CONCRETE FILLED STEEL TUBE ARCH

Nebraska Department of Roads

Project Number SPR-1 (03) 560

NDOR
Nebraska
Department of Roads

University of Nebraska
Lincoln

July 2006

CONCRETE FILLED STEEL TUBE ARCH

NDOR Project Number SPR-1 (03) 560

PRINCIPAL INVESTIGATOR

Maher K. Tadros

Charels J. Vranek Professor of Civil Engineering

University of Nebraska-Lincoln

Amgad F. Morgan Girgis

Research Assistant Professor

University of Nebraska-Lincoln

Sponsored by

Nebraska Department of Roads

University of Nebraska-Lincoln

July 2000

TECHNICAL REPORT DOCUMENTATION PAGE

1. Report No. SPR-1 (03) 560	2. Government Accession No.	3. Recipient's Catalog No.
1. Title and Subtitle Concrete Filled Steel Tube Arch		2. Report Date January 4, 2006 3. Performing Organization Code
4. Author(s) Dr. Maher K. Tadros and Dr. Girgis		5. Performing Organization Report No.
6. Performing Organization Name and Address Department of Civil Engineering University of Nebraska-Lincoln Omaha, Nebraska 68182-0178		7. Work Unit No. 8. Contract or Grant No. SPR-P1(04) P571
9. Sponsoring Agency Name and Address Nebraska Department of Roads Bridge Division P. O. Box 94759 Lincoln, NE 68509-4759		10. Type of Report and Period Covered Draft Report 11. Sponsoring Agency Code
12. Supplementary Notes		

13. Abstract

Ravenna viaduct spans a major route of the Burlington Northern Santa Fe Railroad. Approximately 60 trains per day pass under the bridge. There are very tight restrictions on the vertical clearance above the tracks, the horizontal distance to any pier, and the amount of time rail traffic can be interrupted. The bridge is 174 ft. long to span over 6 sets of rail tracks, two main lines and four sidings. Since this section of track is a major route for the railroad, the amount of time the tracks can be closed is limited to a few hours, and only a limited number of closures. Maintaining the existing road grade and providing the required vertical clearance above the railroad tracks limited the depth of the structure to 35 in.

The old bridge was scheduled to be replaced because it was structurally deficient and functionally obsolete. The vertical clearance above the tracks was less than 23 ft, the horizontal clearance from the pier to the track was less than 13 ft, and the horizontal clearance at the south abutment was 8.5 ft to the track. In addition, the railroad wanted additional space on the south side to extend two side tracks through the bridge opening. The grade coming off the bridge to the north was 7 % and touchdown was at the south end of town's main street. To solve all these concerns, a bridge with a long span and a very shallow superstructure depth was needed. The answer appeared to be a truss or a tied arch.

This paper report presents a practical solution for the clearance limitation through utilizing a unique arch bridge system. The report describes in detail the rapid construction sequencing, and the laboratory tests performed at the University of Nebraska to clarify some of the design issues that the designers were facing. This prefabricated developed system is suitable for accelerated construction, as well as the constraint of working over live main railroad tracks.

14. Keywords: Confinement, steel tube, Arch Bridge, Ravenna, Post-Tensioning, Self-Consolidating Concrete.		15. Distribution Statement	
16. Security Classification (of this report) Unclassified	17. Security Classification (of this page) Unclassified	18. No. of Pages 144	22. Price

Form DOT F1700.7 (8-72)

DISCLAIMER

The contents of this report reflect the views of the authors who are responsible for the facts and the accuracy of the data presented herein. The contents do not necessarily reflect the official views or policies of the Nebraska Department of Roads, nor of the University of Nebraska-Lincoln. This report does not constitute a standard, specification, or regulation. Trade or manufacturers' names, which may appear in this report, are cited only because they are considered essential to the objectives of the report. The United States (U.S.) government and the State of Nebraska do not endorse products or manufacturers.

ACKNOWLEDGEMENTS

This project was sponsored by the Nebraska Department of Roads (NDOR) and the University of Nebraska-Lincoln (UNL). Special thanks are extended to David Fritz of NDOR who was the lead designer of the bridge; Lynden VanderVeen of NDOR who contributed to the design; and Dana Hartung of NDOR who developed the plans and a very attractive scale model of the bridge. They did their work under the capable guidance of Assistant Bridge Engineer Dan Sharp. The authors wish also to thank Lyman Freemon, State Bridge Engineer, whose vision and leadership made this project a reality. Assistant Bridge Engineer, Sam Fallaha, provided valuable leadership and technical support throughout the project. Thanks go to Moe Jamshidi, Materials and Research Engineer and his associates Amy Starr, Lieska Halsey, and Jodi Gibson of NDOR for their valuable feedbacks.

Kelvin Lein, manager of the structures research lab at the Peter Kiewit Institute, and Jeremy Boweres, research assistant of UNL put in significant effort in the experimental work. Also, thanks goes to Ning Wang, research assistant of UNL, for her contributions in the bridge Finite Element 3D Model.

TABLE OF CONTENTS

TECHNICAL REPORT DOCUMENTATION PAGE ..... **I**

DISCLAIMER ..... **II**

ACKNOWLEDGEMENTS ..... **III**

TABLE OF CONTENTS ..... **IV**

TABLE OF FIGURES ..... **IX**

TABLE OF TABLES ..... **XVI**

SECTION 1: INTRODUCTION **1**

1.1 PROBLEM STATEMENT 1

1.2 OBJECTIVE 1

1.3 SCOPE AND LAYOUT 1

SECTION 2: SYSTEM SELECTION **3**

2.1 SITE DESCRIPTION 3

2.2 INVERTED TEE (IT) SYSTEM 4

2.3 PLATE GIRDER SYSTEM 5

2.4 PARALLEL TIED ARCH SYSTEM (CHOSEN SYSTEM) 6

2.4.1 SYSTEM DESCRIPTION 6

2.4.2 FLOOR BEAM SELECTION 12

2.4.2.1 PRECAST PANEL FLOOR BEAM SYSTEM 12

2.4.2.2 STEEL FLOOR BEAM SYSTEM 13

2.4.3 OTHER RECENT ARCH BRIDGES 14

2.4.3.1 HOUSTON SPUR 527 OVER SOUTHWEST FREEWAY 14

2.4.3.2 ARCH BRIDGE OVER THE BRNO-VIENNA EXPRESSWAY 16

SECTION 3: EFFECTIVE FLANGE WIDTH 18

3.1 INTRODUCTION AND CURRENT CODE REQUIREMENTS 18

3.2 LITERATURE REVIEW 19

SECTION 4: SYSTEM ANALYSIS 25

4.1 SECTION PROPERTIES 25

4.1.1 CROSS SECTION 1: STEEL SECTIONS ONLY 25

4.1.2 CROSS SECTION 2: STEEL SECTIONS WITH CONCRETE 26

4.1.3 CROSS SECTION 3: POST-TENSIONED SECTIONS 26

4.1.4 CROSS SECTION 4: SYSTEM WITH COMPOSITE DECK 26

4.1.5 HANGER PROPERTIES 27

4.2 OVERALL SYSTEM ANALYSIS; LOAD DISTRIBUTION 27

4.2.1 GRAVITY LOADING 27

4.2.2 LIVE LOADING 37

4.2.3 WIND LOADING 40

4.3 ELEMENT CAPACITY 41

4.3.1 BOTTOM CHORD 42

4.3.2 TOP CHORD 44

4.3.3 HANGER CONNECTION 45

4.3.4 CROSS BEAM RATING 45

4.4 COMPOSITE ACTION CALCULATIONS 47

4.4.1 SHEAR STUDS 47

4.4.2 INTERACTION BETWEEN TUBE AND ENCASED CONCRETE 49

SECTION 5: FULL SCALE SPECIMEN PRODUCTION 53

5.1 INTRODUCTION 53

5.2 BOTTOM CHORD FABRICATION 53

5.2.1 STEEL FABRICATION AND HARDWARE PLACEMENT 53

5.2.2 CONCRETE POUR AND POST-TENSIONING 60

5.3 END PIECE FABRICATION 64

5.4 TOP CHORD FABRICATION 68

SECTION 6: SPECIMEN TESTING 70

6.1 TOP CHORD SPECIMEN TESTING 70

6.1.1 HOLLOW STEEL TUBE 70

6.1.2 CONCRETE FILLED TUBE 71

6.2 BOTTOM CHORD ULTIMATE STRENGTH 74

6.3 HANGER CONNECTION FATIGUE 77

6.4 HANGER CONNECTION ULTIMATE 81

SECTION 7: CONSTRUCTOR RESPONSE 84

7.1 CONSTRUCTOR INTEREST 84

7.2 BIDDING 85

7.3 COST ANALYSIS 86

SECTION 8: EFFECTIVE FLANGE WIDTH TESTING 88

8.1 OBJECTIVES 88

8.2 INTRODUCTION 88

8.3 TESTING PROGRAM 89

8.3.1 SPECIMEN FABRICATION 89

8.3.2 SPECIMEN DETAILS 93

8.3.2.1 SHEAR STUD CONNECTORS 94

8.3.2.2 DECK SLAB 96

8.3.3 TESTING THE SPECIMEN 97

8.3.3.1 TEST 1 97

8.3.3.2 TEST 2 98

8.3.3.3 TEST 3 99

8.3.3.4 TESTS 4, 5, 6 AND 7 100

8.4 RESULTS AND DISCUSSION 101

SECTION 9: ARCH BRIDGE FINITE ELEMENT MODELING 106

9.1 OBJECTIVES 106

9.2 INTRODUCTION 106

9.3 MODELING 106

9.3.1 HANGERS MODELING 106

9.3.2 ARCH TOP CHORD MODELING 107

9.3.3 ARCH BOTTOM CHORD MODELING 108

9.3.4 DECK SLAB MODELING 109

9.3.5 TURNDOWN BEAM MODELING 109

9.3.6 CROSS-BEAM MODELING 110

9.4 LOADINGS AND ANALYSIS 111

9.5 RESULTS AND DISCUSSION 112

9.5.1 RESULTS IN THE TRAFFIC DIRECTION 112

9.5.2 RESULTS PREPENDICULAR TO TRAFFIC 115

9.5.3 DISCUSSION ON STRESS DISTIBUTION ALONG THE MID-SPAN CROSS SECTION WIDTH 116

9.6 IMPACT OF USING 70 PERCENT OF TOTAL SLAB WIDTH ON BOTTOM CHORD STRENGTH 117

SECTION 10: CONSTRUCTION CHALLENGE 120

10.1 INTRODUCTION 120

10.2 CHOSEN SYSTEMS TO ACCELERATE CONSTRUCTION 120

10.2.1 SUBSTRUCTURE SYSTEM 120

10.2.2 SUPERSTRUCTURE CONSTRUCTION SYSTEM SELECTIONS ... 121

10.2.3 SUPERSTRUCTURE LIFTING OPTIONS 125

SECTION 11: CONCLUSIONS AND RECOMMENDATIONS 129

SECTION 12: IMPLEMENTATION 131

REFERENCES 132

APPENDICES 136

APPENDIX A: TRANSVERSE STABILITY OF THE ARCHES ..... (ON CD)A-1

APPENDIX B: MIX DESIGN ..... (ON CD)B-1

APPENDIX C: BOTTOM CHORD STRENGTH INTERACTION DIAGRAM DATA ..... (ON CD)C-1

APPENDIX D: SECTION PROPERTIES CALCULATION FOR THE FE MODELING ..... (ON CD)D-1

TABLE OF FIGURES

Figure 2.2-1 Typical Inverted Tee bridge cross section 4

Figure 2.2-2 Workers form the deck of a typical IT bridge system 4

Figure 2.2-3 The Ravenna Viaduct using the IT system 5

Figure 2.4.1-1 Elevation view showing components of the chosen system 7

Figure 2.4.1-2 Ravenna Arch Bridge cross section for the chosen system 8

Figure 2.4.1-3 Ravenna Arch Bridge scale model 9

Figure 2.4.1-4 Ravenna Arch Bridge roadway profile 9

Figure 2.4.1-5 Metal decking and foam supports the concrete slab 11

Figure 2.4.2.1-1 Precast panel floor beam system 12

Figure 2.4.2.1-2 Precast Panel longitudinal section 13

Figure 2.4.3.1-1 Houston Arch Bridge on Spur 527 over Highway US 59 15

Figure 2.4.3.2-1 Arch Bridge crossing the Brno-Vienna expressway 16

Figure 3.2-1 Actual stress distribution with imposed constant stress distribution acting on effective flange width b_E 19

Figure 4.1.1-1 2 x 12 in. x ½ in. diameter top chord and 24 in. x 24 in. x ½ in. bottom chord 25

Figure 4.2.1-1 Stage 1 loading 29

Figure 4.2.1-2 Moment distribution due to Stage 1 loading 29

Figure 4.2.1-3 Axial forces due to Stage 1 loading 29

Figure 4.2.1-4 Stage 2 loading 30

Figure 4.2.1-5 Moment distribution from Stage 2 loading 30

Figure 4.2.1-6 Axial forces from Stage 2 loading. 31

Figure 4.2.1-7 Loading due to post-tensioning 31

Figure 4.2.1-8 Moment distribution from post-tensioning 32

Figure 4.2.1-9 Axial forces from post-tensioning 32

Figure 4.2.1-10 Loading due to deck weight 33

Figure 4.2.1-11 Moment distribution from deck weight 33

Figure 4.2.1-12 Axial forces due to deck weight 33

Figure 4.2.1-13 Loading due to barrier weight 33

Figure 4.2.1-14 Moment distribution due to barrier weight 34

Figure 4.2.1-15 Axial force distribution due to barrier weight 34

Figure 4.2.1-16 Loading due to the future wearing surface 35

Figure 4.2.1-17 Moment distribution due to the future wearing surface 35

Figure 4.2.1-18 Axial force due to the future wearing surface 36

Figure 4.2.2-1 Three AASHTO Standard HS20 truck loading 36

Figure 4.2.2-2 ASHTO Standard three lane loading 37

Figure 4.2.2-3 Moment envelope due to live loading. Three HS20 trucks control the design 38

Figure 4.2.2-4 Axial force envelope due to live loading 39

Figure 4.2.3-1 Design loads used for the lateral stability analysis 39

Figure 4.2.3-2 RISA 3D model used for bi-axial stress distribution 40

Figure 4.3.1-1 Bottom chord positive moment interaction diagram 43

Figure 4.3.2-1 Top chord moment interaction diagram 44

Figure 4.3.4-1 Three HS20 Loadings of the cross beam 46

Figure 4.4.1-1 Cross section used for the composite action calculation 47

Figure 4.4.1-1 Longitudinal forces calculation.....49

Figure 5.2.1-1 The bottom chord in fabrication 54

Figure 5.2.1-2 Bottom chord end plate.....55

Figure 5.2.1-3 Post tensioning anchor plates before modification 55

Figure 5.2.1-4 DSF's 19-0.6" diameter post tensioning hardware, before installation.....56

Figure 5.2.1-5 Post tensioning anchor plates after the edges are trimmed. 57

Figure 5.2.1-6 Installed internal post tensioning hardware 57

Figure 5.2.1-7 End plate with grouting hole.....58

Figure 5.2.1-8 Chair supporting post tensioning duct 58

Figure 5.2.1-9 #4 bar holding down the ducts 59

Figure 5.2.2-1 Tensioning the strands 62

Figure 5.2.2-2 Using the special hardware 62

Figure 5.2.2-3 Pipe fitting welded around grout access hole 63

Figure 5.3-1 End specimen elevation view.....65

Figure 5.3-2 Connection base plate 66

Figure 5.3-3 Connection elements.....66

Figure 5.3-4 Connection elements, as seen from below 67

Figure 5.3-5 Spherical nut seated in dish plate.....67

Figure 5.4-1 The hollow tube was filled by pumping from the bottom 69

Figure 5.4-2 A high flow mix was used to fill the specimen.....69

Figure 6.1.1-1 Hollow steel tube test setup 70

Figure 6.1.1-2 Hollow steel tube final deflection 71

Figure 6.1.2-1 Concrete filled tube test setup 72

Figure 6.1.2-2 Concrete filled tube testing in progress 73

Figure 6.1.2-3 The center of the tube, immediately after cutting open, showing the visible moisture 73

Figure 6.2-1 Point loading of Ravenna Bottom Chord test specimen 74

Figure 6.2-2 The bottom chord test specimen in place and in early stages of loading 75

Figure 6.2-3 The bottom chord test specimen in advanced stages of loading 76

Figure 6.2-4 The bottom chord test specimen as it approaches ultimate deflection 77

Figure 6.3-1 Special plates were used to seat the mounting rods perpendicular to the load 78

Figure 6.3-2 The connection specimen mounted upside-down in the load frame 79

Figure 6.3-3 The connection specimen mounted beneath the 110 kip actuator 79

Figure 6.3-4 The wedge plate was mistakenly fabricated too small 80

Figure 6.3-5 Corrective stiffeners 81

Figure 6.4-1 The test setup, as seen from the floor of the PKI Structures Laboratory 83

Figure 6.4-2 The test setup, as seen from below, on the specimen's level 83

Figure 8.3.1-1 Shooting the studs 90

Figure 8.3.1-2 Beam connection. 90

Figure 8.3.1-3 Longitudinal and cross beams layout 91

Figure 8.3.1-4 Forming the deck slab and installing the reinforcement 92

Figure 8.3.1-5 Specimen ready to be tested 92

Figure 8.3.2-1 Layout of the specimen 93

Figure 8.3.2.1-1 Distribution of the shear studs along beam C 94

Figure 8.3.2.1-2 Distribution of the shear studs along Beam D 95

Figure 8.3.2.1-3 Shear stud configurations of the longitudinal beams 96

Figure 8.3.2.2-1 Deck reinforcement 97

Figure 8.3.3.1-1 Test 1 loading locations 98

Figure 8.3.3.2-1 Location of the strain gauges for Test 2 99

Figure 8.3.3.3-1 Load application for test 3 100

Figure 8.3.3.4-1 Load application for tests 4, 5, 6 and 7 101

Figure 8.4-1 Test 2 Results 102

Figures 8.4-2 Test 3 steel strain gauge readings 102

Figures 8.4-3 Test 3 concrete strain gauge readings 103

Figures 8.4-4 Test 3 load-deflection curve 104

Figure 8.4-5 Test 6 lead deflection curve 104

Figure 9.3.2-1 Arch top chord element 105

Figure 9.3.3-1 Arch bottom chord element 107

Figure 9.3.4-1 Deck slab element 108

Figure 9.3.5-1 Turndown beam element.....109

Figure 9.3.6-1 Cross-beam element.....110

Figure 9.4-1 RISA 3D Model 111

Figure 9.5.1-1 3D model bottom chord element axial force.....112

Figure 9.5.1-2 2D model bottom chord element axial force.....113

Figure 9.5.1-3 3D Model bottom chord element moment about Z-Z direction..113

Figure 9.5.1-4 2D Model bottom chord element moment about Z-Z direction.....114

Figure 9.5.2-1 Pictures of the member numbers of the 3D model 114

Figure 9.5.2-2 Mid-span member numbers 116

Figure 9.5.3-1 3D model output deck slab axial stresses along the bridge mid-span.....117

Figure. 9.6-1 Ravenna bottom chord interaction diagram using 100% and 70% from deck slab.....119

Figure 10.2.1-1 Construction of substructure 121

Figure 10.2.2-1 Construction of the two arches 122

Figure 10.2.2-2 Arches temporary bracing.....122

Figure 10.2.2-3 Cross beams and metal decking installation 123

Figure 10.2.2-4 Post-tensioning the tie beams.....123

Figure 10.2.2-5 Deck slab reinforcement installation 124

Figure 10.2.2-6 Deck slab post-tensioning 124

Figure 10.2.2-7 Railing Construction 125

Figure 10.2.3-1 Superstructure lifting options I 126

Figure 10.2.3-2 Superstructure lifting options II 127

Figure 10.2.3-3 Superstructure lifting options III.....127

Figure 10.2.3-4 Installation of the first arch 128

TABLE OF TABLES

Table 4.3.4-1 Dead loads and bending moments 45

Table 4.4.1-1 Shear studs calculations 48

Table 4.4.2-1 Longitudinal forces calculations 51

Table 8.3.2.2-1 Concrete strength development with time 97

Table 8.4-1 Predicted and tested loads for tests 4 through 7.....105

Table 9.5.2-1 Axial forces of the deck cross section.....115

SECTION 1: INTRODUCTION

1.1 PROBLEM STATEMENT

The NDOR, Bridge Division, is faced with the challenge of providing a 175 ft single span bridge with a structural depth not exceeding 35 in. for the Ravenna Viaduct. The only way to meet this challenge is by using a truss or a tied arch system. A tied arch would require less fabrication labor and would be more aesthetically pleasing than a truss. An innovative steel tube parallel arch system was investigated by NDOR and University of Nebraska personnel and was found to be feasible. The slender arch would only be possible due to the high performance steel and concrete to be used, and due to use of new theories recognizing a significant increase in capacity of concrete that is confined inside a steel tube.

1.2 OBJECTIVE

The immediate goal of this research is to provide technical justification for the design and detailing of the Ravenna Viaduct arch system. The results of the research will form the basis for standardizing the system for future use in applications where superstructure depth is severely limited.

1.3 SCOPE AND LAYOUT

This report is divided into eleven sections. Section one provides the introduction and layout of this report. Section two describes how the Ravenna Viaduct system was selected and gives some examples in the United States as well as in Europe of previously

successfully arch bridges built the past. Section three is a literature review of the effective flange width. Section four provides the analysis of the arch bridge. Section five shows the specimens that were fabricated to cover the production issues. Section six describes the tests that were preformed on the arch bridge elements. Section seven shows the contractors response and acceptance to this project details and innovations. Section eight describes the tests that were preformed to investigate the effective deck slab width and the results. Section nine shows the bridge finite element model and its results. Section ten describes the construction challenges and sequence of the bridge. Section eleven provides conclusions and recommendations.

SECTION 2: SYSTEM SELECTION

2.1 SITE DESCRIPTION

Ravenna, Nebraska, is located in central Nebraska, just northwest of Grand Island. Nebraska Highway 2 passes south of the city, and Route 68 cuts directly through town. Visitors to town pass over the Ravenna Viaduct as they approach town on Route 68 from the south.

The viaduct passes over a major hub of the Burlington Northern Santa Fe Railroads. Because of this, there are very tight restrictions on the depth of the bridge members, the type of work that can be done over the railway, and the amount of time the rails can be closed. The bridge is 174 ft. long to pass over 6 sets of rail tracks. Because this particular section of track is a major hub for the line, the amount of time the railroad below can be closed is limited to a few hours, and only a very limited number of closures. Railroad restrictions limit the depth of the structural members to 35 in.

Ravenna is a rural town of approximately 2,300 people. Special considerations include designing the bridge to take a tractor load, potentially 3 tractors wide. Additionally, there are no Ready-Mixed concrete producers in Ravenna. The closest are located in Grand Island or Kearney, both about 35 miles away.

Several systems were discussed as the initial concept for the new Ravenna Viaduct. In the end the drawbacks of each conventional system led to the Arch bridge concept.

2.2 INVERTED TEE (IT) SYSTEM

A typical Inverted Tee (IT) system cross section is shown below in *Figure 2.2-1*. One major drawback to this system is the method used to form the cast-in-place deck. *Figure 2.2-2* shows a typical deck being formed with the IT system. Plywood is placed between the stems, the overhang is formed and the deck is placed. With this project, however, worker time spent over the railroad must be limited. This system would require extensive time spent over the railroad, posing a risk to both the workers and the railroad.

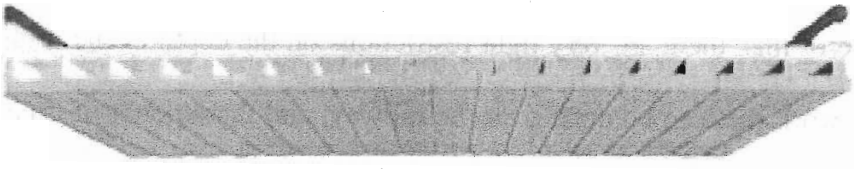

Figure 2.2-1 – Typical Inverted Tee bridge cross section [Ref. 11]

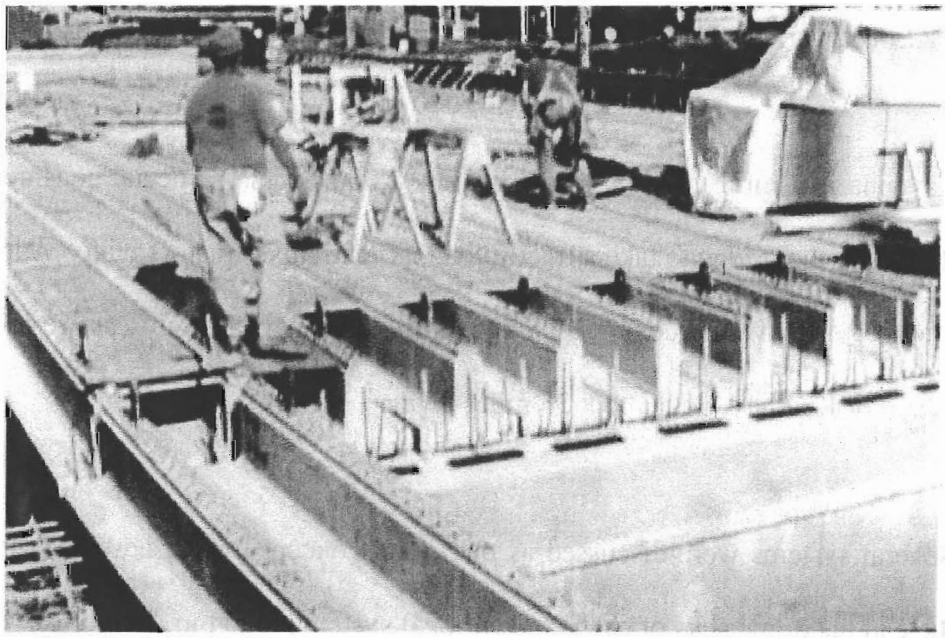

Figure 2.2-2 - Workers form the deck of a typical IT bridge system [Ref. 11]

As previously mentioned, because of the railroad the structural depth must be limited to 35 in. At this depth, the maximum distance a typical IT system can span is 100 ft. Therefore, a pier would be necessary with this system. Due to the rail traffic, constructing this pier would be both difficult and expensive. Railway service would have to be postponed, and not resumed until after the construction was completed and cleaned up. *Figure 2.2-3* shows this system.

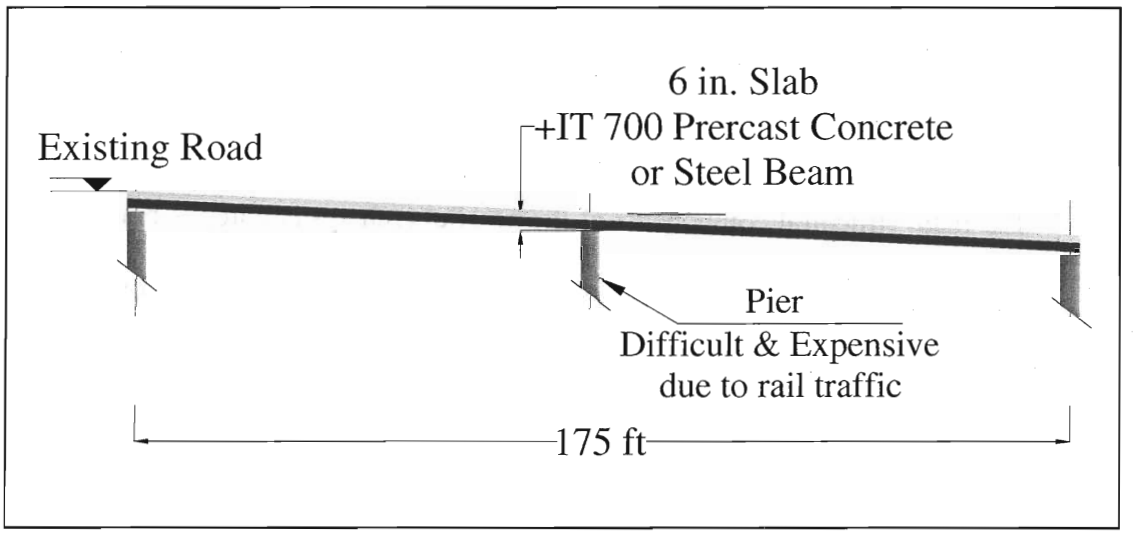

Figure 2.2-3 – The Ravenna Viaduct using the IT system.

2.3 PLATE GIRDER SYSTEM

A plate girder system has similar drawbacks as the IT system. A structural depth of less than 35 in. is not possible without a pier. Additionally, this system requires workers spending significant time over the railroad forming for the cast-in-place deck.

2.4 PARALLEL TIED ARCH SYSTEM (CHOSEN SYSTEM)

2.4.1 SYSTEM DESCRIPTION

The parallel arch system provides a unique solution to these problems. Namely, the system provides a structural depth less than 35 in., does not require the use of a pier, and keeps worker time over the railroads to a minimum. Additionally, a majority of the assembly and construction can be done before the bridge is over the railroad. The bridge is then launched into place. This slender arch system is only possible because of new high performance steel and concrete, and new theories recognizing the increased strength of confined concrete.

The main structural components of the parallel arch system are: 1) bottom chords; 2) top chords; 3) floor beams; 4) hangers; and 5) deck. *Figure 2.4.1-1* shows the components for the chosen system visible in an elevation view. A cross section appears in *Figure 2.4.1-2*, and a scale model appears in *Figure 2.4.1-3*.

The system allows for a minimum structural depth by using the bottom chord as a tension tie and the top chord as a compression strut. In this way, the moment in the girder is reduced by this bottom chord/top chord couple.

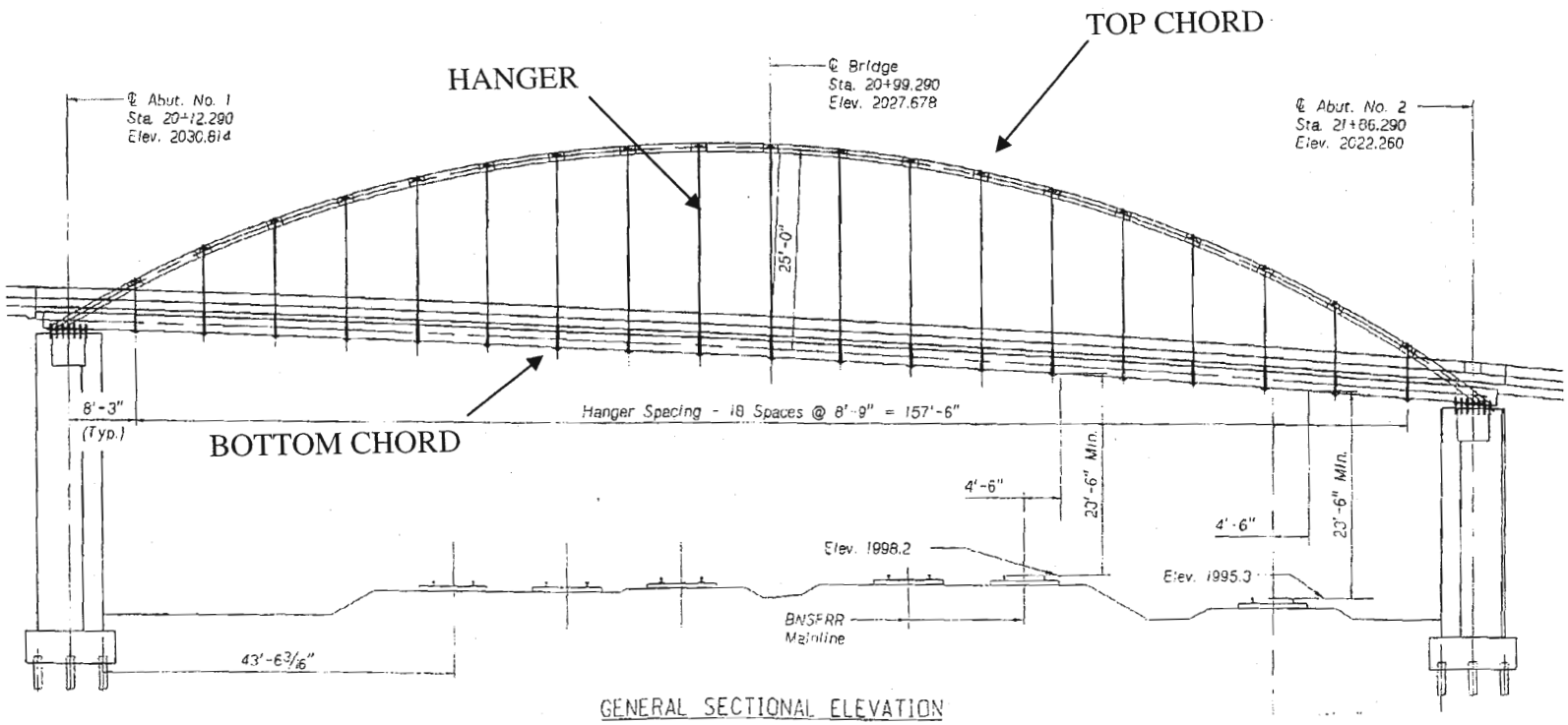

Figure 2.4.1-1 – Elevation view showing components of the chosen system.

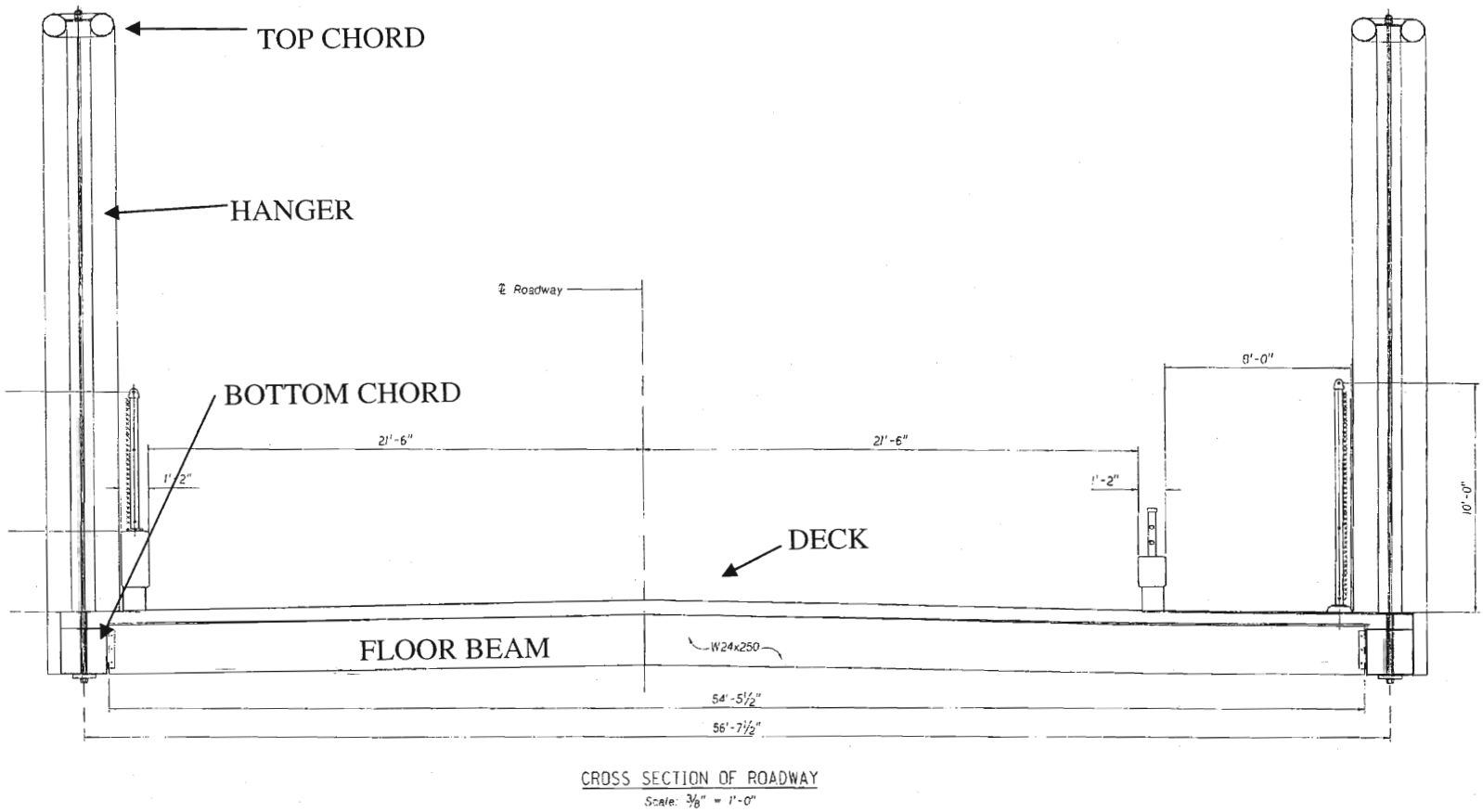

Figure 2.4.1-2– Ravenna Arch Bridge cross section for the chosen system.

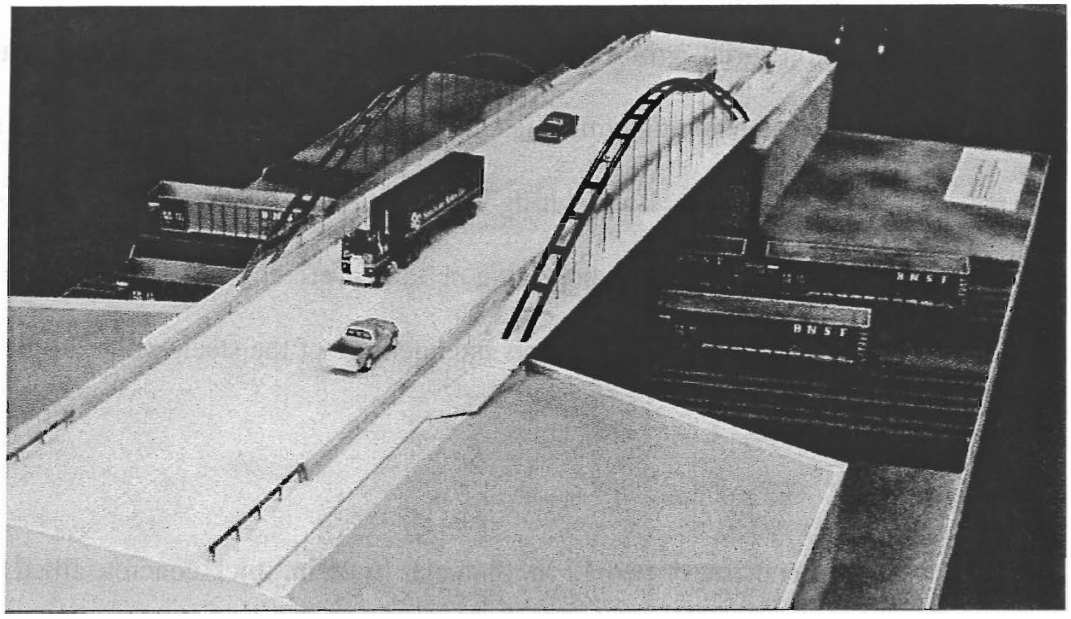

Figure 2.4.1-3 – Ravenna Arch Bridge scale model (By Dana Hartung, NDOR).

The bridge is 56 ft. 7 ½ in. wide, and has a span of 174 ft. The peak of the arch is 25 ft. above the roadway elevation. The roadway profile has a maximum 7 % slope as shown in *Figure 2.4.1-4*.

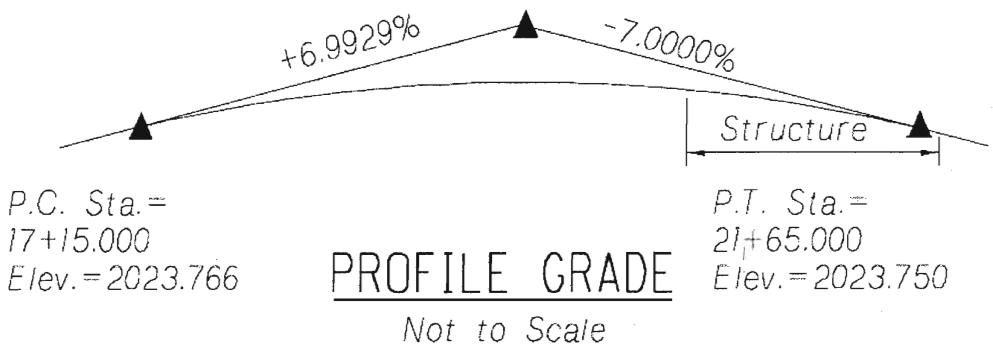

Figure 2.4.1-4 – Ravenna Arch Bridge roadway profile.

The bottom chords are 24"x24"x½" concrete filled steel tubes. Each tube is post-tensioned with 38 fully tensioned 0.6" diameter strands. The post-tensioning ducts are

grouted with non-shrink grout. The bottom chord is the most innovative feature of the system. The post-tensioning eliminates the concern over fatigue in the splice by keeping the section in net compression during loading. The concrete filling makes the post-tensioning more efficient by providing a larger effective area to sustain the post-tensioning load. The concrete prevents the buckling of the steel, while the steel confines the concrete.

Each top chord consists of two 12 in. diameter by ½ in. thick concrete filled steel tubes. The arch is the primary compression member in the system. There are no braces connecting the top chords. This is highly desirable for aesthetic reasons. The lack of horizontal braces also provides unlimited overhead clearance. At the peak, the arches are 25 ft. above the roadway grade.

The independent arches were accomplished by placing the concrete filled pipes next to each other. This greatly increased the moment of inertia in the lateral direction, and gave space to connect the hangers.

1¾ in. diameter high strength threaded rods serve has hangers. The rods reach between the top chord and the bottom chord at 8 ft. 9 in. spacing.

The floor beams are W24x250 and are also spaced at 8 ft. 9 in. on-center. Their selection is discussed in the following section.

The composite deck is 8" thick, and utilizes a longitudinal unbonded monostrand post-tensioning system. The 0.6" diameter strands are spaced at 6" on-center. The metal decking for the concrete slab can be assembled with the rest of the bridge before being launched. *Figure 2.4.1*-5 shows the metal decking supporting the concrete slab. In this way, worker time over the railroad is kept to a minimum.

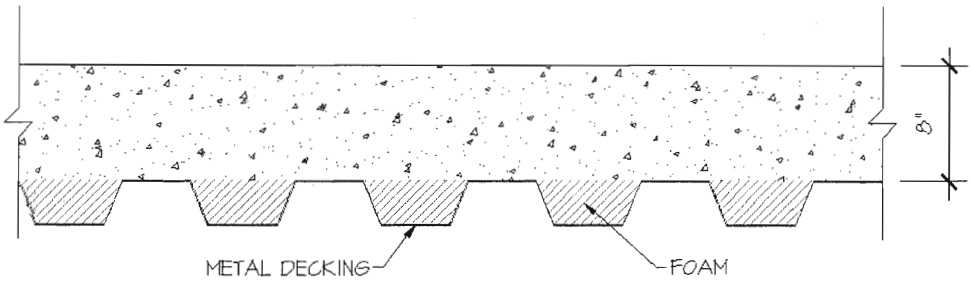

Figure 1.4.1-5 – Metal decking and foam supports the concrete slab.

2.4.2 FLOOR BEAM SELECTION

Spanning under the roadway between the two bottom chords will be floor beams. Design of the floor beams offers several challenges. The floor beams must be an efficient, economic section spanning approximately 55 ft. between the two bottom chords. The floor beams must be limited to a depth equal to or less than the bottom chords (30"). As previously discussed, work over the railway must be minimized. Consequently, the system must provide an easy way to construct the deck.

2.4.2.1 PRECAST PANEL FLOOR BEAM SYSTEM

One alternative system is a rapid construction precast concrete floor panel system. The casting of each panel would involve two precast stages. The first would be the casting of two regular 55 ft. IT500 sections. The second stage would involve forming an 8 in. deck on 4 or 5 diaphragms. The panels are then placed side by side for the length of the bridge, and the joint between the panels is grouted. *Figure 2.4.2.1-1* below shows the cross section of a typical panel proposed in this system, and *Figure 2.4.2.1-2* shows a longitudinal section.

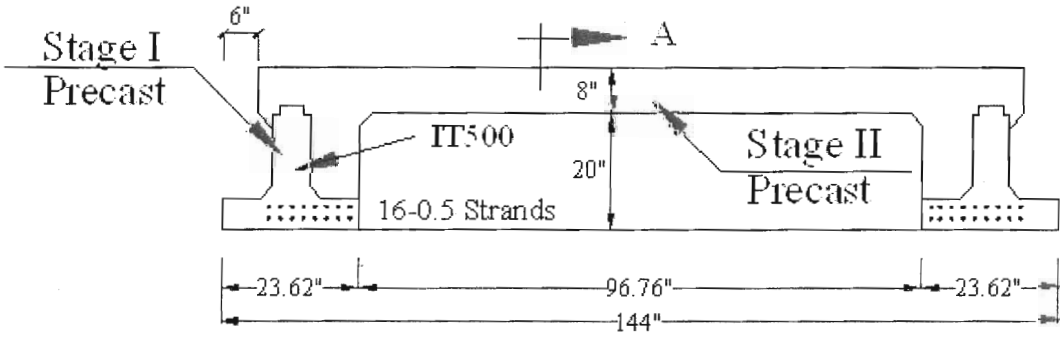

Figure 2.4.2.1-1 – Precast panel floor beam system

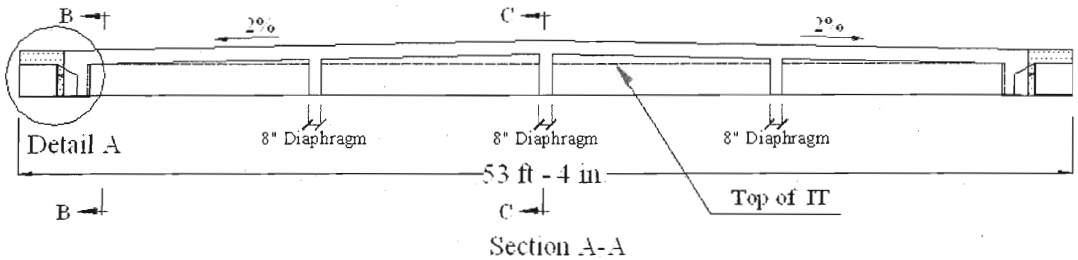

Figure 2.4.2.1-2 – Precast Panel longitudinal section.

There are several advantages to this system. First, the deck can have a higher compressive strength then a conventional cast in place (CIP) deck. The life cycle of the deck is closer to the IT, significantly longer than a CIP deck. The only field work involved is the connection to the bottom chords and grouting between the adjacent panels. Most importantly, however, is that once the gap between panels is grouted the strength of each "floor beam" is effectively doubled. The prestressing and the effective deck width used for strength are doubled to carry the live load and the super-imposed dead load (S.I.D.L.). This enables a standard IT500 to span 55 ft., giving a span to depth ratio of approximately 33.

2.4.2.2 STEEL FLOOR BEAM SYSTEM

The other option for the floor beam system is a more customary steel design. Because the span for the floor beams is only 55 ft., choosing a steel section under the required 35 in. depth is not a problem. Because the floor beams, and the metal decking for the riding surface, can be attached to the girders before the bridge is launched, this system also reduces worker time above the tracks.

The major advantage to this system is constructor familiarity. The arch system itself is already unconventional for a constructor. Additionally, more conventional connections can be used because both the bottom chords and the floor beams are then structural steel.

Although the precast panel floor system offers many advantages, and should be explored further in future projects, it was thus decided to use the steel beam floor system for the Ravenna Viaduct. As mentioned previously, the steel floor beams are W24x250 spaced at 8 ft. -9 in. on-center.

2.4.3 OTHER RECENT ARCH BRIDGES

2.4.3.1 HOUSTON SPUR 527 OVER SOUTHWEST FREEWAY

Designers at the Texas Department of Transportation recently used a tied arch bridge system on Spur 527 over US Highway 59 [Ref. 20]. Because of the freeway traffic below the bridge, similar depth restrictions and safety precautions were incorporated into the design.

The bridge is 47 ft. wide and spans 224 ft. over the freeway. The system is very similar to the Ravenna concept. Both the bottom and top chords of this bridge are built up steel tube sections. The bottom chord is post-tensioned, and is ultimately encased in concrete. *Figure 2.4.3.1-1* shows a picture of the completed bridge.

One of the biggest differences in the overall system is the way the arches are tied together. The Houston arches are 45 ft. apart, and tied together along the length of the

arch (above the roadway) with steel sections. The Ravenna Viaduct utilizes the deck as a structural tie between the two arches.

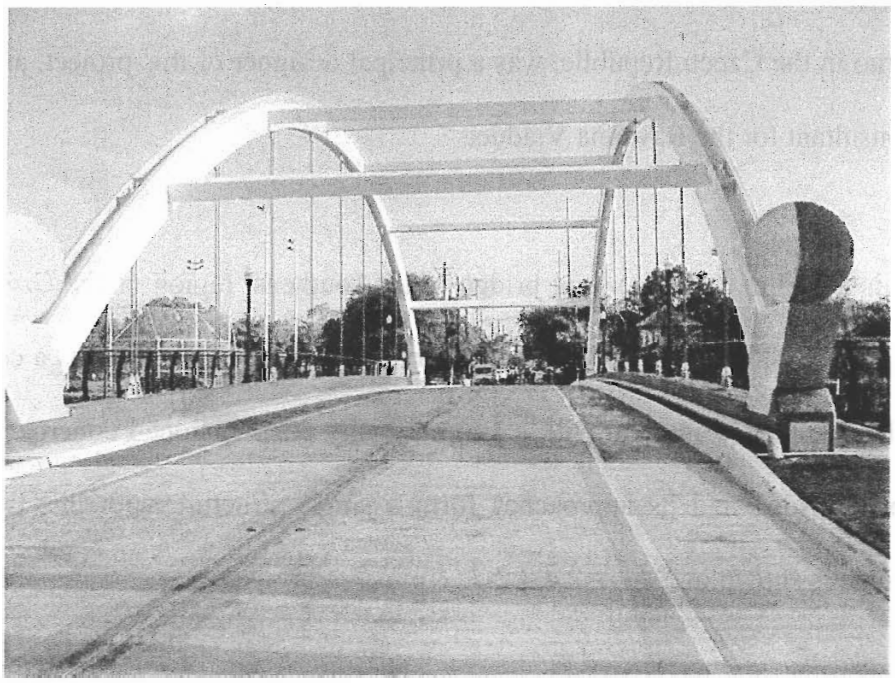

Figure 2.4.3.1-1 – Houston Arch Bridge on Spur 527 over Highway US 59. (Courtesy of the Texas Department of Transportation)

Another significant difference between the Houston and Ravenna bridges is the floor system. The Houston system uses an 11 in. thick longitudinally post-tensioned precast floor system. A CIP riding surface is then poured.

An additional notable difference between the two systems is the difference in the hangers. The Houston Bridge uses 1⅝ in. diameter structural cables that are adjusted after the deck is placed. This is probably done in order to balance the dead load positive and negative moments. The Ravenna system uses 1¾ in. threaded rods, and there are no plans for adjustment after erection.

2.4.3.2 ARCH BRIDGE OVER THE BRNO-VIENNA EXPRESSWAY

Another recent arch bridge of interest to designers is the Arch Bridge over the Brno-Vienna expressway [Ref 1.3]. Dr. Jiri Strasky, a professor at the Technical University of Brno in the Czech Republic, was a principal designer of this project, and also served as a consultant for the Ravenna Viaduct.

This a 110 m. (361 ft.) long bridge in the southeast region of the Czech Republic. The bridge is esthetically pleasing and structurally unique. The arch is a concrete filled steel tube completely integral with a longitudinally post-tensioned concrete bridge deck. The entire bridge and its approaches form a single structure with just two supports. The bridge is shown in *Figure 2.4.3.2-1.*.

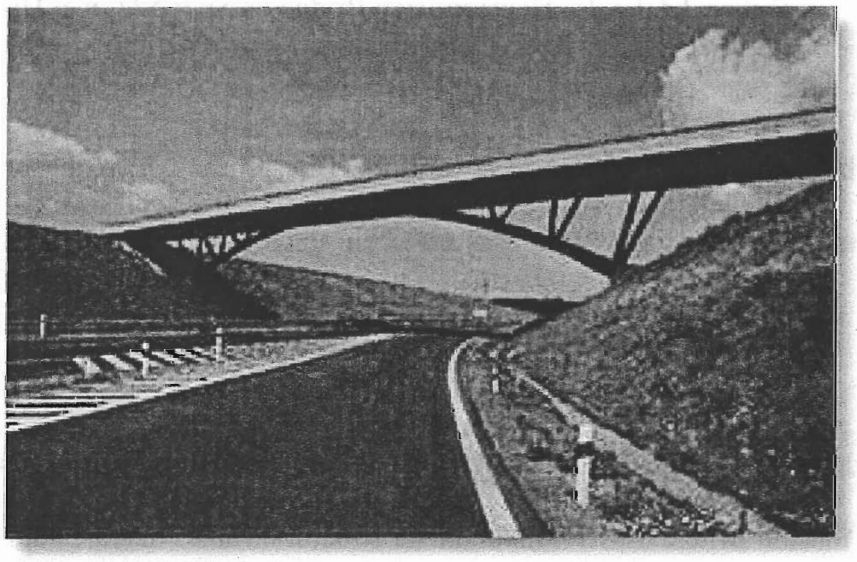

Figure 2.4.3.2-1 – Arch Bridge crossing the Brno-Vienna expressway. [Ref. 1.3]

Of particular interest to the Ravenna Viaduct designers was the filling of the main arch tube with concrete. The compressive strength of the mix used was 50 MPa (7250 psi). It

is noted that the water to cement ratio was kept as low as possible to eliminate the risk of excess water freezing. A superplasticizer helped create a mix with the desirable high flow characteristics.

The tubes were filled using an innovative procedure. The concrete was pumped from the bottom to the top of the arch where it was fitted with three vent tubes. The middle short tube was sealed when concrete reached the top, but the concrete continued to be pumped until several cubic feet had passed out the top of the two 3-m high tubes. This was done in order to use the pressure head created by the vent tube to help consolidate the pumped concrete. The first few cubic feet were wasted to ensure the concrete in the tube was of high quality and any bleed water was expelled at the beginning.

SECTION 3: EFFECTIVE FLANGE WIDTH

3.1 INTRODUCTION AND CURRENT CODE REQUIREMENTS

One of the most interesting aspects of the design of the Ravenna Viaduct was the discussion on how much of the deck to assume acts compositely with the girders. This parameter is called effective flange width.

AASHTO LRFD 4.6.2.6.1 [Ref. 2] states that, for interior beams, the effective flange width may be taken as the least of:

- One-quarter of the effective span length
- 12.0 times the average depth of the slab, plus the greater of web depth or one-half the width of the top flange of the girder
- The average spacing of the adjacent beams

For exterior beams, the effective flange width may be taken as one-half the effective width of the adjacent interior beam, plus the least of:

- One-eighth of the effective span length
- 6.0 times the average depth of the slab, plus the greater of one-half the web depth or one-quarter of the width of the top flange of the basic girder;
- The width of the overhang.

AISC LRFD SPECIFICATION FOR STRUCTURAL STEEL BUILDINGS Section I3.1 [Ref. 17] states that the effective width of the concrete slab is the sum of the effective widths for each side of the beam center-line, each of which shall not exceed:

1. one-eighth of the beam span, center-to-center of supports;
2. one-half the distance to the center-line of the adjacent beam; or
3. the distance to the edge of the slab.

3.2 LITERATURE REVIEW

The stiffness of a beam acting compositely with its deck is often two to three times the stiffness of the steel beam acting alone [Ref. 9] so the issue is of great importance to the design of the Ravenna Viaduct. The extent to which the deck contributes to the stiffness of the system is dependent on the distribution of normal stresses, which vary transversely in the slab. *Figure 2.2-1* shows a typical distribution.

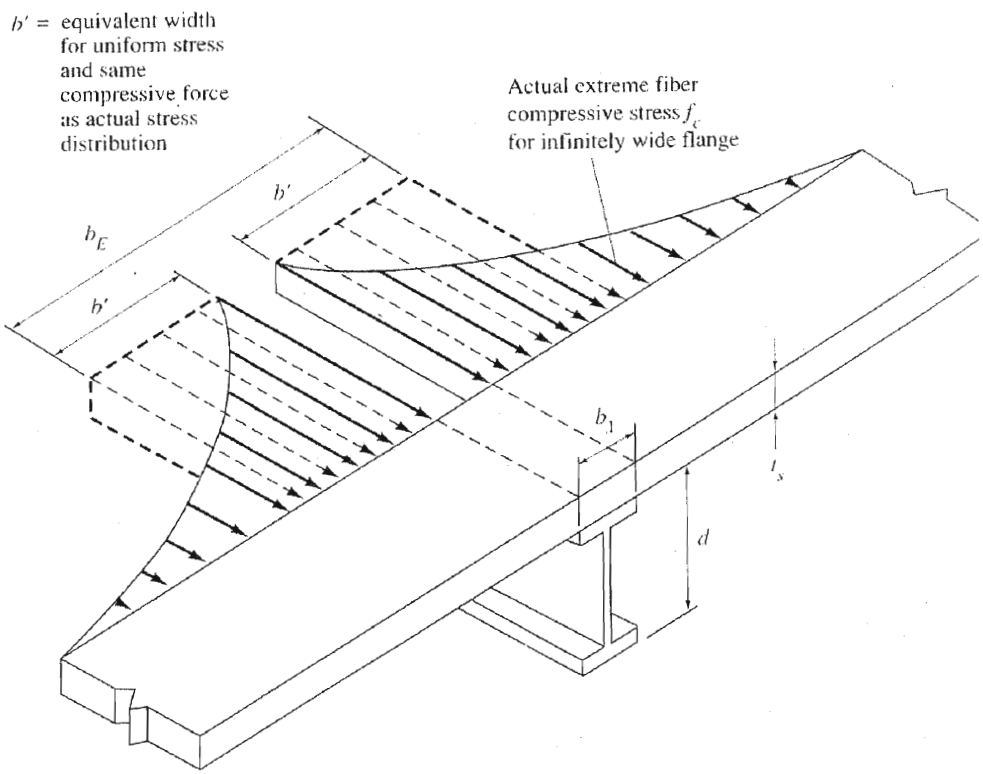

Figure 3.2-1 – Actual stress distribution with imposed constant stress distribution acting on effective flange width b_E [Ref. 2.4]

The varying stresses in the transverse direction are due to what is called the shear lag effect. This effect in the slab is traditionally analyzed using the governing partial differential equations, while beam bending behavior is used to analyze the steel beam that the deck is made composite with [Ref. 7]. Therefore, the problem of determining to what extent the two act together becomes very complex.

The effective flange width is a tool designers use to simplify the problem that a complicated, variable stress distribution causes. The effective flange width code solution assumes a rectangular stress distribution over a specified limited width. This limited width is defined in the codes as described previously.

Several historical studies have produced approximations to estimate how much of the deck is acting compositely with the girder. These studies include Schade [Ref. 27], Sechler [Ref. 28], Lee [Ref. 14], Reisner [Ref. 24], Fan and Heins [Ref. 10], Pantazopoulou and Moehle [Ref. 22], Amra and Nassif [Ref. 3], and Song and Scordelis [Ref. 29]. Each of these studies was conducted to develop simplified equations to estimate effective flange width.

Reisner [Ref. 24] concluded with a hypothesis that the distribution of normal stresses in the flange can be approximated by a second order parabolic curve. His solution gives the following expression for effective flange width:

$$b_m = \frac{\left[\int_0^b \sigma_z(x)dx\right]}{\sigma_{z,\max}}$$

Where: $\sigma_{z,max}$ = maximum stress at the junction point of the web and flange plates; $\sigma_z(x)$ = normal stress distribution in the flange plate; and b_m = one side of the effective width.

In a more celebrated study, von Karman [Ref. 13] constructed a solution accounting for the complicated interaction between the two elements and corresponding analysis methods. The solution is, of course, quite complex. Assumptions used to develop the stress function include an infinitely large flange, and a very small thickness when compared to the depth of the beam. The bending of the top flange as a beam is neglected, and the forces are transmitted to the flange in a way that creates a two dimensional problem.

Assuming equilibrium in von Karman's solution gives the following expression for effective flange width [weigh in motion study]:

$$b_m = L/\pi(3 + 2\nu - \nu^2) \qquad \text{(simple span)}$$
$$b_m = 0.85L/\pi(3 + 2\nu - \nu^2) \qquad \text{(continuous span)}$$

Where: b_m = one side of the effective flange width; L = span length; and ν = Poisson's ratio.

Timoshenko [Ref. 34] developed the same solution, and Metzer [Ref. 18] and Miller [Ref. 19] used that approach to solve the case of a single T-beam with infinite flange width subjected to a concentrated load at midspan.

Chen et al. [Ref. 7] in an interim report give a brief historical background on the history of the current code restrictions, and the following is a summary from their report.

The "Final report of the special committee on concrete and reinforced concrete" of 1916 first introduced the ¼ span length and 12 times the slab thickness provisions. This was based on current engineering practice, a study of concrete T beams by Talbot [Ref. 33] and other studies. Although there was some debate over its adoption, and several other limits were being used at the time, the discussion and variations died down after the 1916 report provisions were published.

The provisions first appeared in the 1936 AISC specifications, and the 1944 AASHTO Standard Specifications. The definition of effective flange width has remained essentially the same in AASHTO Standard since the provisions were first introduced.

Until 1986 the requirements were the same in both AISC and AASHTO Standard. In 1986, however, AISC dropped the use of slab thickness in the determination of effective flange width.

As the Load and Resistance Factor Design (LRFD) method was developed, the effective flange width definition from AASHTO standard was adopted. Therefore, its use, although originally adopted in an allowable stress design, is also used in the determination of ultimate capacity.

The research suggests that effective flange width is greatly underestimated with current codes. Important parameters in the calculation include the type of loading, degree of interaction, span length, and slab width [Ref. 3]. Cheung and Chan [Ref. 8] found that for most practical bridges, girder size and deck thickness had very little effect on the effective width.

Elhelbawey et al., [Ref. 9] who used weigh in motion technology to determine slab participation, concludes that effective flange widths from testing are relatively higher than those from design codes. Elhelbawey et al. also points out that the current AASHTO limitations were the result of research that was performed on simple-span, nonskewed bridges, and no correction facors are defined for use in other situations. Loo and Sutandi, [Ref. 15] who focused on T-Beams, concluded that most American and international codes are unduly conservative for beams under a uniformly distributed loads.

The most current research is the NCHRP 12-58 study by the aforementioned Chen et al. [Ref. 7]. The study reviewed all foreign and domestic field and laboratory results, analytical studies, and specifications regarding effective slab widths for all types of

concrete structures. The study also compared all existing methodologies in this area, and used a finite element based analytical investigation of the issue.

NCHRP 12-58, in the interim report summary of findings, states that there is little or no justification in retaining the 12t limitation in the AASHTO specifications. The study recommends laboratory and field experiments on structural configurations with widely spaced supporting girders, if verification of the finite element analysis is desired.

The Ravenna Viaduct, as discussed in later sections, only needs to count on the full deck for composite actions to meet recommended deflection limits. In regards to strength, the system is sufficient relying solely on the concrete filled steel tube acting as the bottom tie, with no contributions from the slab. It appears from the literature review that a significant portion of the slab, if not the whole slab, does, in fact, act compositely with the bottom chord.

Researchers are continuing this investigation with an experimental program studying a full size composite system with similar characteristics.

SECTION 4: SYSTEM ANALYSIS

4.1 SECTION PROPERTIES

Section properties are calculated for each stage of construction. These stages are: 1) Steel sections only; 2) Steel sections filled with concrete; and 3) Composite sections with post tensioning; 4) System with composite deck. Section properties for each of these stages are shown below.

4.1.1 CROSS SECTION 1: STEEL SECTIONS ONLY

TOP CHORD: *Figure 4.1.1-1* shows the top chord steel sections.

A = 36.13 in.^{2}

I = 598.37 in.^{4}

BOTTOM CHORD: *Figure 4.1.1-2* shows the bottom chord steel section.

A = 47.00 in.^{2}

I = 4327.92 in.^{4}

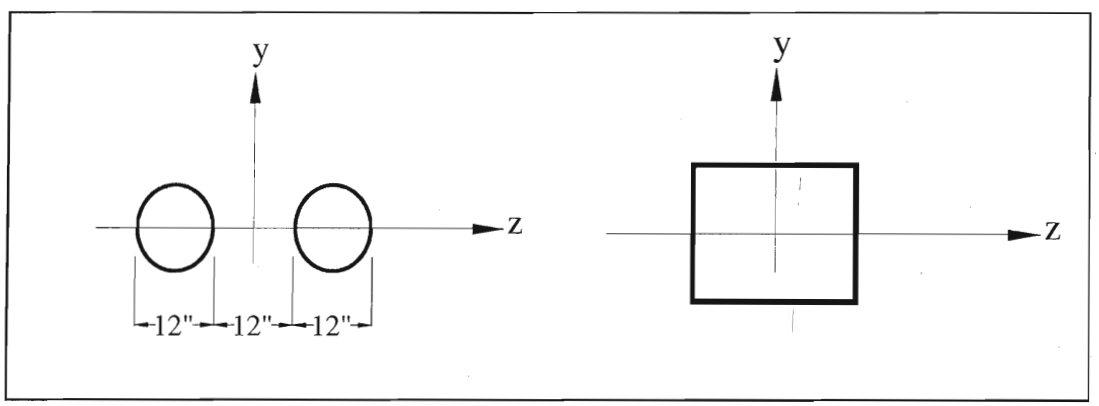

Figure 4.1.1-1 - 2 x 12 in. x ½ in. diameter top chord and 24 in. x 24 in. x ½ in. bottom chord.

4.1.2 CROSS SECTION 2: STEEL SECTIONS WITH CONCRETE

TOP CHORD:

Area = 71.67 in^2 Steel Equivalent — Area = 383.29 in^2 Conc. Equivalent

I_z = 867.14 in^4 Steel Equivalent — I_z = 4637.56 in^4 Conc. Equivalent

I_y = 11184.8 in^4 Steel Equivalent — I_y = 59817.8 in^4 Conc. Equivalent

BOTTOM CHORD:

Area = 145.91in^2 Steel Equivalent — Area = 780.36 in^2 Conc. Equivalent

I_z = 8688.33 in^4 Steel Equivalent — I_z = 46,466.36 in^4 Conc. Equivalent

4.1.3 CROSS SECTION 3: POST-TENSIONED SECTIONS

TOP CHORD:

Area = 71.67 in^2 Steel Equivalent — Area = 383.29 in^2 Conc. Equivalent

I_z =867.14in^4 Steel Equivalent — I_z = 4637.56 in^4 Conc. Equivalent

BOTTOM CHORD:

Area = 154.16 in^2 Steel Equivalent

I_z = 9127.36 in^4 Steel Equivalent

4.1.4 CROSS SECTION 4: SYSTEM WITH COMPOSITE DECK

Half of the deck width is assumed to act compositely with each bottom chord. See Section 2 for a more detailed explanation of this decision.

TOP CHORD:

Area = 71.67 in^2 Steel Equivalent — Area = 383.29 in^2 Conc. Equivalent

I_z = 867.14in^4 Steel Equivalent — I_z = 4637.56 in^4 Conc. Equivalent

BOTTOM CHORD:

Area = 502.96 in^2 Steel Equivalent

I_z = 38650.64 in^4 Steel Equivalent

y_b = 22.80 in.

4.1.5 HANGER PROPERTIES

The hangers are 1 ¾ in. diameter steel rods spaced at 8 ft.-9 in. The cross sectional area is 2.39 in.,^{2} and the hanger is made of 150 ksi grade steel.

4.2 OVERALL SYSTEM ANALYSIS; LOAD DISTRIBUTION

4.2.1 GRAVITY LOADING

Loads calculated here and in subsequent sections are for each individual arch:

TOP CHORD SELF WEIGHT:

Steel only = $W_s = 2x\ A_s\ (3.4) = 2 \times 18.064 \times 3.4 = 122.835$ lb/ft

Concrete filling = $W_s = 2\ [A_c(150)] = 2[\frac{95.033}{144} \times 150] = 197.985$ lb/ft

BOTTOM CHORD SELF WEIGHT:

Steel only = $W_s = A_s\ (3.4) = 47 \times 3.4 = 160.0$ lb/ft

Steel with Concrete filling = $W_s = A_c\ (150) = \frac{23x23}{144} \times 150 = 551.042$ lb/ft

FLOOR BEAM SELF WEIGHT:

W24X250 L = 56 ft. -7.5 in. @ 8 ft.- 9 in.

P_b=W.L/2=54.625 X 250/(2x1000)= 6.828 kips @ 8 ft.-9 in.

METAL DECKING:

$W = 0.004\ k/ft^2$

$P_{md} = (8.75-1.0985) \times (54.625/2) \times 0.004 = 0.836$ kips @ 8 ft. – 9 in.

DECK SLAB WEIGHT:

At this point in the analysis, the slab is assumed to be 8 in. thick. Slab loading is taken by the floor beams, and then applied to the bottom chord as a series of point loads.

$P_s = 8.75 \times (8/12) \times (58.625/2) \times 0.15 = 25.648$ kips @ 8 ft. – 9 in.

BARRIERS:

$W_b = 0.4$ k/ft

FUTURE WEARING SURFACE:

The future wearing surface weight is also carried by the floor beams to the bottom chord. It is assumed that the future wearing surface is only applied between the barriers.

$P_{ws} = 8.75 \times (43/2) \times 0.02 = 3.76$ kips @ 8 ft. – 9 in.

A RISA model was then created and run to determine the distribution of the dead loading in the system. For all following RISA models, a negative moment value represents a positive bending moment (tension in bottom fibers). A positive axial force equals a compressive force. Stage 1 loading is the effects of steel own weight, floor beams, and metal decking. The loading is resisted by Cross Section 1. *Figure 4.2.1-1* shows the loading. *Figure 4.2.1-2* shows the moment distribution, and *Figure 4.2.1-3* shows the axial force distribution. The maximum deflection due to Stage 1 loading is 1.38 in. and occurs at node 29.

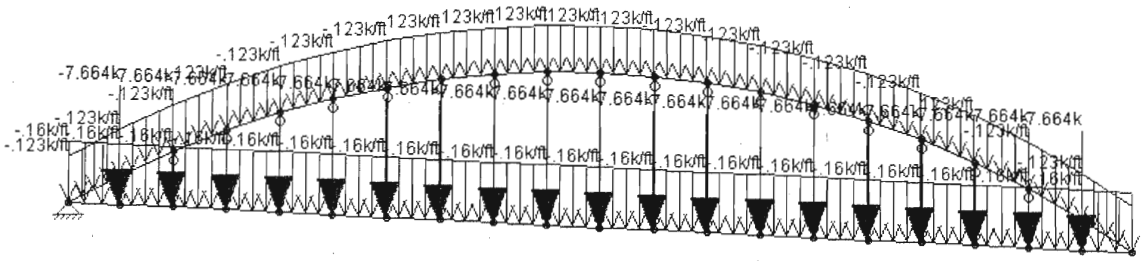

Figure 4.2.1-1 – Stage 1 loading

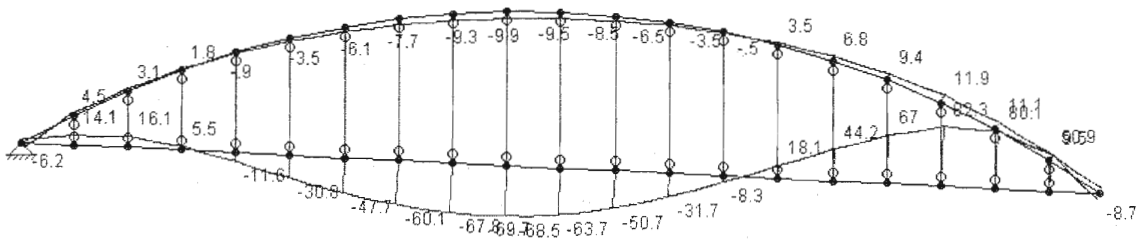

Figure 4.2.1-2 – Moment distribution due to Stage 1 loading.

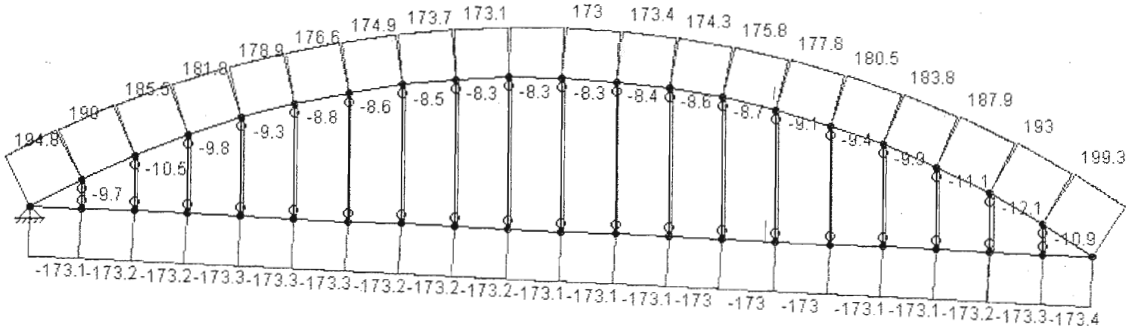

Figure 4.2.1-3 – Axial forces due to Stage 1 loading.

Stage 2 loading includes the added concrete weight of the filled top and bottom chords. The loads are resisted by Cross Section 1, as the concrete in the tubes contributes nothing to the stiffness at this point *Figure 4.2.1-4* shows the loading. *Figure 4.2.1-5* shows the moment distribution, and *Figure 4.2.1-6* shows the axial force distribution. The maximum deflection due to Stage 2 loading is 0.87 in. and occurs at node 29.

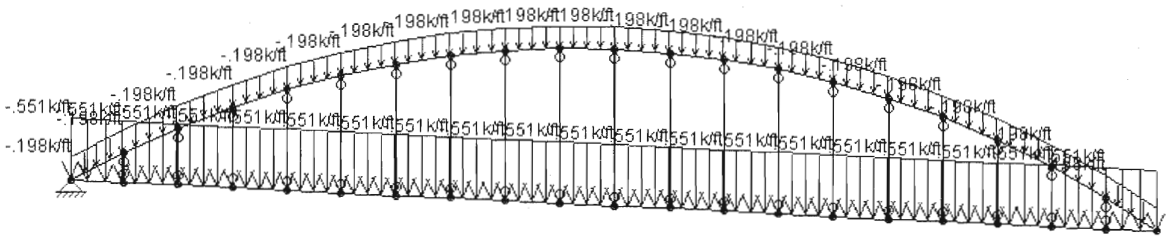

Figure 4.2.1-4 – Stage 2 loading.

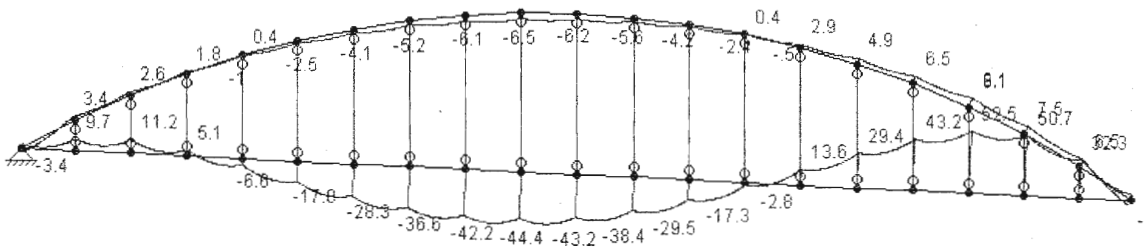

Figure 4.2.1-5 – Moment distribution from Stage 2 loading.

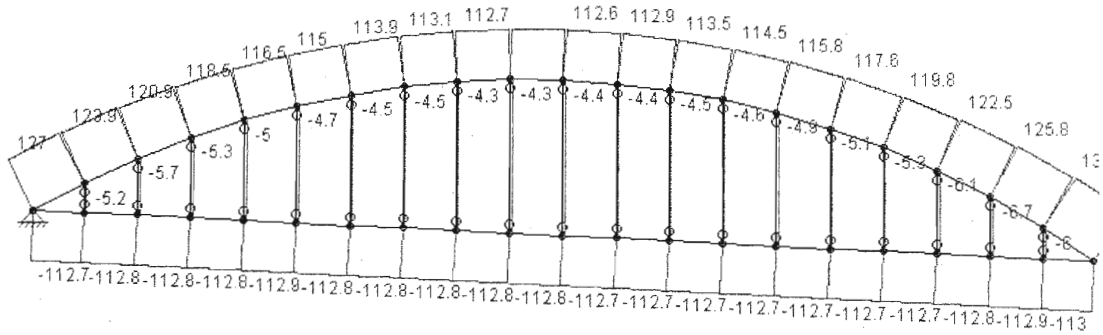

Figure 4.2.1-6 – Axial forces from Stage 2 loading.

Stage 3 loading accounts for the post-tensioning, and is resisted by Section 2. *Figure 4.2.1-7* shows the loading. *Figure 4.2.1-8* shows the moment distribution, and *Figure 4.2.1-9* shows the axial force distribution. The initial post-tensioning axial load = 2 x 19 x 0.217 x 270 x 0.78 x 0.95 = 1650 kips. The Initial Post-tensioning Moment = 1650 (11.6 - 4)/12 = 1045 ft-k. The post tensioning loading was input by releasing the axial force in the hangers.

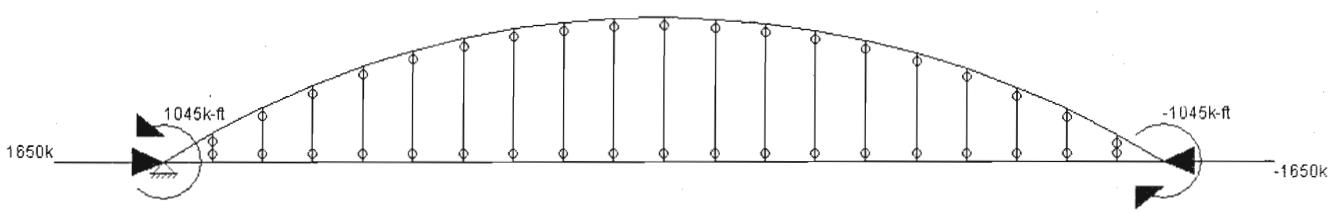

Figure 4.2.1-7 – Loading due to post-tensioning

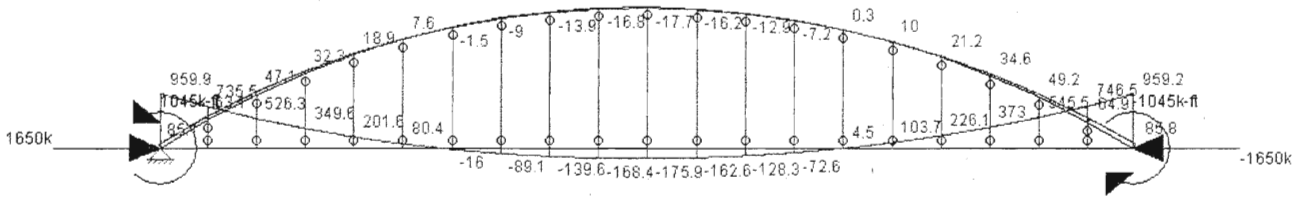

Figure 4.2.1-8 – Moment distribution from post-tensioning

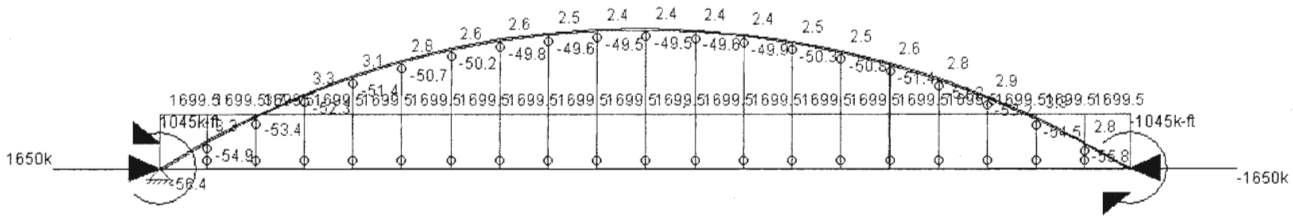

Figure 4.2.1-9 – Axial forces from post-tensioning

Stage 4 loading is the dead weight due to the placement of the deck. Therefore, the section is not yet composite with the deck, and acts as cross section 3. *Figure 4.2.1-10* shows the loading. *Figure 4.2.1-11* shows the moment distribution, and *Figure 4.2.1-12* shows the axial force distribution. The maximum deflection due to Stage 4 loading is 1.69 in. at node 29.

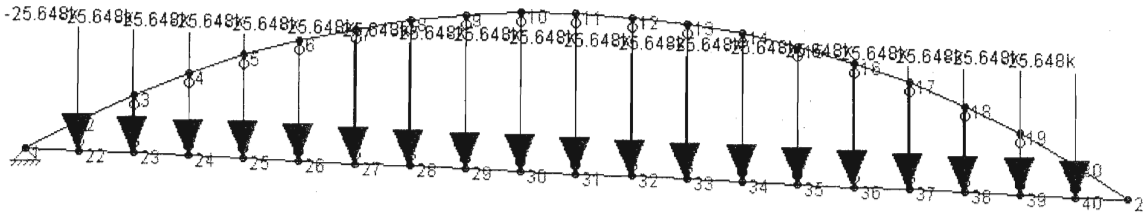

Figure 4.2.1-10 – Loading due to deck weight.

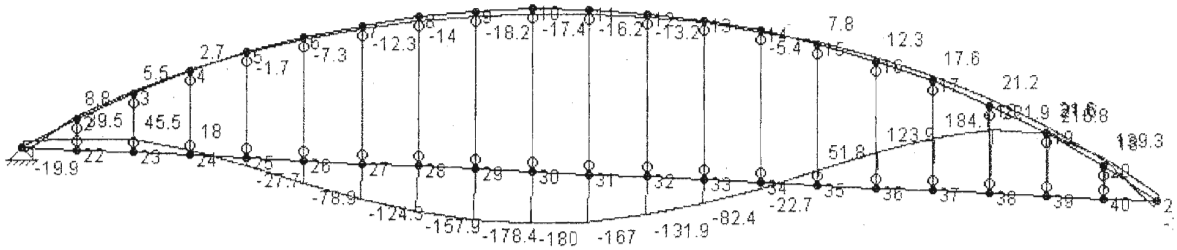

Figure 4.2.1-11 – Moment distribution from deck weight.

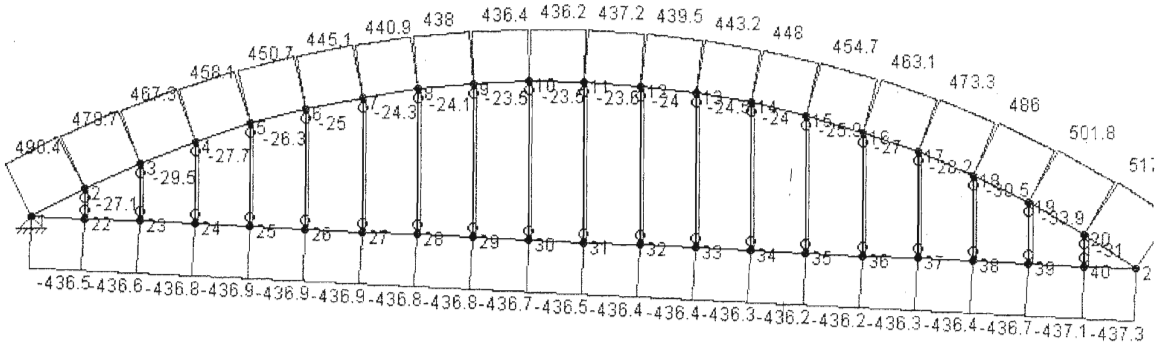

Figure 4.2.1-12 – Axial forces due to deck weight.

Stage 5 loading acts on the composite cross section (Cross Section 4) and consists of the barrier weight. *Figure 4.2.1-13* shows the loading, *Figure 4.2.1-14* shows the moment distribution, and *Figure 4.2.1-15* shows the axial force distribution. The maximum deflection due to Stage 5 loading is 0.139 in. at hanger 30.

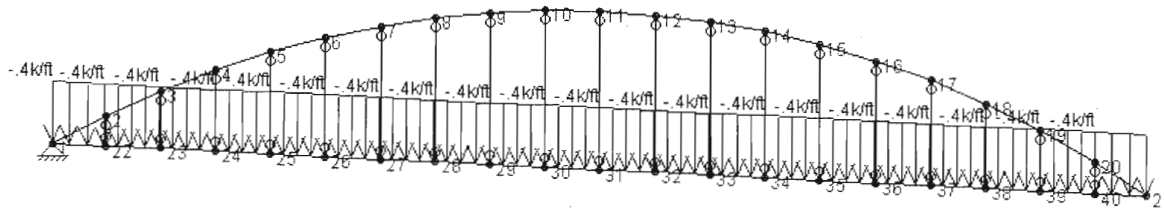

Figure 4.2.1-13 – Loading due to barrier weight.

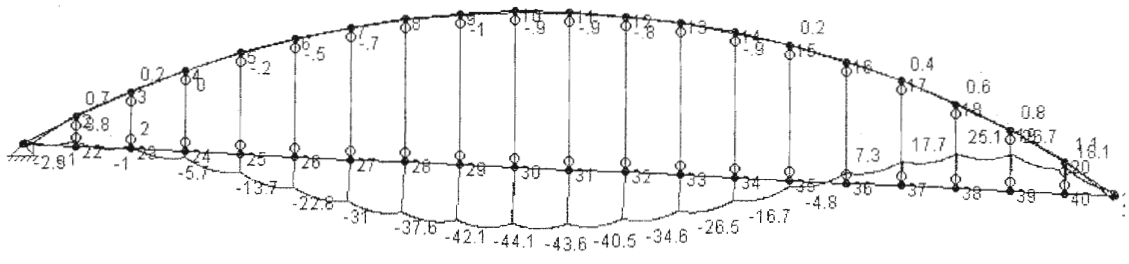

Figure 4.2.1-14 – Moment distribution due to barrier weight.

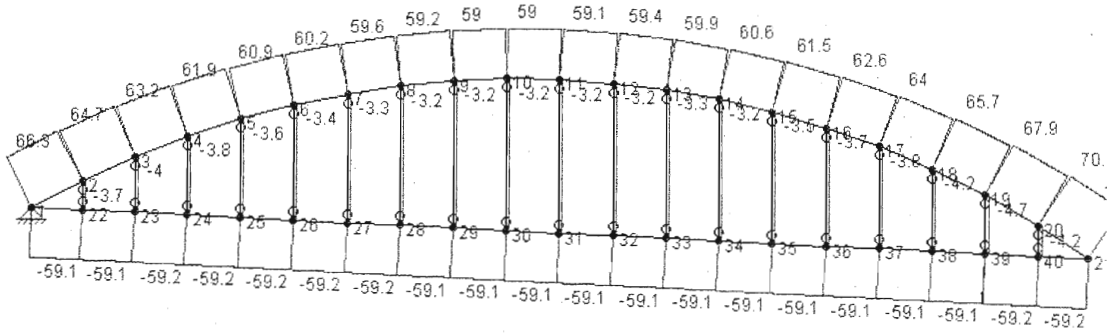

Figure 4.2.1-15 – Axial force distribution due to barrier weight.

Stage 6 loading acts on the composite cross section (Cross Section 4) and consists of the future wearing surface. *Figure 4.2.1-16* shows the loading, *Figure 4.2.1-17* shows the moment distribution, and *Figure 4.2.1-18* shows the axial force distribution. The deflection due to the future wearing surface is negligible.

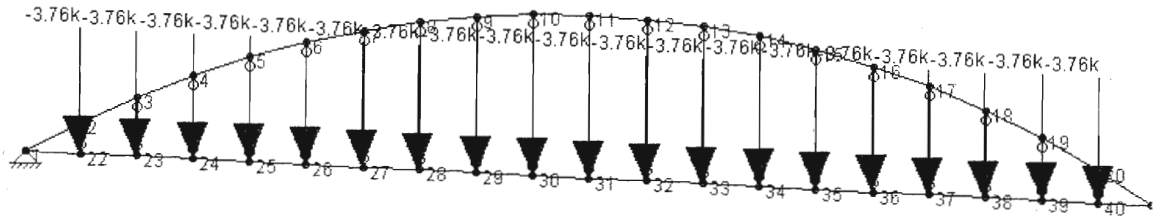

Figure 4.2.1-16 – Loading due to the future wearing surface.

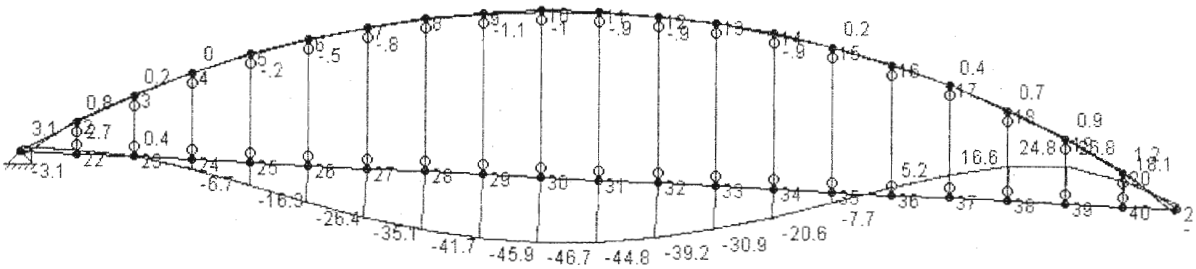

Figure 4.2.1-17 – Moment distribution due to the future wearing surface.

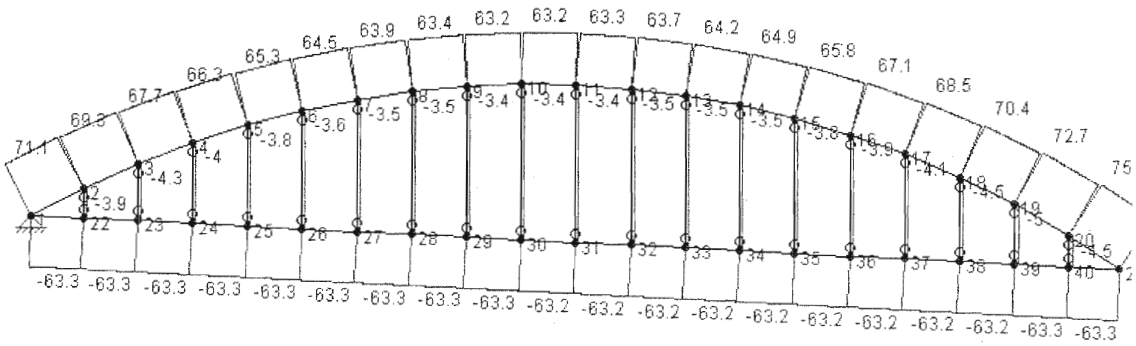

Figure 4.2.1-18 – Axial force due to the future wearing surface.

4.2.2 LIVE LOADING

Stage 7 loading consists of the controlling live load combination specified in the AASHTO Standard Specifications. The required combinations include One HS25 Truck, Two HS25 Trucks, 3 HS25 Trucks, One lane loaded, two lanes loaded, and three lanes loaded. A three HS20 loading is shown below in *Figure 4.2.2-1*, and the three lane loading is shown in *Figure 4.2.2-2*. The HS20 loading is later converted though the load factor to the required HS25 loading. This combination controls the design.

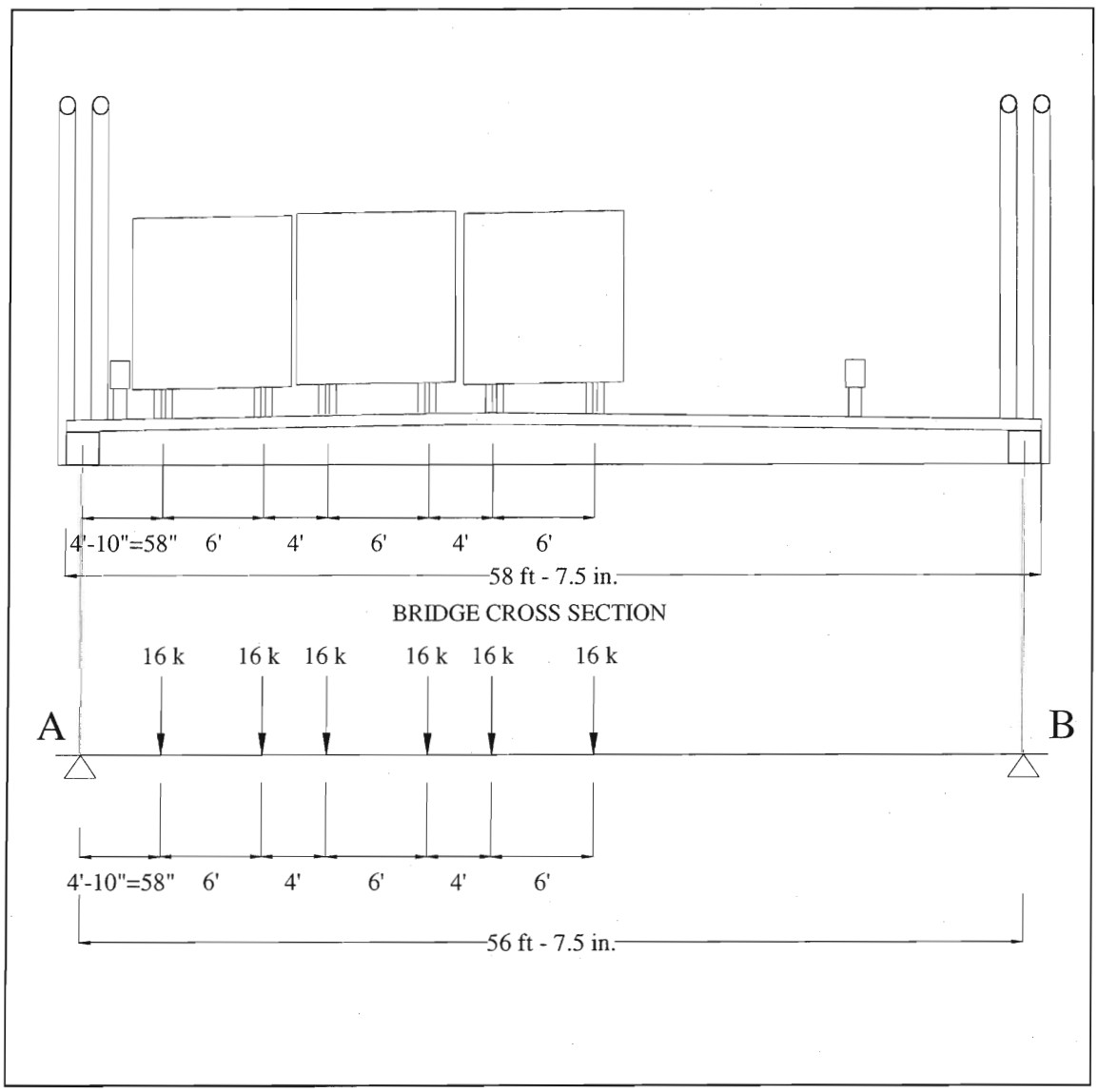

Figure 4.2.2-1 – Three AASHTO Standard HS20 truck loading.

$$R_A = 16x6 - \frac{16X(4.833 + 10.833 + 14.833 + 20.833 + 24.833 + 30.833)}{56.625} = 65.767kips$$

$$\text{Impact factor} = \frac{50}{174 + 125} = 0.167$$

Presence factor = 0.9

Load factor = 65.767 x 1.25 (HS25) x 1.167 x 0.9/32 = 2.7

The 1.25 factor converts the response from the HS20 loading to that of the HS25 loading.

The 32 factor is used to normalize the load factor.

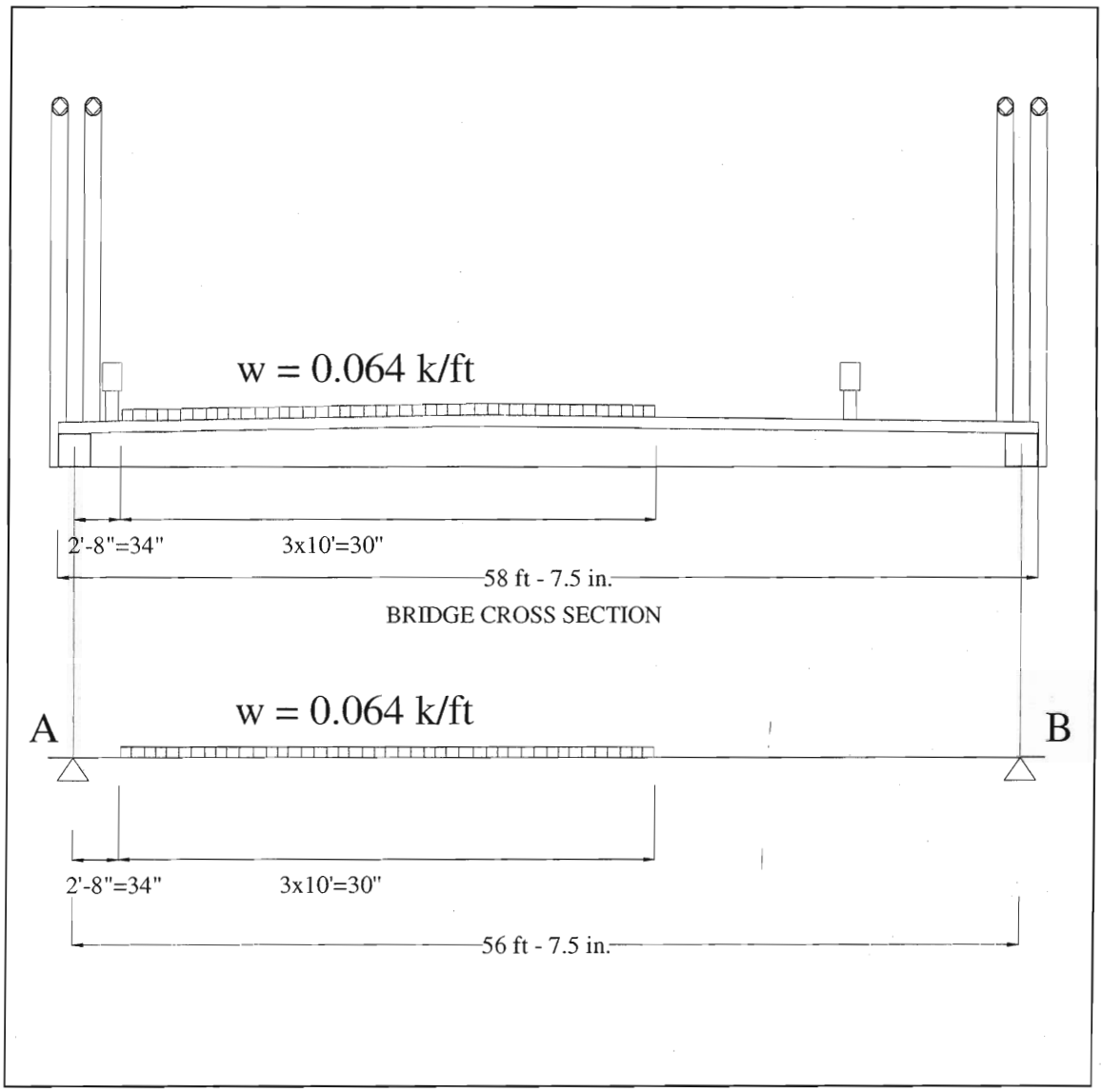

Figure 4.2.2-2 - ASHTO Standard three lane loading.

In the same way as the dead loads, the live loading was analyzed with RISA. The bending moment envelope is shown in *Figure 4.2.2-3* and the axial force envelope is shown in *Figure 4.2.2-4*. The maximum deflection due to live loading is approximately 2.4 in. at node 26. The live load deflection limit in AASHTO Standard is L/800 = 2.61 in. Therefore, the design satisfies live load deflection limits.

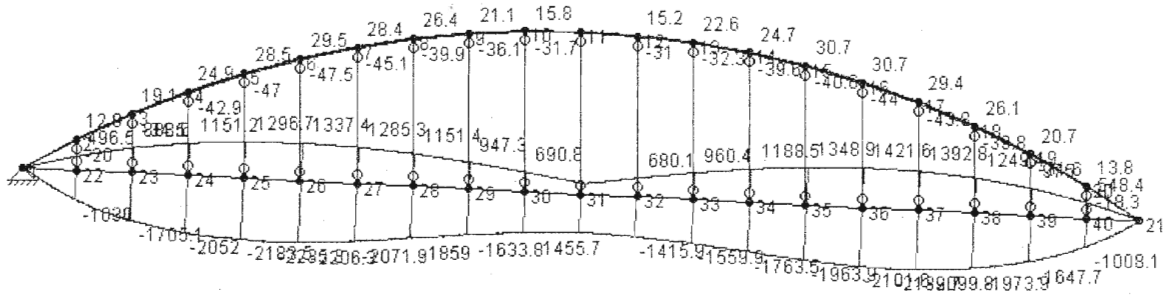

Figure 4.2.2-3 – Moment envelope due to live loading. Three HS20 trucks control the design.

Figure 4.2.2-4 – Axial force envelope due to live loading.

4.2.3 WIND LOADING

The lateral stability of the system was considered with a bi-axial stress analysis. The design loads used are those found in the AASHTO Standard specifications, and are shown in *Figure 4.2.3-1*. A 3D model was developed to determine the maximum bending moments and axial forces in the arch as it will be shown later in sections 4 and 9 and Appendix C. The maximum fiber stresses accounted for the axial load and the bending moments in both directions. The maximum fiber stresses were found to be adequately below allowable values.

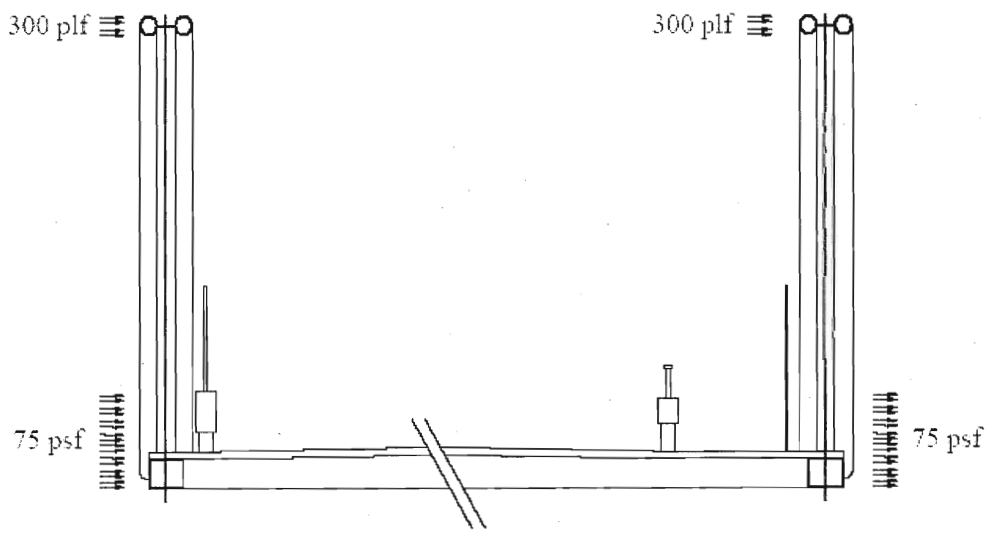

Figure 4.2.3-1 – Design loads used for the lateral stability analysis.

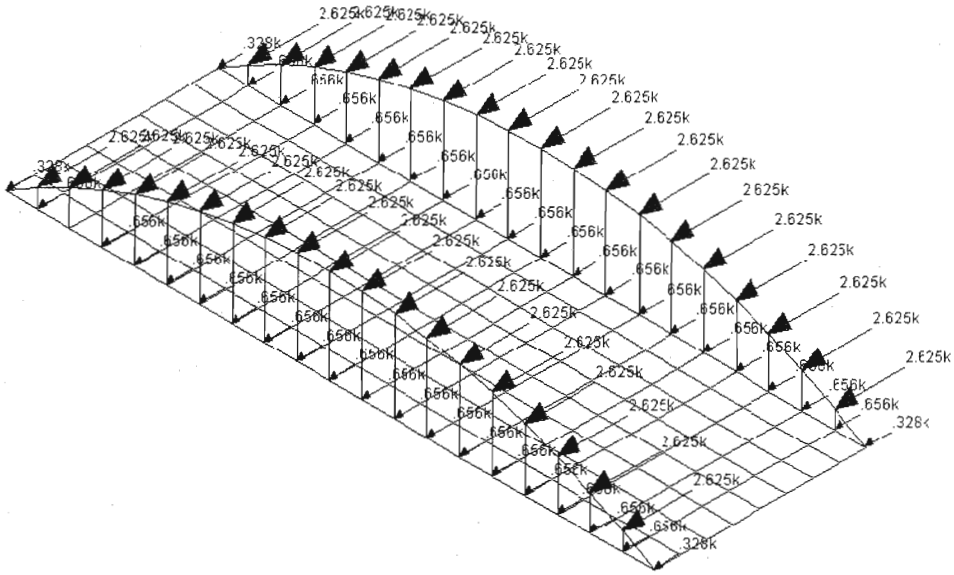

Figure 4.2.3-2 – RISA 3D model used for bi-axial stress analysis.

4.3 ELEMENT CAPACITY

Both the bottom and top chords sustain axial and bending loads. Therefore, the only way to determine the adequacy of the section is by developing axial-moment interaction diagrams for each of the main components.

The interaction diagrams are based on the strength design method utilizing strain compatibility. This method computes the ultimate capacity of a section by using established ultimate values for strain and a linear strain distribution.

After the interaction diagram showing the element capacity is developed, the values are reduced by the appropriate strength reduction factor. The maximum axial and bending load combinations on the actual bridge are factored and then plotted on the diagram. As

long as the loading point falls within the area enclosed by the interaction diagram the section is considered safe.

4.3.1 BOTTOM CHORD

An interaction diagram was developed for both the positive and negative moment cases. The load combination used to plot the loading point was: $1.25M_{DL} + M_{SEC} + 1.75M_{LL}$. The maximum positive moment combination was 5305.8 k-ft at node 27. The maximum negative moment combination was -2273.7 ft-k at node 38. The axial loads on the section were almost equal at each node. The factored axial load combination was 1507.1 k tension. The axial load combination was almost constant at each node, and used the factored combination $1.25P_{DL} + 1.75P_{LL}$.

Both the negative and positive loading points were safely within the interaction diagrams. For the positive moment, the live load factor could be increased to 3.17 before reaching the sections capacity. For the negative moment loading, the live load factor could be increased to 2.56 before reaching the capacity of the section. *Figure 4.3.1-1* shows the positive and the negative moment interaction diagram. The coordinated of the interaction diagram is shown in Appendix C.

An important point to note is that the following interaction diagrams are exceedingly conservative. This is due in part to a disregard of the increase in ultimate strain and ultimate stress that results from confinement of the concrete by the steel sections. Research suggests that incremental strength gain due to confinement can be expressed as

4.1 times the lateral confinement pressure [Ref. 25]. The effect of confinement in rectangular sections is less developed than circular sections. There is ongoing research exploring the effect confinement has on concrete [Ref. 32].

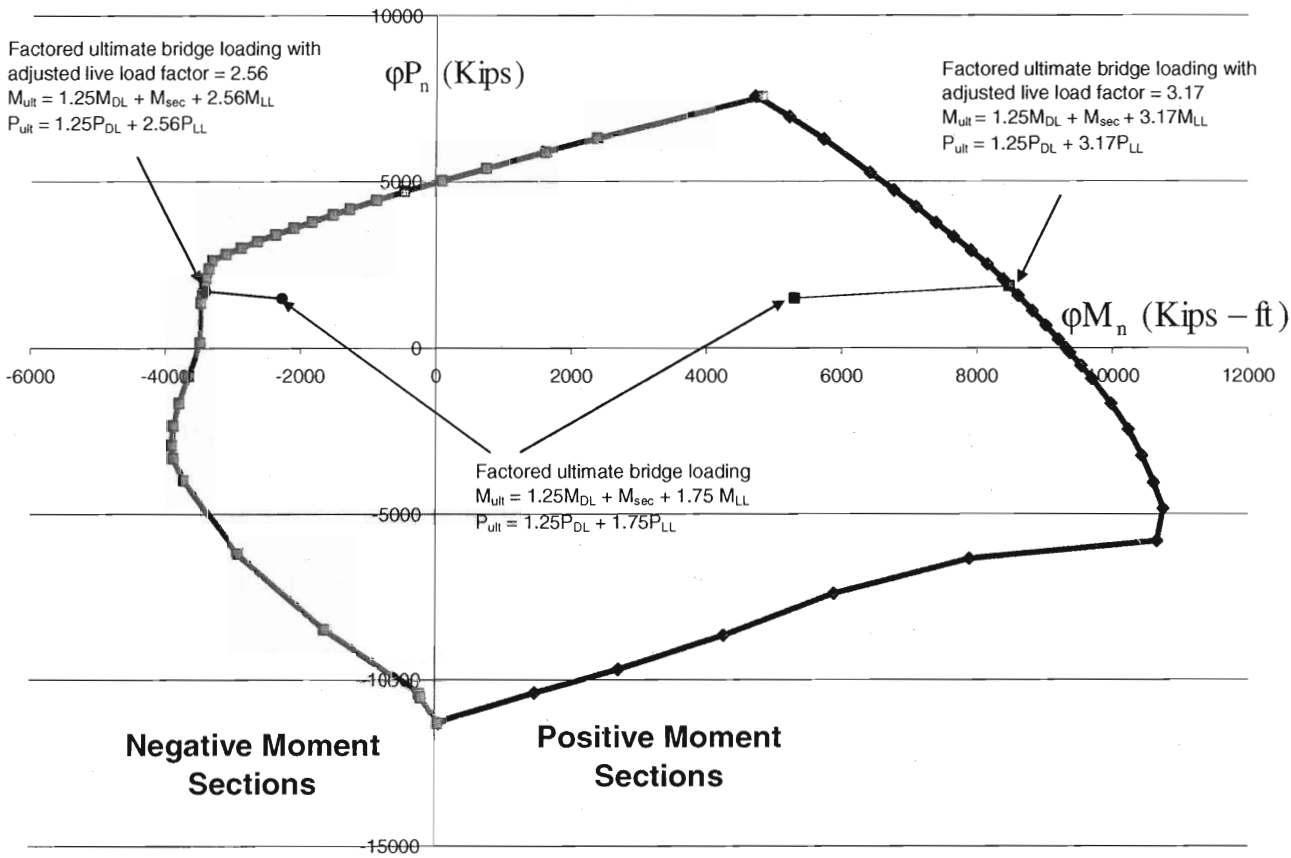

Figure 4.3.1-1 Bottom chord positive and negative moment interaction diagram..

4.3.2 TOP CHORD

In the same way as the bottom chord, interaction diagrams were developed for the top chord loading. The top chord is a symmetric section, so positive and negative moments have the same effect. Unlike the bottom chord, the effects of confinement are considered [Ref. 32].

The factored load combination used for the top chord is $1.25M_{DL} + M_{PT} + 1.75M_{LL}$. The maximum factored moment in the top chord is 67.8 k-ft in node 19. The axial force is effectively constant at each node. The factored maximum axial force in the top chord is 861.6 k. The top chord interaction diagram is shown in *Figure 4.3.2-1.* When plotted on the interaction diagram for the top chord, the loading is safely within the diagram. The live load factor could be increased from 1.75 to 5.20 before the top chord fails.

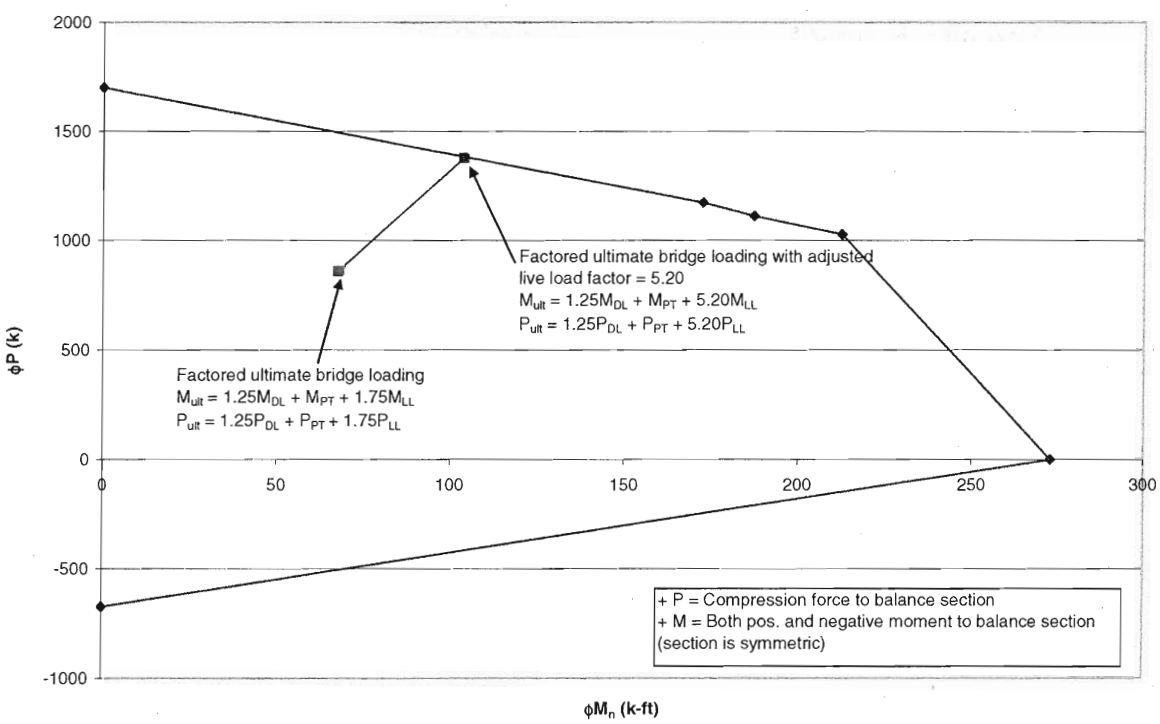

Figure 4.3.2-1 - Top chord interaction diagram.

4.3.3 HANGER CONNECTION

The maximum force in the threaded rod hangers resulting from the dead load stages (Stages 1 through 6) is 62.84 kips. The maximum force in the threaded rod hangers resulting from the live load case is = 19.71 kips at member 58. Therefore, the loading cycles between approximately 63 and 83 kips. The capacity of this connection was verified primarily through testing in the PKI Structures Lab, discussed in Section 6. The specimen was tested in fatigue and in pure tension until failure. The ultimate load recorded was 385 k, providing a capacity to demand ratio of 4.6.

4.3.4 CROSS BEAM RATING

The cross-beam was calculated as a 56 ft-7.5 in. simply supported beam. Table 3.3.4-1 shows the dead loads and the corresponding bending moments of the cross-beam.

Table 4.3.4-1 - Dead loads and bending moments

	Loads (kip/ft)	Mid-Span Moments (k-ft)
Steel Self-Weight (k/ft)	0.250	100.20
Metal Decking	0.035	14.03
Deck Slab	0.875	350.70
Future Wearing Surface	0.175	70.14

Three HS20 loadings are shown below in Figure 4.4-1. The HS20 loading was later converted though the load factor to the required HS25 loading. An impact factor of 33% and a presence factor of 0.9 were used.

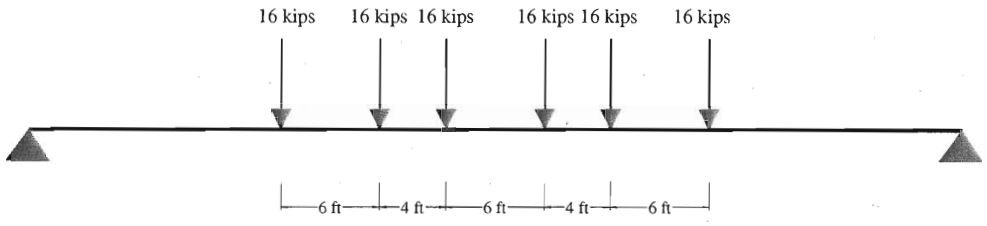

Figure 4.3.4-1 – Three HS20 Loadings of the cross beam

The calculated live load moment was 1491 k-ft. The factored bending moment was calculated as follows:

1.25 (100.2+14.03+350.70) + 1.5(70)+1.75 (1491)= 3295.41 k-ft.

The factored bending moment due to dead loads only was calculated as follows:

1.25 (100.2+14.03+350.70) + 1.5(70) = 686.16 k-ft..

The cross-section consisted of W24X 250 and a 7.5 in. deck slab. A 3 in. haunch was assumed between the I-beam and the deck slab. The flange effective width was taken as the spacing between the cross-beams which was equal to 8ft-9in. This was less than quarter the span and almost equal to slab thickness times 12 added to the beam top flange width. Based on the cross-section properties and full composite action, the plastic neutral axis (PNA) was in the I-beam top flange. The nominal moment capacity was calculated to be 5,507.6 k-ft, and 4,681.5 k-ft. when accounting for the strength reduction factors. Consequently, the strength of the cross-beams was larger than the factored moment. The cross-beam rating capacity was calculated using the following equation.

$$\text{Rating} = \frac{\phi M_n - M_u(\textit{due to deadLoads})}{M_{LL}} = \frac{4{,}681.5 - 686.16}{1491} = 2.680$$

4.4 COMPOSITE ACTION CALCULATIONS

4.4.1 SHEAR STUDS

The whole deck was assumed to act composite with the bottom chord for the purpose of calculating shear connectors on the bottom chord. Section 3 has a complete discussion of this decision. *Figure 4.4.1-1* shows the dimensions used in this calculation. The shear force due to the final loading stage is considered. The main equation used is the standard shear flow equation, but using the cracked section moment of inertia [Ref. 16].

$$v_b = \frac{VQ}{I_{cr}} \times \left(12 \frac{in}{ft}\right)$$

The following calculations are done using 1 ¼ in. diameter studs.

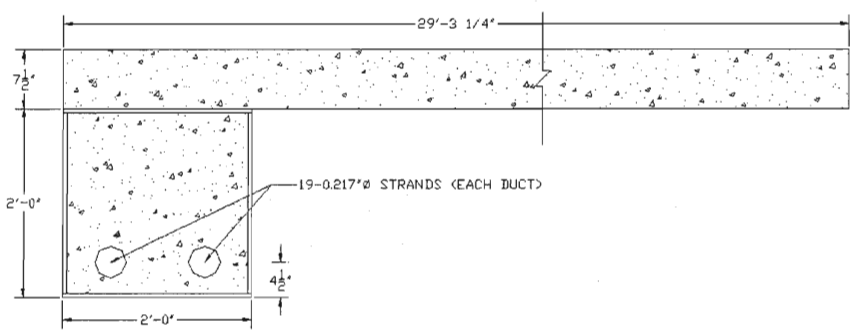

Figure 4.4.1-1 Cross section used for the composite action calculation.

b (in) =	351.75		
kd (in) =	5.90		
$A_{comp}(in^2)$	274.48	SE	(Steel Equivalent)
Q (in^3) =	809.72	SE	
I_{cr} (in^4)=	19812.01	SE	
γ =	1.75		

Stud size used (f") =	1.250
f'_{ci} (ksi) =	4
Strength per Stud, Q_n (k) =	71

Table 4.4.1-1 Shear studs calculations

node	x (in)	x(ft)	V (k)	γv_b (k/ft)	studs/ft
0	0	0.00	158	135.61	2
1	384	32.00	131	112.43	2
2	768	64.00	111	95.27	2
3	1152	96.00	99	84.97	2
4	1536	128.00	88	75.53	2
5	1920	160.00	83	71.24	2
6	2304	192.00	91	78.10	2
7	2688	224.00	96	82.39	2
8	3072	256.00	98	84.11	2
9	3456	288.00	98	84.11	2
10	3840	320.00	94	80.68	2
11	4224	352.00	94	80.68	2
12	4608	384.00	96	82.39	2
13	4992	416.00	94	80.68	2
14	5376	448.00	90	77.24	2
15	5760	480.00	84	72.09	2
16	6144	512.00	89	76.39	2
17	6528	544.00	88	75.53	2
18	6912	576.00	98	84.11	2
19	7296	608.00	109	93.55	2
20	7680	640.00	129	110.72	2
21	8064	672.00	157	134.75	2

The strength of each 1 ¼ in. diameter stud is taken to be double that of the ⅞ in. stud. This is a conservative assumption [Ref. 4]. γ is a conservative load factor. With ⅞ in. diameter studs, the spacing goes up to 4 studs per foot through node 1, and then to 3 studs per foot.

4.4.2 INTERACTION BETWEEN TUBE AND ENCASED CONCRETE

In order to transfer shear force between the tube concrete and the surrounding steel tube, some type of connector must be used. The bottom chord uses the corner braces for this purpose. These braces are spaced at 2 ft. intervals along the length of the bottom chord. The following analysis determines if the braces are sufficient, and what size of weld is necessary.

Cross section three is used for the analysis. The section properties are repeated here:

Area = 154.16 in.^{2} Steel Equivalent

I_z = 9127.36 in.^{4} Steel Equivalent

y_b = 11.6 in. Steel Equivalent

Next, the maximum moment difference was found for all loading cases. This moment difference is transferred over 8 ft. - 3 in.

M_1 = 960 k-ft

M_2 = 735.5 k-ft

The longitudinal forces from bending are represented in the following Figure:

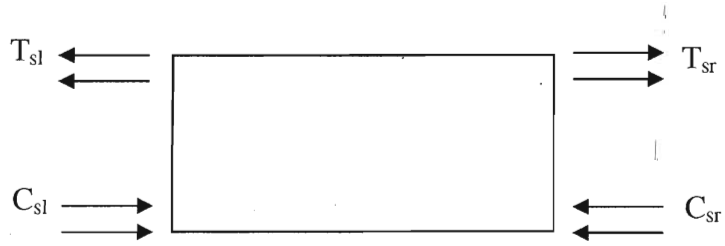

Figure 4.4.2-1 longitudinal forces calculation

Where T_{sl} = Tension Steel Left

C_{cr} = Compression Concrete Right

The area each force acts upon is then computed. For example, T_{sl} (Tension Steel Left) acts on two areas: 1) A rectangle across the top of the box, and 2) rectangles extending from the neutral axis up to the bottom of the previously mentioned rectangle. Therefore, the areas acted upon by T_{sl} are:

1) 24" * 0.5" = 12 in^2
2) (24" – 11.6" – 0.5") * 0.5" * 2 = 11.9 in^2

The next step is to calculate the average stress acting on each area. The average stress on each T_{sl} area is:

1) (960 k-ft) * (12"/ft) * (23.75" – 11.6") / (9127.36 in^4) = 15.34 ksi
2) (960 k-ft) * (12"/ft) * ((24" – 11.6" – 0.5")/2) / (9127.36 in^4) = 7.51 ksi

The force on each area (stress x area) is calculated as:

1) (24" * 0.5") * (15.34 ksi) = 184.02 k
2) ((24" – 11.6" – 0.5") * 0.5" * 2) * (7.51 ksi) = 89.36 k

The following table shows the results for each force:

Table 4.4.2-1 Longitudinal forces calculations

Location	Area (in^2)	Stress (ksi)	Force (k)
T_{sl}	12.00	15.34	184.02
	11.90	7.51	89.36
T_{cl}	50.97	7.51	382.74
C_{cl}	47.54	7.01	333.02
C_{sl}	12.00	14.33	171.90
	11.10	7.01	77.76
T_{sr}	12.00	11.74	140.89
	11.90	5.75	68.42
T_{cr}	50.97	5.75	293.04
C_{cr}	47.54	5.36	254.96
C_{sr}	12.00	10.97	131.62
	11.10	5.36	59.53

To obtain the shear force resisted by the plane between the concrete and the steel, the difference between the forces carried by each material is calculated:

$$(T_{sr} - T_{sl}) - (T_{cr} - T_{cl}) = (140.89 + 68.42 - 184.02 - 89.36) - (293.04 - 382.74)$$

$$= 25.63 \text{ k}$$

It is then necessary to calculate the area of the weld resisting this force. The braces will be located every 2 ft, but were originally designed at every 4 ft. Therefore, in design, there are two sets of braces within every 99 in. 99 in. is used because it is the distance over which the considered moment is transferred. The brace is 2 in. wide and 3/8 in. thick. Because the tops of the braces are not welded to the top plate of the girder, the total length of resisting weld every 99 in. is (2" + 2" + 2" + 2") x 2 = 16 in.

The eccentricity of the weld was taken as 0 because there was no information on the location of the top connectors. The researchers recommend that the braces be placed as high as possible. Ignoring the eccentricity is conservative in this calculation.

The weld stress was then calculated by dividing the shear force by the area of the weld (1/4" weld): 25.63 k / (0.25" x 16") = 6.41 ksi. This is compared to the shear strength of the weld: 0.60 x 50 ksi = 30 ksi > 6.41 ksi O.K.

SECTION 5: FULL SCALE SPECIMEN PRODUCTION

5.1 INTRODUCTION

Because the Ravenna Arch Bridge is such a unique project, there is much that can be learned from the production and testing of full scale specimens. By creating these specimens, any difficulties in production can be noted, and then planned for in the actual bridge fabrication. Additionally, the bottom chord specimen and hanger connection specimen were tested in the PKI Structures Lab (see Section 6).

5.2 BOTTOM CHORD FABRICATION

5.2.1 STEEL FABRICATION AND HARDWARE PLACEMENT

Capital Contractors in Lincoln, Nebraska, fabricated a full scale specimen of the bottom chord. UNL researchers were on-hand to learn from the experience. *Figure 5.2.1-1* shows the bottom chord in the middle of fabrication. This picture shows three of the four plates that make up the bottom chord tube walls of the 40 ft. specimen already welded together. The end plates are already in place. The top plate has been left off to allow for the post-tensioning hardware to be installed. The tube is 24" x 24", and the plates are ½" thick.

The two holes in each end plate are 6 ½" in diameter to fit the post-tensioning anchorage plate. *Figure 5.2.1-2* shows the holes in the end plate. At this point, the smaller hole for grouting access had not been cut in the end plate, so that an exact fit could be made when the anchorage is first placed. The post-tensioning system was purchased from DSF. The 19-0.6" strand system was used and is shown in *Figures 5.2.1-3 and 5.2.1-4* prior to

installation. The components include the wedge plate, wedges, grouting accessories, multiplane anchor (anchorage plates), the PE Trumpet, the duct coupler, and the duct. The wedge plate, wedges, and strands are to be placed after shipment to the PKI Structures Lab.

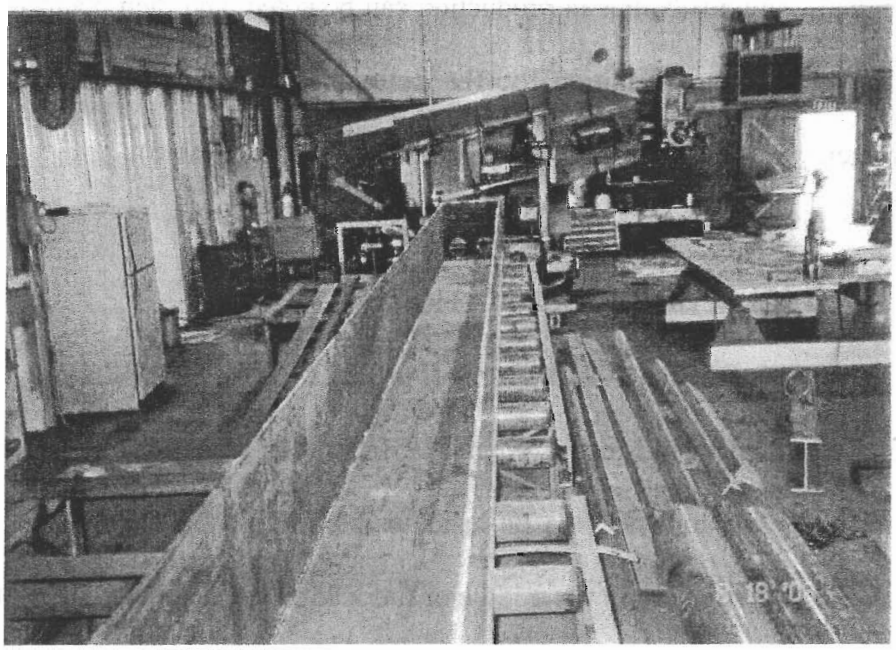

Figure 5.2.1-1 - The bottom chord in fabrication.

The end plate holes were placed so that the center of the strand group was as low as possible. It was determined that 4" from the bottom was as low as the hardware would allow. In order to achieve a more effective depth, it was necessary to modify the anchorage plates. *Figure 5.2.1-5* shows the anchorage plates after modification. Approximately ½ in. was cut from the anchorage. This gives 3 in. of concrete cover below the duct. A 2 in. cover is preferable. To achieve this in the actual bridge fabrication, there are two different possibilities. The anchors could, perhaps, be trimmed further. The other possible solution is to divert the post tensioning ducts. In this way, the

anchorage plates could be left without modification, and the prestressing force could be placed at the optimum depth.

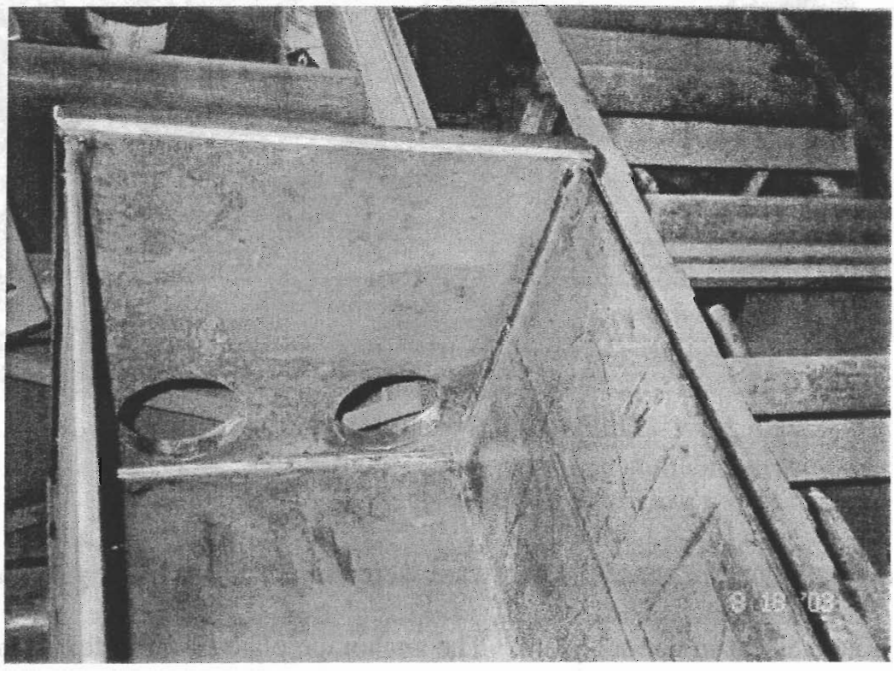

Figure 4.2.1-2 – Bottom chord end plate.

Figure 5.2.1-3 – Post tensioning anchor plates before modification.

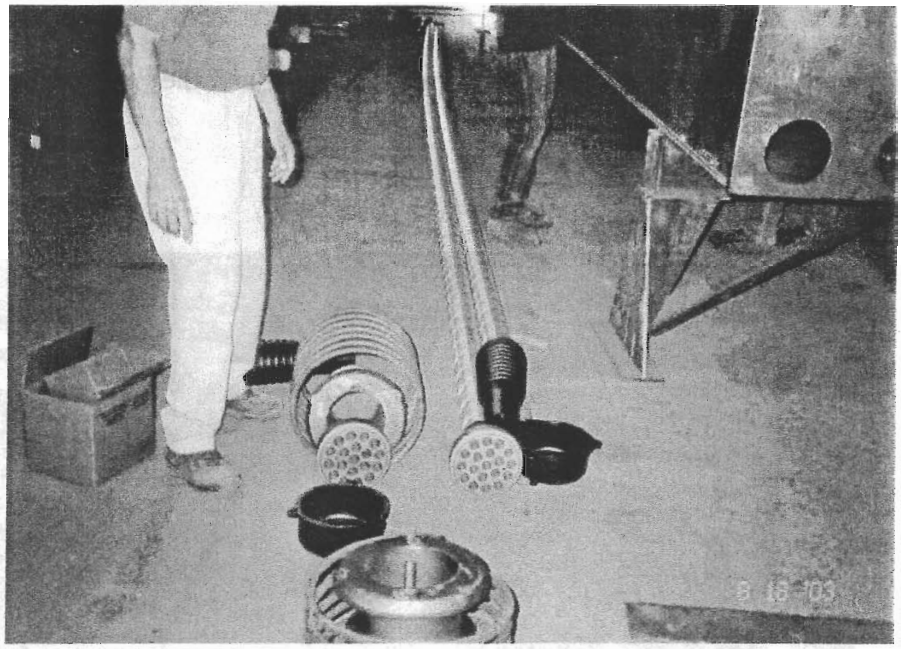

Figure 5.2.1-4 – DSF's 19-0.6" diameter post tensioning hardware, before installation.

The internal components of the hardware were then installed in the tube, and the smaller grout hole was cut in the end plate. The anchorage plates are welded to the inside of the tube. A view of the internal end components can be seen in *Figure 5.2.1-6* and the end plate in *Figure 5.2.1-7*. *Figure 5.2.1-8* shows the chairs used to set the duct in the tube. The chairs are secured to the tube with liquid nails and then tied to the duct, and are spaced at 3 ft.

Researchers were concerned that when the concrete is poured in the tube, the ducts will be displaced upward by buoyant forces. To eliminate the concern, #4 bars were cut and hammered in place directly above the duct at 3 ft. on center. This is shown in *Figure 5.2.1-9*.

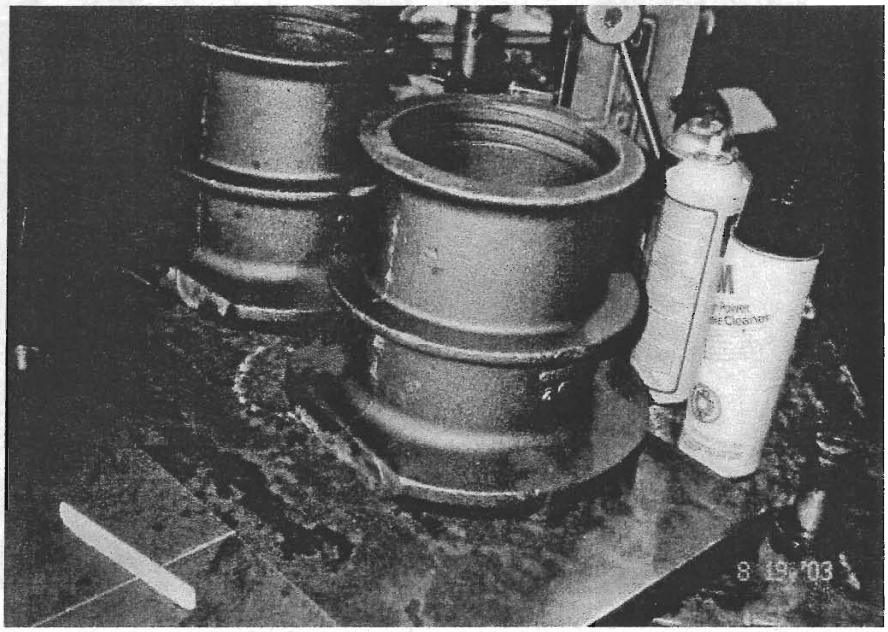

Figure 5.2.1-5 – Post tensioning anchor plates after the edges are trimmed.

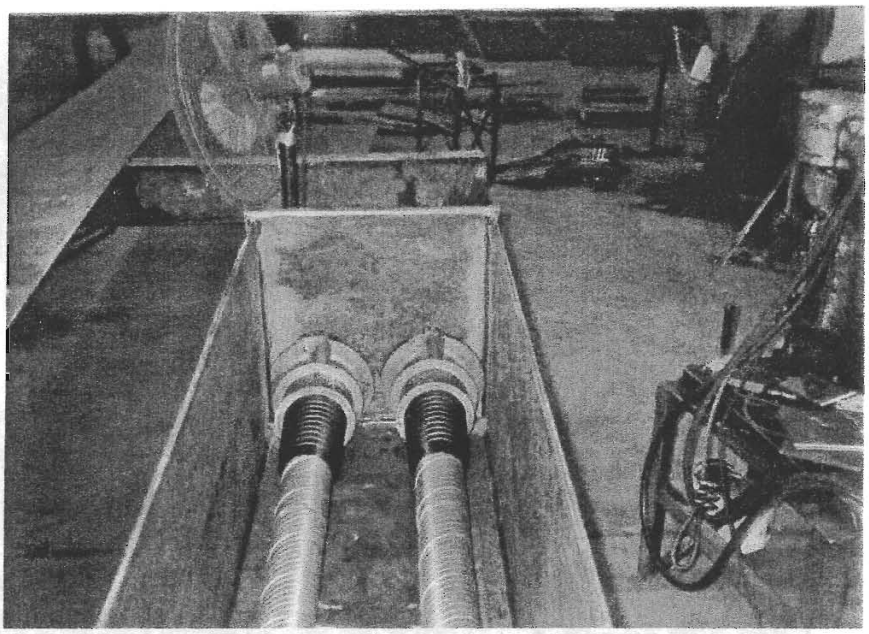

Figure 5.2.1-6 – Installed internal post tensioning hardware.

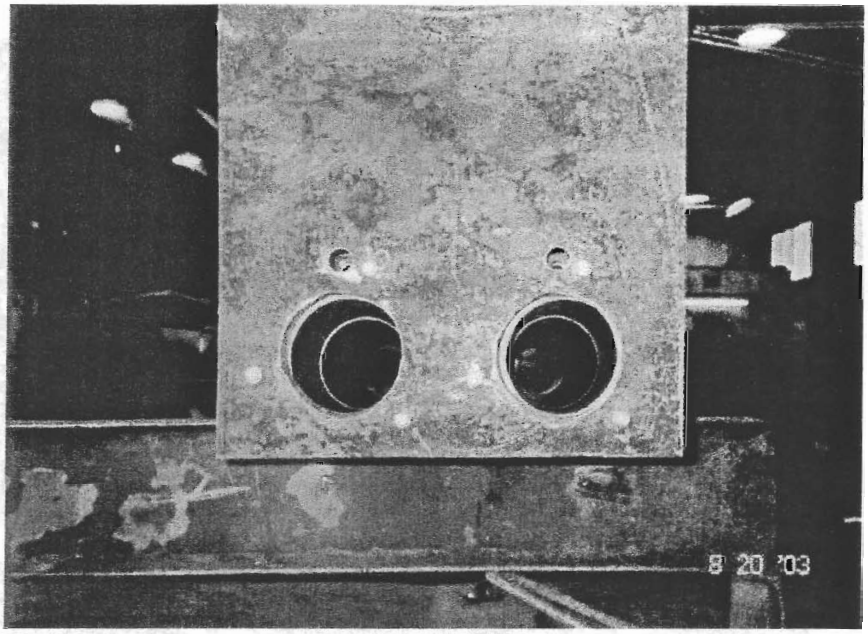

Figure 5.2.1-7– End plate with grouting hole.

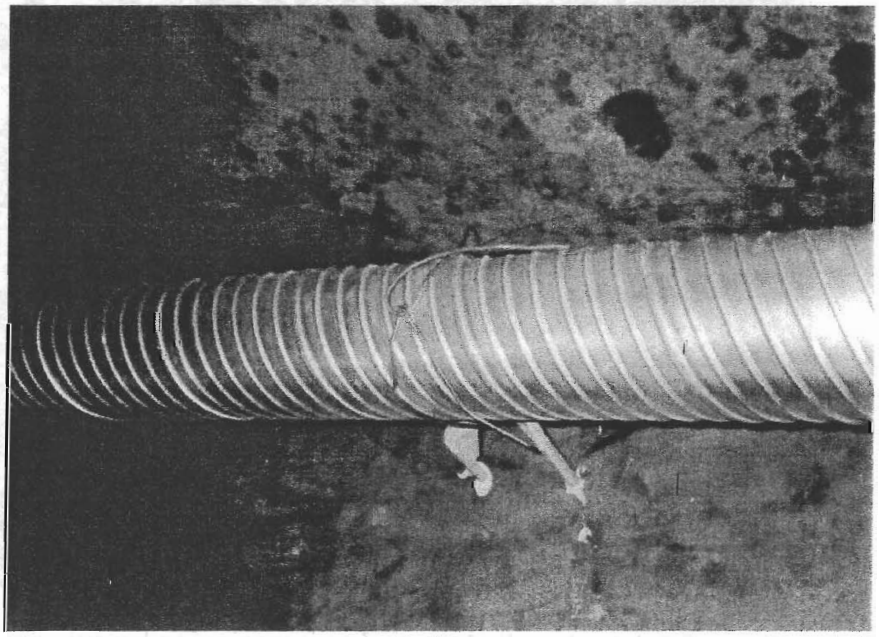

Figure 5.2.1-8 – Chair supporting post tensioning duct.

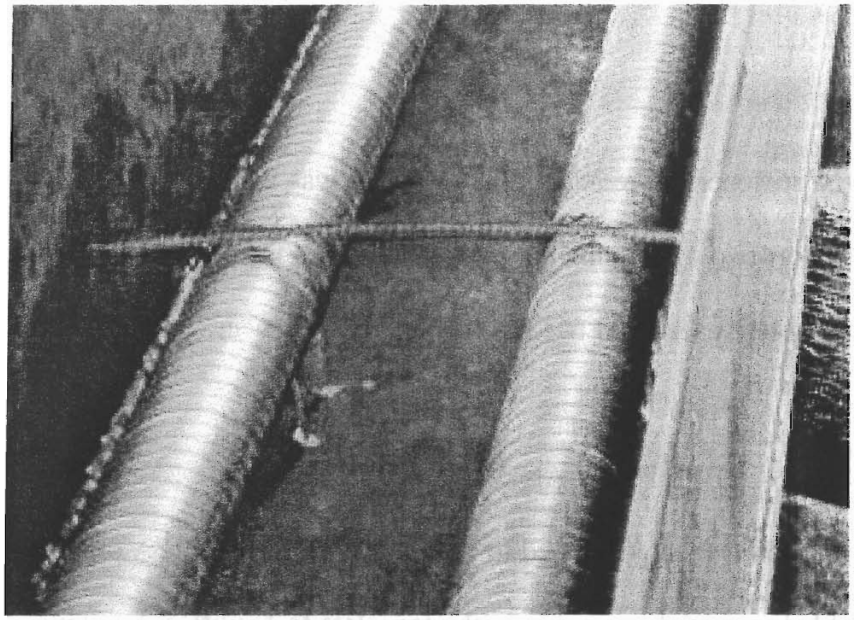

Figure 5.2.1-9 – #4 bar holding down the ducts.

It was suggested that in the real bottom chord, corner stiffeners be provided to keep the wall plates perpendicular to each other. However, in the 40 ft. production specimen, this was not necessary and the corner plates were not provided. The stiffeners also aided in achieving composite action between the concrete and the surrounding steel. The only concern was to make sure there was sufficient room for the concrete to freely flow. The steel corner braces are 2 in. x 2 in., and allow for 1 in. clearance between the stiffener and the corner of the box.

Additionally, in order to solve the aforementioned challenge of keeping the ducts in place, a note in the construction drawings specifies that "the ducts shall be fastened to the tie beams at a maximum interval of 2 ft. to prevent displacement of the ducts during concrete casting."

After the stiffeners were added, the top plate was welded; and the box was closed. The top plate has two 4 in. diameter holes at each end for pumping concrete, and twelve 1 in. diameter holes spaced at 3 ft. to for venting and to ensure complete filling of the tube.

5.2.2 CONCRETE POUR AND POST-TENSIONING

The specimen was then shipped to the PKI Structures Lab. A pipe fitting was purchased and welded around the opening in the top plate to facilitate the pumping of the concrete. As the pumped concrete reached each hole, it was plugged. Using the procedure, designers can be sure the tube is completely filled.

The concrete mix used was a self-consolidating mix with a spread test of 30" and a 28 day strength of approximately 7000 psi. Appendix A contains the mix design. As indicated by the 30" spread, the mix was easy to pump, and self-leveled as the tube filled. The spread was measured using the Inverted Slump Flow Test Method [Ref. 12]. Unfortunately, the test mix took several days to gain any significant strength.. Researchers decided it would best to wait until the mix reached 4000 psi to begin post-tensioning. Because the original test mix did not gain strength very fast, post-tensioning was delayed.

Therefore, researchers suggest a variation to the production test mix. This mix can be found in Appendix B. The suggested mix achieved a comparable spread, a 1 day strength

of 2,300 psi, and a 7 day strength of 8000 psi. The aggregate used in the recommended mix includes NDOR's 47B Sand-Gravel, C33 Sand, and ½" BRS Limestone.

Because of a steel shortage, it was not possible for researchers to purchase the needed 38 strands. Instead, only 20 strands (10 per duct), or just over half of the design, were placed in the tube. First, the wedge plate was welded onto the end plate. Then each strand was labeled on both ends before being strung through the tube. This allowed researchers to be confident that the same strand was in the same hole of the wedge plate at each end. A wedge grip was then placed over each strand and secured in the wedge plate.

Each strand was tensioned using a mono-strand jack. *Figure 5.2.2-1* shows a strand being tensioned. The small hydraulic pump can be seen on the ground, and the jack is straddling a strand. Using a table, the required tension was converted to a pump pressure. Each strand was initially tensioned to 202.5 ksi, or 44 kips. After all the strands were loaded, "lift off" tests were preformed to determine the true level of prestress, after initial losses. By doing several of these, it was determined that each strand was tensioned to approximately 37 kips, or 170.5 ksi. This is approximately a 16% loss.

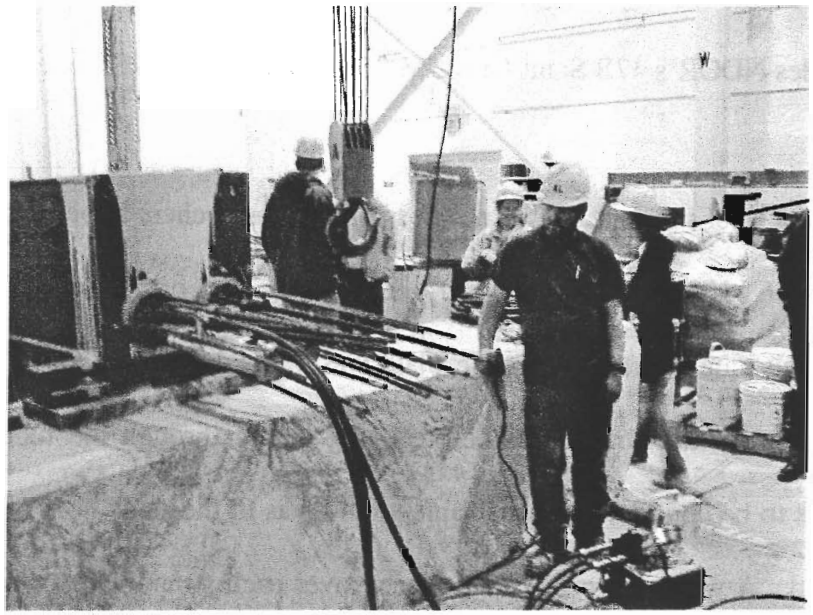

Figure 5.2.2-1 – Tensioning the strands.

In order to use the mono-strand jack in what is typically thought of as a multi-strand jack application, a special piece of hardware had to be fabricated. This small steel tube, shown in *Figure 5.2.2-2*, was placed around the head of the jack, and was used to bear against the wedge plate, instead of the wedges themselves.

Figure 5.2.2-2 – Using the special hardware.

Each strand group was tensioned symmetrically, working from the outside in. Several people worked together to balance the jack in place until the load begin to apply.

Following post-tensioning, the duct was grouted. Shrinkage data for the grout can be found in Appendix C. A very simple grout consisting of Type I cement (94 lb. bag) and water (5 gallon) was used. A standard 2 in. diameter pipe fitting was purchased and welded around each grout access hole.

As was previously mentioned, only 10 strands were used in each duct, although each anchor plate is designed for 19. Therefore, a toggle bolt and washer were used in each empty hole to block the grout. *Figure 5.2.2-3* shows this arrangement, including the added pipe fitting discussed above. The bolt and washer did not hold the pressure completely, requiring a tub to be placed to collect the excess grout.

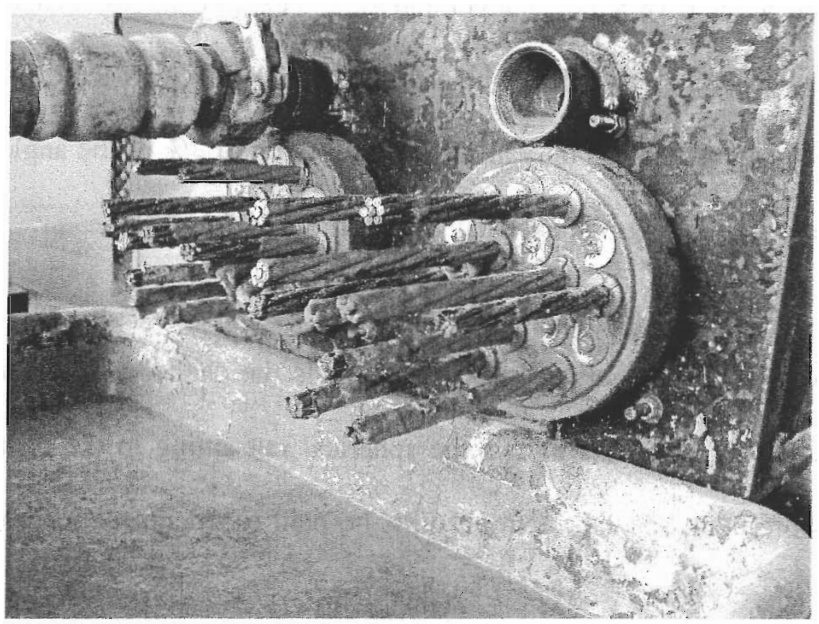

Figure 5.2.2-3 – Pipe fitting welded around grout access hole.

5.3 END PIECE FABRICATION

Capital Contractors also fabricated a full scale specimen of a 10 ft. end piece. This piece contains the bottom to top chord connection, as well as the first bottom to top chord hanger. *Figure 5.3-1* shows an elevation view of the specimen, and *Figure 5.3-2* shows the large base plate. Note the slotted holes to allow for expansion and contraction.

Unlike the bottom chord specimen, this specimen was not load tested, and was only produced to discover any challenges or special considerations in fabrication. A separate specimen was fabricated to test the hanger to top chord connection (see Sections 6.3 and 6.4).

The hanger to top chord connection must facilitate the transfer of a vertical load to non-perpendicular member. This connection consists of a solid steel wedge plate, a dish plate, a spherical nut, two connection plates, and a bearing plate (see *Figures 5.3-3 and 5.3-4*). The angle between the hanger and the top chord changes at each hanger location. The dish plate and spherical nut help transfer this vertical load to the top chord, but manufacturer specifications only allow a contribution of 2% of the angle. Therefore, the wedge plate angle changes at each hanger location.

The connection on the finished specimen reveals the challenge in seating the spherical nut correctly. *Figure 5.3-5* shows the spherical nut sitting in the dish plate. To help avoid this problem, special attention must be paid to tolerances in production of these

pieces. Additionally, the 12 in. x 12 in. wedge plate was fabricated incorrectly. Instead, the dimensions are 10 in. x 8 in. on this production specimen and the testing specimen.

In order to avoid having water pond in this connection, weep holes were to be cut in the appropriate locations. In the production specimen however, the weep holes were placed in the wrong location, or the plate was installed upside down. *Figure 5.3-3* shows the connection with standing water after a storm. Note the weep holes just below the bearing plate.

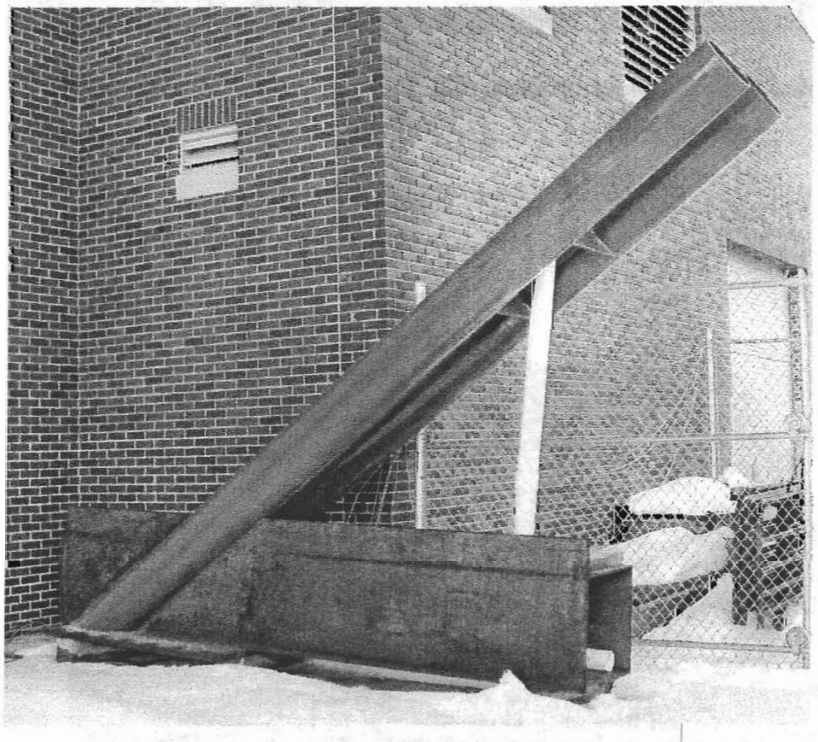

Figure 5.3-1- End specimen elevation view.

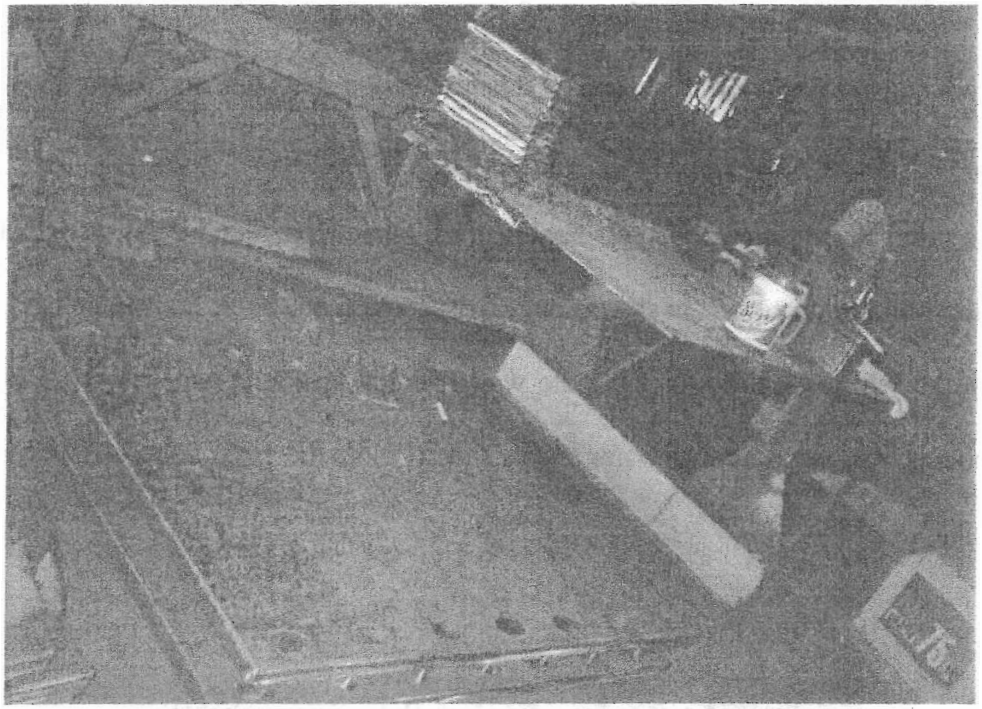

Figure 5.3-2- Connection base plate.

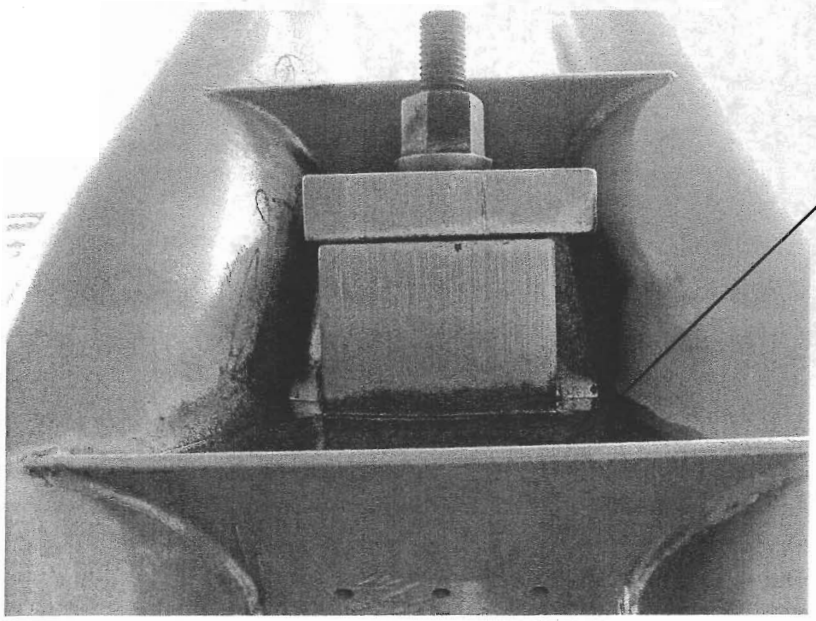

Figure 5.3-3 – Connection elements.

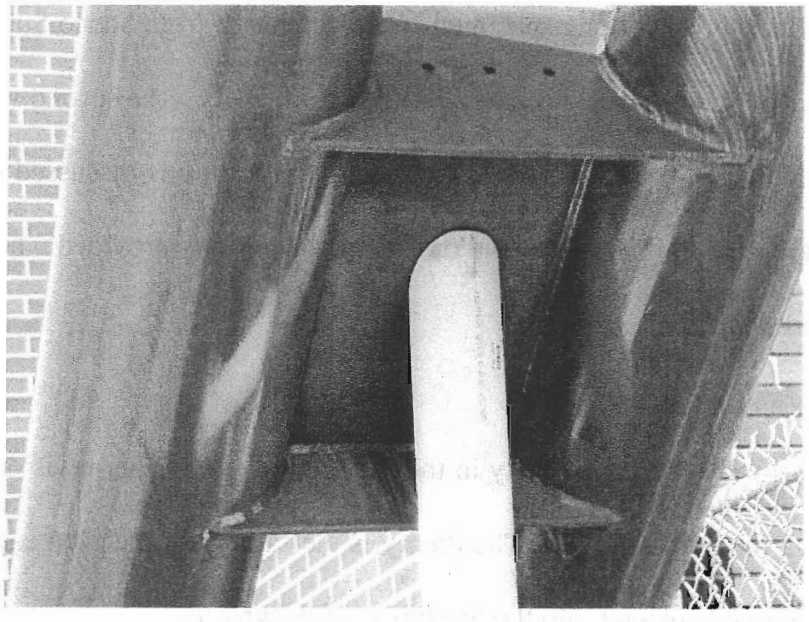

Figure 5.3-4 – Connection elements, as seen from below.

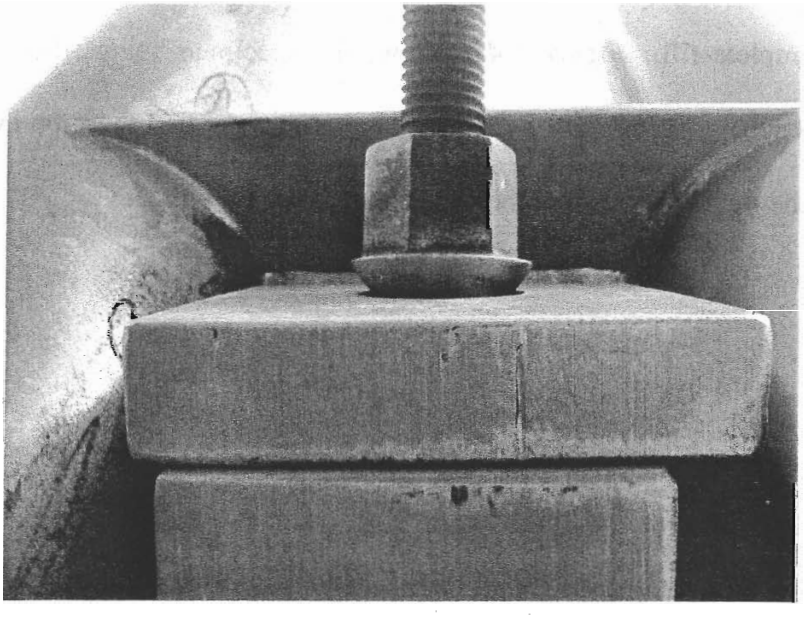

Figure 5.3-5 – Spherical nut seated in dish plate.

5.4 TOP CHORD FABRICATION

Two 10 in. diameter 21 ft. long specimens were purchased from Scoco Supply in Omaha. One was later filed with concrete at the PKI Structures Lab. The second was left hollow, and both specimens were then tested in flexure. The testing is discussed in Section 6.1. The results are then compared to show the increased capacity provided when the concrete and steel work together.

The specimens were fabricated early in the design process; further revisions changed the design to a 12 in. diameter tube. The theory is the same, and the fabrication and testing still provide valuable insight into the feasibility of the project.

In order to ensure the specimen was fully filled with concrete, it was filled while leaning at a steep angle, and the concrete was pumped from bottom to top. An air vent at the top ensured a complete fill. *Figure 5.4-1* shows the specimen being filled. As with the bottom chord specimen, the mix used flowed nicely, and filled the tube evenly. *Figure 5.4-2* shows the mix flowing from the truck.

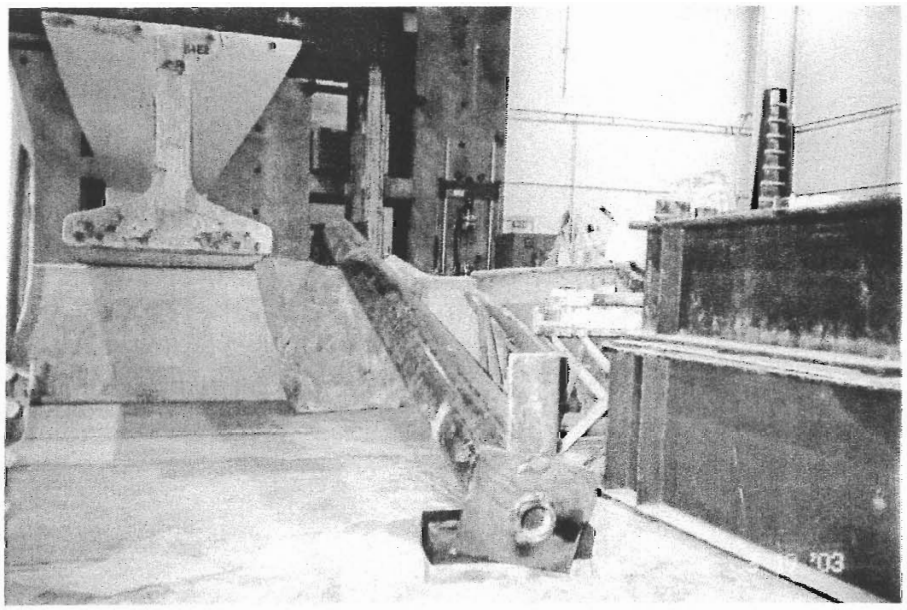

Figure 5.4-1 – The hollow tube was filled by pumping from the bottom.

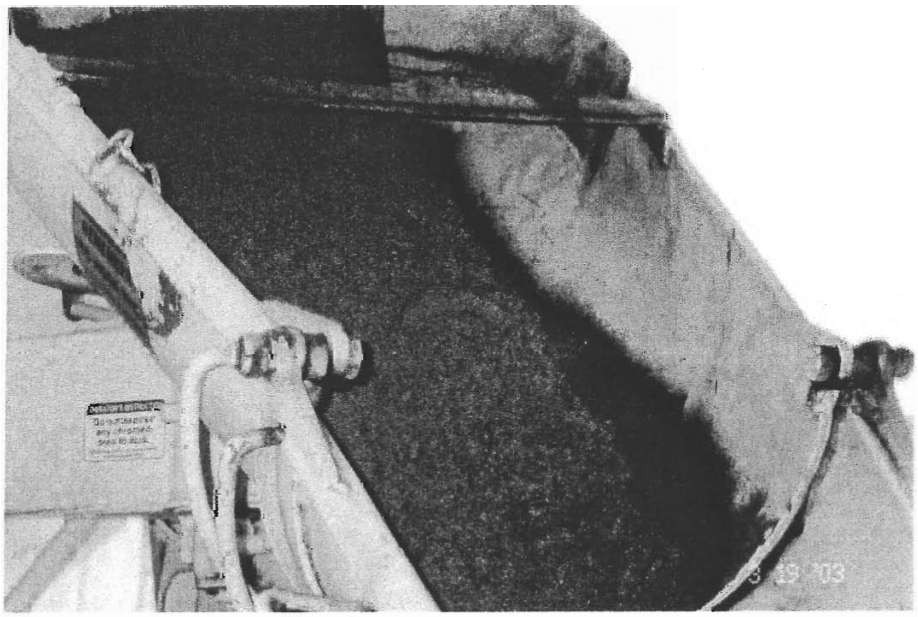

Figure 5.4-2 – A high flow mix was used to fill the specimen.

SECTION 6: SPECIMEN TESTING

6.1 TOP CHORD SPECIMEN TESTING

As discussed in the previous section, two 10 in. diameter 21 ft. long specimen were fabricated at Capital Contractors. One was later filed with concrete at the PKI Structures Lab. The second was left hollow, and both specimens were then tested in flexure. The results are then compared to show the increased capacity provided when the concrete and steel work together.

6.1.1 HOLLOW STEEL TUBE

The hollow specimen was tested as a 20 ft. simple span with a single point load at midspan. The load was applied using a 110 kip hydraulic jack. *Figure 6.1.1-1* shows the test setup with the hollow tube, and *Figure 6.1.1-2* shows the test nearing completion. The specimen stopped taking force at an ultimate load of 39.8 kips, and reached a deflection of 10.7 in.

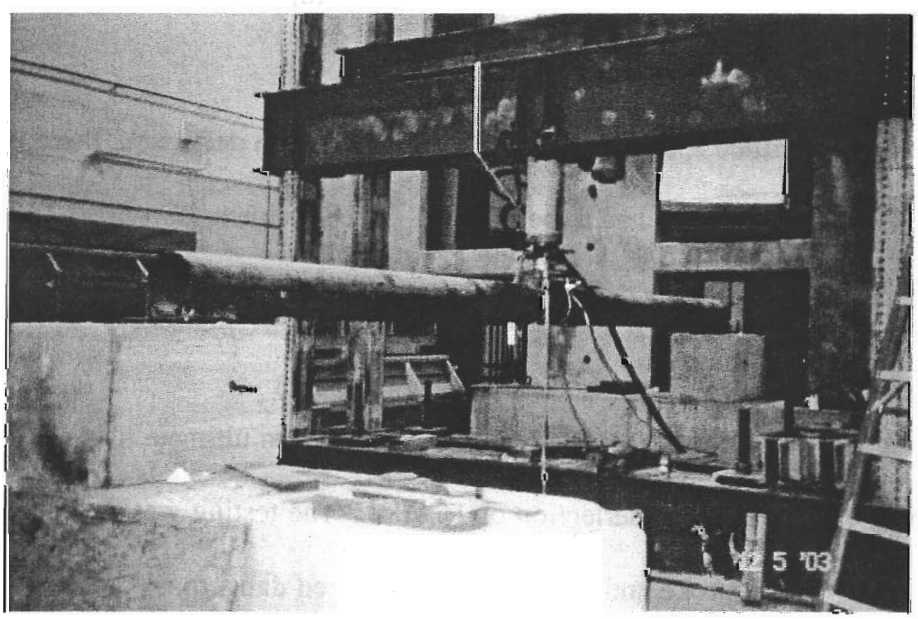

Figure 6.1.1-1– Hollow steel tube test setup.

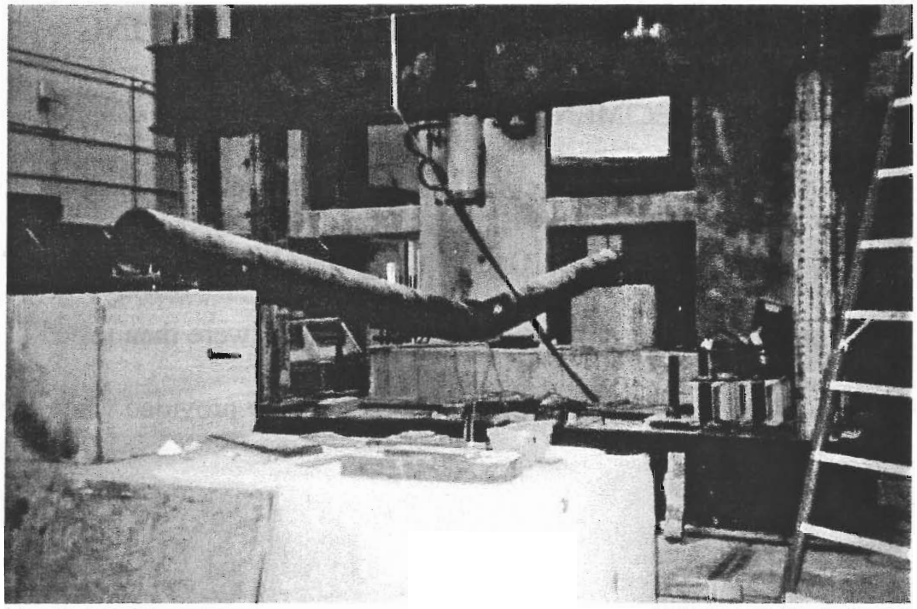

Figure 6.1.1-2– Hollow steel tube final deflection.

6.1.2 CONCRETE FILLED TUBE

The concrete filled tube was tested in the same way as the hollow tube. Therefore, the specimen was tested as a 20 ft. simple span, with a single point load. This way, a comparison is possible and a determination can be made on the effectiveness of filling the tube with concrete. *Figure 6.1.2-1* shows the test setup with concrete filled tube.

As the concrete filled specimen reached a 10 in. midspan deflection, there was a problem with the jack, and the load had to be released. The specimen rebounded 2 ½ in., leaving a 7 ½ in. permanent midspan deflection.

The jack was reset and the testing resumed, reaching an ultimate load of 55.3 kips. The specimen was loaded to a deflection of 16 ½ in. The testing was then stopped, because the jack ran out of stroke and the specimen appeared dangerous. *Figure 6.1.2-2* shows

the specimen as it nears its ultimate deflection. Therefore, the added concrete increased the capacity of the tube in flexure by almost 40%.

After the testing was completed, the tube was cut open to inspect the quality of the concrete fill. *Figure 6.1.2-3* shows the tube cross section after testing, 65 days following the pour. Researchers were surprised to discover a 3 in. diameter circle at the very center of the tube that still retained visible moisture. The confining effect of the steel prevented excess moisture from escaping. This is not believed to affect the strength of the concrete. It is also interesting to note that visible moisture on the cut surface disappeared approximately four seconds after being cut, leaving a dry concrete surface.

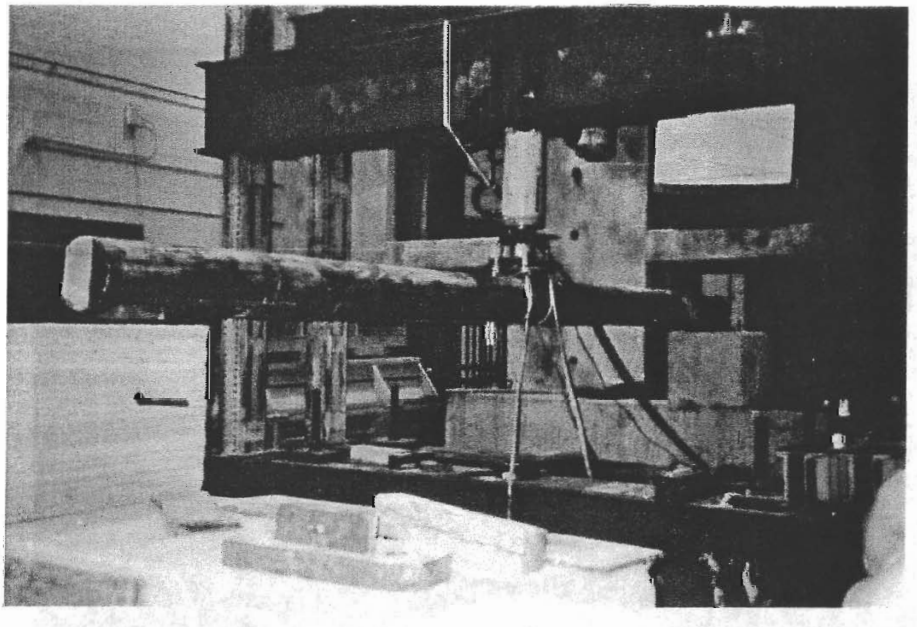

Figure 6.1.2-1– Concrete filled tube test setup.

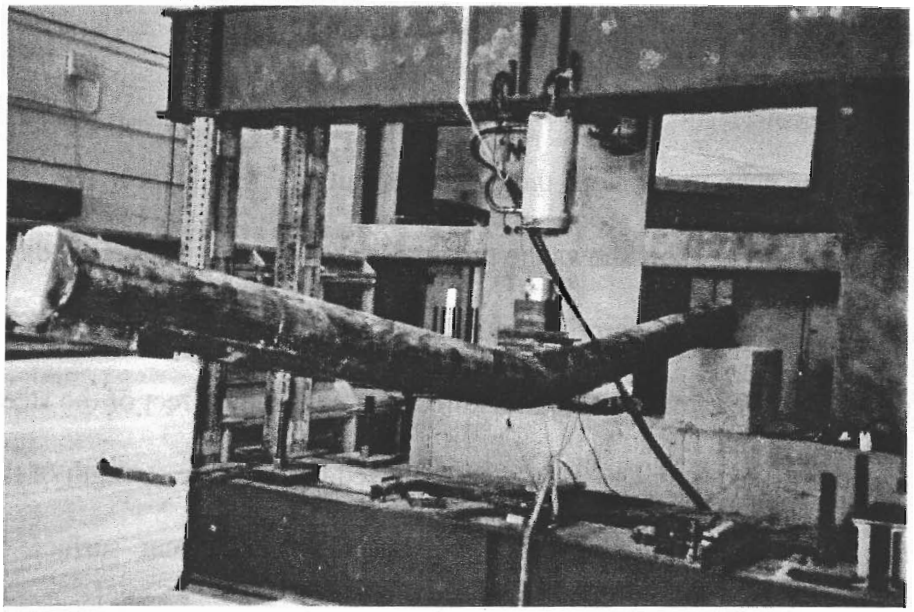

Figure 6.1.2-2 – Concrete filled tube testing in progress.

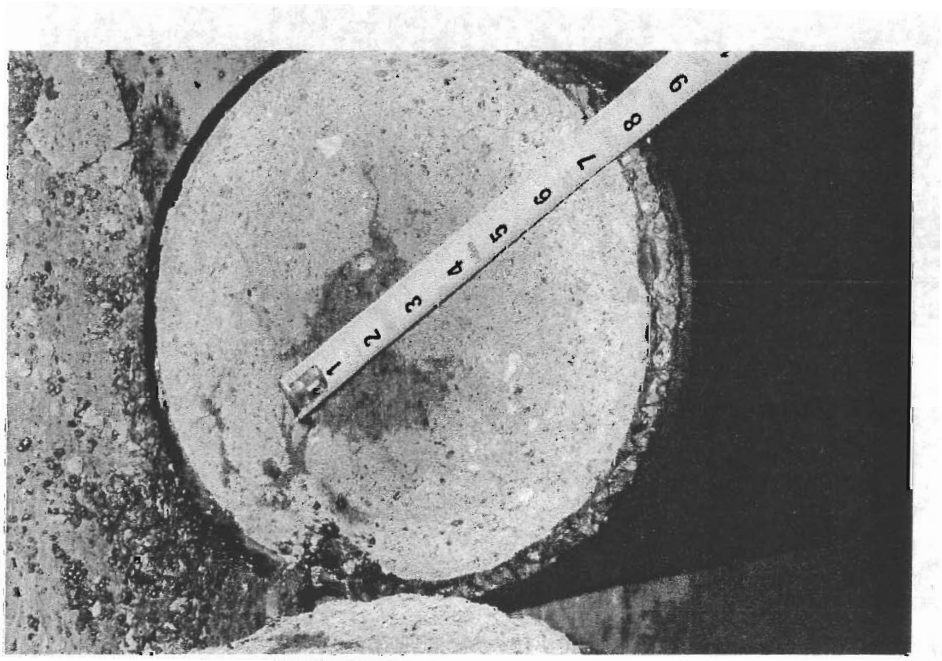

Figure 6.1.2-3 – Visible moisture in center of tube.

6.2 BOTTOM CHORD ULTIMATE STRENGTH

Because the Ravenna Arch Bridge is such a unique design, the bottom chord full scale specimen was tested to ensure the theory used to evaluate the capacity matches experimental data. Section 4.2 discusses the required element capacity, Section 4.3.1 discusses the expected element capacity, and Section 5.2 discusses the fabrication of the bottom chord.

After the grout in the post-tensioning duct had gained strength, the specimen was ready to be tested. The specimen was tested as a 39 ft. 3 in. span. Two 300 kip hydraulic jacks were used to create point loading at 13 ft. 7 ½ in. from each support. The loading is placed at this position because the lab has support locations every 12 ft. The loading diagram is shown in *Figure 6.2-1.* The specimen in early stages of loading is shown in *Figure 6.2-2.*

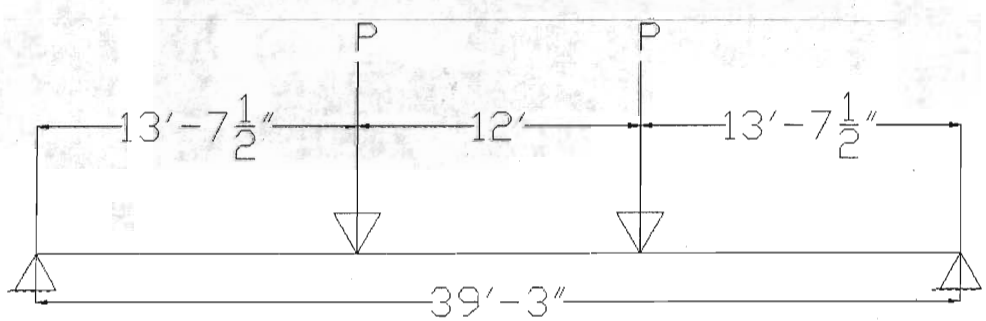

Figure 6.2-1 – Point loading of Ravenna Bottom Chord test specimen.

Eight strain gauges were prepared and placed in order to collect strain data throughout the loading. These were located at midspan, and others at mid-distance between the load and the pier.

The same strain compatibility approach used to calculate the capacity of the final, fully-tensioned, bottom chord was used to calculate the expected capacity of the test specimen. If the specimen behaves as predicted, designers can feel more comfortable with the actual bottom chord that was sized using the same theory.

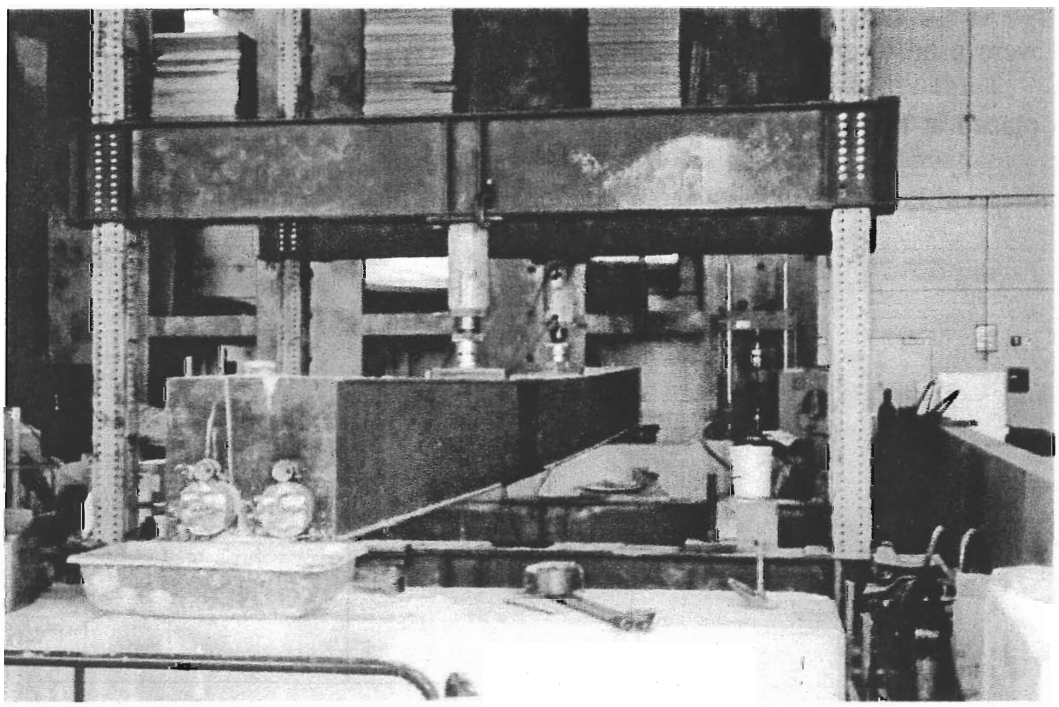

Figure 6.2-2 – The bottom chord test specimen in early stages of loading.

The test specimen, with 20 fully tensioned strands, was expected to have a capacity of 3125 k-ft, or 230 kips per jack, and a deflection at ultimate load of 4.5 in. This calculation, as does the analysis of the real bottom chord, makes an assumption for the

ultimate strain in the concrete. Confinement is known to raise the ultimate strain above the traditionally assumed values of 0.003; Confinement theory is still in early stages of development at the University of Nebraska and other research institutions.

The testing proceeded smoothly, and was continued until the output indicated the specimen was taking no additional load. *Figures 6.2-3 and 6.2-4* show the specimen as it nears its ultimate deflection.

The specimen stopped taking additional load at an ultimate force of 445,176 lbs. or approximately 231 kips per jack, and a deflection at ultimate load of 4.52 in. The results are incredibly close to the predicted values of 230 kips per jack and 4.5 in. of deflection.

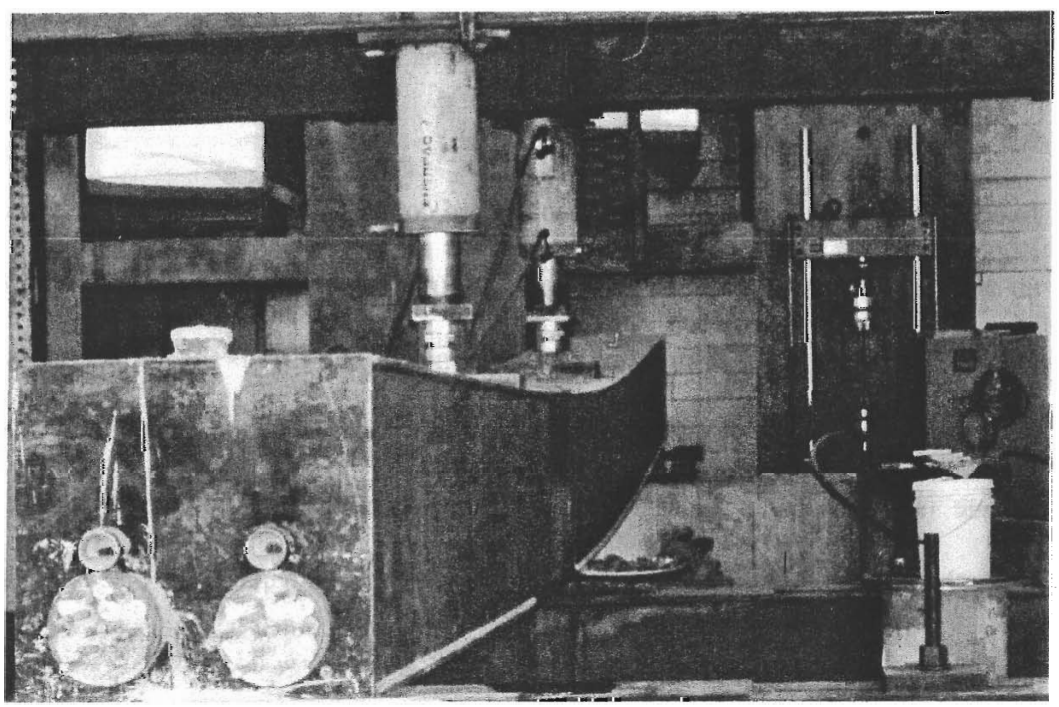

Figure 6.2-3 – The bottom chord test specimen in advanced stages of loading.

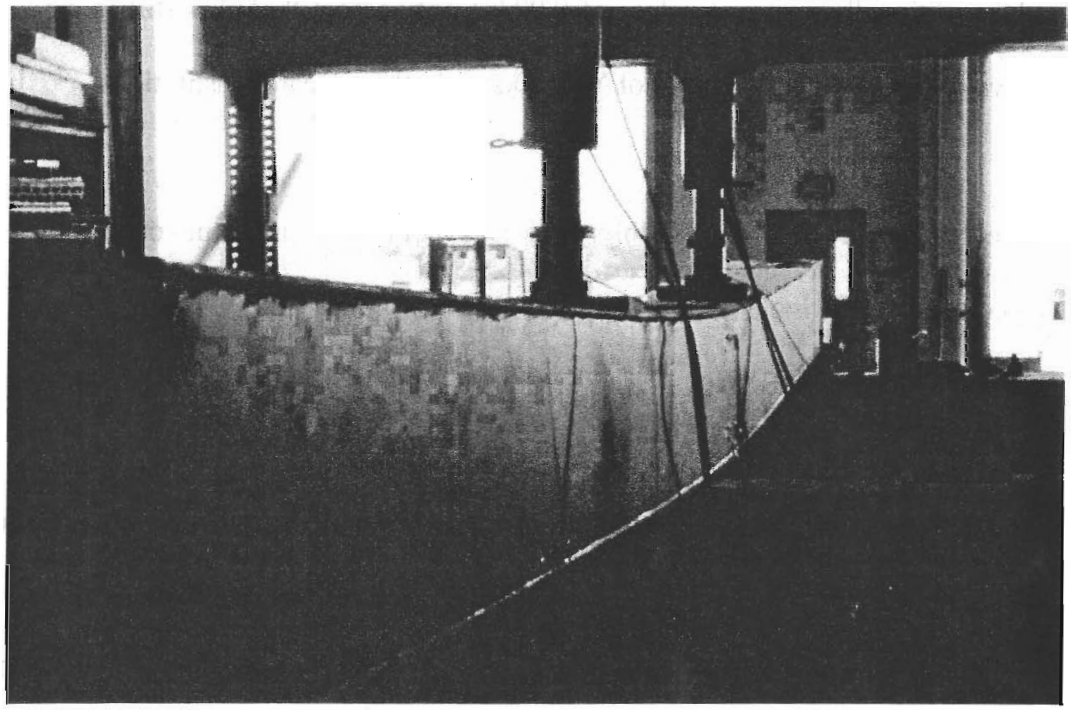

Figure 6.2-4– The bottom chord test specimen as it approaches ultimate deflection.

6.3 HANGER CONNECTION FATIGUE

In addition to the production hanger/top chord connection piece discussed in Section 5.3, an additional connection specimen was constructed specifically for testing. There are two main concerns that testing hopes to eliminate. The first is the connection's capacity under cyclic service loading (fatigue). The determination of the connection's capacity in fatigue is discussed in this section. The other concern is the connection's ultimate strength. Determination of the specimen's ultimate load capacity is discussed in Section 6.4.

The connection was mounted underneath a 110 kip MTS actuator. In order to be able to place the actuator, the specimen was tested upside-down. In order to mount the specimen and keep the threaded rod vertical, several steps had to be completed. First, two 6 ft. x 8 in.x 8 in. hollow steel sections were placed in each tube. After the steel sections were positioned inside the tube, steel plates were welded around the hollow steel sections, effectively closing off the tubes. Grout was then pumped into the tube through a small opening cut in the top of the tube. The filling of the tube was confirmed by the noting of concrete squirting out another small vent hole.

After the concrete was set, the specimen was mounted with four high strength threaded rods through the HSS. A special plate arrangement was used to ensure the loading was perpendicular to the connection. A spherical nut was welded to the plate assembly.

The specimen was loaded by applying the cyclic load to the threaded rod. *Figures 6.3-1* though *6.3-3* show this arrangement.

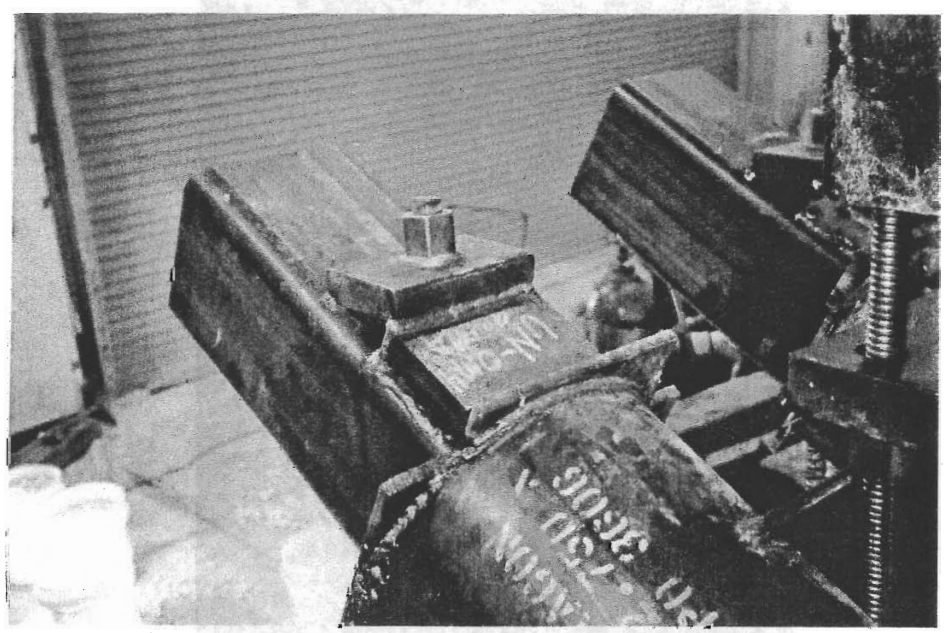

Figure 6.3-1 – Special plates were used to seat the mounting rods perpendicular to the load.

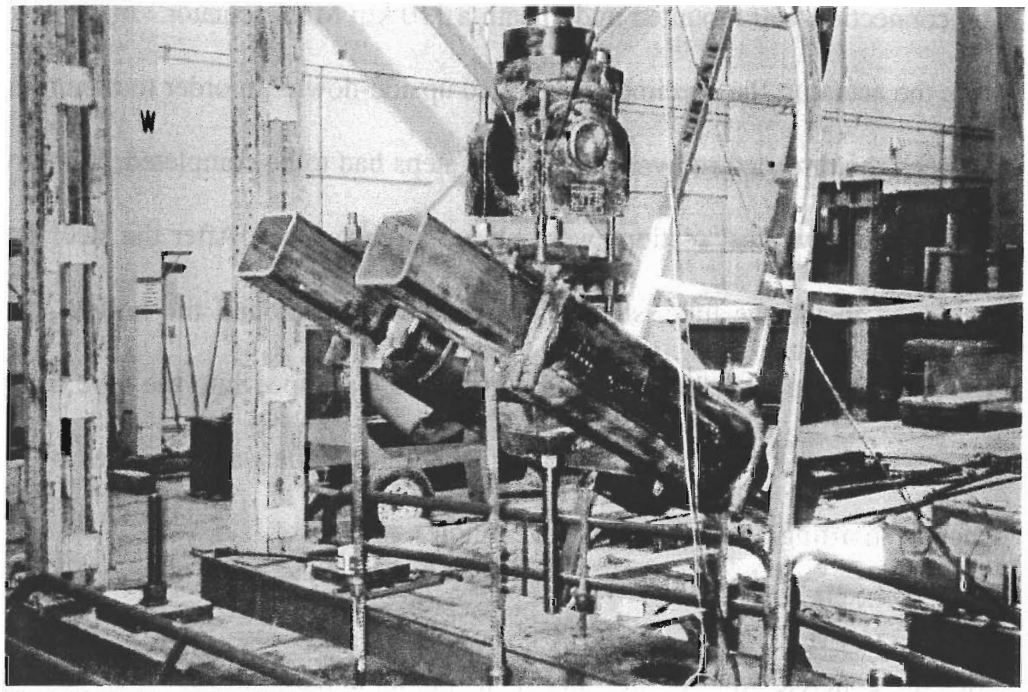

Figure 6.3-2 – The connection specimen mounted upside-down in the load frame.

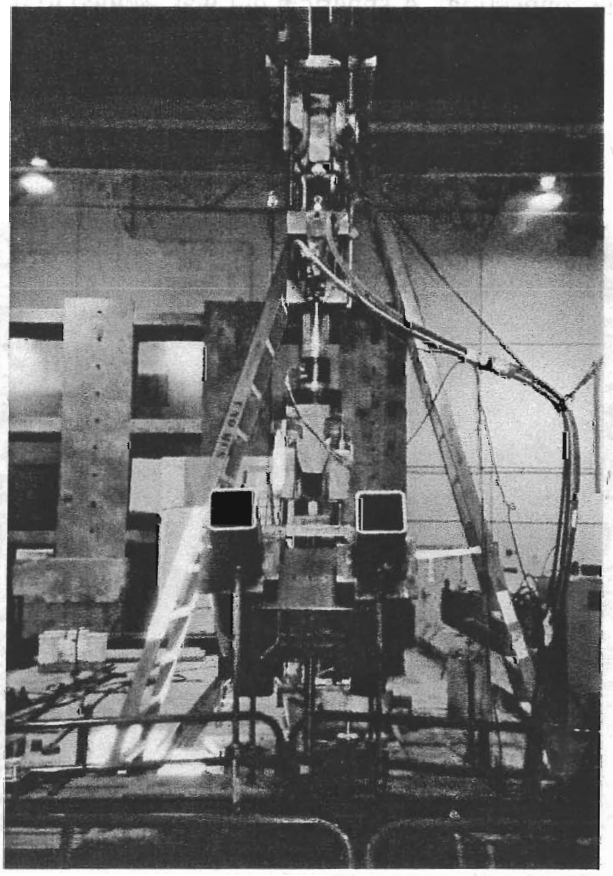

Figure 6.3-3 – The connection specimen mounted beneath the 110 kip actuator.

Only one notable modification was made to the test specimen. The plans call for the triangular wedge plate to be 12 in. x 12 in. at the base. The test specimen was mistakenly fabricated with a 10 in. x 8 in. wedge plate instead. The calculated plate capacity was not sufficient to span between the tubes without the correct sized wedge plate. In order to ensure that this fabrication error does not cause a failure of the test, two stiffener plates were added. This was a bigger concern for the ultimate test (see Section 6.4). The small wedge plate is shown in *Figure 6.3-4*, and the stiffener plates are shown in *Figure 6.3-5*.

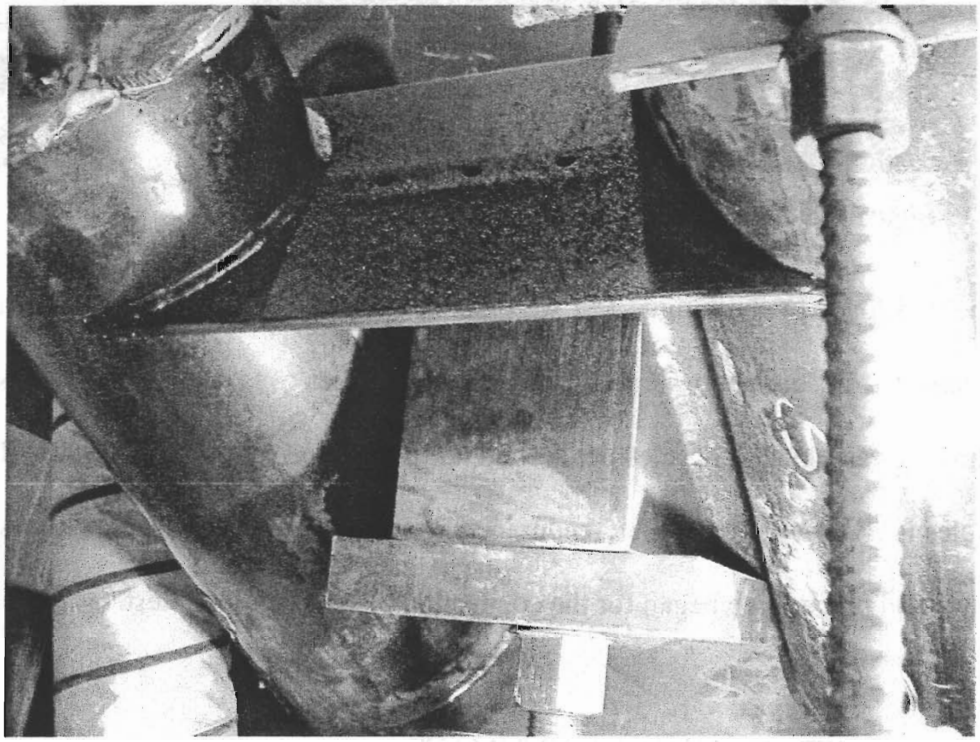

Figure 6.3-4 – The wedge plate was mistakenly fabricated too small.

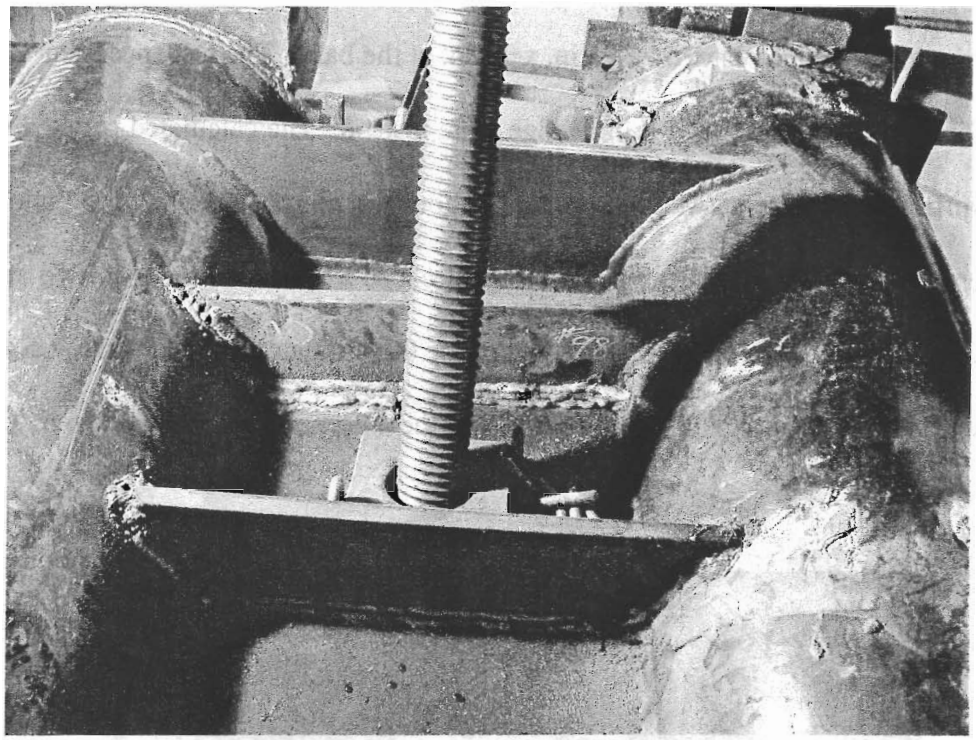

Figure 6.3-5 – Corrective Stiffeners

The end loads of the fatigue test were set at the service load end levels in the hangers obtained from the analysis. Therefore, the specimen was run between 65 k and 85 k. The test was run at 2.5 cycles per second, until reaching two million cycles. Two million cycles is a commonly accepted endurance limit [Ref. 21]. The specimen was then taken down and preparation began for the connection ultimate strength test.

6.4 HANGER CONNECTION ULTIMATE

After completing two million cycles at service load levels, the specimen was tested to failure. This was done to determine its ultimate capacity, and perhaps more importantly, its mode of failure.

Analysis of the connection led researchers to expect the threaded rod to yield before any of the connection components. This is preferable, as a yielding failure is safer than a sudden fracture failure. The yield strength of the 1 ¾ in. high strength treaded rod used in the project is specified as 320 kips. The ultimate strength is specified as 400 kips.

Great effort was made to ensure the specimen failed before any of the test setup failed. *Figure 6.4-1* shows the test setup from the floor of the PKI Structures Lab, and *Figure 6.4-2* shows the setup from below the lab floor, where the specimen was. Two 300 kip jacks were used one either side of the threaded rod to apply the vertical load. In order to keep the loading in line with the threaded rods, each end of the connection had to be shimmed until was bearing against the support beams.

Deflection of the specimen was determined by measuring the stroke of the jack. The jack began at a stroke of 2 in. The table below shows the progression of the deflection.

Load (k)	Jack Stroke (in.)
115	2
167	2 1/6
220	2 1/3
253	2 3/4
300	2 7/8
339	3 1/2
385	5 7/8

After the specimen reached 385 kips it quite taking any more load, and the yielding of the threaded rod could be seen. The total deflection was nearly 4 in.

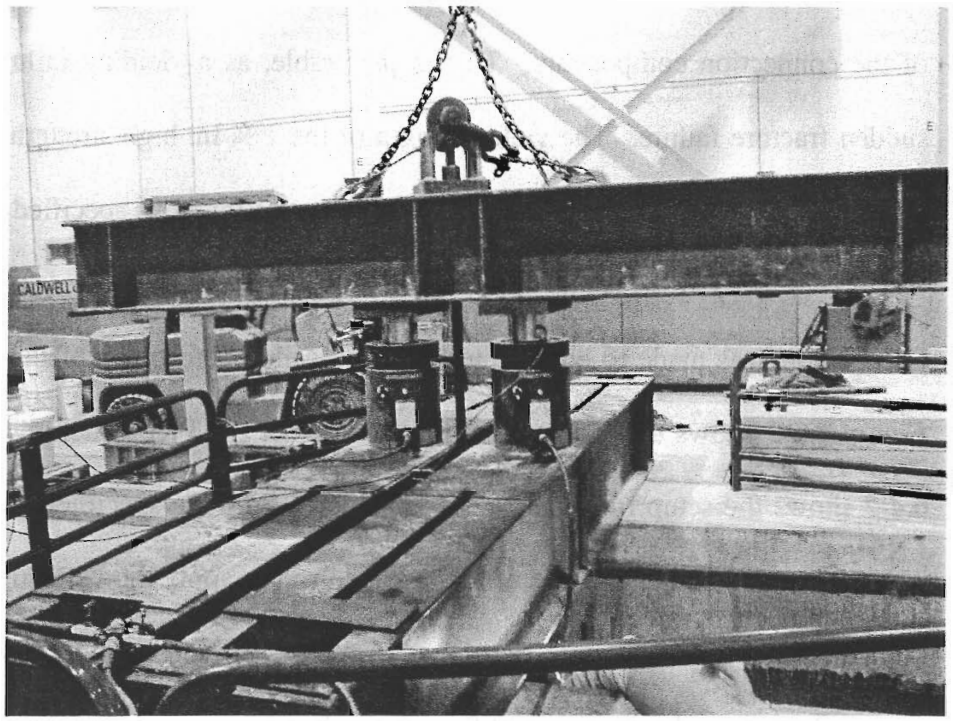

Figure 6.4-1 – The test setup, as seen from the floor of the PKI Structures Laboratory.

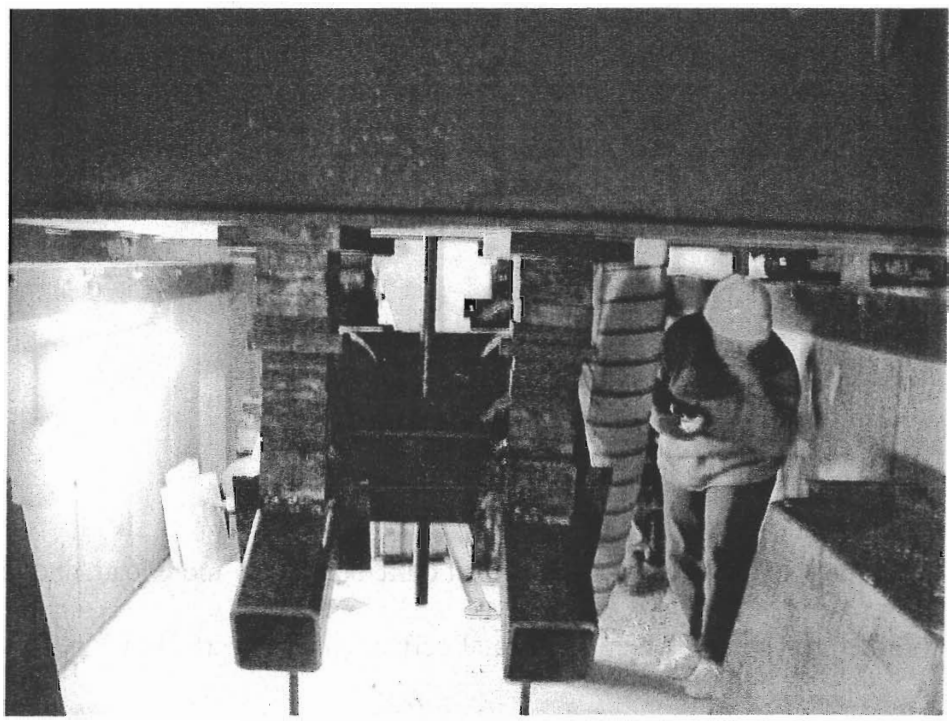

Figure 6.4-2 – The test setup, as seen from below, on the specimen level.

SECTION 7: CONSTRUCTOR RESPONSE

7.1 CONSTRUCTOR INTEREST

A pre-bid meeting was held at 1:30 on August 11, 2004 in the auditorium at the Nebraska Department of Roads' central office building. The purpose of the meeting was to allow bidders to ask questions about the project as the prepared their bids.

The pre-bid meeting was well attended, with 10 general contractors represented, and 29 people in attendance. In regards to the bridge design, there were several questions asked.

There were several questions regarding the structural elements. A few questions focused on the launching process. It was asked how many floor beams need to be assembled with the arches at the time of launching. This is an issue because it is thought that reducing the number of floor beams in place at the time of launching would lessen the weight. The answer given was that it is necessary to have at least one on each ends, and probably one in the middle. Additionally, the floor beams directly over the railroad should be in place before launching to reduce the amount of work over the railroad. Therefore, the number of floor beams could probably be reduced, but not significantly.

The bracing of the arches was also briefly discussed. It is understood that the connection with the tie beam will prevent the arches from flattening out. The more critical stability problem during erection is that of keeping the arches vertical. For that reason, temporary bracing between the two arches will be used. It was mentioned that the constructor should pick the bridge up near the corners, near the support locations.

Another point of concern for the constructors was the amount of time the railroad below could be closed for construction. At the time of the meeting, the answer was a maximum 8 hour window, and only if planned out well in advance. A one to two hour window should be easier to obtain. The importance of the constructor establishing an open dialogue with Burlington Northern Santa Fe was emphasized.

There was some constructor concern about the ease with which the steel sections could be filled with concrete. They were reassured that the testing in the lab had gone smoothly, and there is no reason to believe there would be any problem in the field.

A question was asked about the specific language in the contract documents which states that the bottom chord can be tensioned as soon as the 6000 psi strength is met. It was clarified that the bottom chord could be tensioned no sooner than the specified strength is met. This is not a requirement to tension as soon as 6000 psi strength is met, but that the constructor may proceed at any time after the strength is achieved.

7.2 BIDDING

As indicated by the attendance at the pre-bid meeting, constructor interest in this project was high. Constructor interest was further proved with seven bids made for the Ravenna Viaduct.

The successful bid was made by Christensen Bros., Inc., of Cherokee, IA. The bid was $4,212,903.12 for the whole project, including $2,149,401.15 for the bridge portion.

The second place bidder was Capital Contractors, Inc., of Lincoln, NE. The bid was $4,247,399.18, including $2,250,955.00 for the bridge portion. The difference in the successful and second place bid was 0.8188%. The highest overall bid was $4,850,537.87, or 5.1353% higher than the winning bid.

The bridge portion bid ranged from the winning bid of $2,149,401.15 to $2,720,408.85 in the highest bid.

7.3 COST ANALYSIS

The Ravenna Arch Bridge has a very unique design, but one that could possibly serve as a NDOR standard design for similar spans. The system works well, is esthetically pleasing, and releases designers and the public from the monotony of traditional stringer bridge design. In the end, however, the decision comes down to, of course, the cost considerations. Is this bridge cost effective?

A good average cost for a traditionally designed stringer bridge in our area is $75/ft^2 of deck area. The Ravenna Arch Bridge effectively covers 10,200.75 ft^2. Therefore, a traditional design covering the same square footage would cost $765,056.

As discussed in the previous section, the bridge portion of the Ravenna Arch Bridge costs \$2,149,401.15. This comes out to \$210.71/ ft^2. This is almost three times the cost of the traditional design. However, if the cost of mobilization, approach slab concrete and steel, and bridge removal is not considered, the cost goes down to a more reasonable \$163/ ft^2.

It is important to note that cost of a unique concept can be expected to come down as the design is used more often, and constructors become more familiar with the system.

SECTION 8: EFFECTIVE FLANGE WIDTH TESTING

8.1 OBJECTIVES

The objectives of this section are to investigate the effective flange width that is needed to act compositely with the arch bridge bottom chord and to investigate the possibility of increasing the minimum distance for shear connectors required by the current code provisions.

8.2 INTRODUCTION

The effective slab width is a concept used in flexural analysis of concrete T-beams and concrete-steel composite beams to simplify the computation of flange bending stresses. The effective flange width is the width of the flange in which the stresses are assumed to be constant instead of taking the more accurate parabolic shape of stresses. The resultant force and the point of application of the resultant force in the flange should be the same in both cases.

The effective flange width is an important parameter for the design and analysis of composite beams. The effective flange width has a direct effect on the member strength as well as its serviceability. Results of the experimental tests were compared to an effective flange width that is equal to the spacing between the cross-beams for the interior cross-beams and equals to half of the spacing plus the overhang for the exterior cross-beams. This approach was selected as it is least conservative when compared to bridge code requirements. Further analysis can be performed by researchers and designers as explicated in Section 3.

8.3 TESTING PROGRAM

To achieve the objectives of this study, steel beams were assembled and a concrete slab was poured at top of these steel beams and tested as described below. The steel frame was supported in a longitudinal direction during slab casting using two jacks. The two jacks were released seven days after casting the slab. The concrete strength of the slab at this time was 5,707 psi. Tests 3 and 4 were conducted at the concrete age of 27 days. The average concrete strength at this time was 6,452 psi. The last test was conducted at the concrete age of 36 days with corresponding concrete strength of 6,948 psi.

8.3.1 SPECIMEN FABRICATION

Studs were shot into all steel beams. Longitudinal and cross beams were then connected with angles that were welded to both beams at the UNL structural laboratory. Figure 8.3.1-1 shows the shooting of the studs. Figure 8.3.1-2 and 7.3.1-3 show the connections between the longitudinal and cross beams.

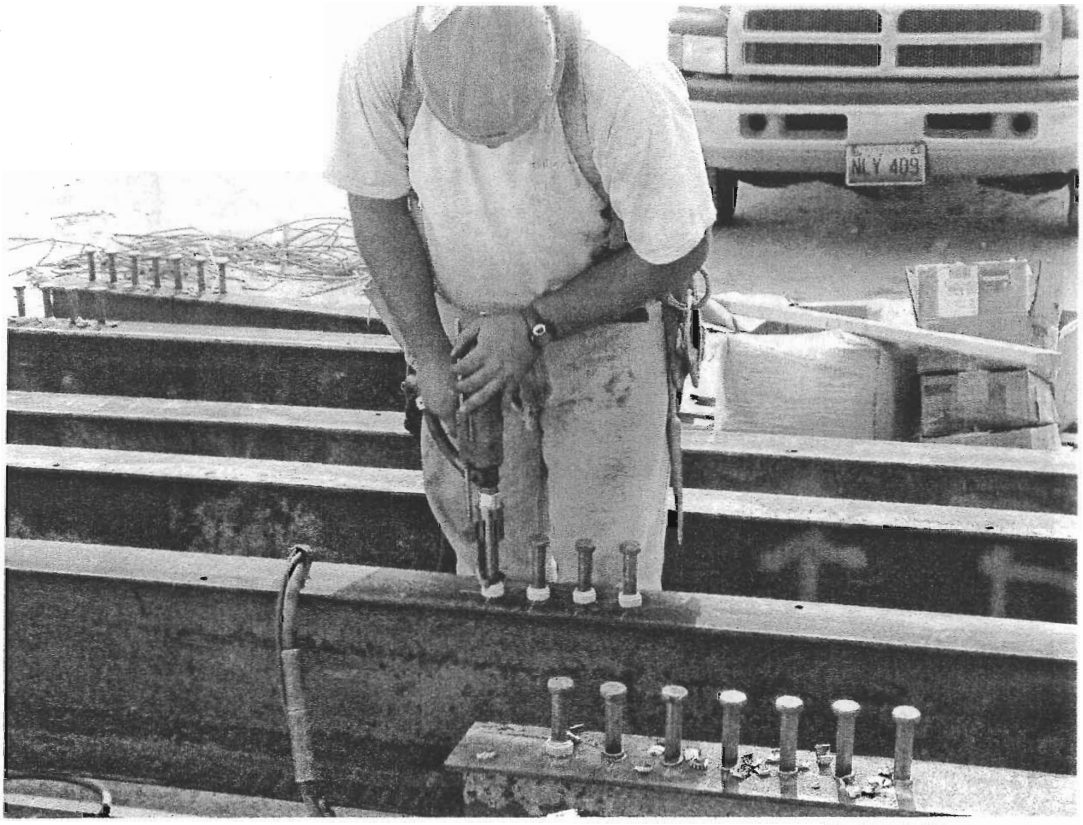

Figure 8.3.1-1 - Shooting the studs

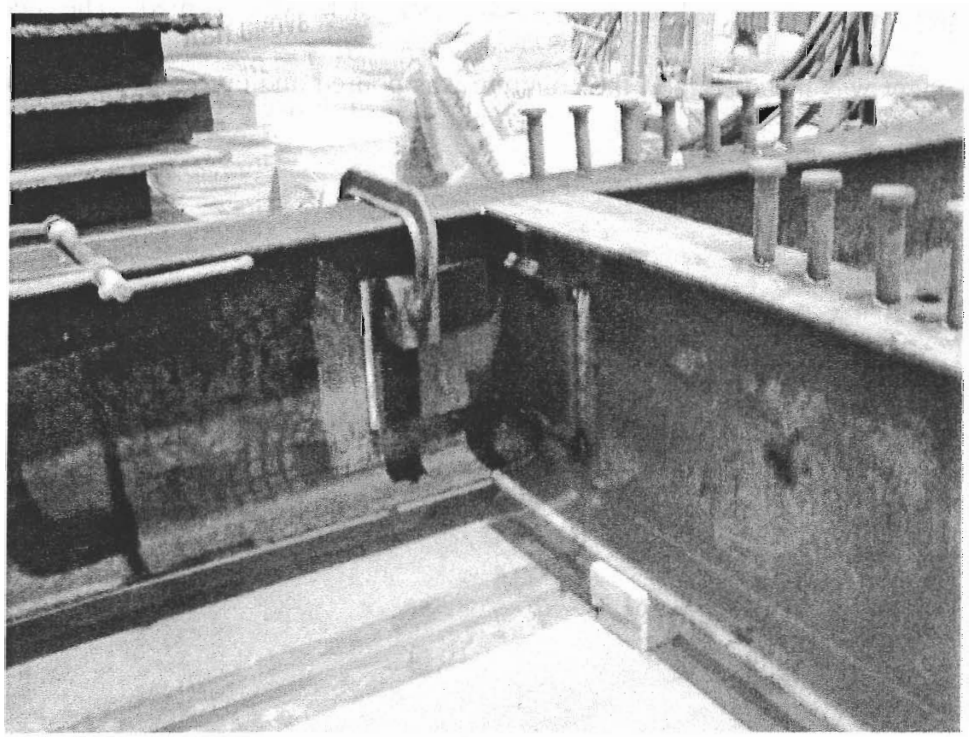

Figure 8.3.1-2 - Beam connection

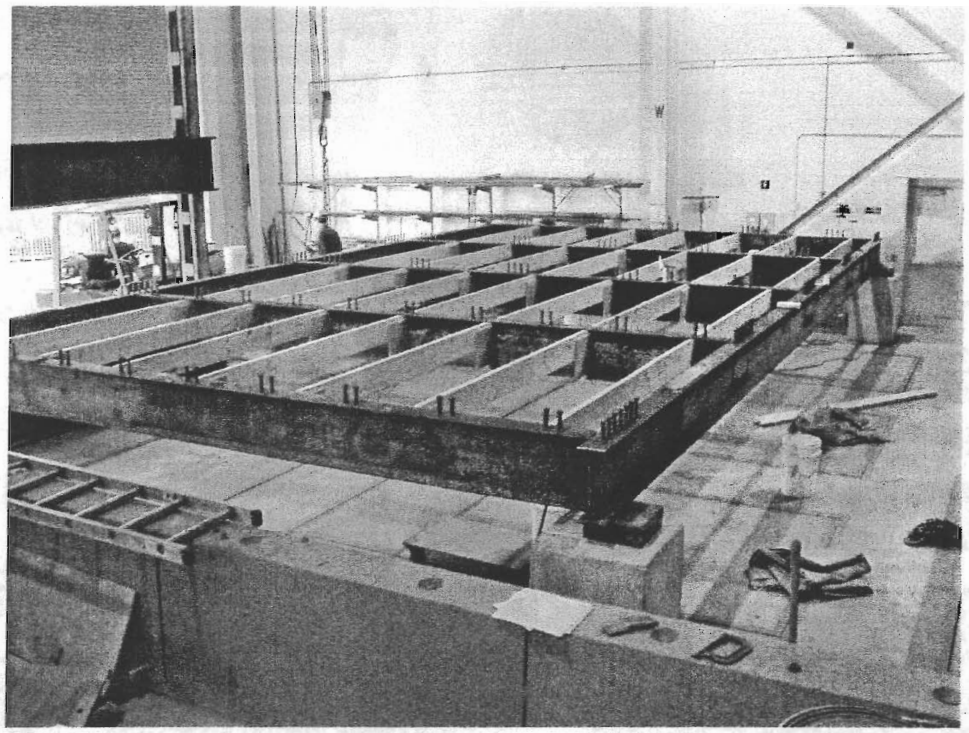

Figure 8.3.1-3 - Longitudinal and cross beams layout

The beams were connected, and then the deck slab was formed. The deck slab reinforcement was installed, and the concrete was poured and cured, as shown in Figure 8.3.1- 4 and 8.3.1- 5.

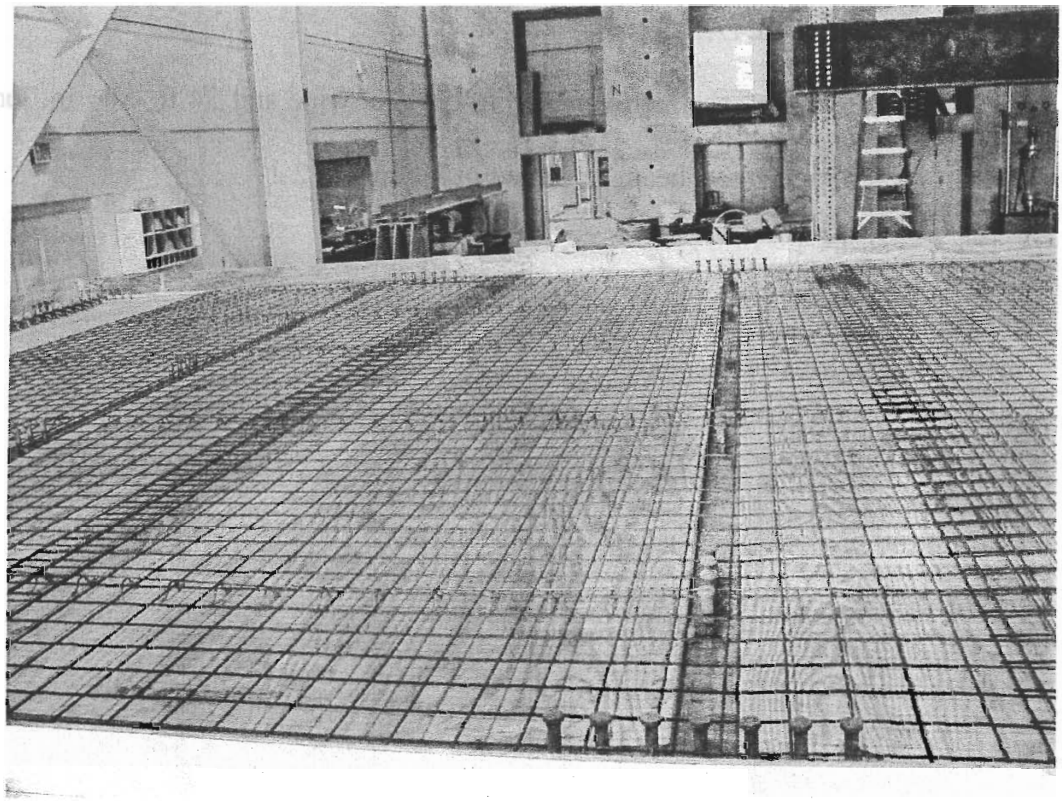

Figure 8.3.1-4 - Forming the deck slab and installing the reinforcement

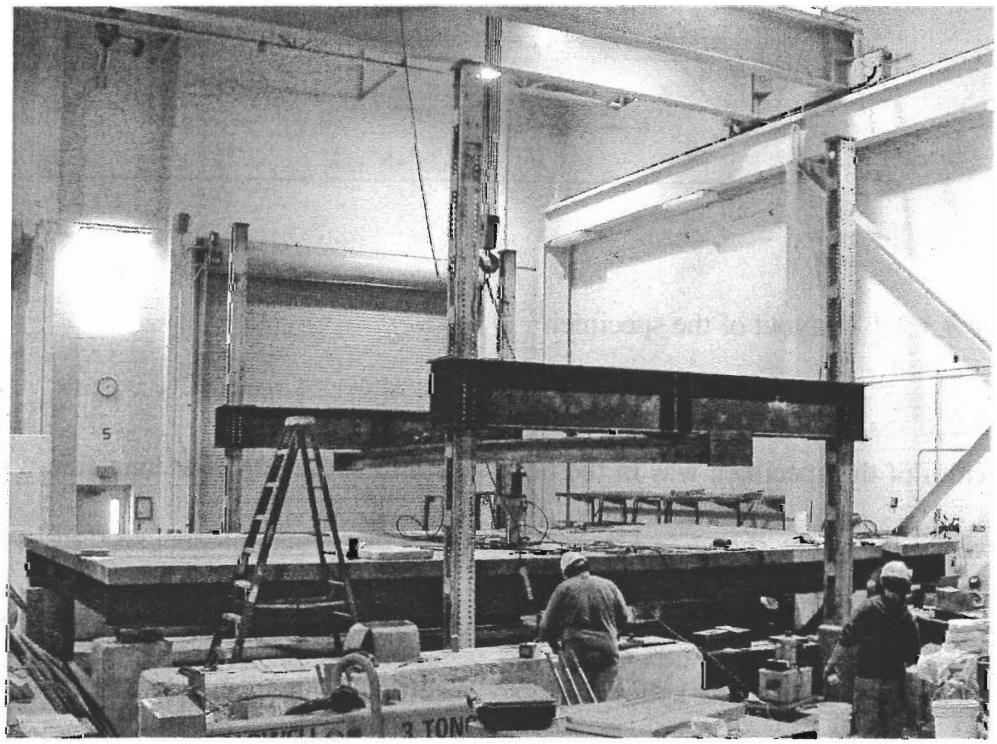

Figure 8.3.1-5 - Specimen ready to be tested

8.3.2 SPECIMEN DETAILS

The dimensions of the specimen were 21 ft -5 ½ in. wide and 34 ft -5 ½ in. long. The layout of the structural steel beams is shows in Figure 8.3.2-1.

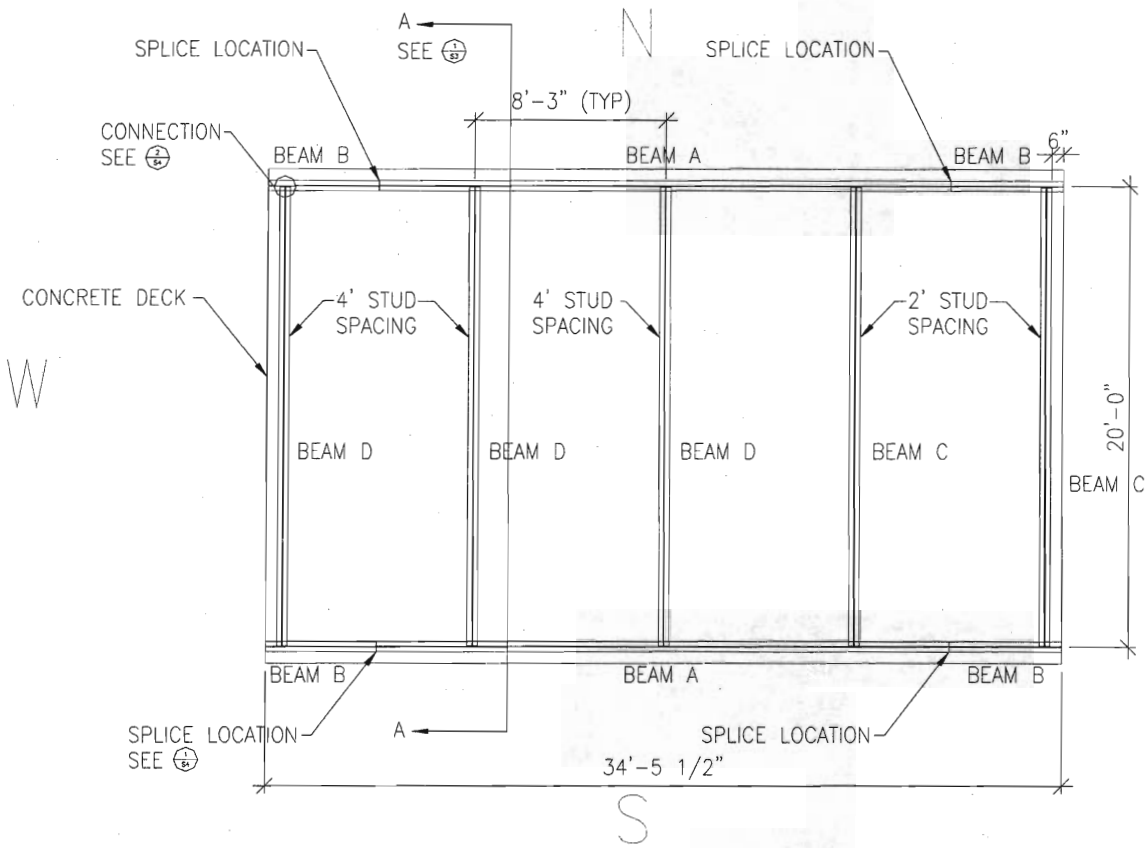

Figure 8.3.2-1 - Layout of the specimen

The width of the specimen was in the north-south direction, and the long side was in the east-west direction as shown in Figure 8.3.1-1. All the structural steel sections were S 15 x 42.9. Two longitudinal beams were created by splicing the beams marked as A and B. The location of the beam splices is also specified on the sketch. The splices were designed and fabricated to have more strength than the steel cross beam in flexure and

shear. The spacing of the steel beams in the transverse direction was 8 ft -3 in., which is reasonably close to the Ravenna Viaduct spacing (8 ft -9 in.).

8.3.2.1 SHEAR STUD CONNECTORS

7/8 in. diameter shear studs were used on top of the beams to provide the full composite action between the steel beams and the concrete slab. Beam C, located in the transverse direction, had clusters of shear studs, spaced 2 ft on center, while beam D had the stud clusters spaced 4 ft on center. Figures 8.3.2.1 - 1 and 8.3.2.1 - 2 show the shear studs distribution along beams C and D.

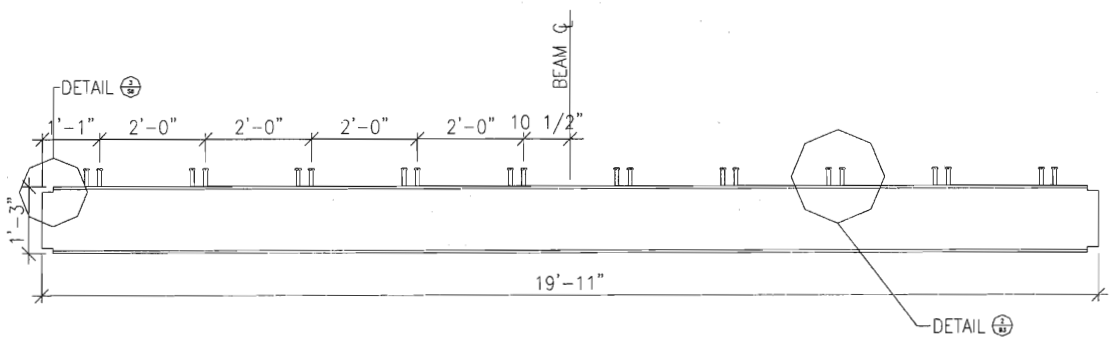

a) Beam C studs layout

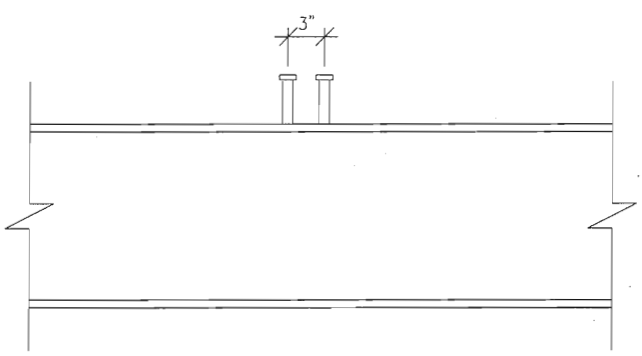

b) Configuration of the stud clusters

Figure 8.3.2.1 - 1 - Distribution of the shear studs along beam C

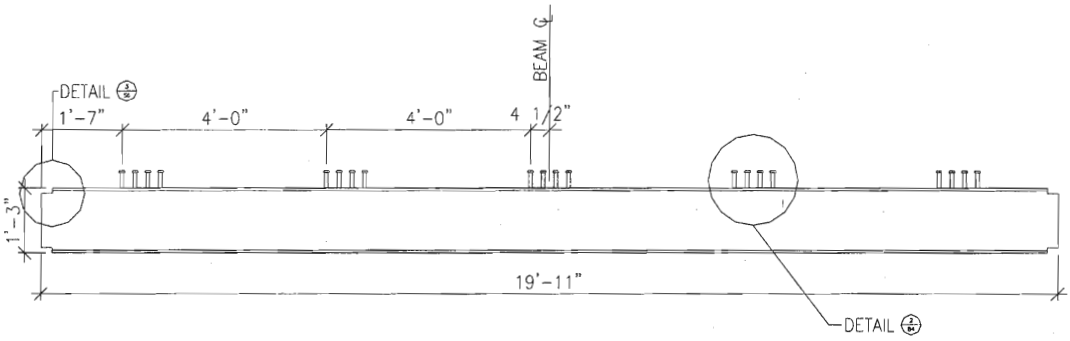

a) Beam D studs layout

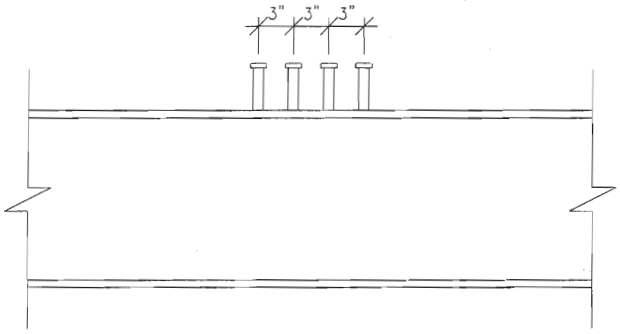

b) Configuration of the stud clusters

Figure 8.3.2.1 - 2 - Distribution of the shear studs along Beam D

The shear studs in the longitudinal beams were clustered at 8 ft each as shown in Figure 8.3.2.1 - 3. The locations of the stud clusters are at the intersections of the cross beams with the longitudinal beams.

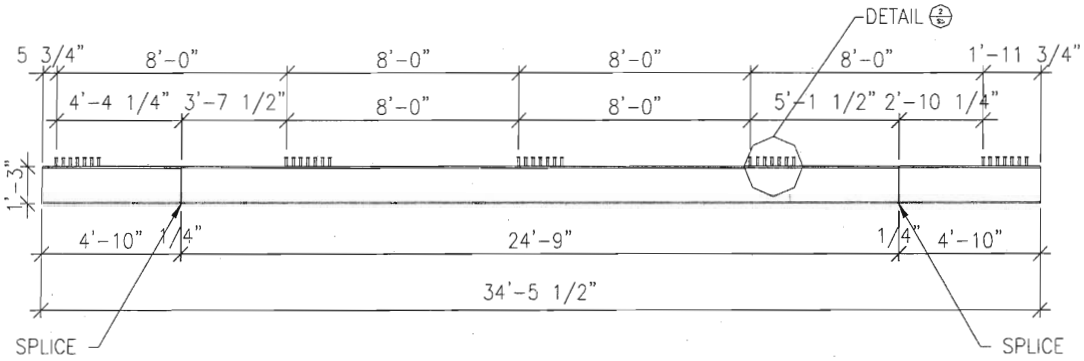

a) Beams A and B studs layout

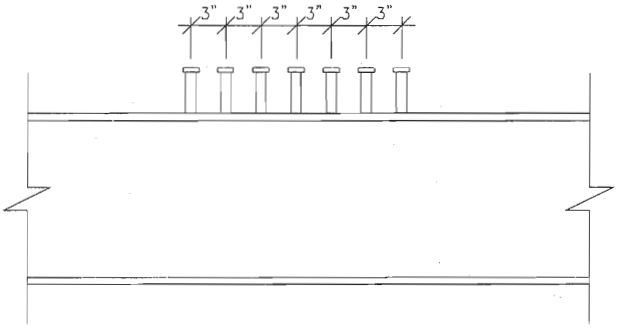

b) Configuration of the stud clusters

Figure 8.3.2.1 – 3 - Shear stud configurations of the longitudinal beams

8.3.2.2 DECK SLAB

A 6 in. deck slab with ¾ in. haunch was reinforced with two layers of WWR (D4xD4 @ 4 x 4). The WWR splices were 4 in. in each direction. The bottom layer had clear cover of 1.5 in., while the top WWR layer had 2 in. clear cover as shown in Figure 8.3.2.2 – 1. The concrete strength development with time is shown in Table 7.3.2.2 – 1.

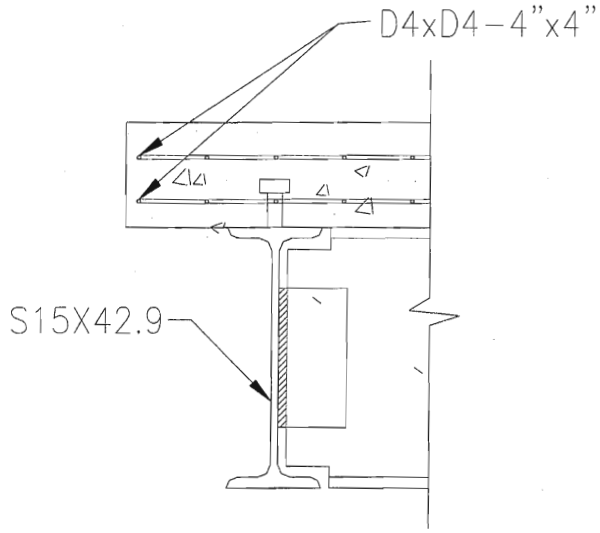

Figure 8.3.2.2 – 1 - Deck reinforcement

Table 8.3.2.2 – 1 - Concrete strength development with time

Day	Strength (psi)
1	1,967
4	4,469
7	5,707
27	6,452

8.3.3 TESTING THE SPECIMEN

A series of seven tests was performed on the specimen.

8.3.3.1 TEST 1

The first test was performed during casting the deck slab. Temporary supports were placed at the mid span of the longitudinal beams during pouring the slab. In this test, four strain gauges were placed on the longitudinal beams at the temporary support location. The strain gauges were placed on the top and bottom flanges of the longitudinal beams as shown in Figure 8.3.3.1-1.

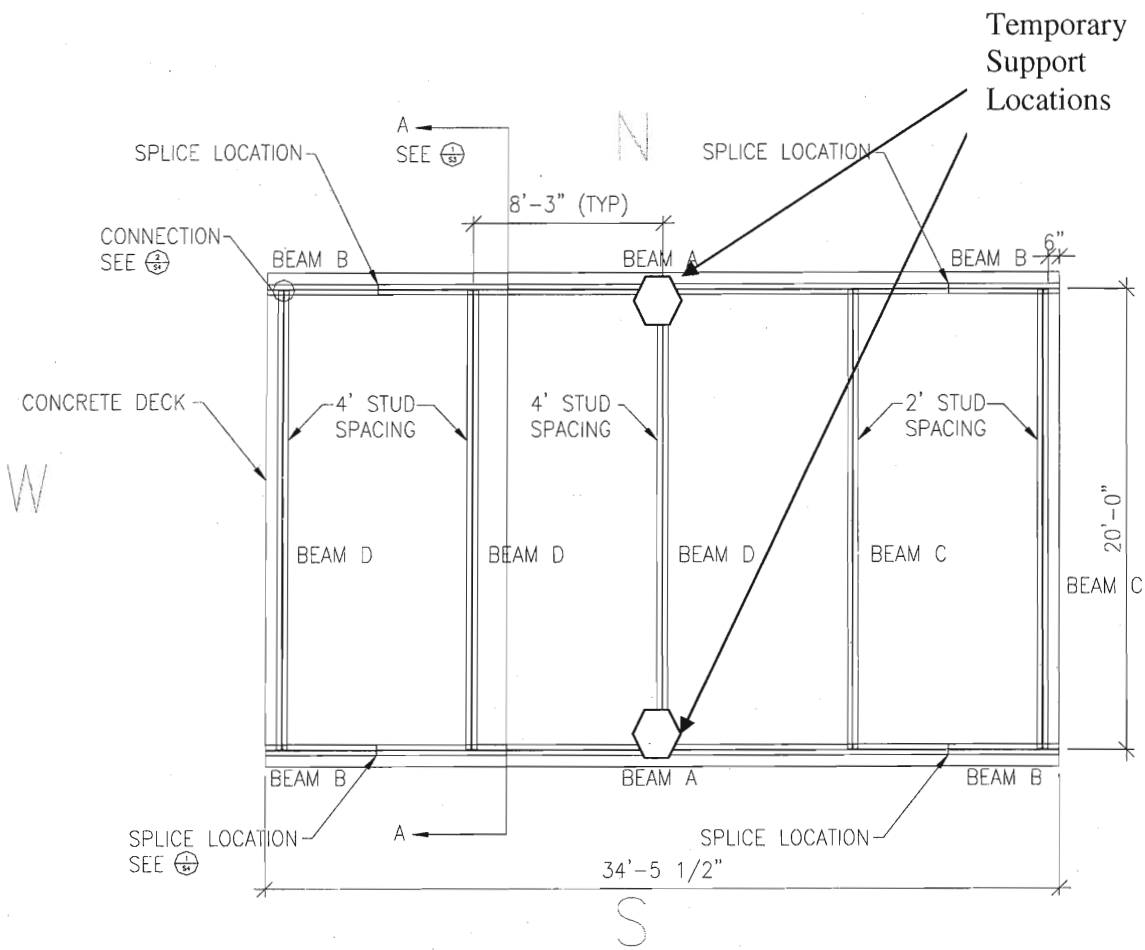

Figure 8.3.3.1-1 – Test 1 loading locations

8.3.3.2 TEST 2

Test 2 was performed by releasing the temporary supports after the concrete slab gained the strength of 5.5 ksi. Releasing the supports underneath the longitudinal beams after the slab hardened results in applying two vertical forces on these longitudinal beams that equal to the reactions from the supports on the composite sections. Nine concrete strain gauges were placed on the top of the concrete slab as shown in Figure 8.3.3.2-1. Four steel strain gauges were placed in the same position as in test 1. Deflection was also measured during the release of the support reactions.

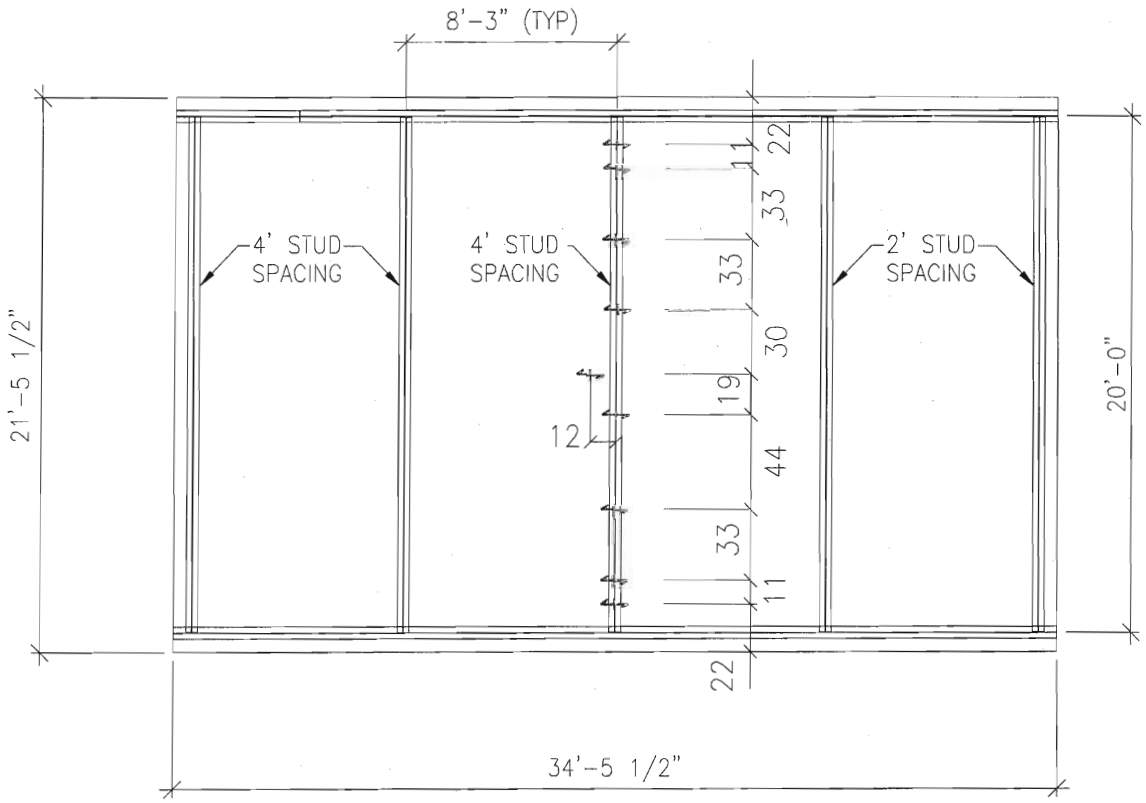

Figure 8.3.3.2-1 – Location of the strain gauges for Test 2

8.3.3.3 TEST 3

In this test, two vertical loads were applied to the specimen instead of releasing the reaction as was done in test 2. Two concentrated point loads were applied above the middle cross-beam as shown in Figure 8.3.3.3-1. Strain gauge locations were similar to those of test 2, with minor modifications to accommodate load locations.

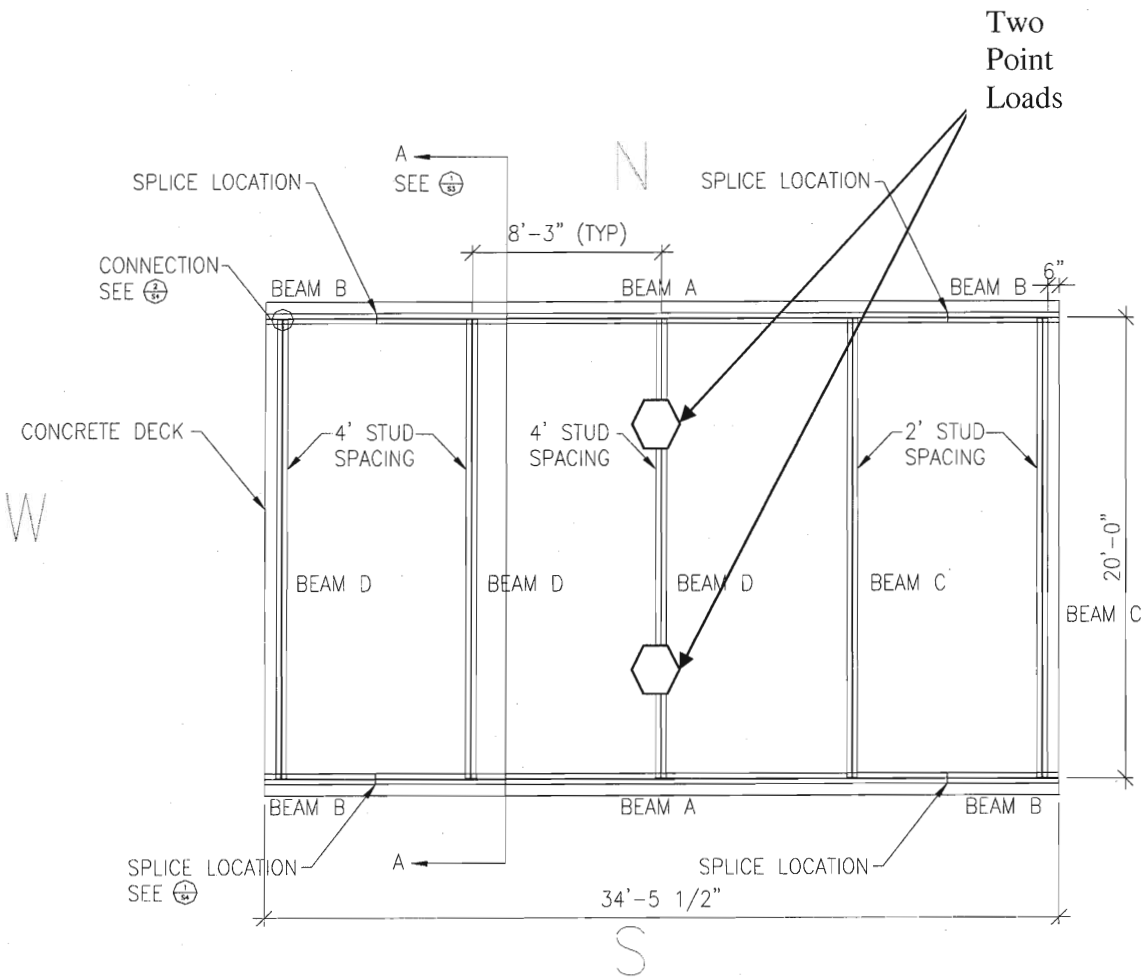

Figure 8.3.3.3-1 - Load application for test 3

8.3.3.4 TESTS 4, 5, 6 AND 7

The following four tests were performed on individual cross-beams. Test 4 was performed on the first beam from the west side of the specimen. Test 5 was performed on the second beam from the west. Test 6 was performed on the first beam from the east side of the specimen. Test 7 was performed on the second beam from the east. Figure 8.3.3.4-1 shows the tested beams.

In these above series of tests, two point loads were applied to each test beam. The location of these two point loads are shown on the same figure. In these tests, the loads

were applied to each of the cross-beams until the load passed the calculated strength of the beam, considering that the effective slab width is the spacing between the cross-beams in tests 5 and 7, and half the cross-beam spacing added to the overhang in tests 4 and 6.

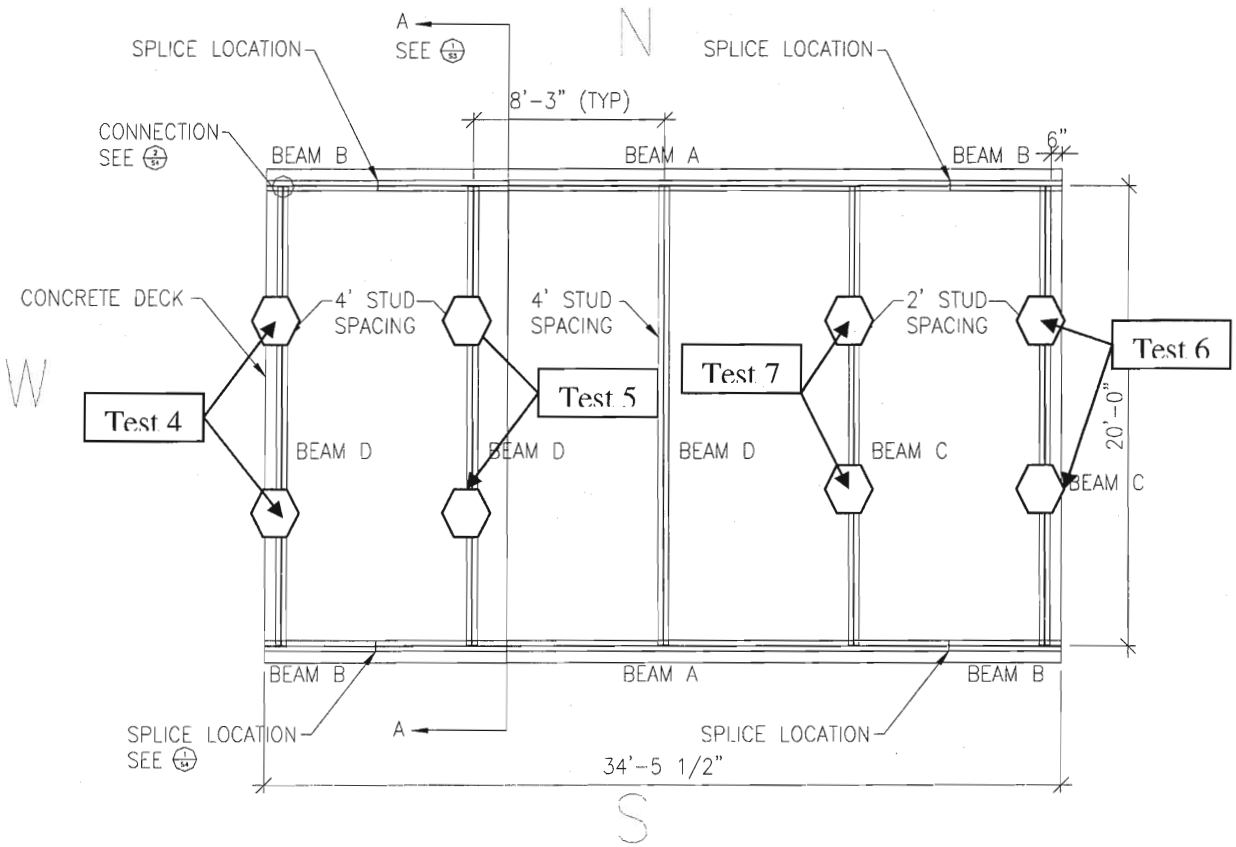

Figure 8.3.3.4-1 - Load application for tests 4, 5, 6 and 7

8.4 RESULTS AND DISCUSSION

For test 2, the predicted and measured deflection were 0.4 in. and 0.44, respectively. The strain gauge readings are presented in Figure 8.4-1.

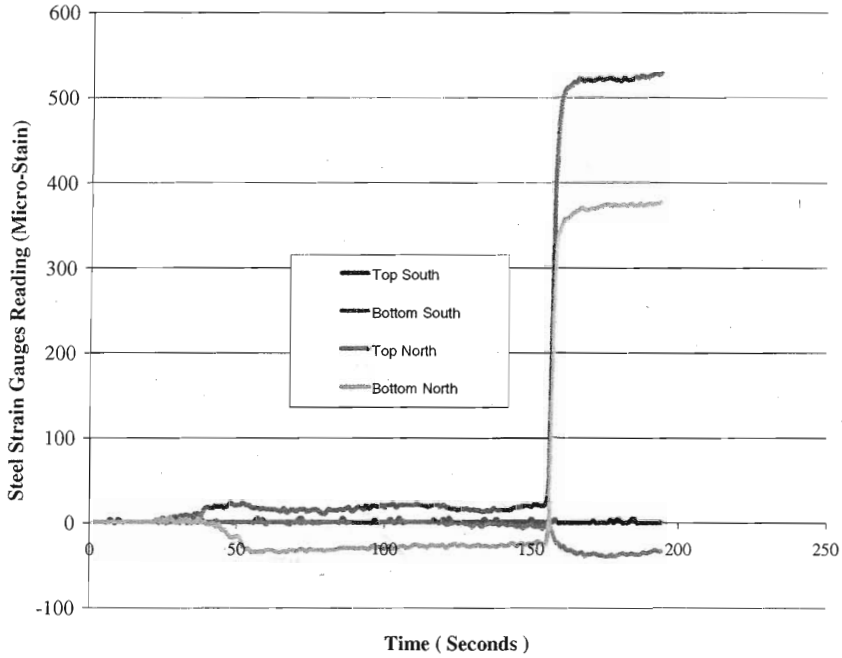

a) Steel strain gauge readings

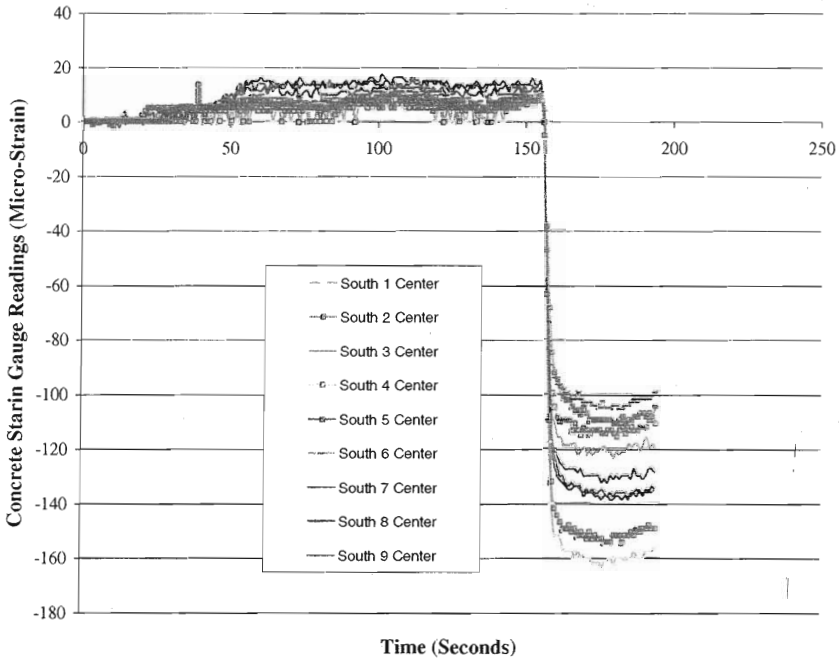

b) Concrete strain gauge readings

Figure 8.4-1 – Test 2 Results

Figures 8.4-2, 8.4-3, and 8.4-4 show the steel strain gauge readings, the concrete strain gauge readings, and the deflection versus loads for test 3.

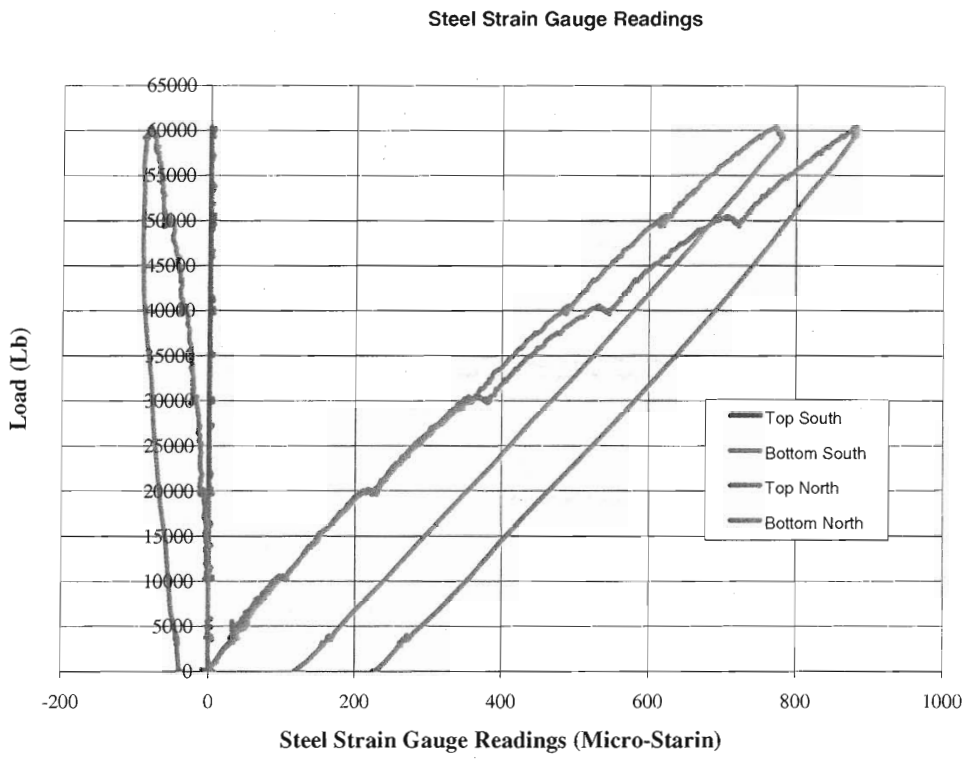

Figures 8.4-2 - Test 3 steel strain gauge readings

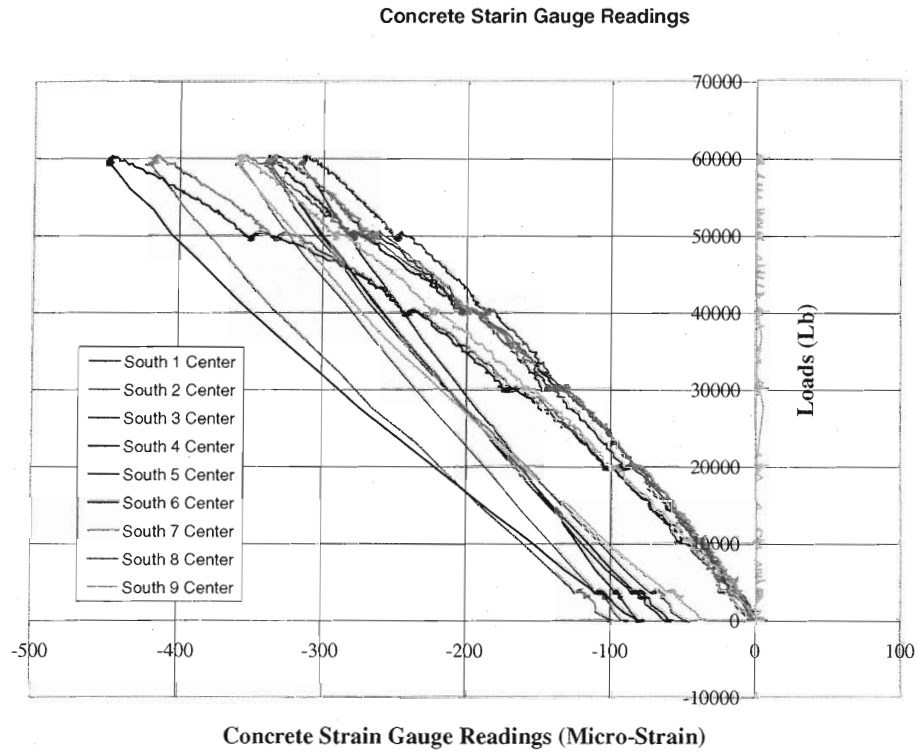

Figures 8.4-3 - Test 3 concrete strain gauge readings

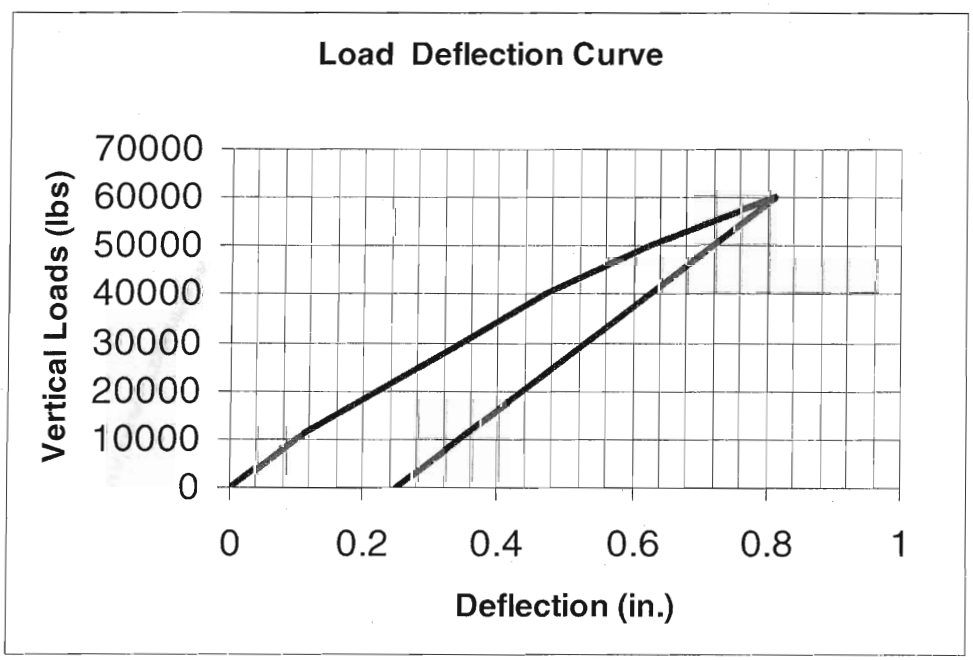

Figures 8.4-4 - Test 3 load-deflection curve

Table 8.4-1 shows the predicted failure and stop loads for tests 4, 5, 6 and 7. Figure 8.4-5 shows an example of a load deflection curve, for test 6.

Table 8.4-1 - Predicted and tested loads for tests 4 through 7

Test Number	Studs Spacing (feet)	Predicted Failure load (kips)	Test Load Release Without Failure (No Load Drop) (kips)
Test 4	4	145	159
Test 5	4	165	173
Test 6	2	165	162
Test 7	2	145	173

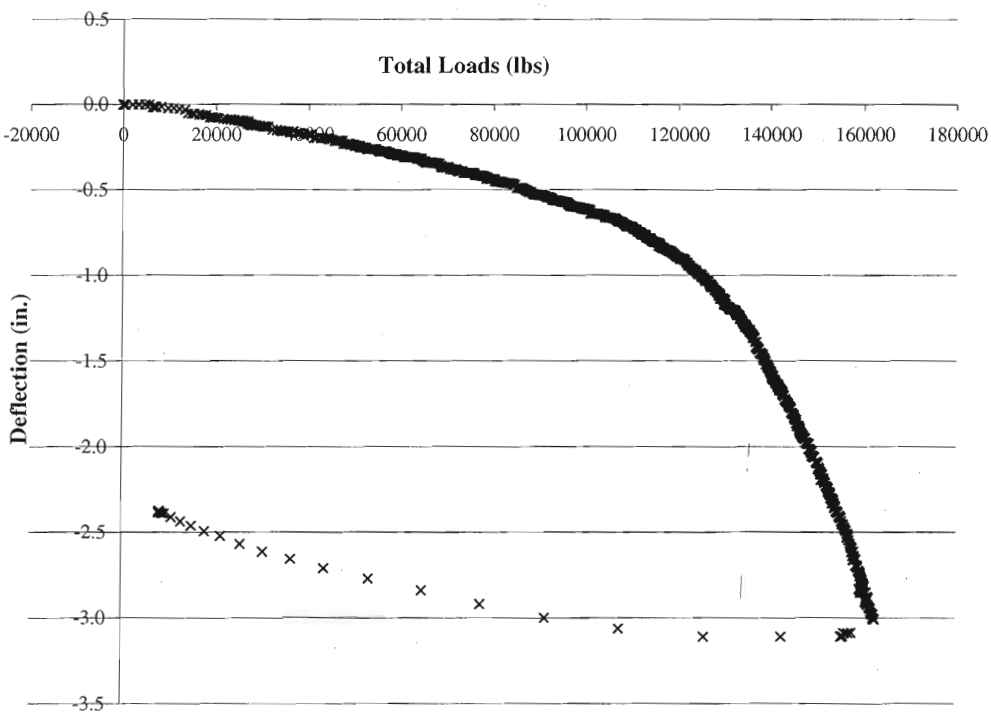

Figure 8.4-5 – Test 6 lead deflection curve

SECTION 9: ARCH BRIDGE FINITE ELEMENT MODELING

9.1 OBJECTIVES

The objectives of this section are to assist the design of the arch bridge and to investigate the effective flange width that is needed to act compositely with the arch bridge bottom chord using the Finite Element Model.

9.2 INTRODUCTION

Two-dimensional finite element modeling was explained in detail in section 4. However this two- dimensional model cannot estimate the effective slab width, which should be considered in the analysis of the bottom chord of the arch bridge. The assumption that was considered in section 4 was that the full width of the slab was acting compositely with the bottom chord of the arch. In this section, a three-dimensional finite element model was created to confirm the assumption of using the full width of the deck slab.

9.3 MODELING

RISA 3D was used to model the bridge. The bridge was modeled at one stage, which was the stage where the deck slab was hardened and there were three trucks on the bridge. Six elements were used to model the different bridge elements as follows.

9.3.1 HANGERS MODELING

The hangers were modeled as beam elements. Both ends were released from moments. The cross-section of this element was circular, with 1.75 in. diameter. The material of the

hanger was steel with Young's modulus equal to 29,000 ksi and yield strength equal to 127 ksi.

9.3.2 ARCH TOP CHORD MODELING

Each arch was composed of two steel pipes grade 50 ksi filled with 8 ksi concrete. The wall thickness of the steel tube was ½ in. as shown in Figure 9.3.2-1. The arch was modeled as a beam element as well. The section properties of this element were modeled as a composite steel transformed section. For simplicity, the arch was modeled as straight, and not curved lines between the hangers . For the material and section properties of the element see Appendix D.

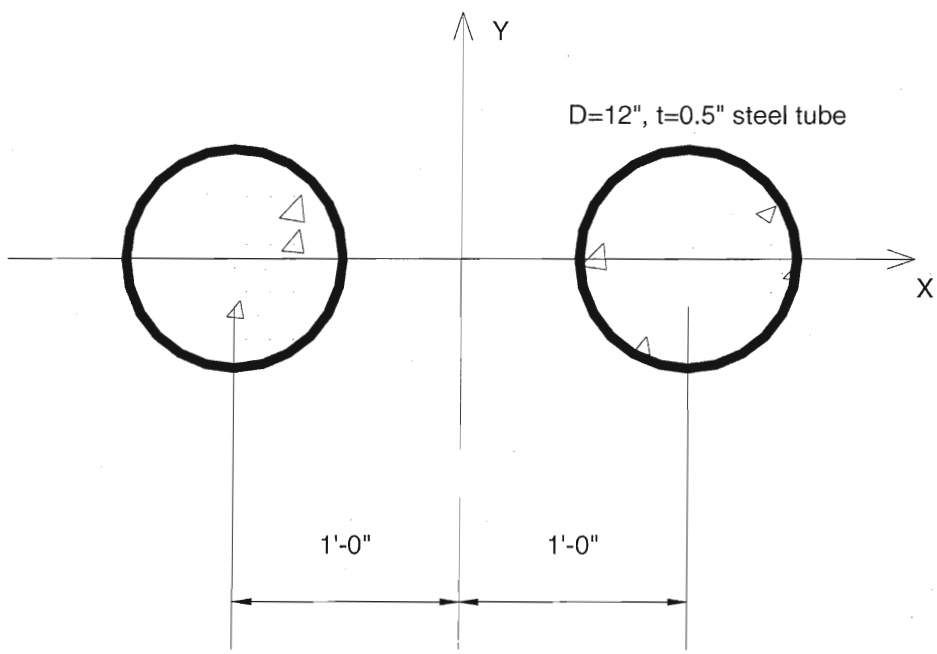

Figure 9.3.2-1- Arch top chord element

9.3.3 ARCH BOTTOM CHORD MODELING

Each bottom chord was composed of 24 in. x 24 in. built-up tube grade 50 steel filled with 8 ksi concrete. The wall thickness of the steel tube was ½ in. Each bottom chord was modeled as a beam element as well. 4ft-61/4 in. of the deck slab was included in the section properties of the bottom chord element. The section properties of this element are the section properties of the composite steel transformed section. For the material and section properties of the element see Appendix D.

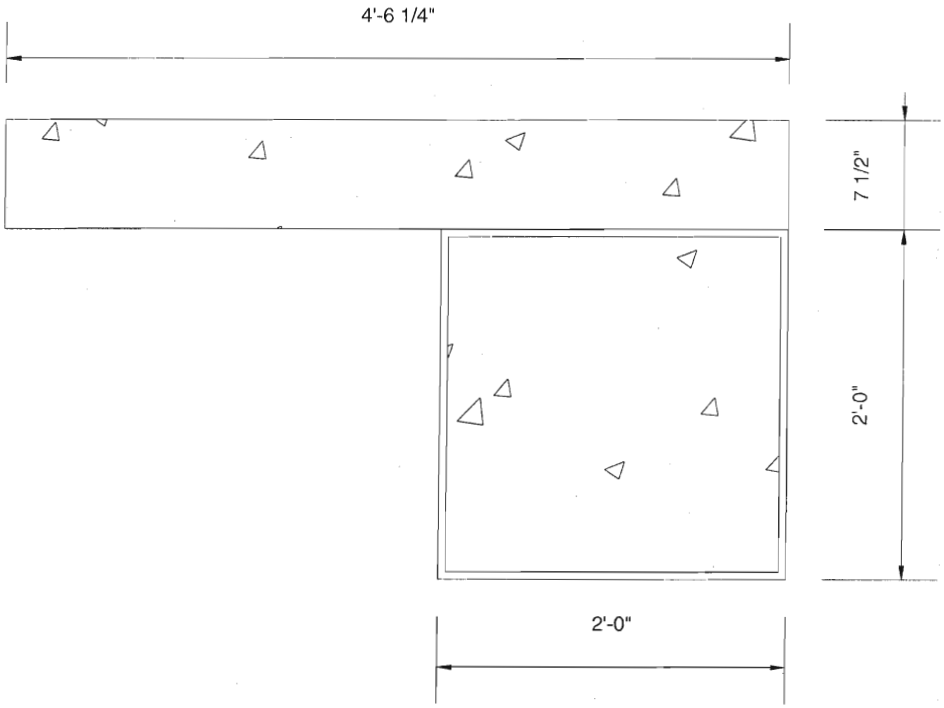

Figure 9.3.3-1- Arch bottom chord element

9.3.4 DECK SLAB MODELING

The deck slab had 7.5 in. concrete structural depth. The deck slab was also modeled as a beam element with a width of 7 ft- 1 in. in the direction of the traffic as shown in Figure 9.3.4-1. The weight of the slab was calculated based on 8 in. thickness. However, the unit weight of the element was reduced to half to account for the unit weight of the slab that was considered in the other direction along the cross-beams as will be shown in the cross-beam element modeling. For the material and section properties of the element see Appendix D

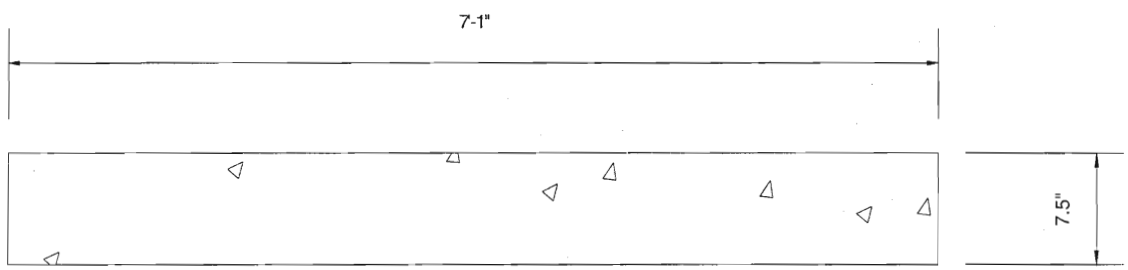

Figure 9.3.4-1- Deck slab element

9.3.5 TURNDOWN BEAM MODELING

The two beams at the end of the two arches were modeled as beam elements as well. Figure 9.3.5-1 shows a cross section of the beam with part of the slab that was considered in modeling this beam. For the material and section properties of the element see Appendix D.

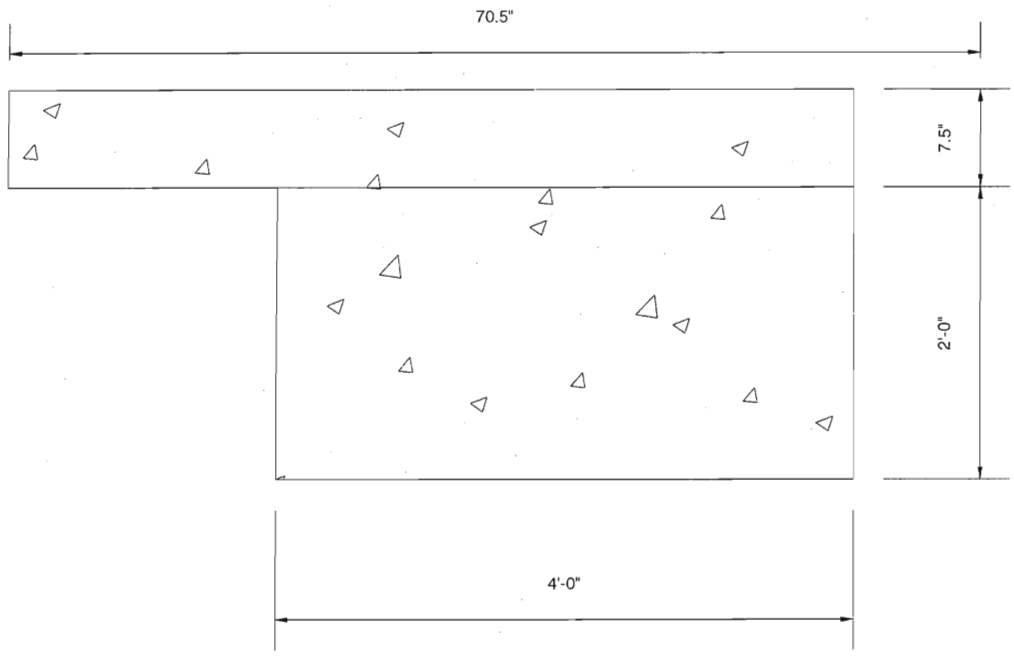

Figure 9.3.5-1- Turndown beam element

9.3.6 CROSS-BEAM MODELING

The cross-beams were designed to be W24 x 250 grade 50 steel. The cross-beams connected the bottom chords of the two arches. The cross-beams were modeled as beam elements as well. 8ft-9 in. from the deck slab is included in the section properties of the bottom chord element. The unit weight of the element was reduced to half to account for the unit weight of the slab that was considered in deck slab element as mentioned earlier. The section properties of this element are the section properties of the composite steel transformed section. For the material and section properties of the element see Appendix D.

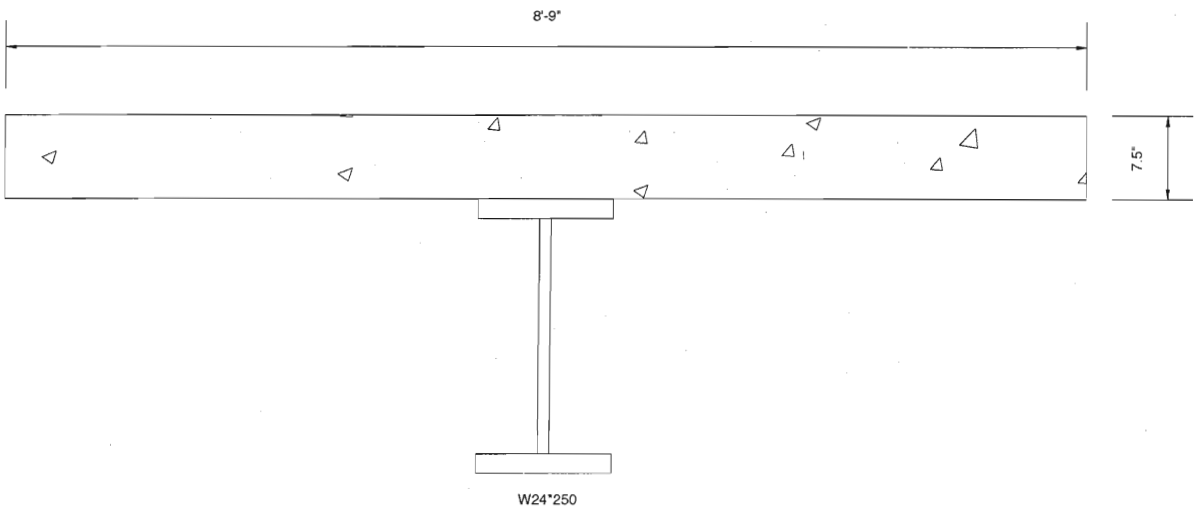

Figure 9.3.6-1- Cross-beam element

9.4 LOADINGS AND ANALYSIS

RISA 3D program was used to run the analysis as mentioned earlier. The bridge was divided into 239 joints, 426 elements. The loads that were considered in the modeling were the total dead load and three HS25. The HS25 truck loading included a presence factor of 0.9, and impact factor of 1.167.

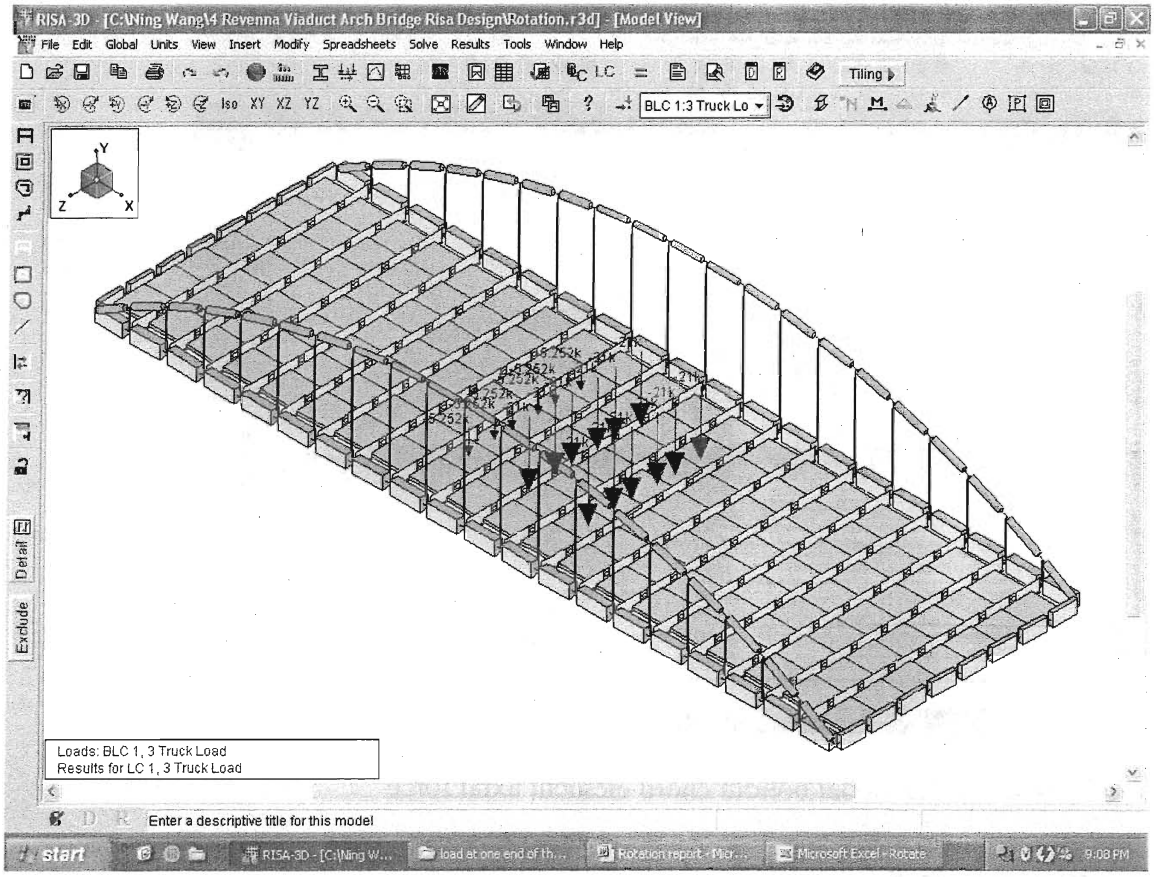

Figure 9.4-1- RISA 3D Model

9.5 RESULTS AND DISCUSSION

9.5.1 RESULTS IN THE TRAFFIC DIRECTION

The forces resulting from the 3D modeling on the bottom chord were much less that the forces from the 2D modeling due to that fact that some of these forces were carried by the deck slab as can be seen from the deference between the axial forces of the 3D and the 2D model shown in Figures 9.5.1-1 and Figures 9.5.1-2 . However the bending moment was not significantly different because the deck slab carried very little moment in the direction of the bottom chord as shown in Figures 9.5.1-3 and Figures 9.5.1-4.

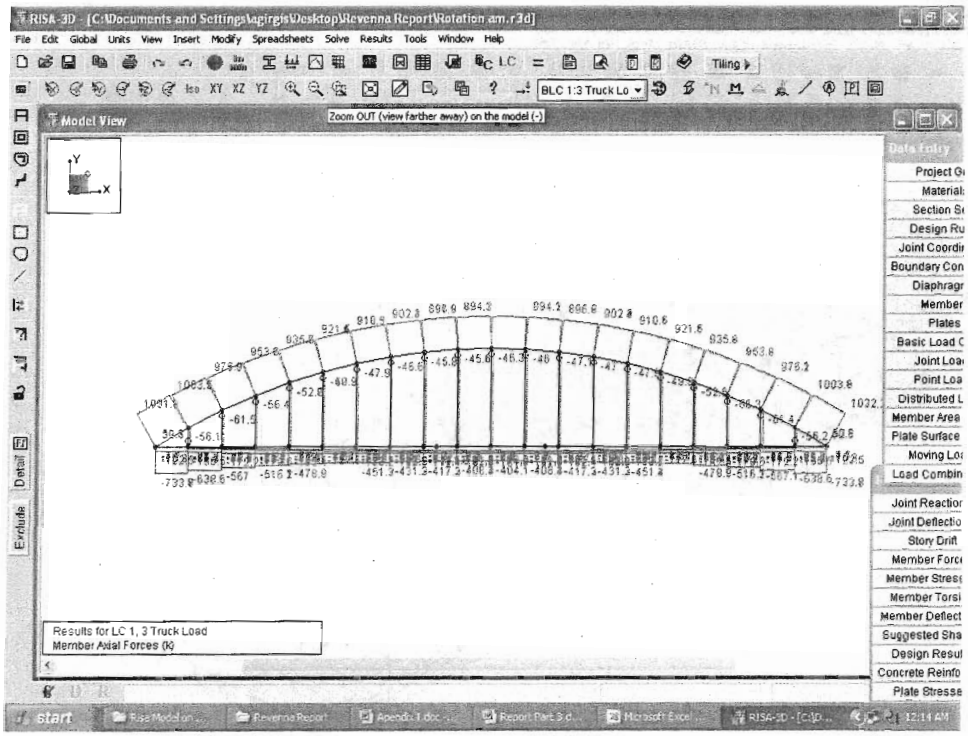

Figure 9.5.1-1- 3D model bottom chord element axial force

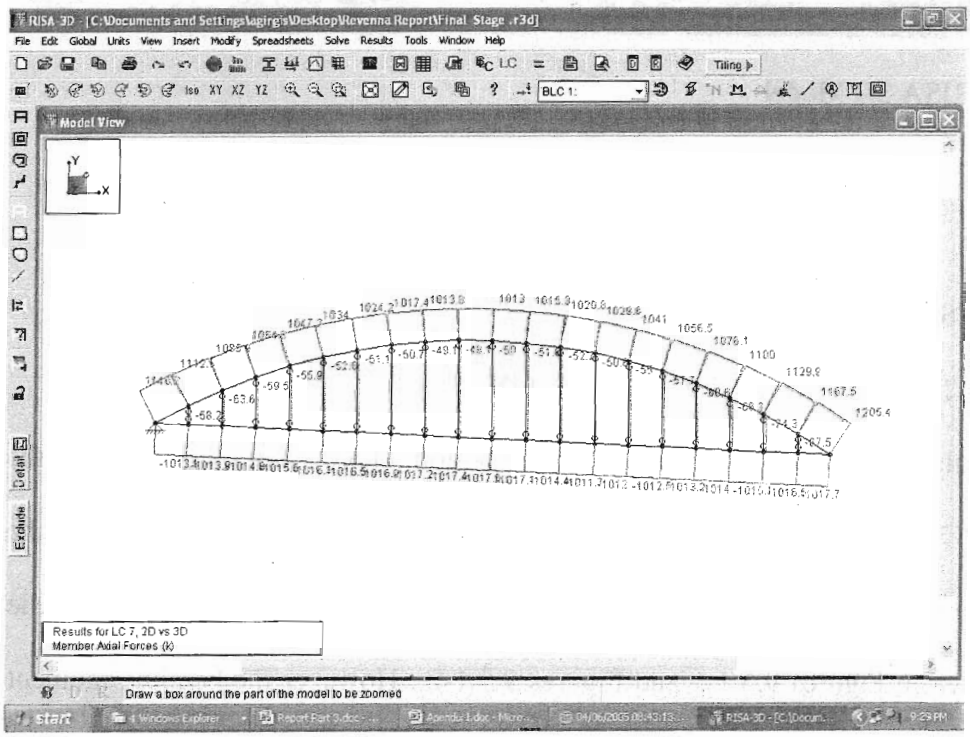

Figure 9.5.1-2 - 2D model bottom chord element axial force

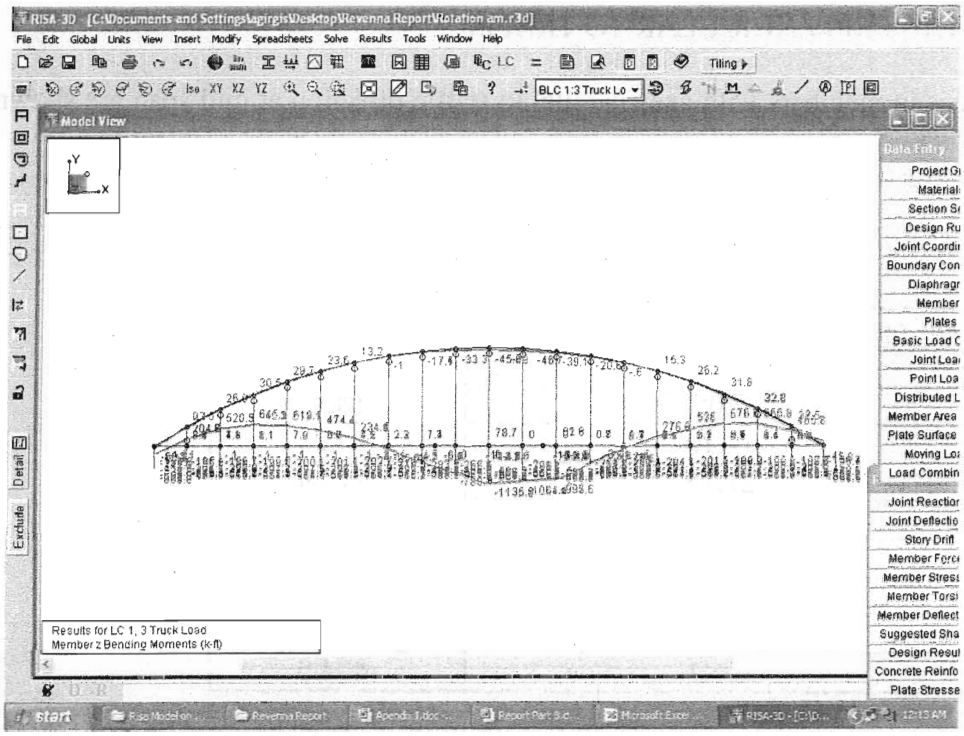

Figure 9.5.1-3- 3D Model bottom chord element moment about Z-Z direction

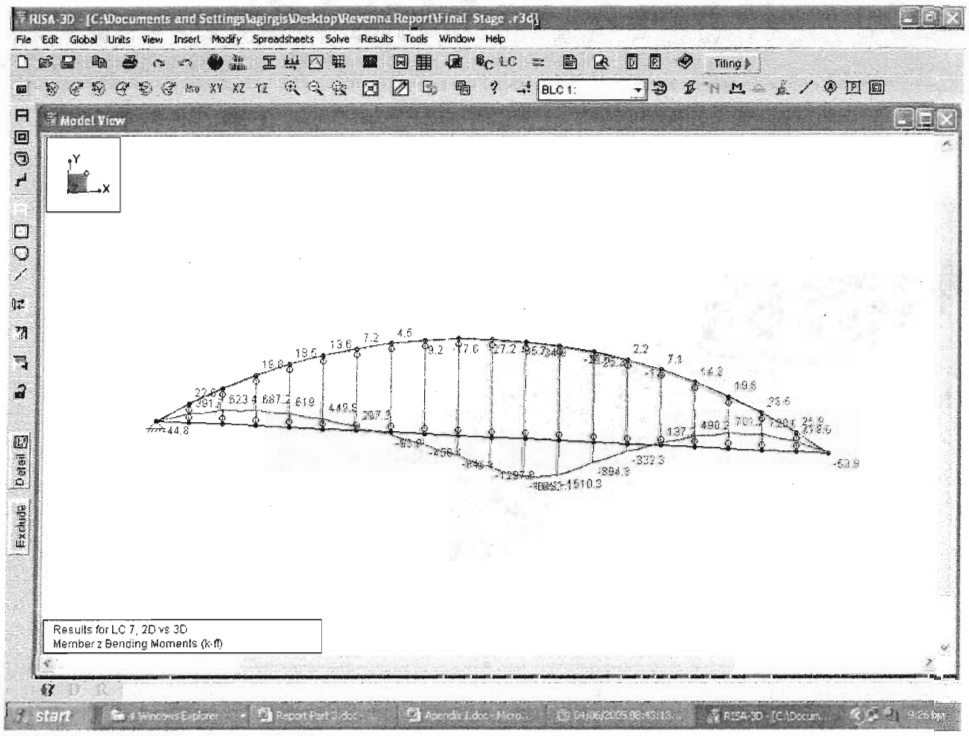

Figure 9.5.1-4- 2D Model bottom chord element moment about Z-Z direction

9.5.2 RESULTS PREPENDICULAR TO TRAFFIC

The axial forces in members with axes parallel to traffic direction at mid span are shown in Table 9.5.2-1 and Figures 9.5.2-1 and 8.5.2-2.

Table 9.5.2-1 Axial forces of the deck cross section

Member	Distance from Left Bottom Chord (ft)	Axial force (kips)
M617	0.00	-440.0
M631	7.05	-182.7
M628	14.10	-142.4
M759	21.15	-113.9
M193	28.21	-103.6
M207	35.26	-113.9
M76	42.31	-142.4
M79	49.36	-181.9
M65A	56.41	-404.0

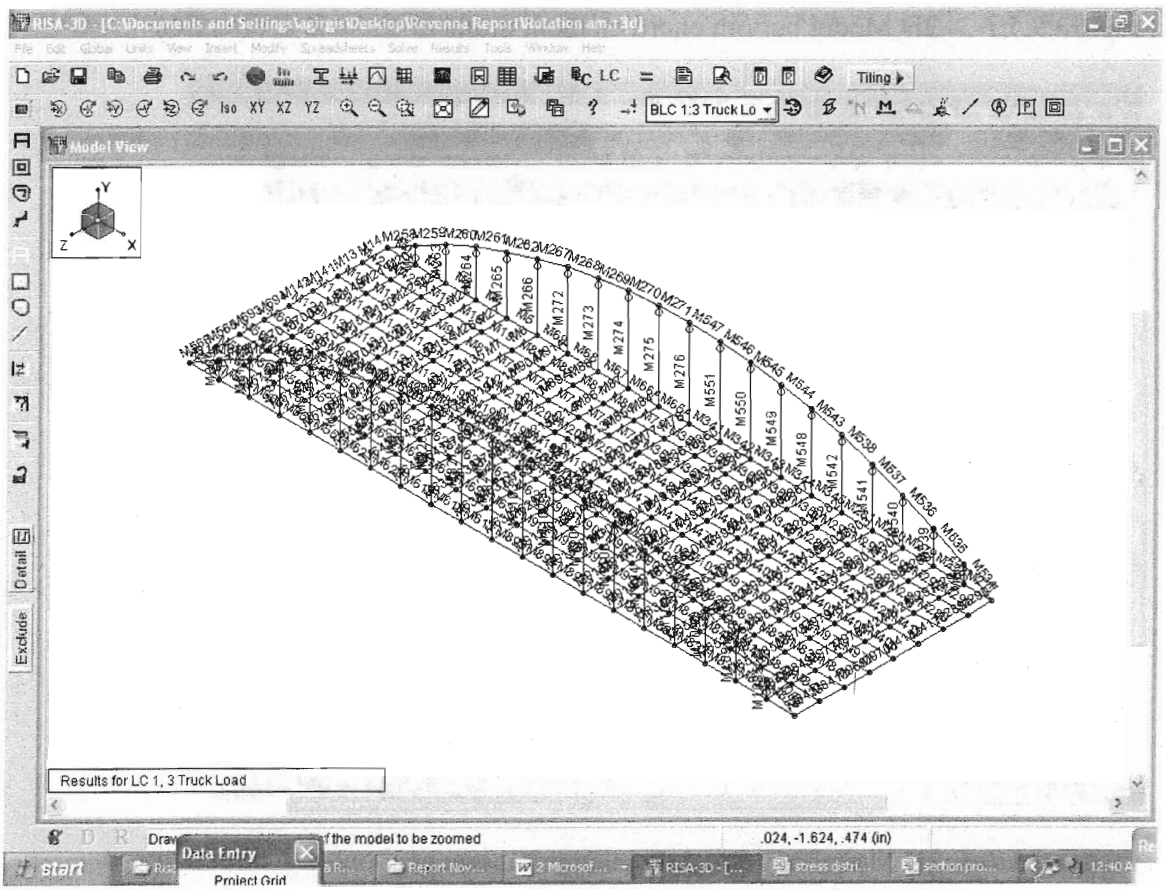

Figure 9.5.2-1 - Pictures of the member numbers of the 3D model

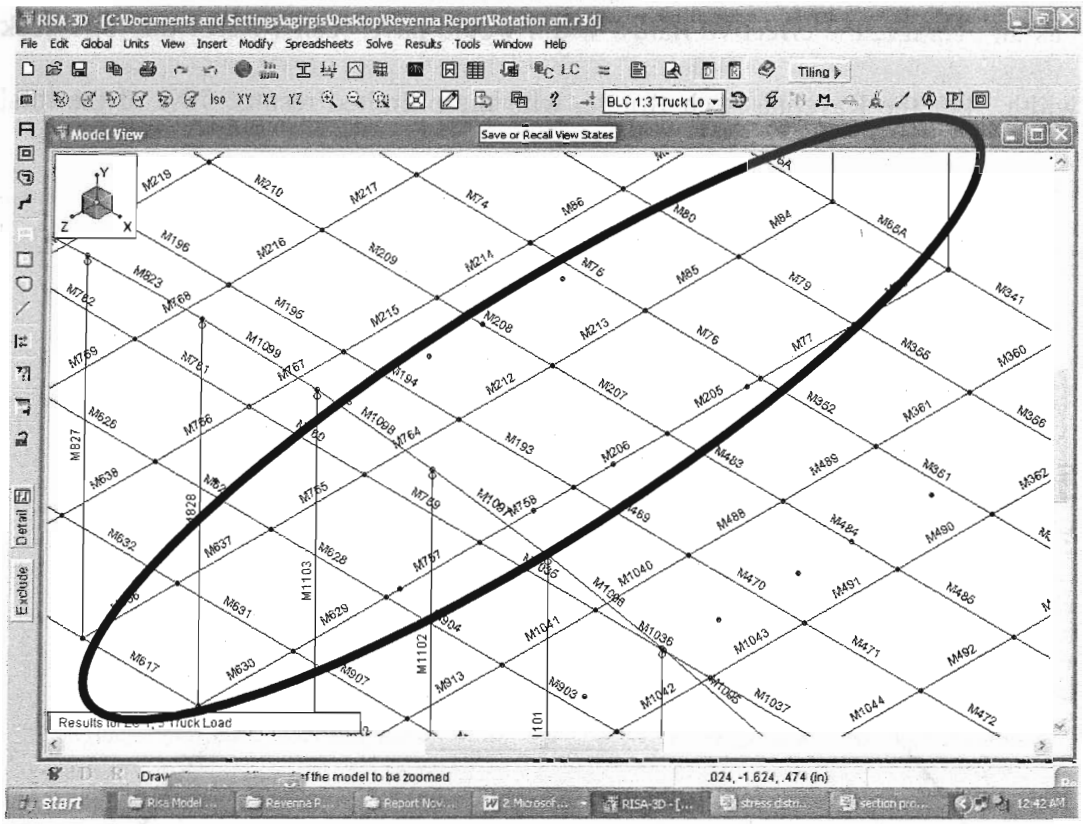

Figure 9.5.2-2- Mid-span member numbers

Stresses were calculated in the slab at the lactation of the bottom chord by distributing the axial tension force over the bottom chord tube and the slab proportionately to their areas. To minimize the variables in calculating the flange effective width, only axial force stresses were distributed along the cross-section of the slab at the bridge mid-span as shown in table 9.5.2-1.

9.5.3 DISCUSSION ON STRESS DISTIBUTION ALONG THE MID-SPAN CROSS SECTION WIDTH

From Figure 9.5.3-1, it can be concluded that the whole width of the cross-section was contributing to the flexural strength of the bottom chord in resisting the external loads on the bridge. However if the maximum stresses in the bridge mid-span cross-section were

taken as an average, the effective flange width would have been 70% of the total deck slab width. For the Ravenna Arch Bridge, with these limited results, 70% of the total deck slab width is proposed as an effective width.

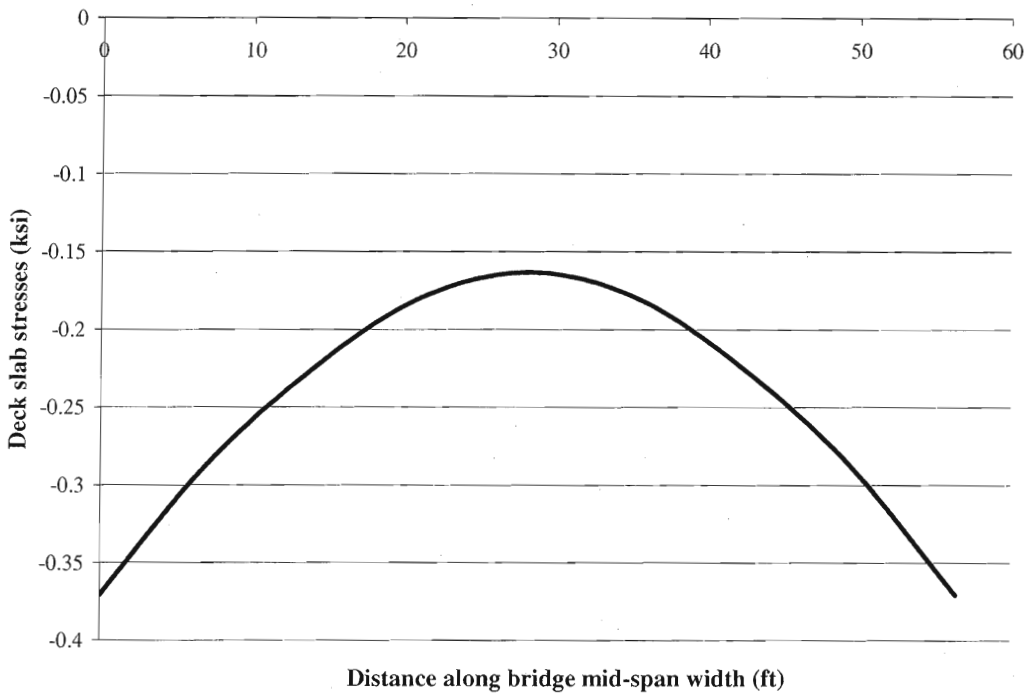

Figure 9.5.3-1 - 3D model output deck slab axial stresses along the bridge mid-span

9.6 IMPACT OF USING 70 PERCENT OF TOTAL SLAB WIDTH ON BOTTOM CHORD STRENGTH

There is little impact when using 70% of the deck slab width on the bottom chord strength. The interaction diagram for the bottom chord is drawn using the full width of the bridge deck slab and 70% of the bridge deck slab width. There are no differences in the negative moment capacity. However there is an eight percent reduction in the live load rating at the positive moment sections as shown in Figure 9.6-1. Refer to Appendix

Cfor the coordinates of the interaction diagram using 100 and 70 percent of the deck slab as an effective width.

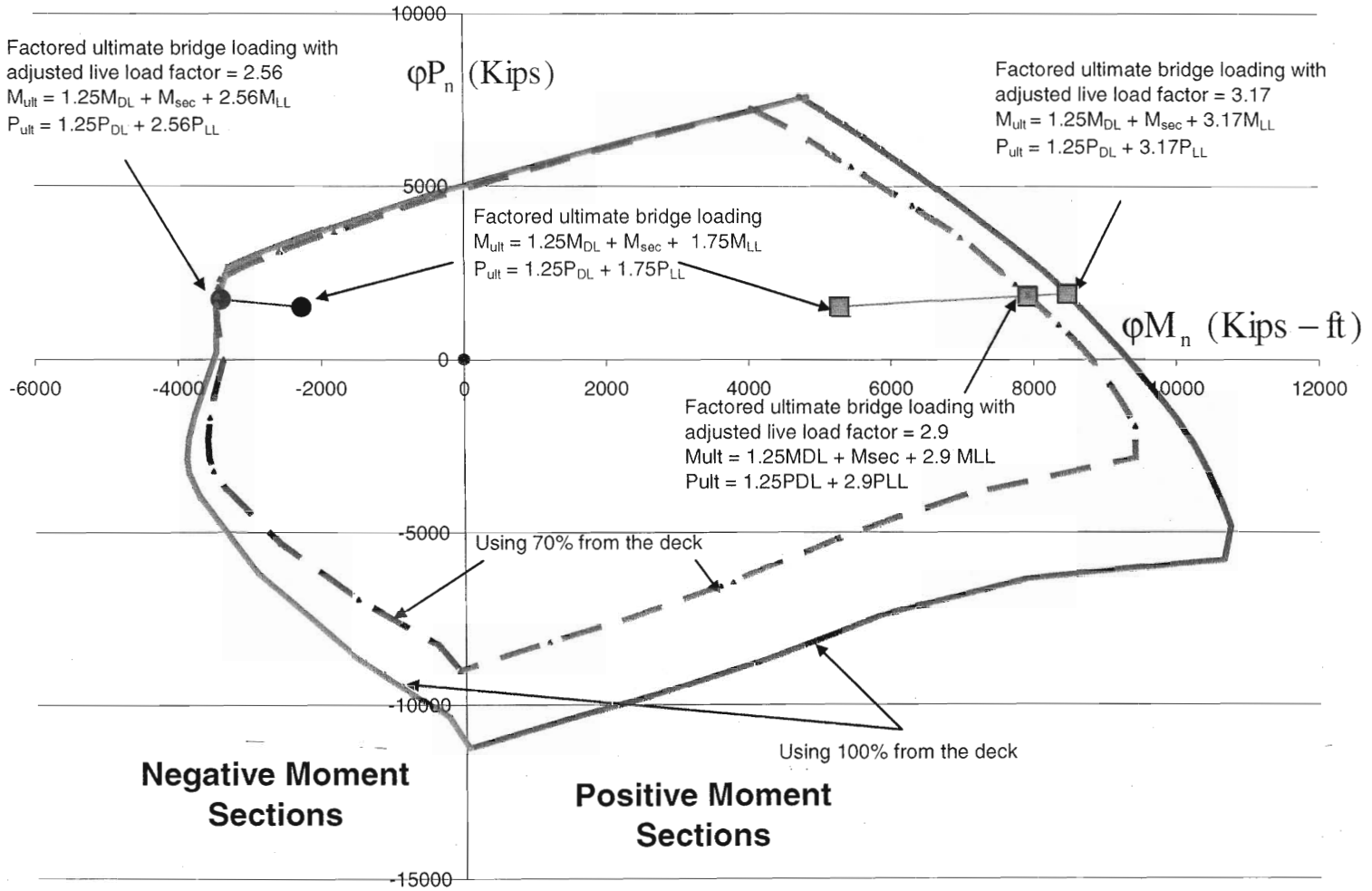

Figure. 9.6-1- Ravenna bottom chord interaction diagram using 100% and 70% from deck slab

SECTION 10: CONSTRUCTION CHALLENGE

10.1 INTRODUCTION

Ravenna viaduct spans a major route of the Burlington Northern Santa Fe Railroad. Approximately 60 trains per day pass under the bridge. There are very tight restrictions on the vertical clearance above the tracks, the horizontal distance to any pier, and the amount of time rail traffic can be interrupted. The bridge is 174 ft. long to span over 6 sets of rail tracks, two main lines and four sidings. Since this section of track is a major route for the railroad, the amount of time the tracks can be closed is limited to a few hours, and only a limited number of closures. The section describes in detail the rapid construction sequencing. Visitors to town pass over the Ravenna Viaduct as they approach town on Route 68 from the south. Route 68 is the main entrance into town from the south, and the only access without having to cross railroad tracks. Thus, it was important to the town to minimize construction time.

This prefabricated developed system was found to be suitable for accelerated construction, as well as the constraint of working over live main railroad tracks. The old bridge was scheduled to be replaced because it was structurally deficient and functionally obsolete.

10.2 CHOSEN SYSTEMS TO ACCELERATE CONSTRUCTION

10.2.1 SUBSTRUCTURE SYSTEM

Typically the time needed to construct the substructure of a bridge can take a large amount of the total project construction time. It was important to have a substructure

system that could be constructed prior to closing the existing bridge or a precast system that can be rapidly built. As shown in *Figure 10.2.1-1*, for the Ravenna Viaduct project a system of 8 ft. dia. drilled shafts with 8 ft. x 6.5 ft columns placed under each corner of the arch was chosen. Since the new bridge is considerably wider than the existing, the substructure system was completed without any major interruptions to traffic.

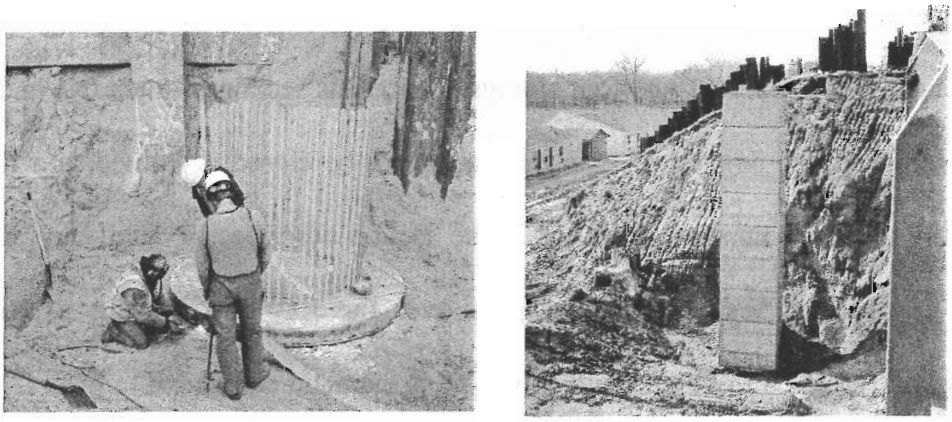

Figure 10.2.1-1- Construction of substructure

10.2.2 SUPERSTRUCTURE CONSTRUCTION SYSTEM SELECTIONS

The selected system was to assemble the two arches on the existing bridge deck, and then install them on the columns and brace them against the old bridge as shown in *Figure 10.2.2-1*. The new bridge is wider than the old bridge, which allowed for the four columns to be built on both sides of the old bridge, and the arches installed on them, without needing to demolish the old bridge. The two arches were braced against each other with temporary bracing as shown in *Figure 10.2.2-2*. The floor beams and the metal decking were installed as the old bridge was demolished as shown in *Figure 10.2.2-3*. A self consolidating concrete was pumped into the arches and tie beam. Post-tensioning was introduced after the concrete gained the required strength as shown in *Figure 10.2.2-4*.

Then deck reinforcement was installed as shown in *Figure 10.2.2-5.* The deck slab was poured and post-tensioned after gaining the required strength as shown in *Figures 10.2.2-6* The temporary cross beams tying the two arches from the top were also removed after the concrete deck gained the required strength. *Figures 10.2.2-7* shows pouring the railing that was done after post-tensioning the deck slab.

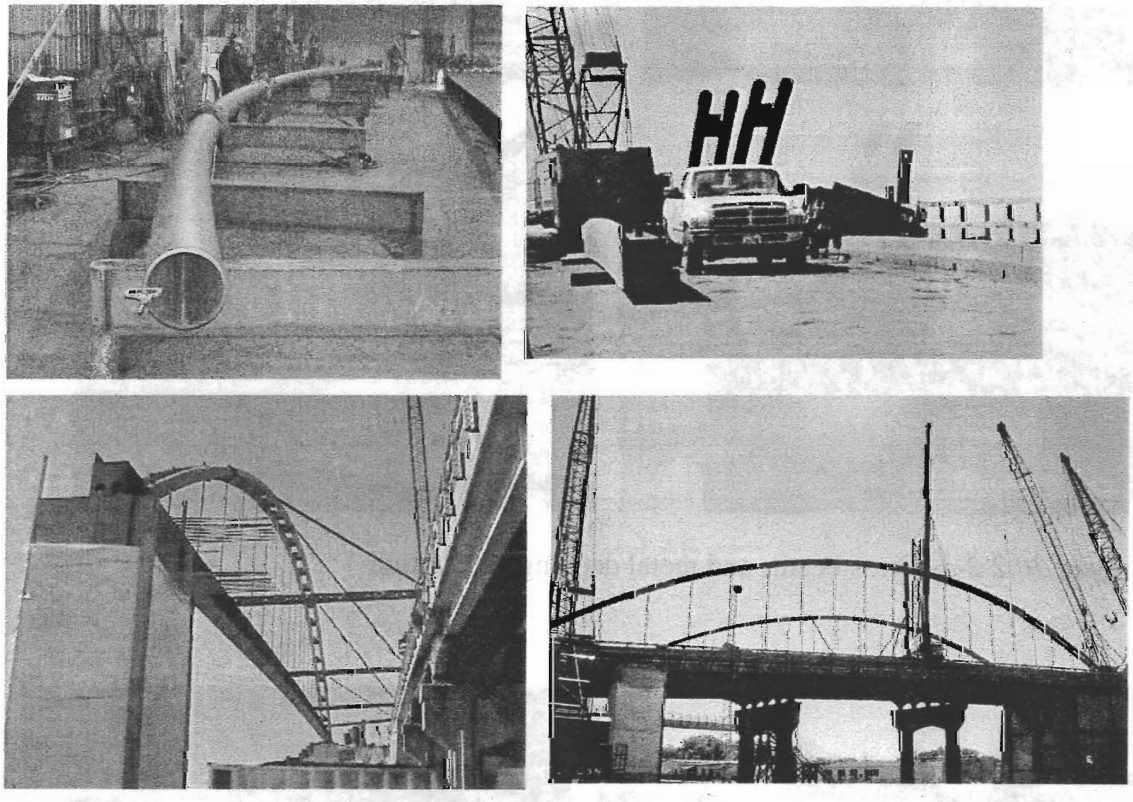

Figure 10.2.2-1- Construction of the two arches

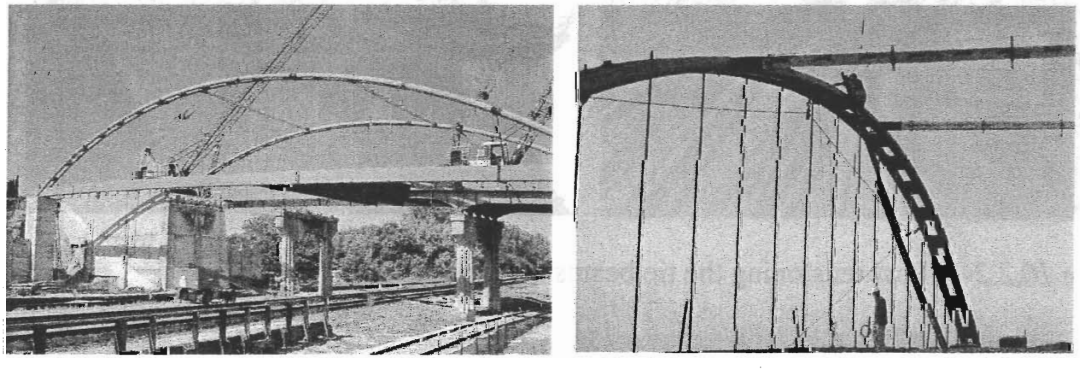

Figure 10.2.2-2- Arches temporary bracing

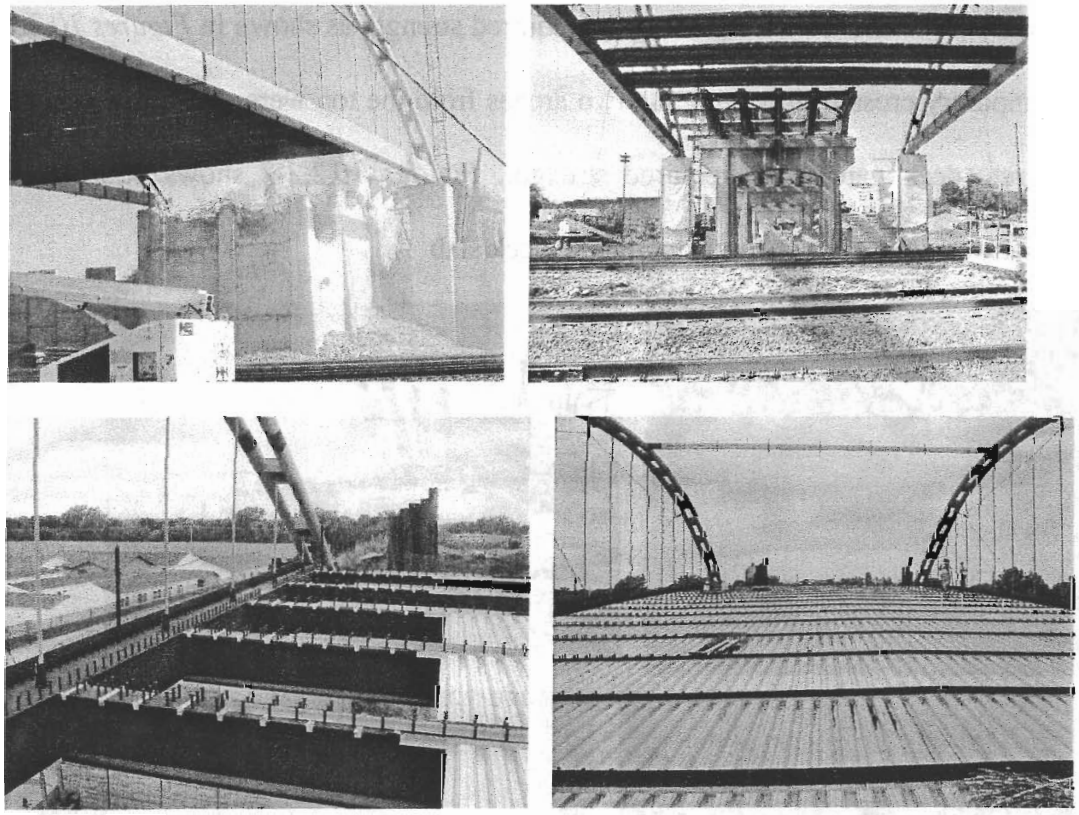

Figure 10.2.2-3- Cross beams and metal decking installation

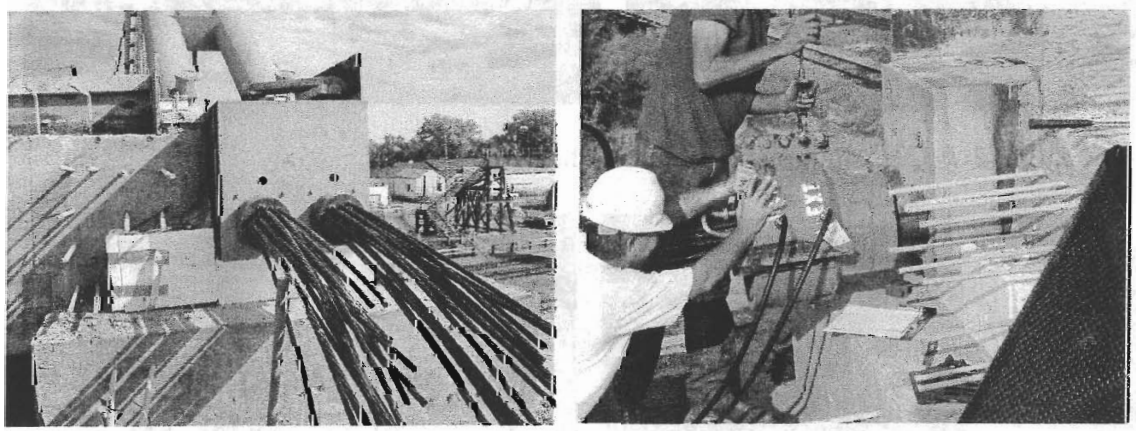

Figure 10.2.2-4- Post-tensioning the tie beams

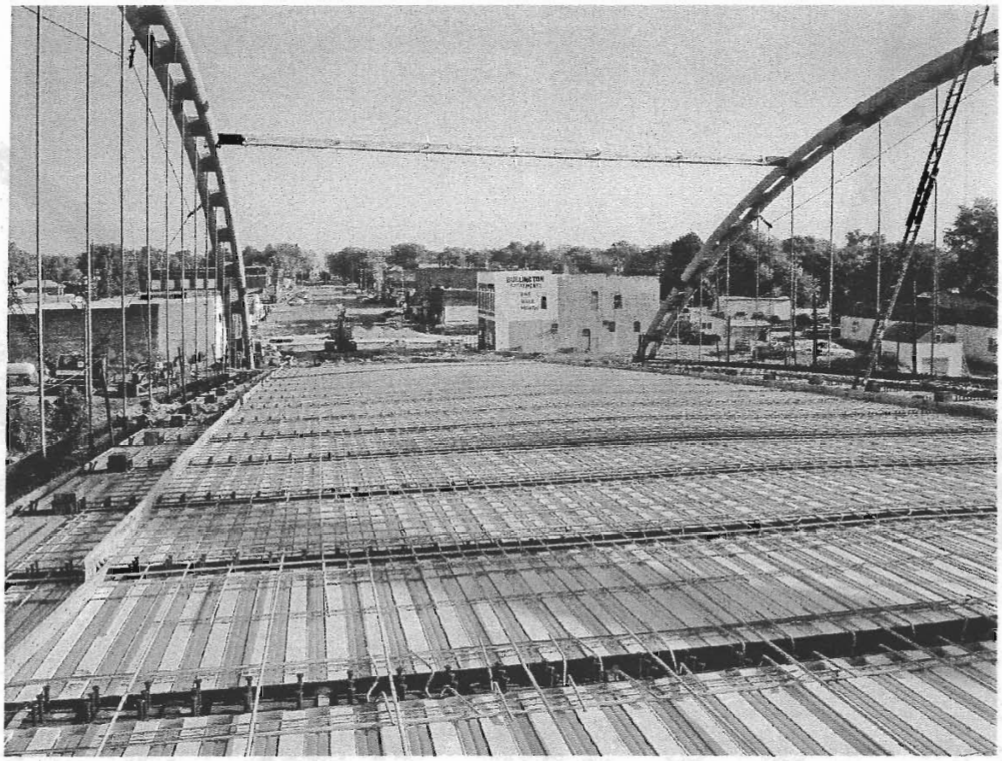

Figure 10.2.2-5- Deck slab reinforcement installation

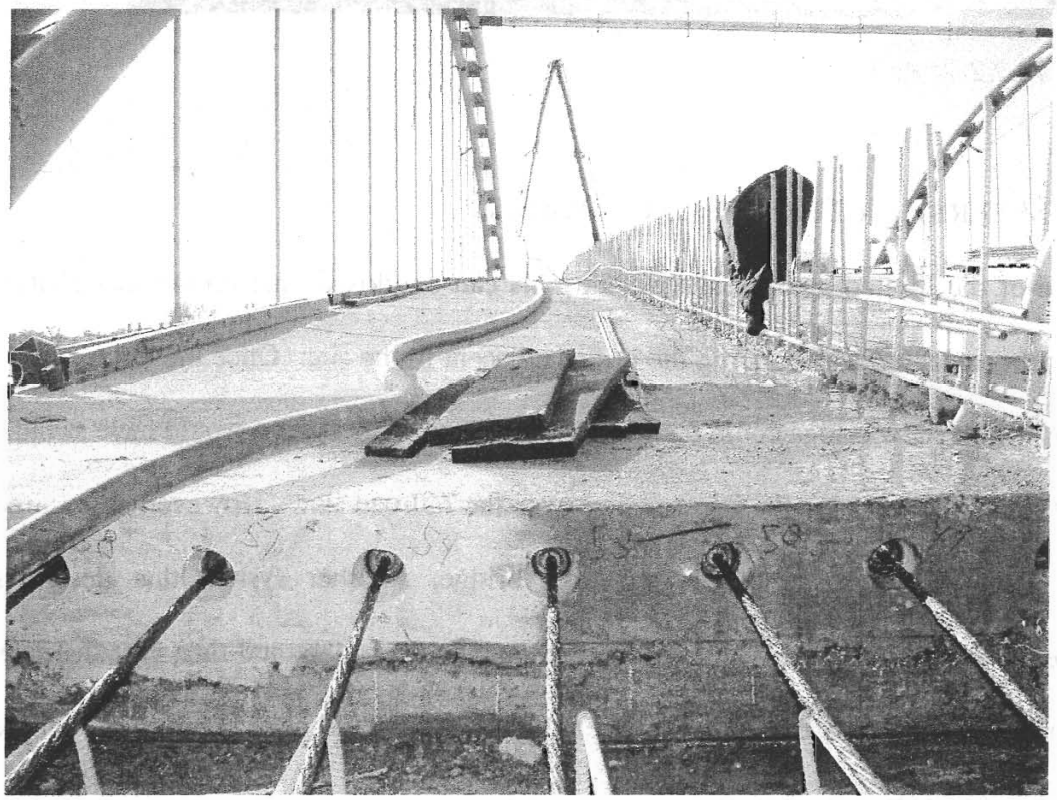

Figure 10.2.2-6- Deck slab post-tensioning

Figure 10.2.2-7- Railing Construction

10.2.3 SUPERSTRUCTURE LIFTING OPTIONS

Because of the limited amount of time the rails can be closed, one option that NDOR personnel considered was building the bridge adjacent to the site. Once the old bridge is demolished, the new bridge could be lifted and installed. This system would have saved a lot of the time needed for the construction over the railroad lines. However, it required higher crane capacities to handle the total bridge. Another system that designers considered was to build the whole bridge without the deck slab, and then cast the deck slab after the bridge was moved into place. This system would have required more time than the first system.

Three options of lifting the bridge elements were investigated. The first option was to build the two arches, connect them with three cross beams, and then install this assembly on the columns. This option would have required two cranes with capacities equal to 41.5 ton each as shown in *Figure 10.2.3-1*.

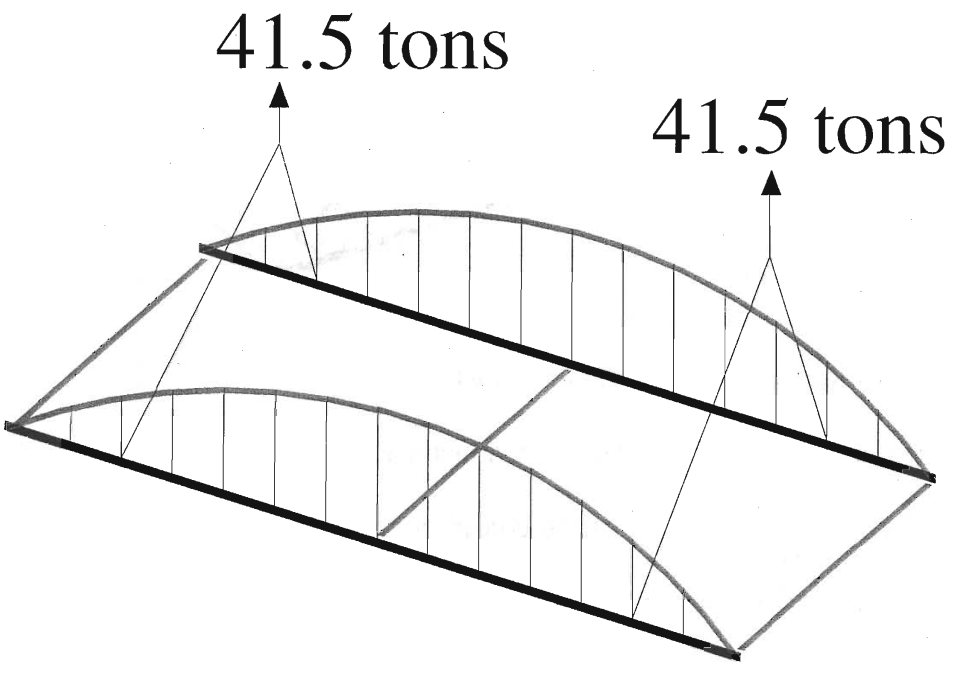

Figure 10.2.3-1- Superstructure lifting options I

The second option that designers were investigating was to assemble the steel structure close to the bridge location without pumping the concrete inside the tubes or pouring the deck slab, and then lift and install the whole assembly on the four columns right after removing or demolishing the old bridge. In this case the arch had to carry the weight of the cross beams and the metal decking without the confined concrete inside the tubes or the post-tensioning. This option required two heavy cranes with capacities exceed 105.6 tons, as shown in *Figure 10.2.3-2*.

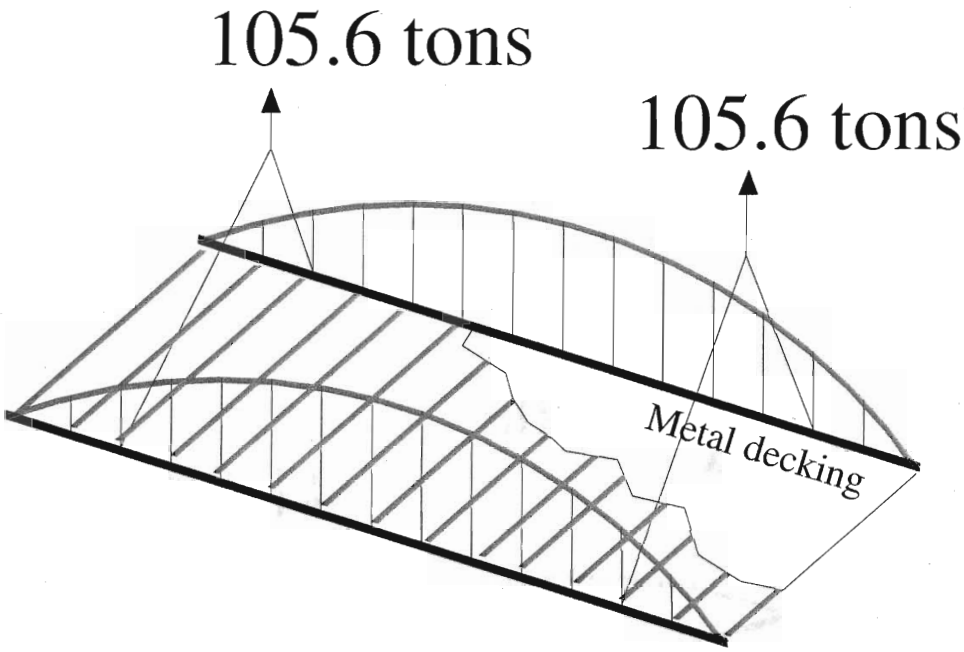

Figure 10.2.3-2- Superstructure lifting options II

The third option was the option that the contractor chose because it required reasonable crane capacity, and yet a big part of the construction was done without interrupting the railroad track service. As shown in *Figure 10.2.3-3, t*his option required utilizing two cranes with capacitates in the range of 20 tons, which were owned by the contractor.

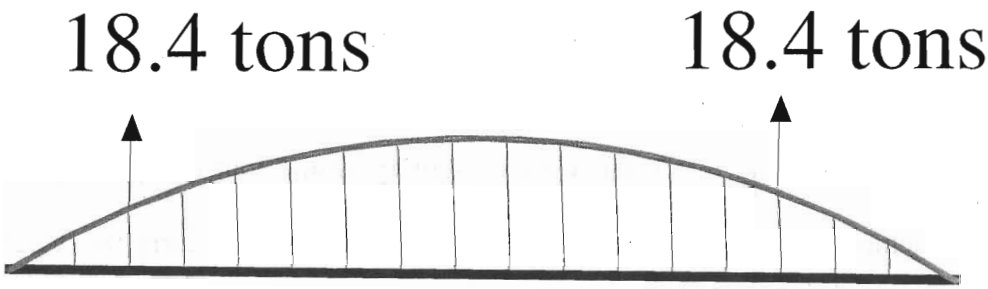

Figure 10.2.3-3- Superstructure lifting options III

Figure 8 shows the actual arch installation, in which three cranes were used. Two of these cranes carried the tied arch from points close to its ends. The third crane was used to prevent the arch from tipping over.

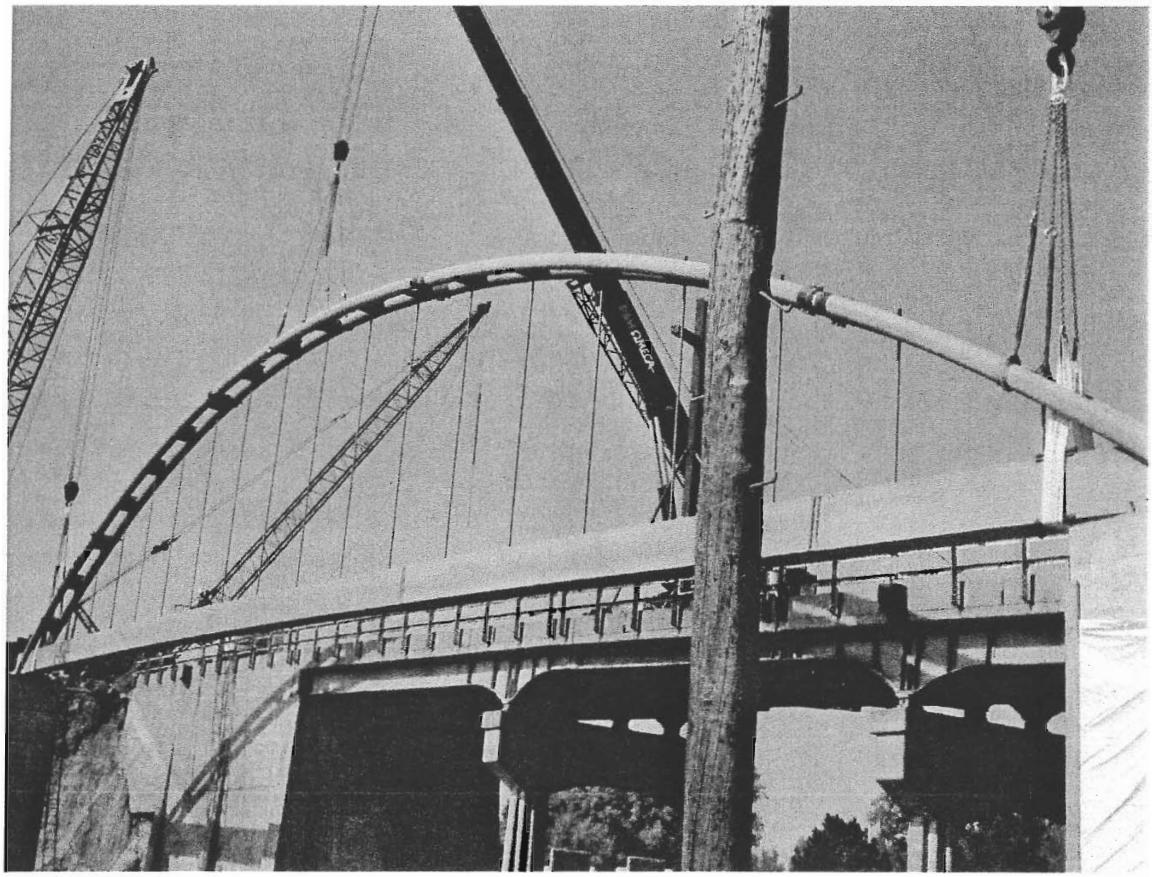

Figure 10.2.3-4- Installation of the first arch

SECTION 11: CONCLUSIONS AND RECOMMENDATIONS

This investigation of the Ravenna Arch Bridge System provides several important conclusions to be applied to future projects. As described in the cost analysis, the Ravenna System is currently uneconomical. However, as constructors become more familiar with the system the cost should be reduced. Additionally, the use of a precast floor system would significantly decrease the cost.

From the literature review, it appears that current code provisions in AASHTO LRFD for effective flange width are unduly conservative. There are no studies to support the retention of the 12t limitation. Additional research, including full scale testing, is recommended.

The effects of confinement are greatest in pure axial members. It is partially for this reason that the arch bridge system is efficient; large bending moments are reduced through the use of axial forces in the top and bottom chords.

As indicated by the bi-axial stress analyis, top ties in an arch system are not always necessary for lateral stability. A thorough analysis of the system is required, and a determination should be made addressing the lateral stiffness of the overall system. In the Ravenna Arch Bridge, the lateral top ties are not necessary.

Through the production of the test specimens, it was determined that fabrication of system components should be monitored closely to ensure proper dimensions. Accurate dimensions, especially in the connection components, are extremely important. Most notably, the spherical nut must be fabricated to precise tolerances outlined in the specifications.

The effective width requirements of most codes seem to be too conservative, even without a diaphragm. The utilization of 4 ft or even 8 ft stud cluster spacing still maintains the full composite action.

Prefabricating the arch saved time and made it possible to finish this project with tight time limitations, however potential options that were discuss in section 10 would have further reduced the construction time of the bridge.

SECTION 12: IMPLEMENTATION

This research was conducted in parallel with he design of the Ravenna Viaduct to verify the design assumptions for the strength of the principal components of the bridge.

The success of this project allows us to use this design concept for future bridge projects which require a long clear span with a very shallow superstructure depth.

REFERENCES

1. AASHTO, Standard Specifications for Highway Bridges, 16th Edition, American Association for State Highway and Transportation Officials, Washington, D.C., 1996.
2. AASHTO LRFD, 2005 and Interim Bridge Design Specifications, Second Edition, American Association of State Highway and Transportation Officials, Washington, D.C.
3. Abu-Amra, T.F., Nassif, H.H., *Effect of Flange Width on the Deflection of Steel Composite Beams,* Department of Civil Engineering, Rutgers, The State University of New Jersey, Paper #: S303, Piscataway, NJ
4. Badie, S.S., Tadros, M.K., "I-Girder/Deck Connection for Efficient Deck Replacement," University of Nebraska, for the Nebraska Department of Roads (NDOR), NDOR Project Number SPR-PL-1(35) P516, December 2000.
5. Bowers, J., "Investigation of an Innovative Arch Bridge System," Master Thesis, University of Nebraska-Lincoln, 2004.
6. Bridge Office Policies and Procedures (BOPP) Manual, Nebraska Department of Roads (NDOR), Lincoln, NE, 2001.
7. Chen, S.S., Aref, A.J., Ahn, I.-S., Chiewanichakorn, M., "Effective Slab Width for Composite Steel Bridge Members," NCHRP Report 12-58, National Cooperative Highway Research Program, Transportation Research Board, Washington D.C., 118 pp.

8. Cheung, M.S., Chan, M.Y.T., "Finite-strip evaluation of effective flange width of bridge girders," *Canadian Journal of Civil Engineering*, Ottawa, Canada, Volume 5, No. 2, pp. 174-185.

9. Elhelbawey, M., Chung, C. F., Sahin, M.A., Schelling, D.R., "Determination of Slab Participation from Weigh-In-Motion Bridge Testing," *Journal of Bridge Engineering*, Vol. 4., No. 3, August 1999, pp. 165-173

10. Fan, H.M., Heins, C.P. *Effective Slab Width of Simple Span Steel I-Beam Composite Bridges at Ultimate Load,* Department of Civil Engineering, Maryland Univ., College Park, 1974.

11. Iowa Department of Transportation, "Inverted Tee Girder Bridges, November 19th 2004 (http://www.dot.state.ia.us/bridge/hrgreen_clinton.html)

12. *Interim Guidelines For The Use Of Self Consolidating Concrete In Precast/Prestressed Concrete Institute Member Plants*, Precast/Prestressed Concrete Institute, Chicago, IL, April, 2003, pp. A1-6 – A1-7.

13. Karman, T. v., "Festschrift August Foppls," *International Association of Bridge Strcutural Engineering*, p. 114, 1923

14. Lee, J.A.N., "Effective Widths of Tee-Beams," *The Structural Engineer,* Vol. 40, No. 1, 1962, pp. 21-27.

15. Loo, Y.-C, Sutandi, T.D., "Effective Flange Width Formulas for T-beams," *Concrete International-ACI*, Vol. 8, No. 2, pp. 40-45, 1986

16. Loov, R.E., Patnaik, A.K. "Horizontal Shear Strength of Composite Concrete Beams With a Rough Interface," *PCI Journal,* January-February, 1994, pp. 48-69.

17. *Manual of Steel Construction*; *Load and Resistance Factor Design*, 3rd Ed. (2001) American Institute of Steel Construction, Washington D.C.

18. Metzer, von W. "Die Mittragende Breite." *Luftfarhtforschung* 4, 1923.

19. Miller, A. "Über die Mittragende Breite." *Luftfarhtforschung* 4, 1, 1929.

20. Modern Steel Construction, "US 59–Houston Gateway," November, 2003.

21. Naaman, A., "Prestressed Concrete Analysis and Design," Techno Press 3000, Ann Arbor, Michigan, 2nd Edition, pp. 59-62.

22. Pantazopoulou, S.J., Moehle, J.P., "Identification of Effect of Slabs on Flexural Behavior of Beams," *Journal of Engineering Mechanics*, *ASCE*, Vol. 116, No. 1, 1990, pp. 91-105

23. PCI Bridge Design Manual, Precast/Prestressed Concrete Institute, Chicago, IL, 1997

24. Reisner, E., "Analysis of shear lag in box beams by principle of minimum potential energy." *Quarterly J. Mech. And Appl. Mathematics,* 4(3), 1964, pp. 268-278

25. Richart, F.E., Brandtzaeg, A., and Brown, R.L., "A study of the failure of concrete under combined compressive stresses." Bull. No. 185, University of Illinois, Engineering Experimental Station, Urbana, Ill., pp 104, 1928

26. Salmon, C.G., Johnson, J.E., "Steel Structures; "Design and Behavior," Prentice – Hall Inc., NJ, 4th Edition, 1996

27. Schade, H.A., "The effective Breadth of Stiffened Plating under Bending Loads," *Trans. SNAME* 59, 1951.

28. Sechler, E.E., *Elasticity in engineering*, California Institute of Technology, Pasadena, Calif, 1952

29. Song, Q., Scordelis, A.C., "Shear-lag analysis of T-, I-, and box beams," *Journal of Structural Engineering*, ASCE, Vol. 116, No. 5, 1990

30. *Standard specifications for highway bridges,* 16th Ed. with 1997 Interim. (1996). American Association of State Highway and Transportation Officials, Washington D.C.

31. Strasky, J., Husty, I., "Arch Bridge crossing the Brno-Vienna expressway," *Institute of Civil Engineering*, Vol. 132, No. 4, November 1999, pp. 156-165

32. Sun, C, Girgis, A., Tadros, M, and Badie, S, "Structural Behavior of Flexural Member with High Strength Concrete," 2003 International Symposium on High Performance Concrete, 2003

33. Talbot, A.N., "Tests of Reinforced Concrete T-Beams (Series of 1906)." *Engineering Experiment Station Bulletin No. 12,* University of Illinois, 1907.

34. Timoshenko, S.P., and Goodier, J.N. (1970). *Theory of Elasticity*, 3rd ed., McGraw-Hill, New York.

APPENDIX A

RAVENNA VIADUCT

TRANSVERSE STABILITY OF THE ARCHES

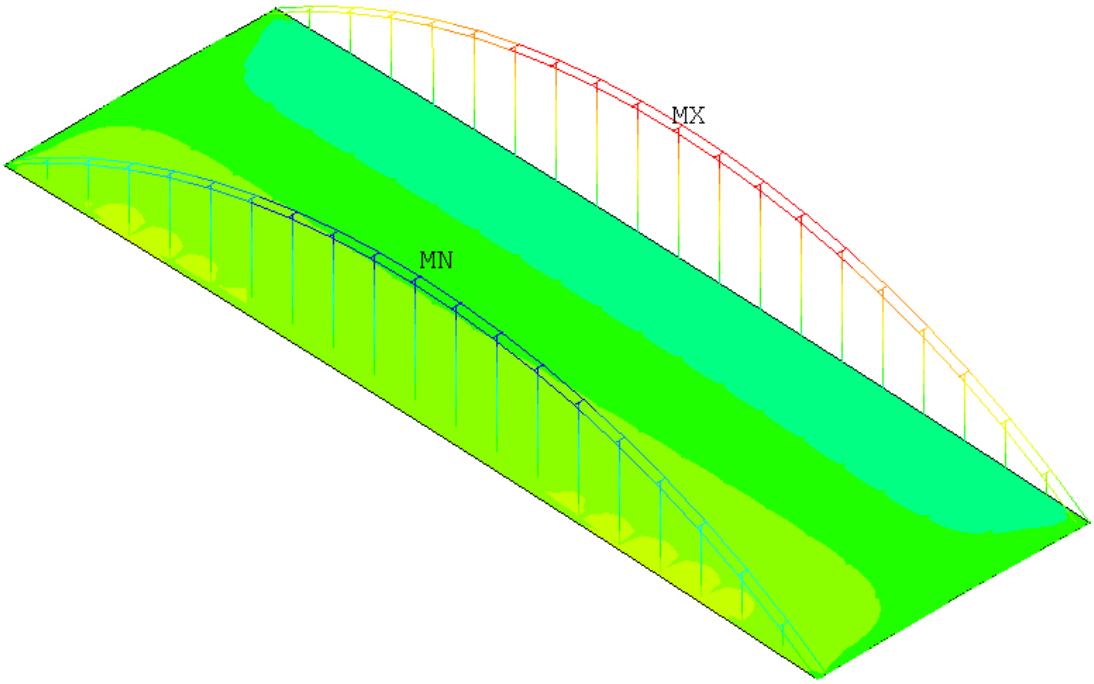

Table of Contents:

1. Description of the analysis
2. Calculation model, section characteristics
3. Natural modes and frequencies
4. Stability of the arch for wind load
5. Stability of the arch for truck and wind load
6. Stability of the arch with an imperfection for truck and wind load
7. Conclusions

Jiri Strasky
Civil Engineer: Arizona (No.32285),California (No.C51868),
Colorado (No.32721),Washington (No. 35077)

1. DESCRIPTION OF THE ANALYSIS

The purpose of the analysis is confirmed the stability of the arches of the Ravenna viaduct. The structure of the Ravenna viaduct is formed by two twin arches fixed into the edge box girders. Both the arches and edge box girder are filled with concrete. The girders are transversally connected by floor beams that support composite deck slab – see Fig.1 and 2. The stability of the arches was determined by non-linear analysis of the 3D structure loaded by wind. The analysis was performed by a program system ANSYS. The arches were modeled by tube elements, the boxes, floor beams and hangers by 3D bar elements, the composite deck slab by shell elements that have both bending and membrane capabilities.

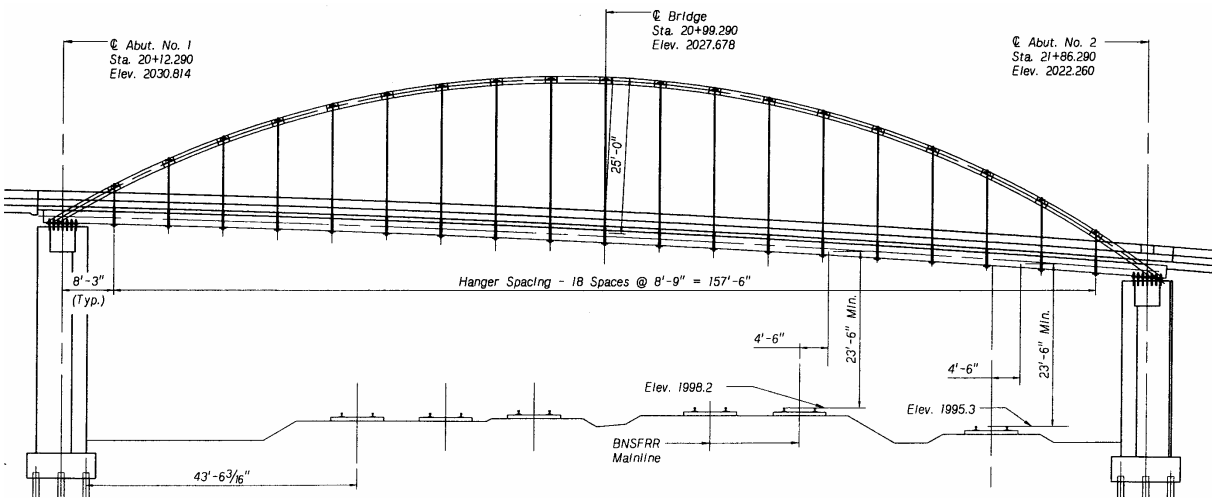

Fig.1.1

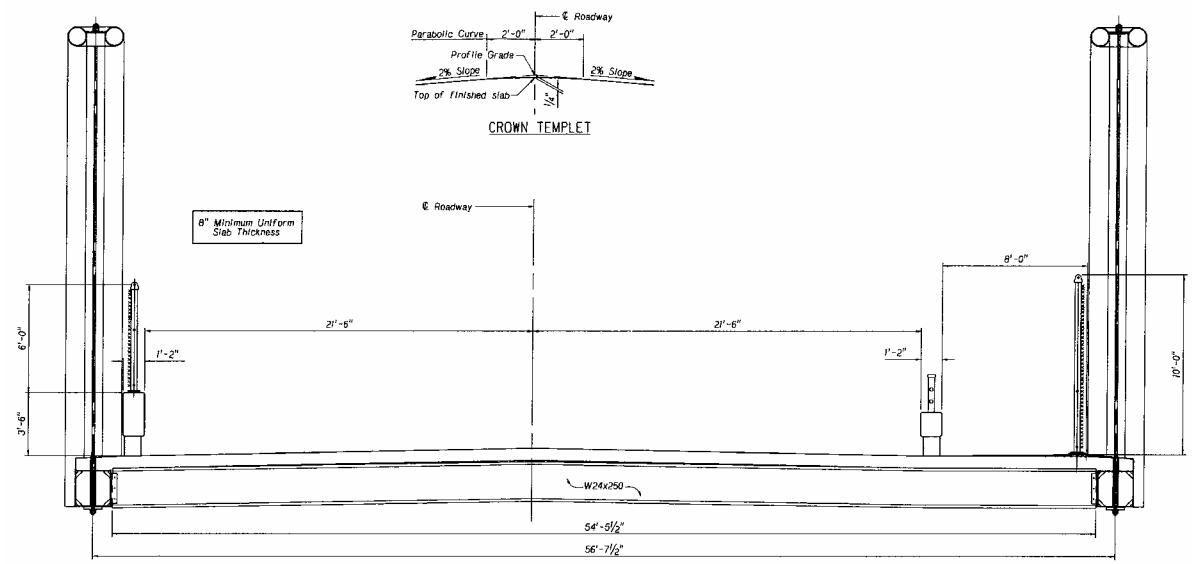

Fig.1.2

The initial state for the non-linear analysis was the stage in which the structure was loaded by dead load and by initial forces in hangers. The initial forces in hangers balanced the dead load of the structure situated between the neighboring hangers. The forces in hangers had the same value and therefore the stresses in the structure had an optimum distribution. Subsequently this structure was non-linearly analyzed for the design wind load (see Fig.1.3) that was gradually increased. The divergence has occurred when the arches have lost their geometric stability.

The analysis was repeated for the structure loaded by HS 20 truck situated at midspan. The influence if imperfection of the geometry of the arches was also considered. It was supposed that the arches were erected with misalignment of 2-in at midspan in a horizontal plane. The misalignment had parabolic curve. This structure was also loaded by HS truck and by gradually increased wind load.

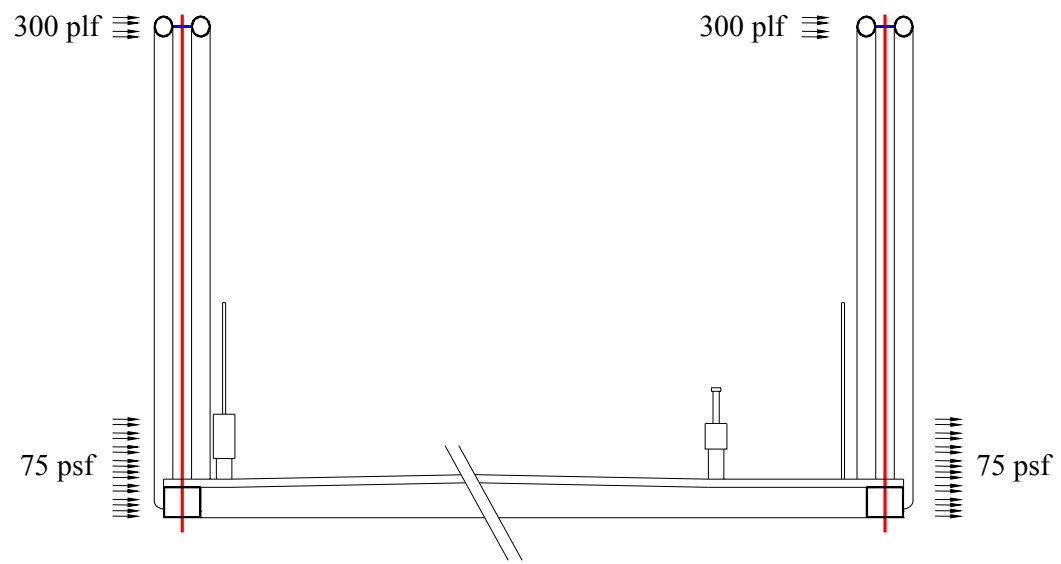

Fig.1.3

2. CALCULATION MODEL, SECTION CHARACTERISTICS

Calculation model and section properties considered in the analysis are evident from Fig.2.1 through 2.4.

Section Properties

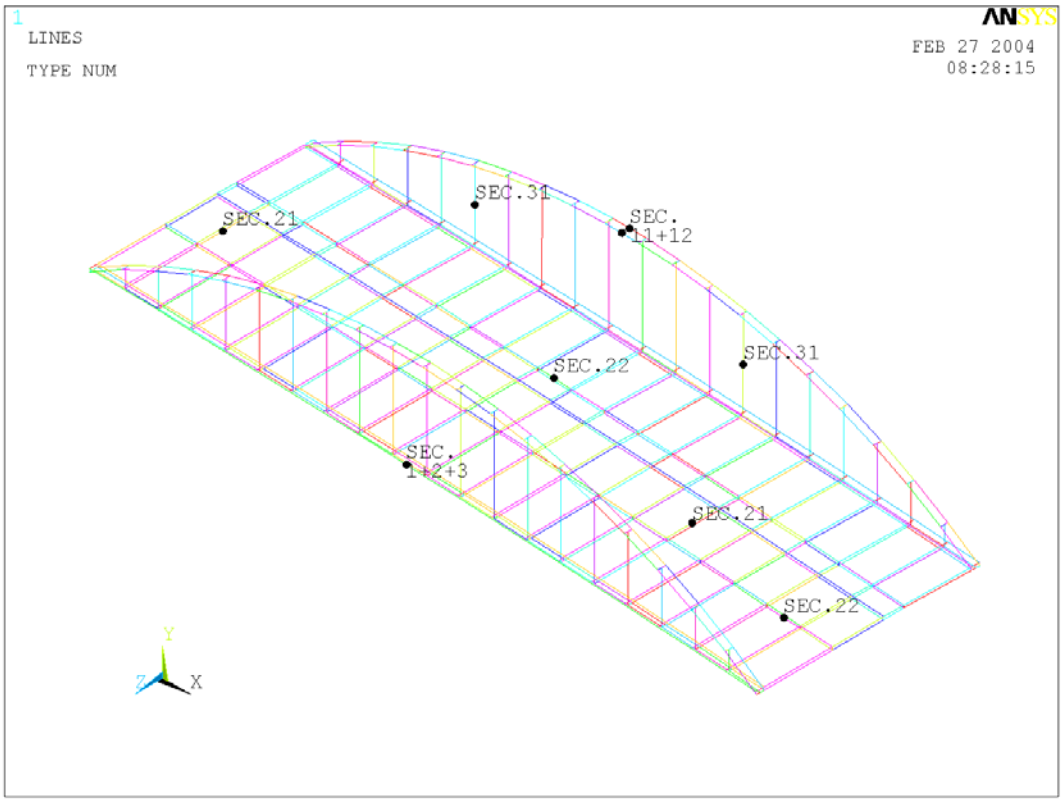

Fig.2.1

NO.	NAME	A [m2]	Iy (horiz. axis) [m4]	Iz (vert. axis) [m4]	It [m4]
2	tie beam – concrete +steel	0.0913	0.353e-02	0.353e-02	0.563e-02
12	arch – concrete + steel	0.0226	0.1784e-03	0.1784e-03	0.3554e-03
21	W24x250 girder	0.047441	0.003531	0.304e-03	0285e-04
31	tie rod	0.001676	0.223e-06	0.223e-06	0.447e-06
51	tie rod – arch connector	0.022419	0.001041	0.727e-04	0.355e-05
71	concrete slab	0.1905	-	-	-

JIRI STRASKY, PH.D.,P.E., 176 CORTE ANITA, GREENBRAE, CA 94904, TEL. (415) 464-0447, FAX.(415) 354 3348
E-mail: j.strasky@usa.net

Calculation Model

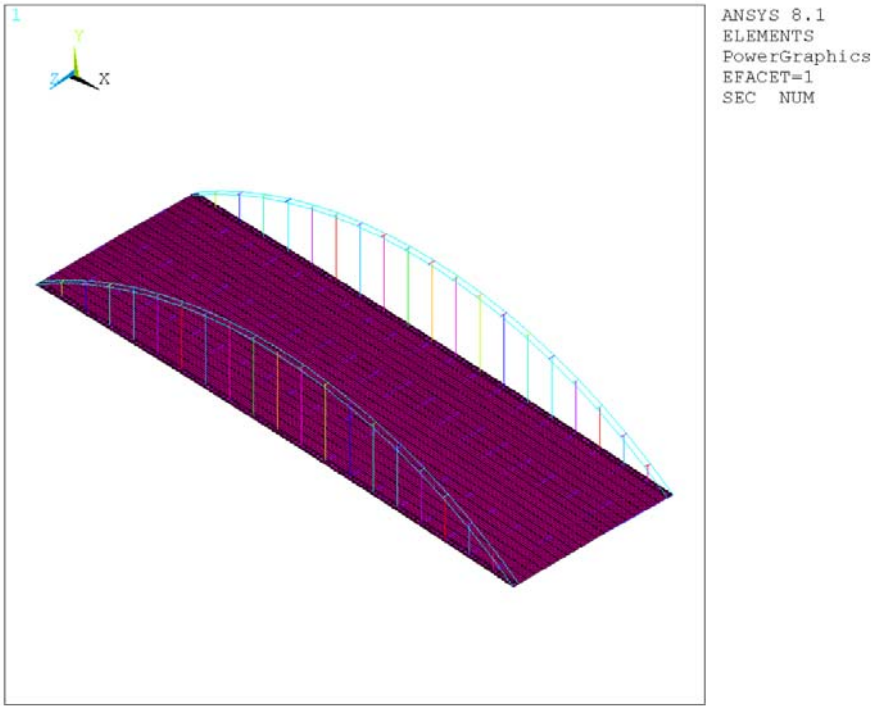

Fig.2.2

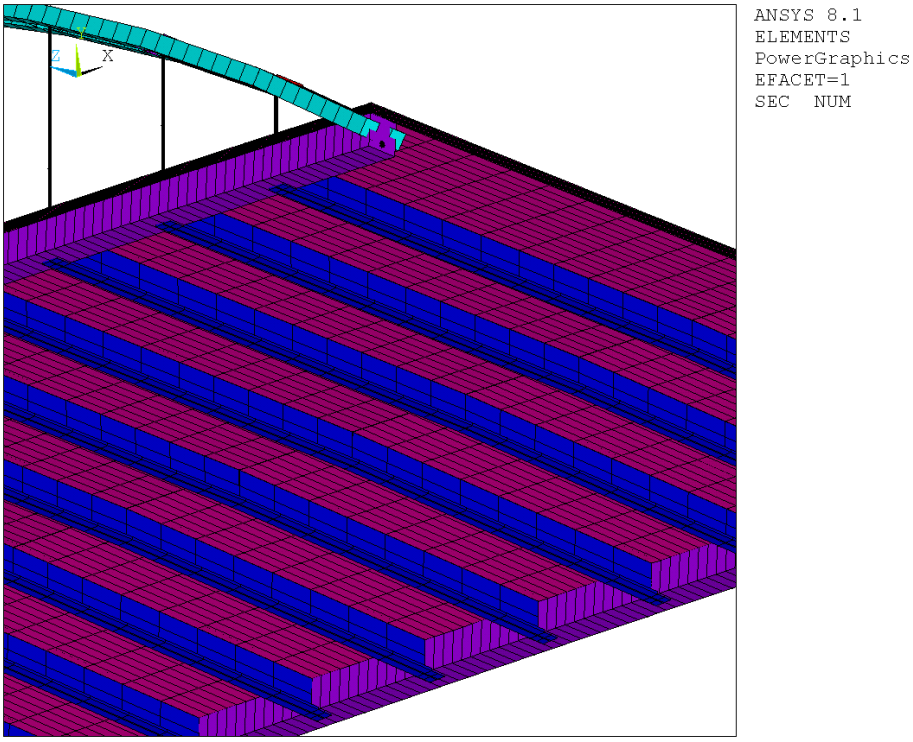

Fig.2.3

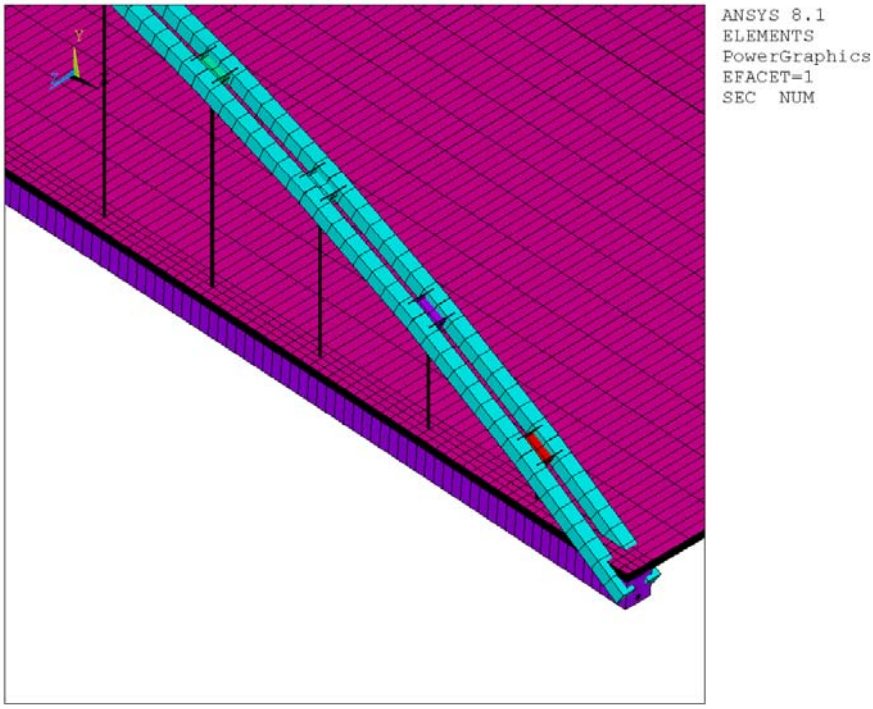

Fig.2.4

EVALUATE MATERIAL PROPERTIES FOR MATERIALS 1 TO 71

MATERIAL NUMBER = 2 EVALUATED AT TEMPERATURE OF 0.0000
EX = 0.19996E+12
NUXY = 0.30000
DENS = 7850.0

MATERIAL NUMBER = 3 EVALUATED AT TEMPERATURE OF 0.0000
EX = 0.19651E+12
NUXY = 0.30000
ALPX = 0.48049E-09
DENS = 7850.0

MATERIAL NUMBER = 12 EVALUATED AT TEMPERATURE OF 0.0000
EX = 0.19996E+12
NUXY = 0.30000
DENS = 7850.0

MATERIAL NUMBER = 21 EVALUATED AT TEMPERATURE OF 0.0000
EX = 0.19996E+12
NUXY = 0.30000
DENS = 7850.0

MATERIAL NUMBER = 31 EVALUATED AT TEMPERATURE OF 0.0000
EX = 0.19996E+12
NUXY = 0.30000
ALPX = 0.54550E-03
DENS = 7850.0

MATERIAL NUMBER = 32 EVALUATED AT TEMPERATURE OF 0.0000
EX = 0.19996E+12
NUXY = 0.30000
ALPX = 0.54550E-03
DENS = 7850.0

```
MATERIAL NUMBER =     33 EVALUATED AT TEMPERATURE OF   0.0000
 EX   =  0.19996E+12
 NUXY =  0.30000
 ALPX =  0.54550E-03
 DENS =   7850.0

MATERIAL NUMBER =     34 EVALUATED AT TEMPERATURE OF   0.0000
 EX   =  0.19996E+12
 NUXY =  0.30000
 ALPX =  0.54550E-03
 DENS =   7850.0

MATERIAL NUMBER =     35 EVALUATED AT TEMPERATURE OF   0.0000
 EX   =  0.19996E+12
 NUXY =  0.30000
 ALPX =  0.54550E-03
 DENS =   7850.0

MATERIAL NUMBER =     36 EVALUATED AT TEMPERATURE OF   0.0000
 EX   =  0.19996E+12
 NUXY =  0.30000
 ALPX =  0.54550E-03
 DENS =   7850.0

MATERIAL NUMBER =     37 EVALUATED AT TEMPERATURE OF   0.0000
 EX   =  0.19996E+12
 NUXY =  0.30000
 ALPX =  0.54550E-03
 DENS =   7850.0

MATERIAL NUMBER =     38 EVALUATED AT TEMPERATURE OF   0.0000
 EX   =  0.19996E+12
 NUXY =  0.30000
 ALPX =  0.54550E-03
 DENS =   7850.0

MATERIAL NUMBER =     39 EVALUATED AT TEMPERATURE OF   0.0000
 EX   =  0.19996E+12
 NUXY =  0.30000
 ALPX =  0.54550E-03
 DENS =   7850.0

MATERIAL NUMBER =     40 EVALUATED AT TEMPERATURE OF   0.0000
 EX   =  0.19996E+12
 NUXY =  0.30000
 ALPX =  0.54550E-03
 DENS =   7850.0

MATERIAL NUMBER =     41 EVALUATED AT TEMPERATURE OF   0.0000
 EX   =  0.19996E+12
 NUXY =  0.30000
 ALPX =  0.54550E-03
 DENS =   7850.0

MATERIAL NUMBER =     42 EVALUATED AT TEMPERATURE OF   0.0000
 EX   =  0.19996E+12
 NUXY =  0.30000
 ALPX =  0.54550E-03
 DENS =   7850.0

MATERIAL NUMBER =     43 EVALUATED AT TEMPERATURE OF   0.0000
 EX   =  0.19996E+12
 NUXY =  0.30000
 ALPX =  0.54550E-03
 DENS =   7850.0

MATERIAL NUMBER =     44 EVALUATED AT TEMPERATURE OF   0.0000
```

JIRI STRASKY, PH.D.,P.E., 176 CORTE ANITA, GREENBRAE, CA 94904, TEL. (415) 464-0447, FAX.(415) 354 3348
E-mail: j.strasky@usa.net

```
 EX   =  0.19996E+12
 NUXY =  0.30000
 ALPX =  0.54550E-03
 DENS =   7850.0

MATERIAL NUMBER =     45 EVALUATED AT TEMPERATURE OF   0.0000
 EX   =  0.19996E+12
 NUXY =  0.30000
 ALPX =  0.54550E-03
 DENS =   7850.0

MATERIAL NUMBER =     46 EVALUATED AT TEMPERATURE OF   0.0000
 EX   =  0.19996E+12
 NUXY =  0.30000
 ALPX =  0.54550E-03
 DENS =   7850.0

MATERIAL NUMBER =     47 EVALUATED AT TEMPERATURE OF   0.0000
 EX   =  0.19996E+12
 NUXY =  0.30000
 ALPX =  0.54550E-03
 DENS =   7850.0

MATERIAL NUMBER =     48 EVALUATED AT TEMPERATURE OF   0.0000
 EX   =  0.19996E+12
 NUXY =  0.30000
 ALPX =  0.54550E-03
 DENS =   7850.0

MATERIAL NUMBER =     49 EVALUATED AT TEMPERATURE OF   0.0000
 EX   =  0.19996E+12
 NUXY =  0.30000
 ALPX =  0.54550E-03
 DENS =   7850.0

MATERIAL NUMBER =     51 EVALUATED AT TEMPERATURE OF   0.0000
 EX   =  0.19996E+12
 NUXY =  0.30000
 DENS =   7850.0

MATERIAL NUMBER =     71 EVALUATED AT TEMPERATURE OF   0.0000
 EX   =  0.24133E+11
 NUXY =  0.20000
 DENS =   2773.3
```

Coordinates

No.	X	Y
2	2.514849	3.999799
5	5.182116	5.267880
8	7.849383	6.343545
11	10.51664	7.240253
14	13.18388	7.968281
17	15.85112	8.535400
20	18.51835	8.947335
23	21.18558	9.208075
26	23.85279	9.320072
29	26.52001	9.284366
32	29.18721	9.100629
35	31.85441	8.767149
38	34.52160	8.280752
44	2.514584	2.547061
45	5.181584	2.475919
46	7.848584	2.397731
47	10.51558	2.312497
48	13.18258	2.220215
49	15.84958	2.120881
50	18.51658	2.014495
51	21.18358	1.901055
52	23.85058	1.780557
53	26.51758	1.652999
54	29.18458	1.518379
55	31.85158	1.376694
56	34.51858	1.227941
57	37.18558	1.072116
58	39.85258	0.909216
62	0.000000	2.612138
77	42.51958	0.739239
78	45.18658	0.562180
79	47.85358	0.378035
80	50.52058	0.186802
81	53.03517	0.000000
82	50.52058	1.722882
83	47.85358	3.310282
84	45.18658	4.677140
85	42.51958	5.843683
86	39.85258	6.825246
87	37.18558	7.633541

JIRI STRASKY, PH.D.,P.E., 176 CORTE ANITA, GREENBRAE, CA 94904, TEL. (415) 464-0447, FAX.(415) 354 3348
E-mail: j.strasky@usa.net

3. NATURAL MODES AND FREQUENCIES

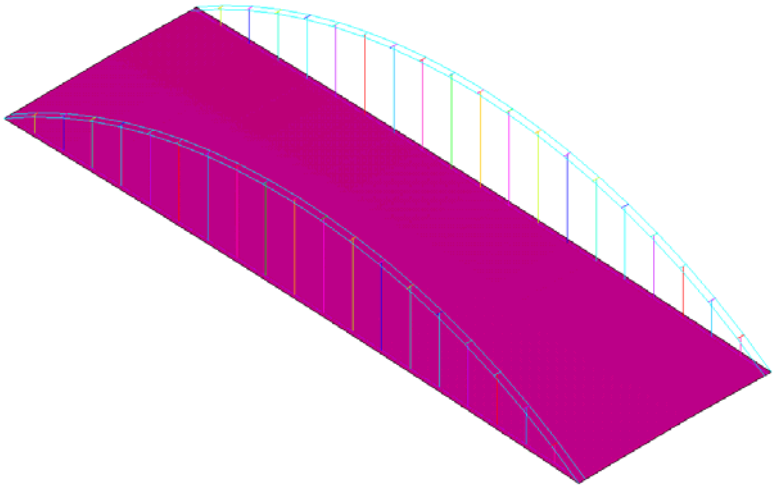

Fig.3.1

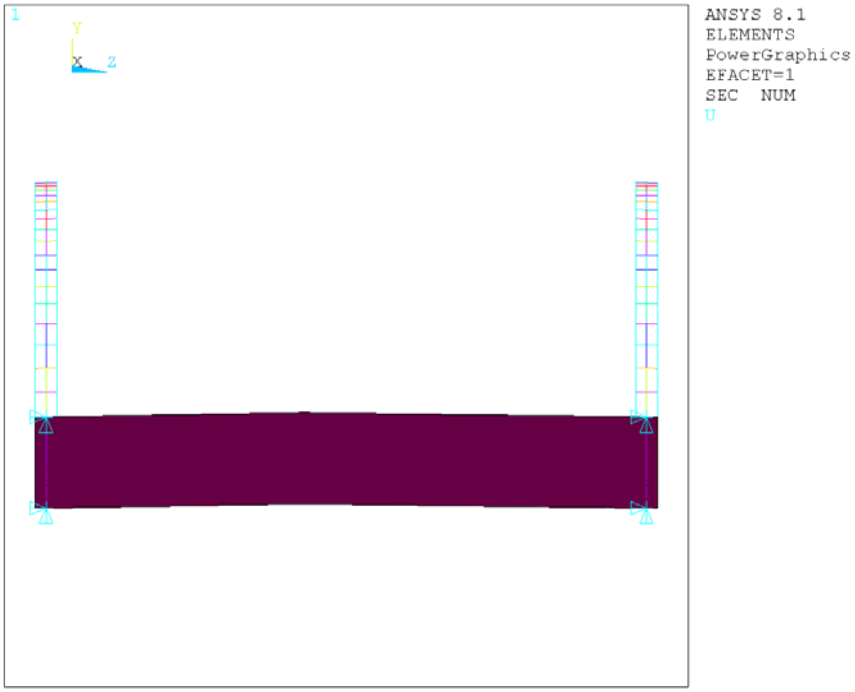

mode	frequency
1	1.2297
2	1.2334
3	1.4440
4	1.5717
5	1.5719
6	1.5748
7	1.5748
8	1.5921
9	1.5923
10	1.5956

modes 4 to 10 is vibration of hangers

Fig.3.2

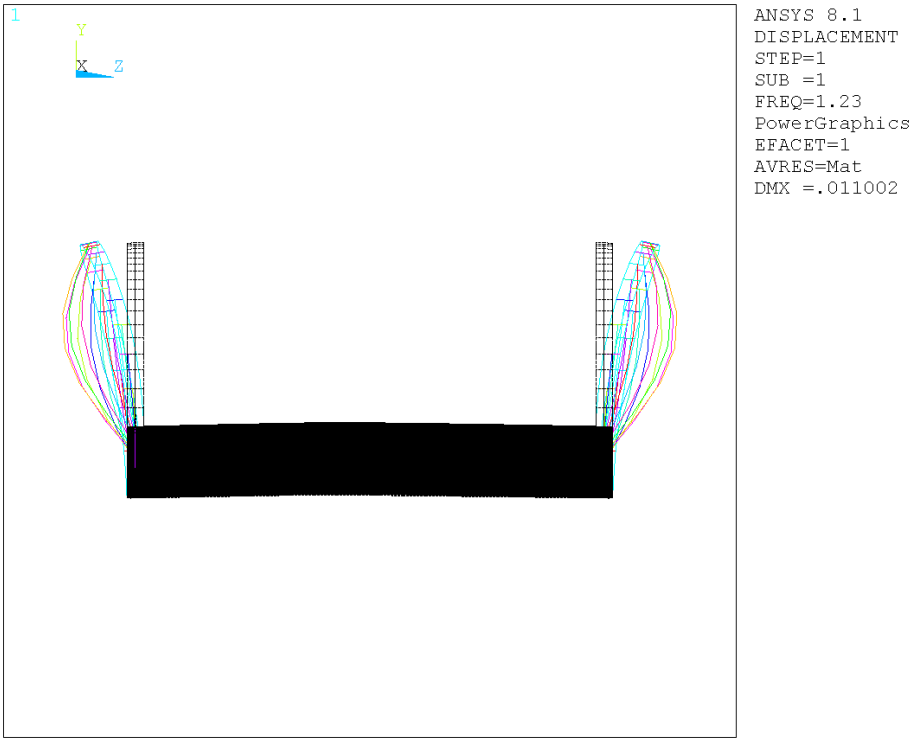

Fig.3.3 f(1)

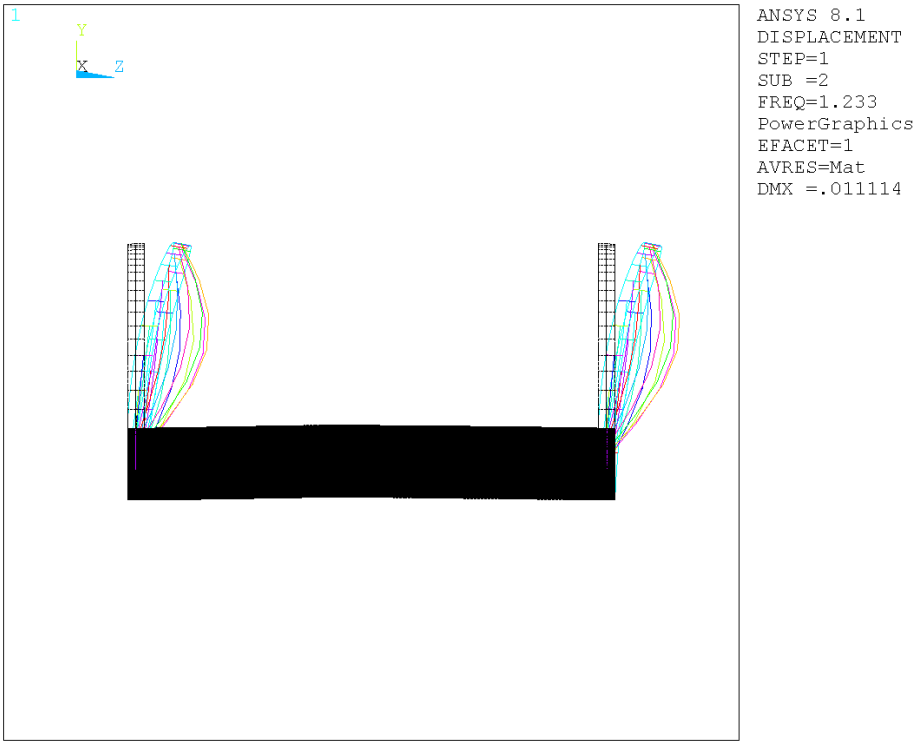

Fig.3.4 f(2)

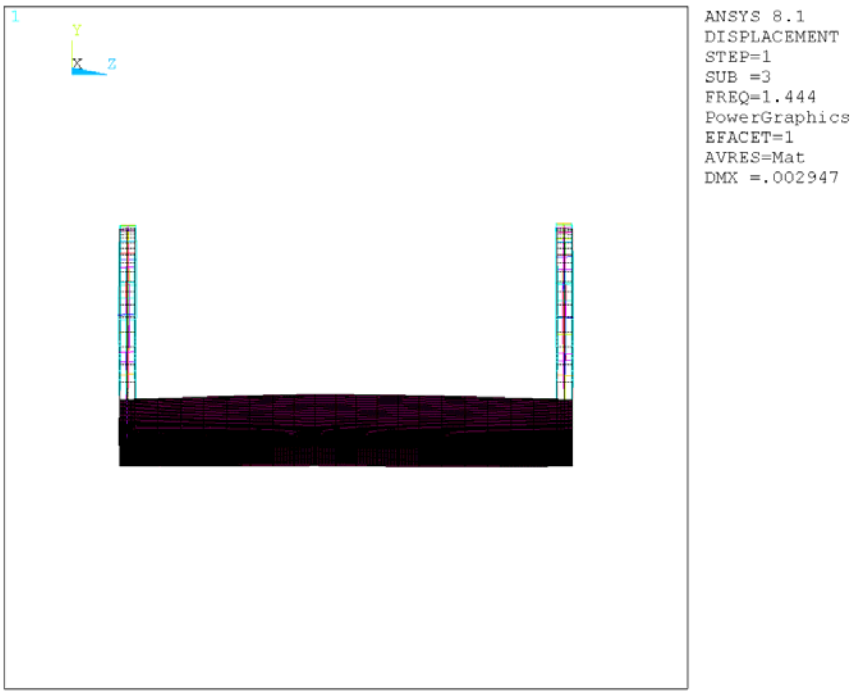

Fig.3.5 f(3)

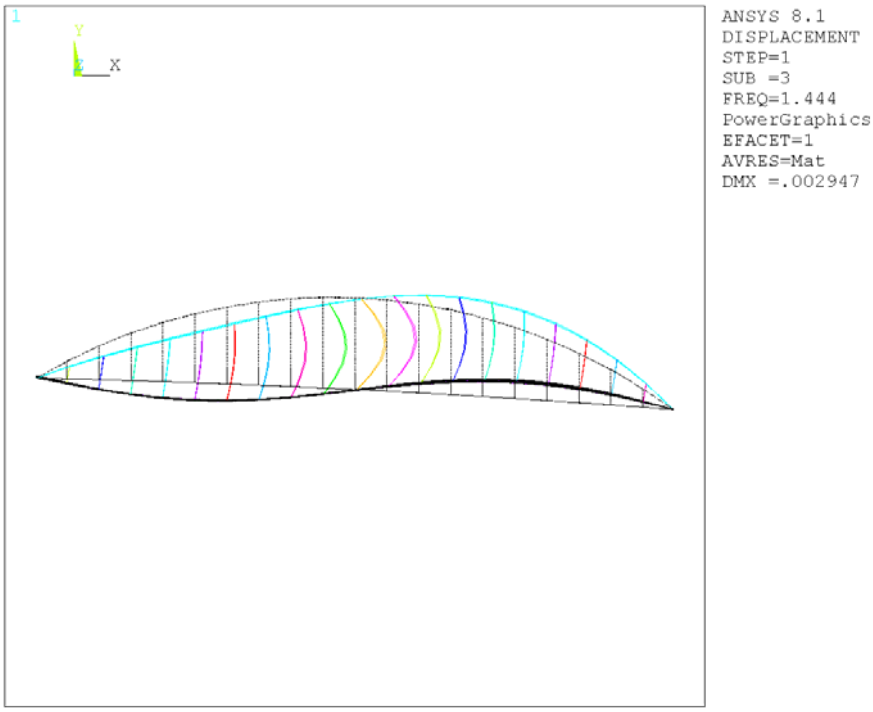

Fig.3.6 f(3)

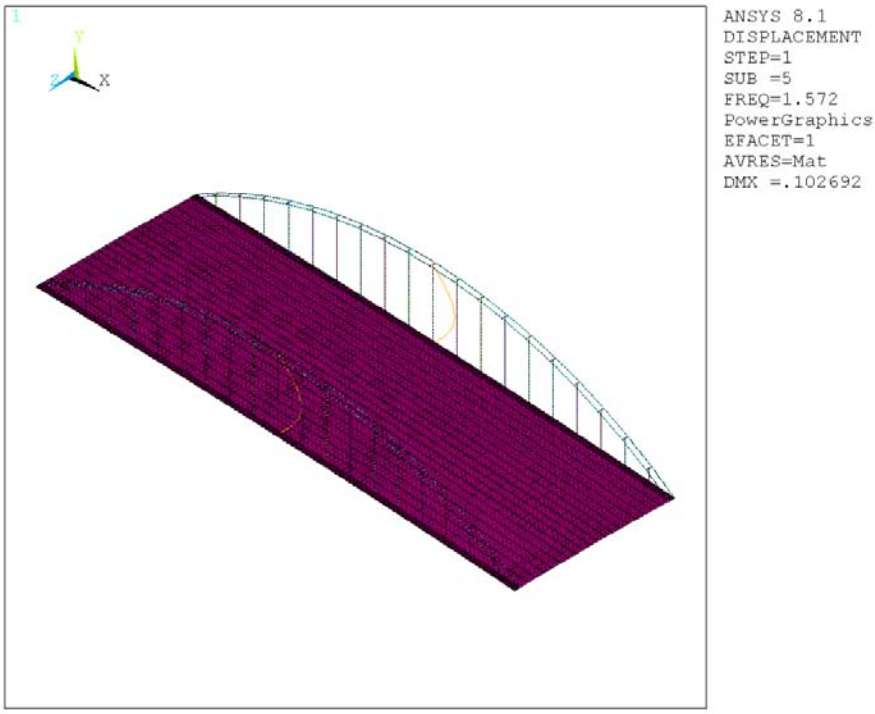

Fig.3.7 f(4)

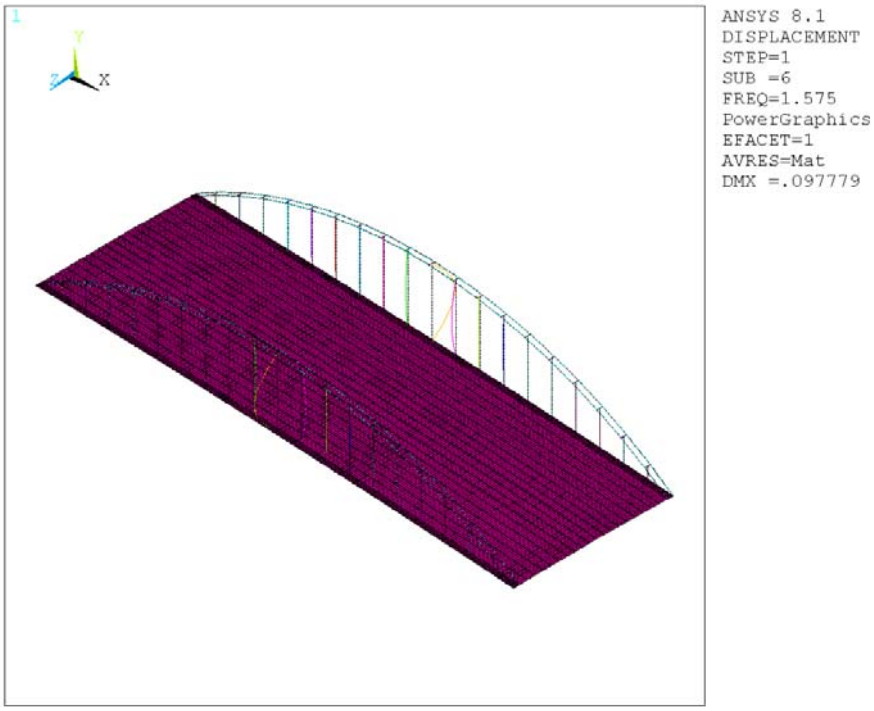

Fig.3.8 f(6)

4. STABILITY OF THE ARCH FOR THE WIND LOAD

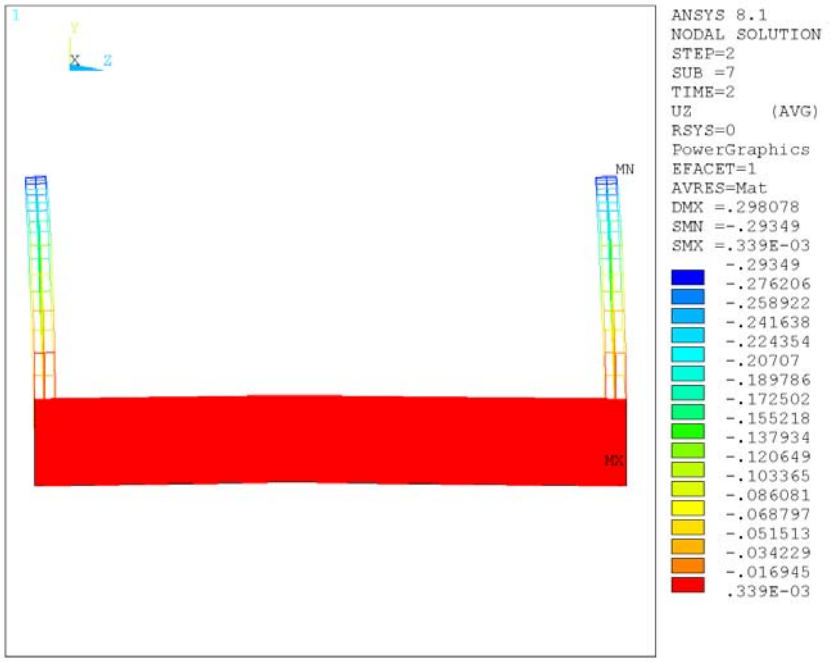

Fig.4.1 step 2- design wind load (initial stage – step 1)

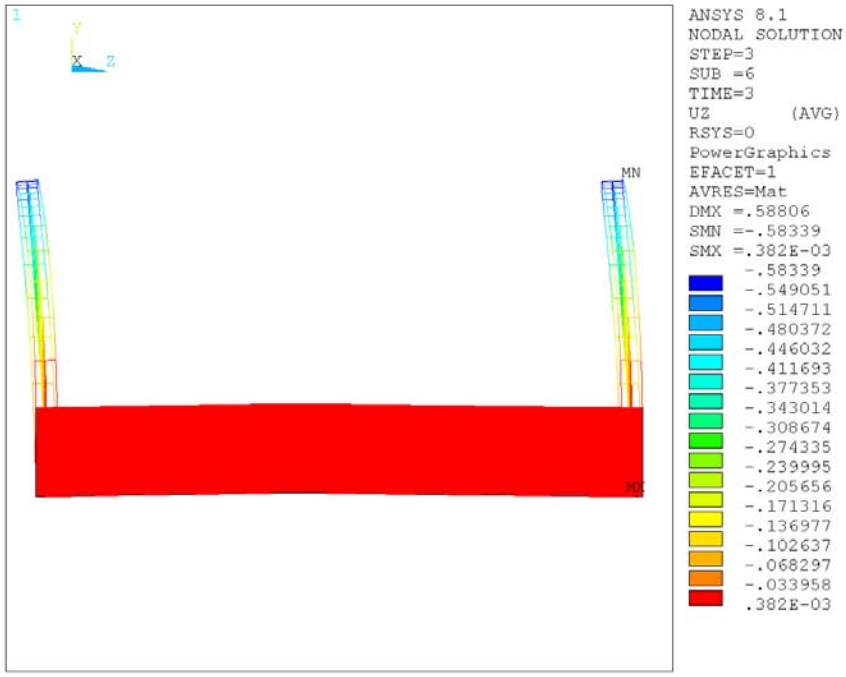

Fig.4.2 step 3 – 2 x design wind load

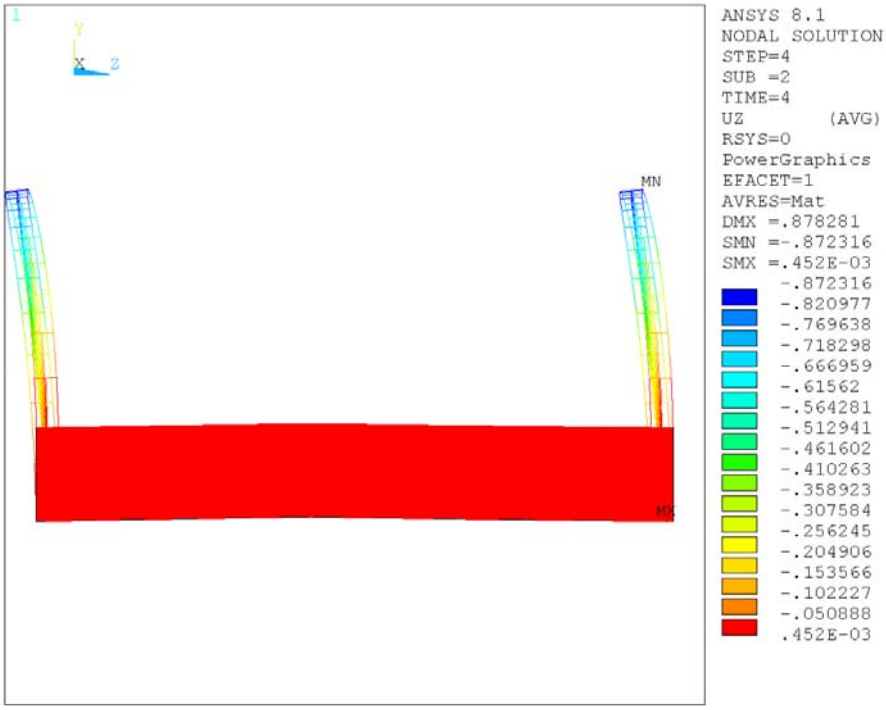

Fig.4.3 step 4 – 3 x design wind load

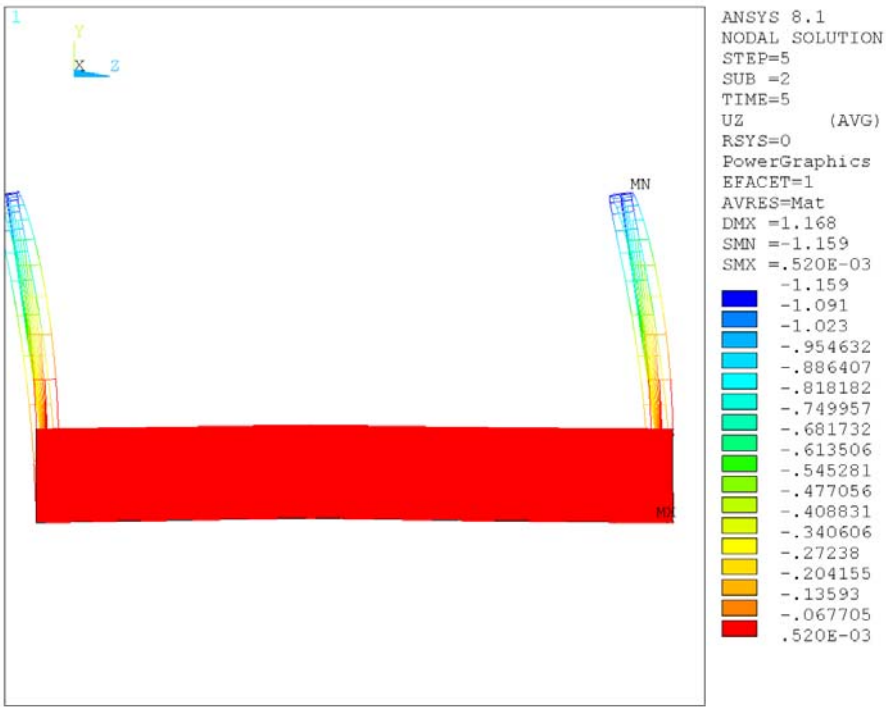

Fig.4.4 step 5 – 4 x design wind load

JIRI STRASKY, PH.D.,P.E., 176 CORTE ANITA, GREENBRAE, CA 94904, TEL. (415) 464-0447, FAX.(415) 354 3348
E-mail: j.strasky@usa.net

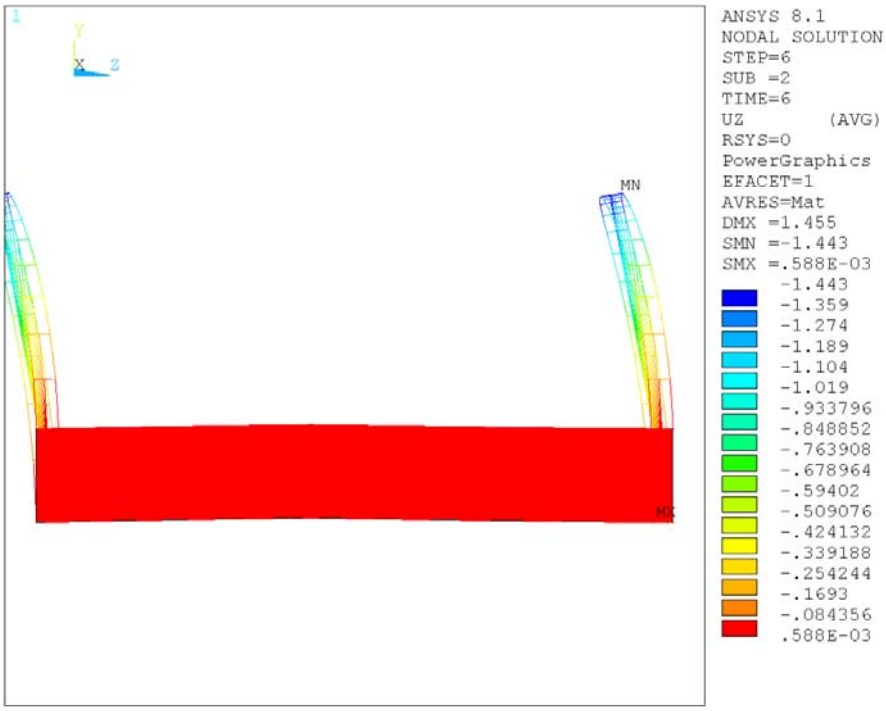

Fig.4.5 step 6 – 5 x design wind load

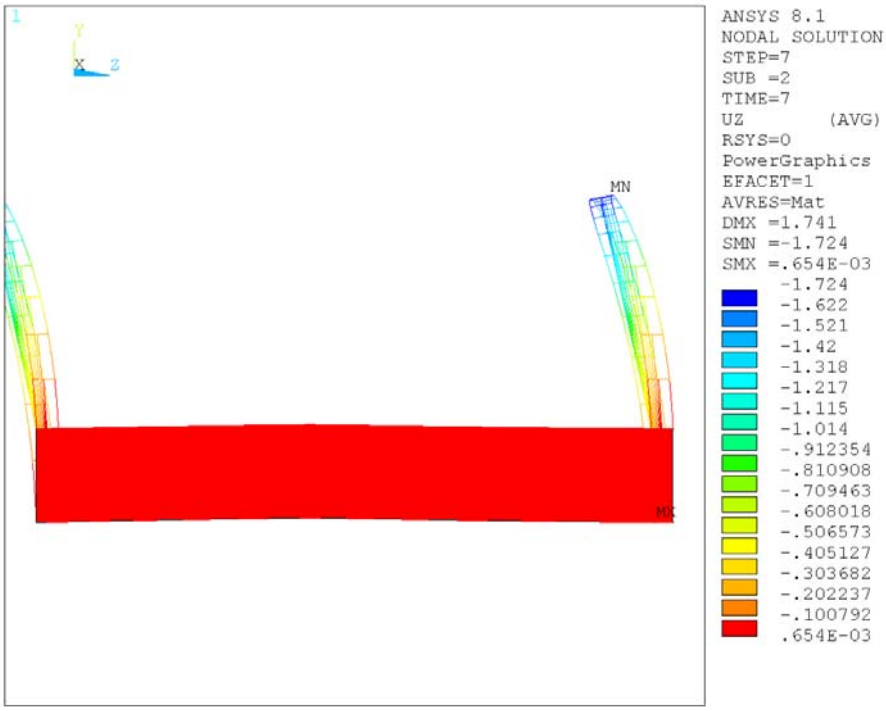

Fig.4.6 step 7 – 6 x design wind load

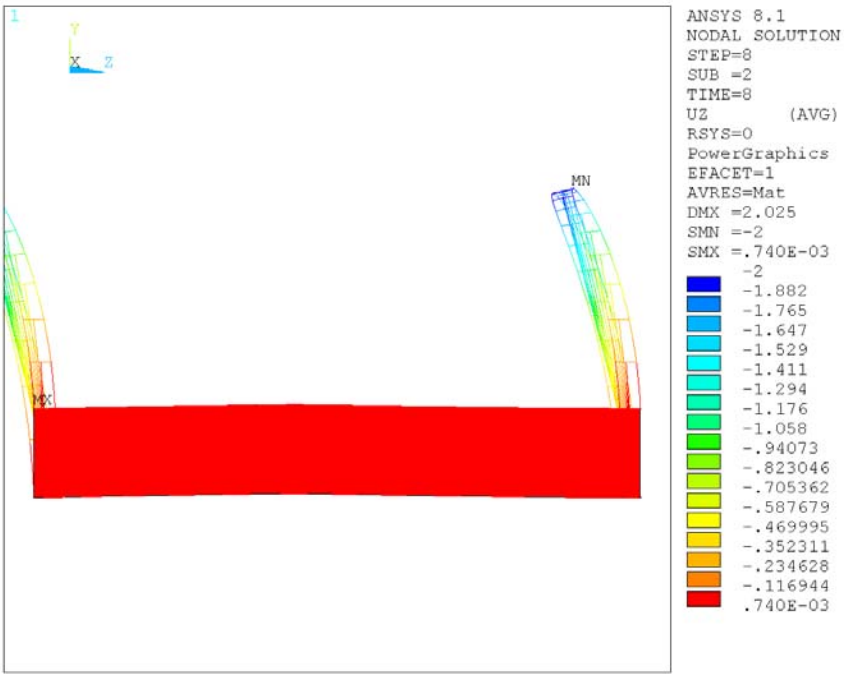

Fig.4.7 step 8 – 7 x design wind load

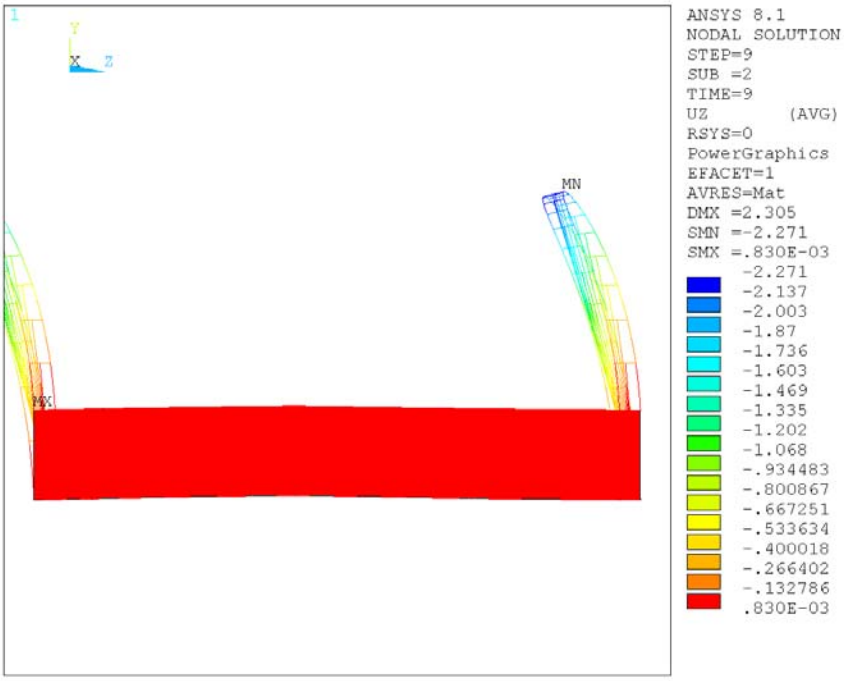

Fig.4.8 step 9 – 8 x design wind load

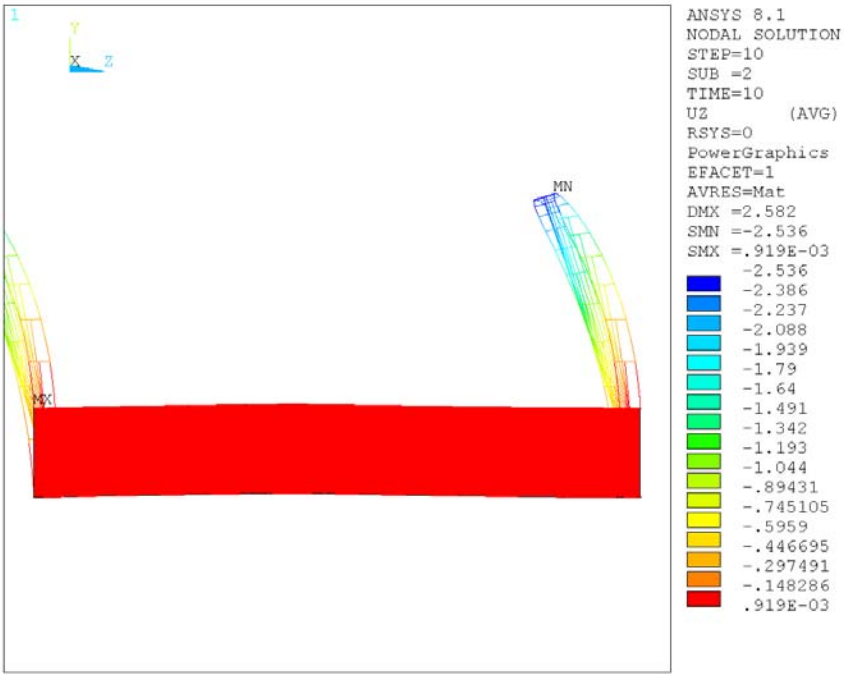

Fig.4.9 step 10 – 9 x design wind load

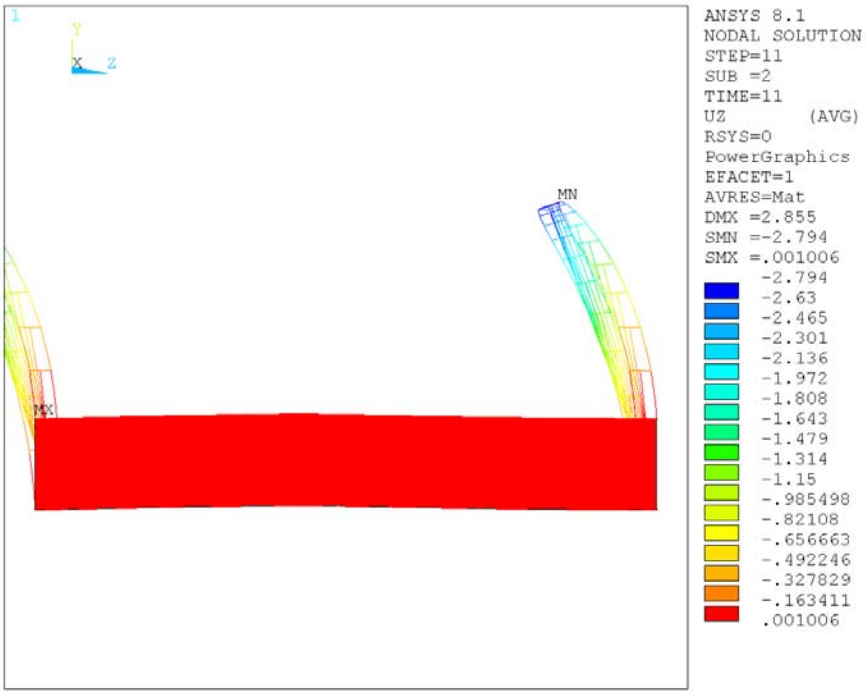

Fig.4.10 step 10 – 9 x design wind load

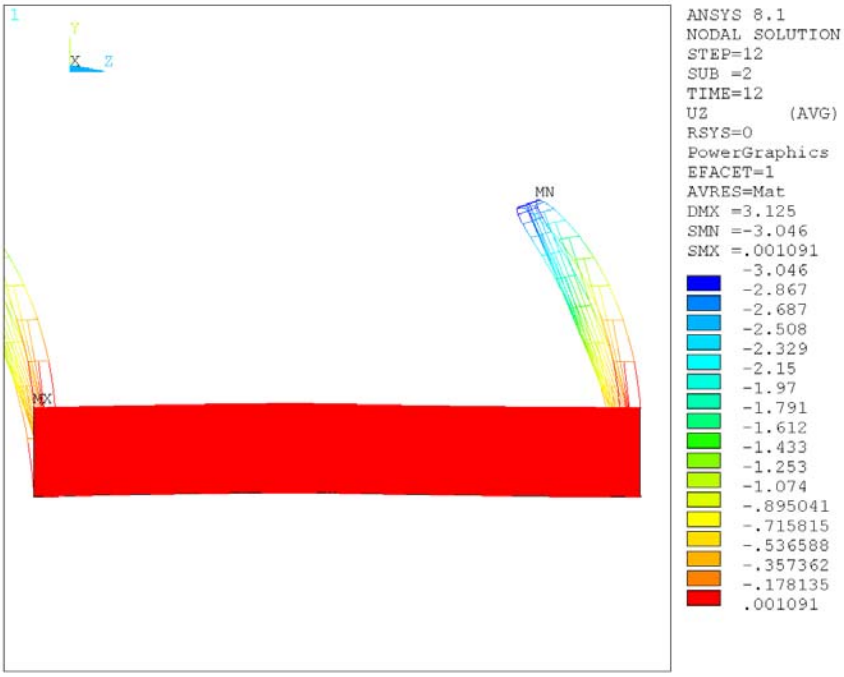

Fig.4.11 step 12 – 11 x design wind load

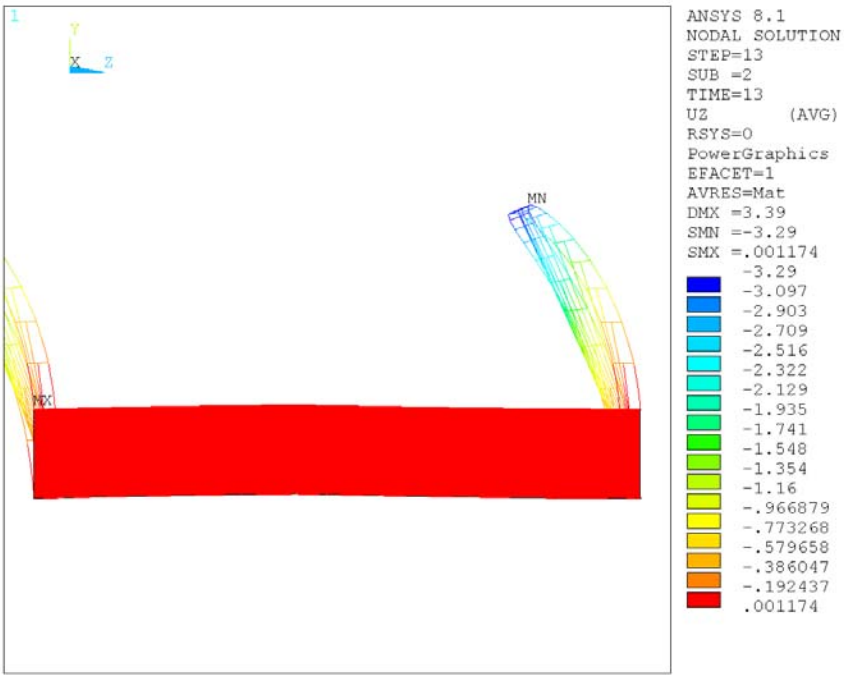

Fig.4.12 step 13 – 12 x design wind load

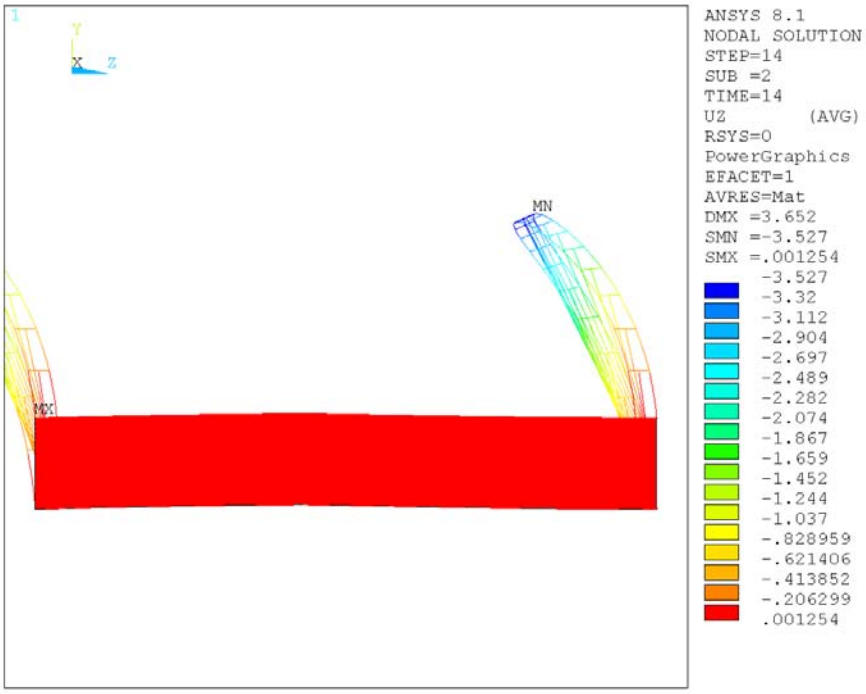

Fig.4.13 step 14 – 13 x design wind load

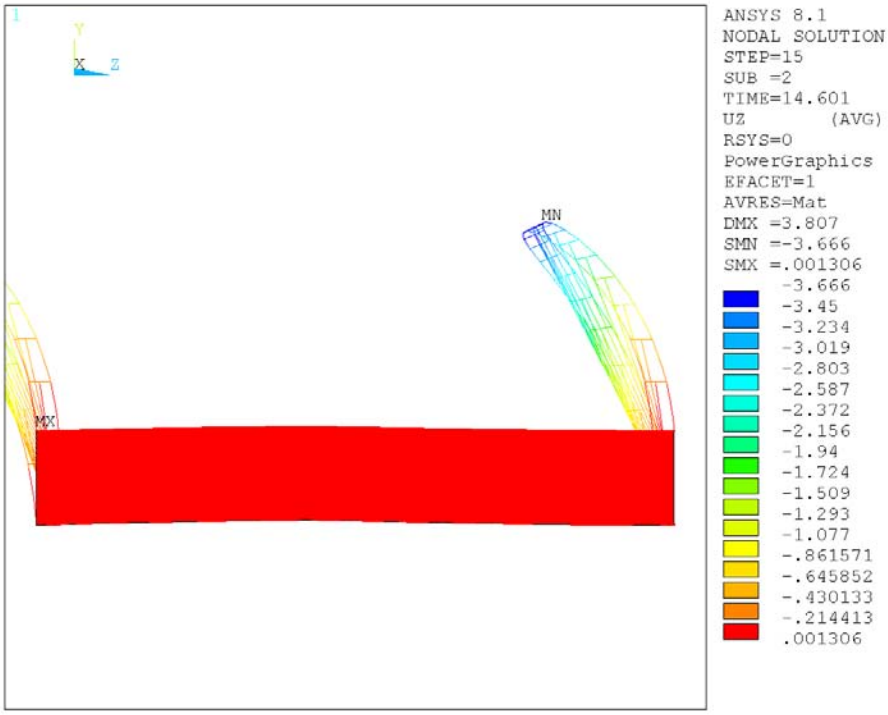

Fig.4.14 step 15 – 14 x design wind load

5. STABILITY OF THE ARCH FOR TRUCK AND WIND LOAD

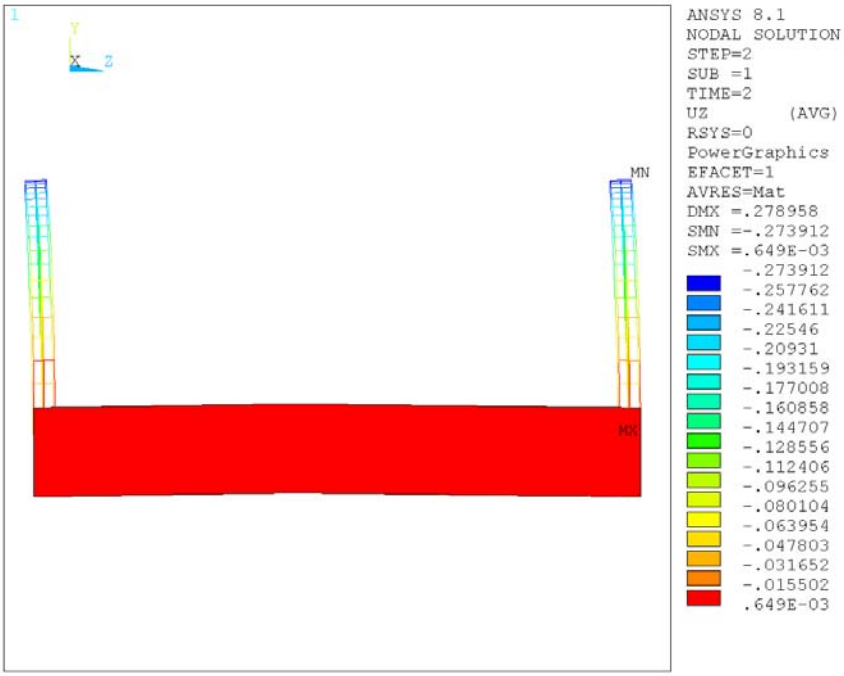

Fig.5.1 step 2- design wind load (initial stage – step 1)

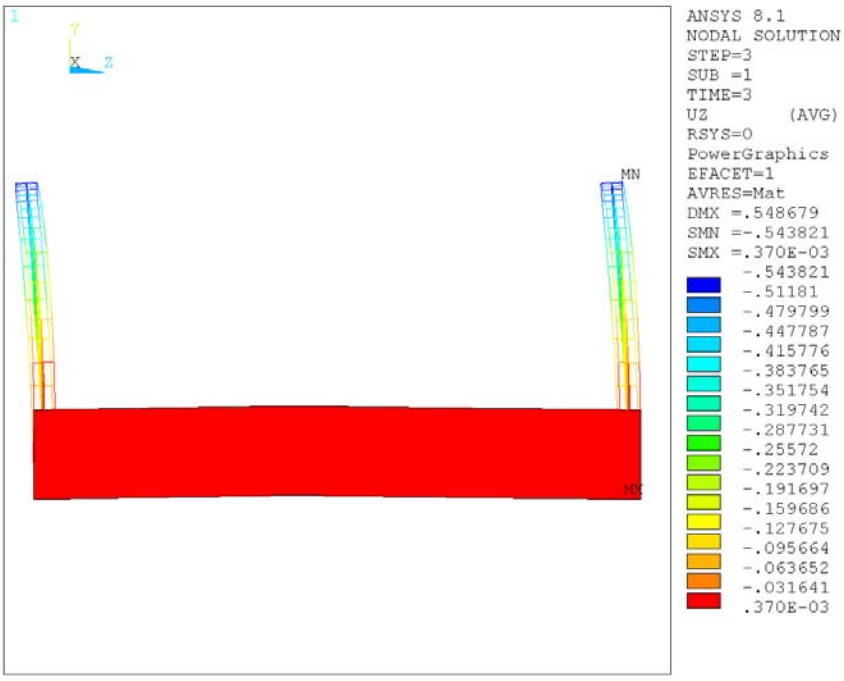

Fig.5.2 step 3 – 2 x design wind load

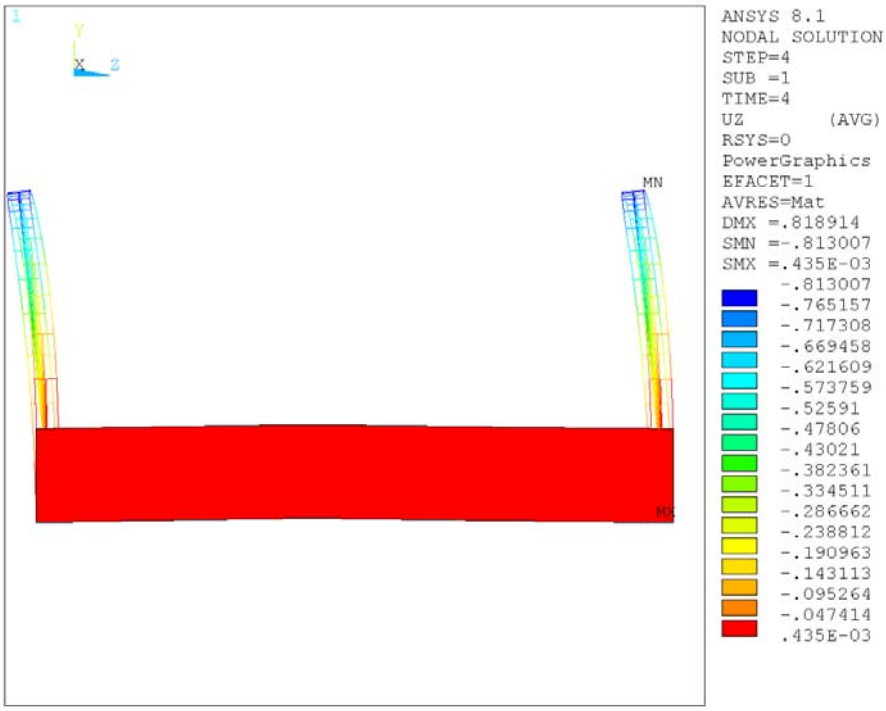

Fig.5.3 step 4 – 3 x design wind load

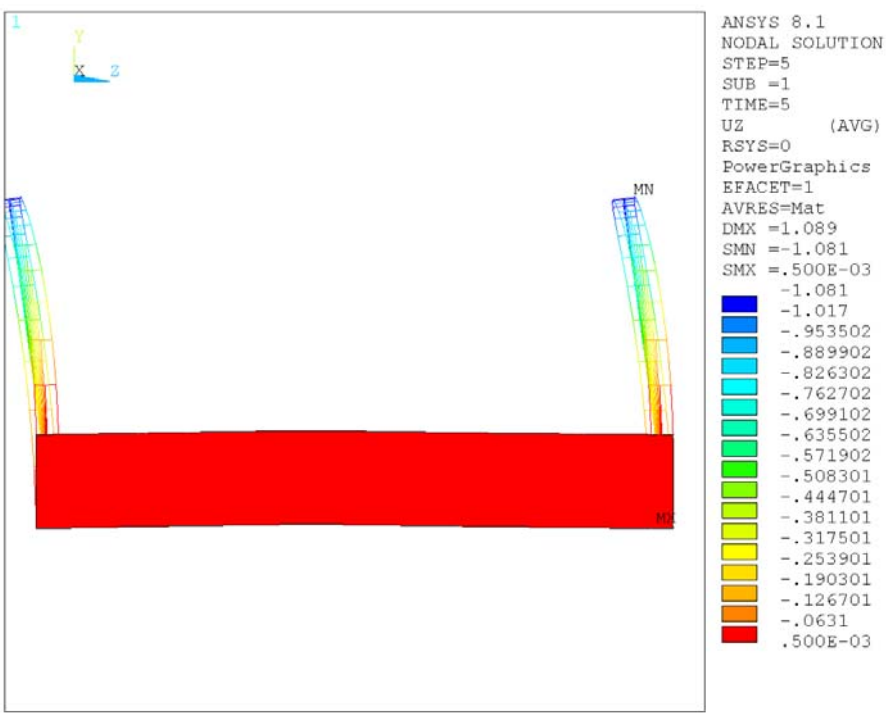

Fig.5.4 step 5 – 4 x design wind load

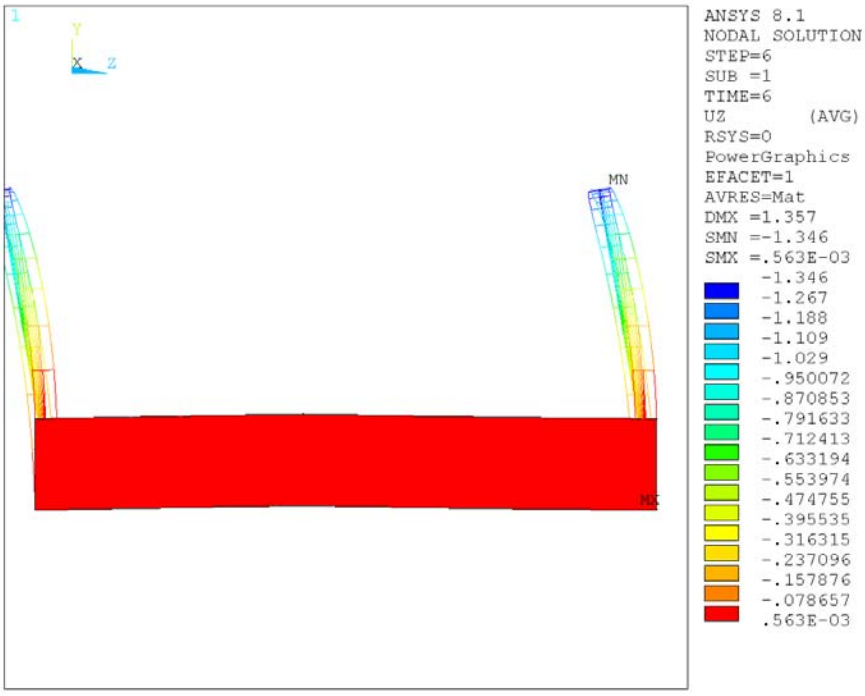

Fig.5.5 step 6 – 5 x design wind load

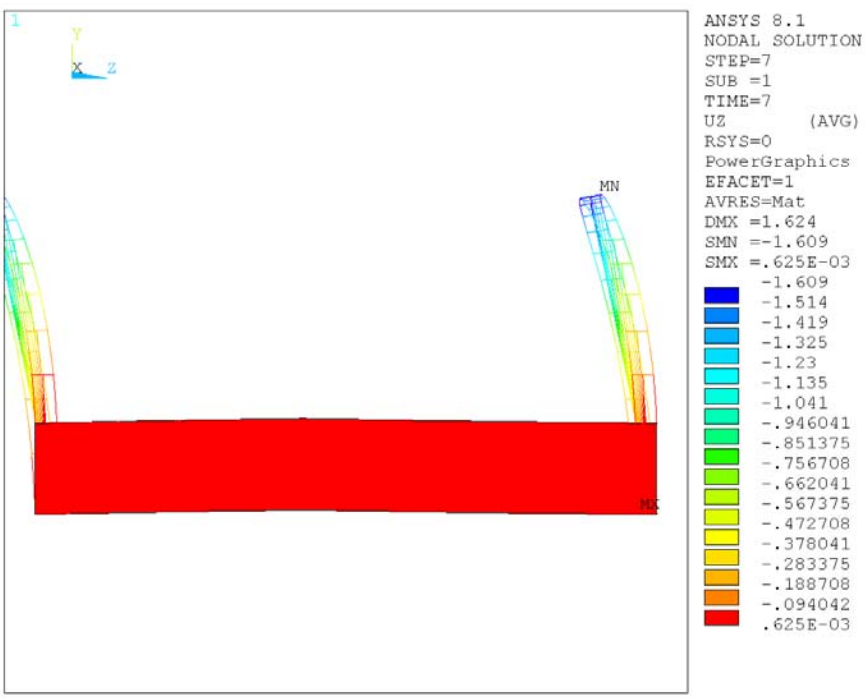

Fig.5.6 step 7 – 6 x design wind load

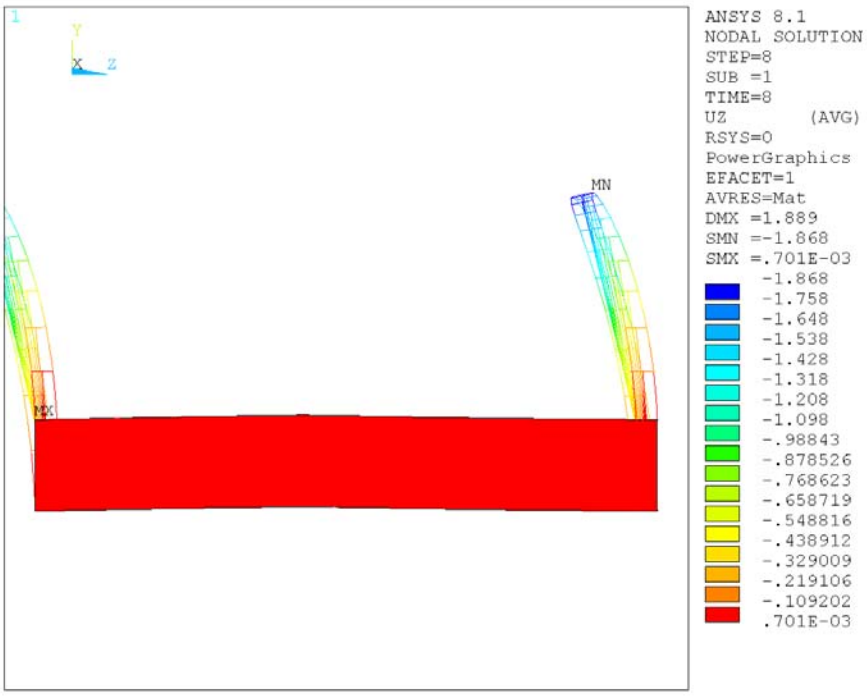

Fig.5.7 step 8 – 7 x design wind load

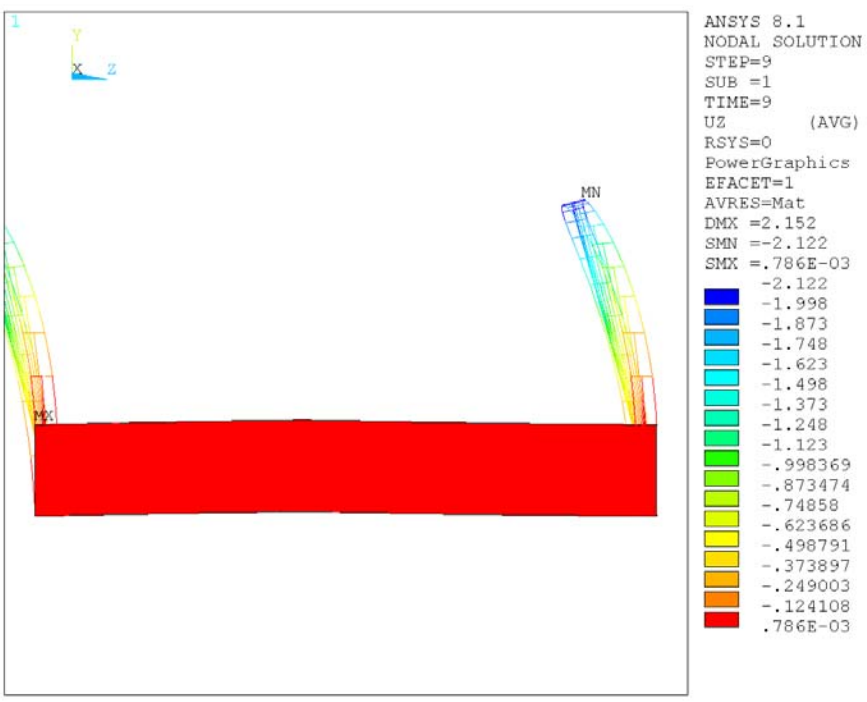

Fig.5.8 step 9 – 8 x design wind load

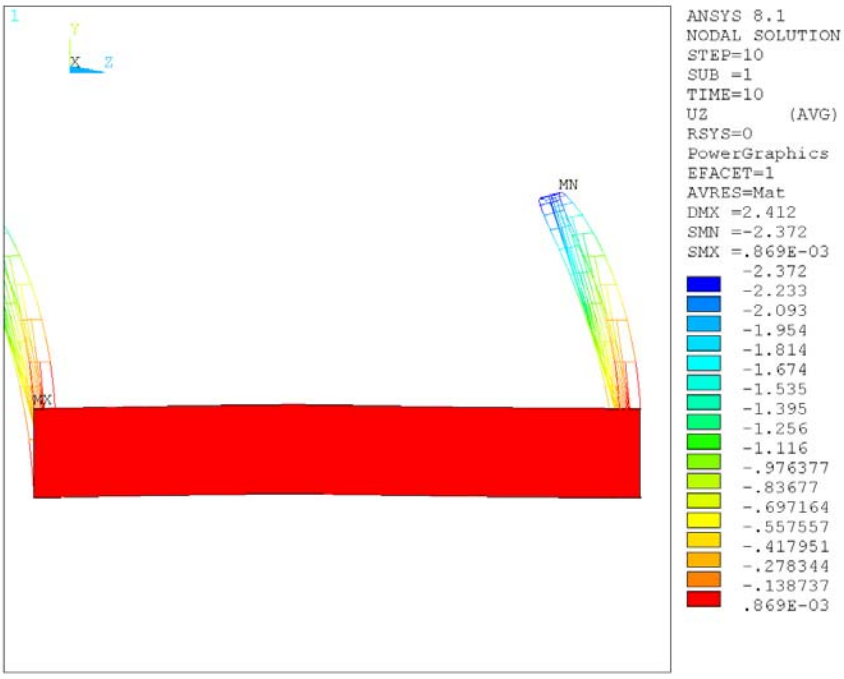

Fig.5.9 step 10 – 9 x design wind load

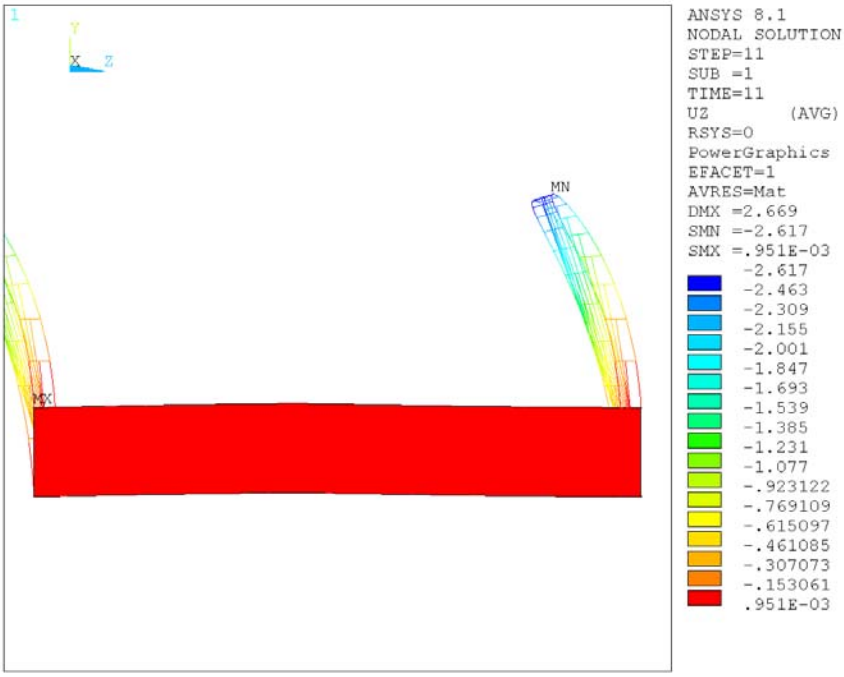

Fig.5.10 step 11 – 10 x design wind load

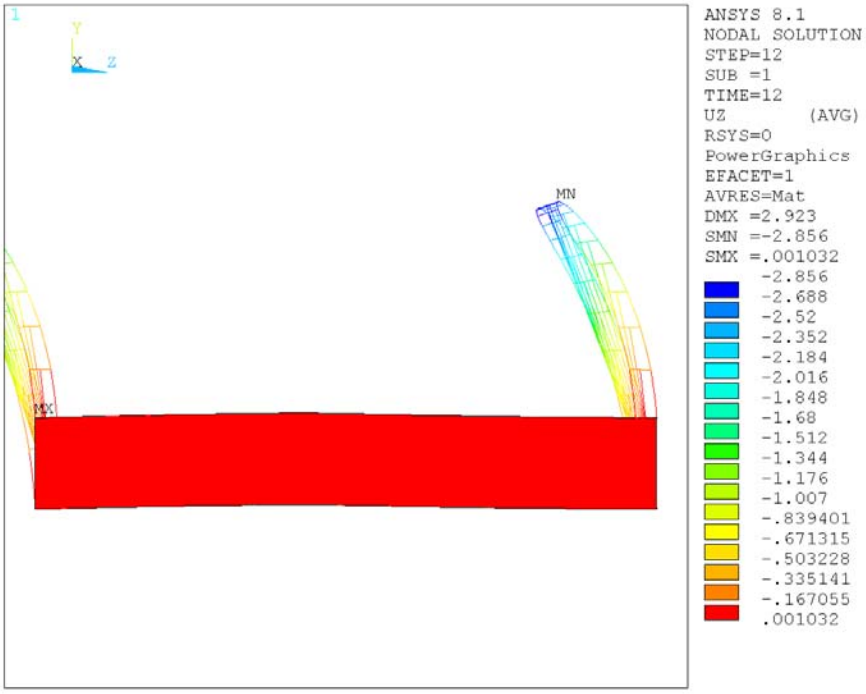

Fig.5.11 step 12 – 11 x design wind load

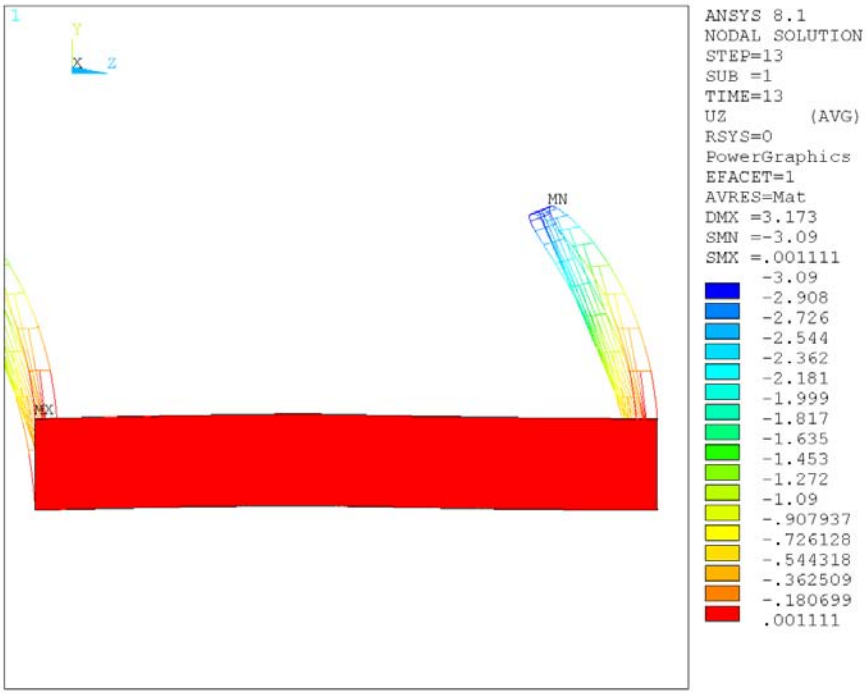

Fig.5.12 step 13 – 12 x design wind load

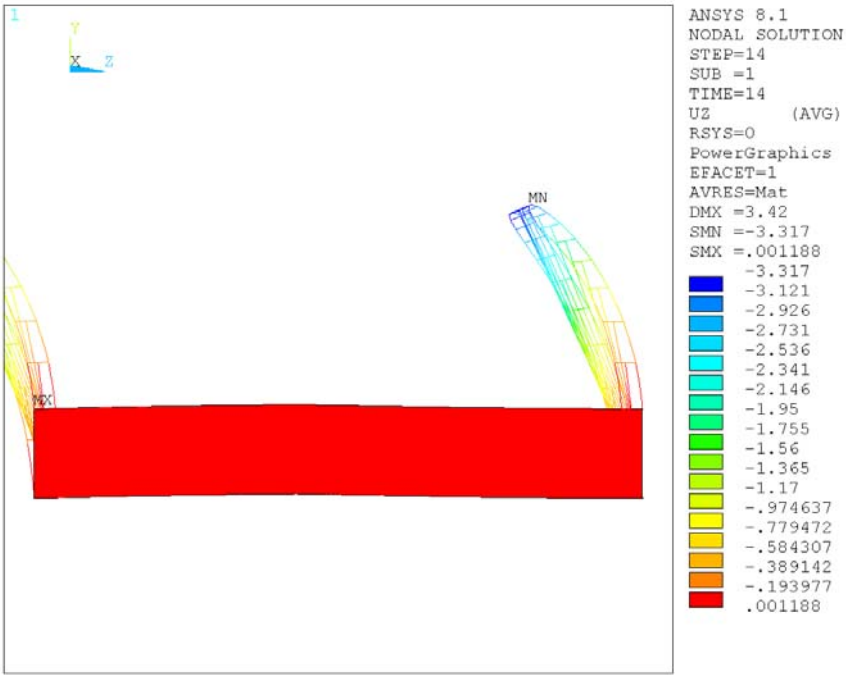

Fig.5.13 step 14 – 13 x design wind load

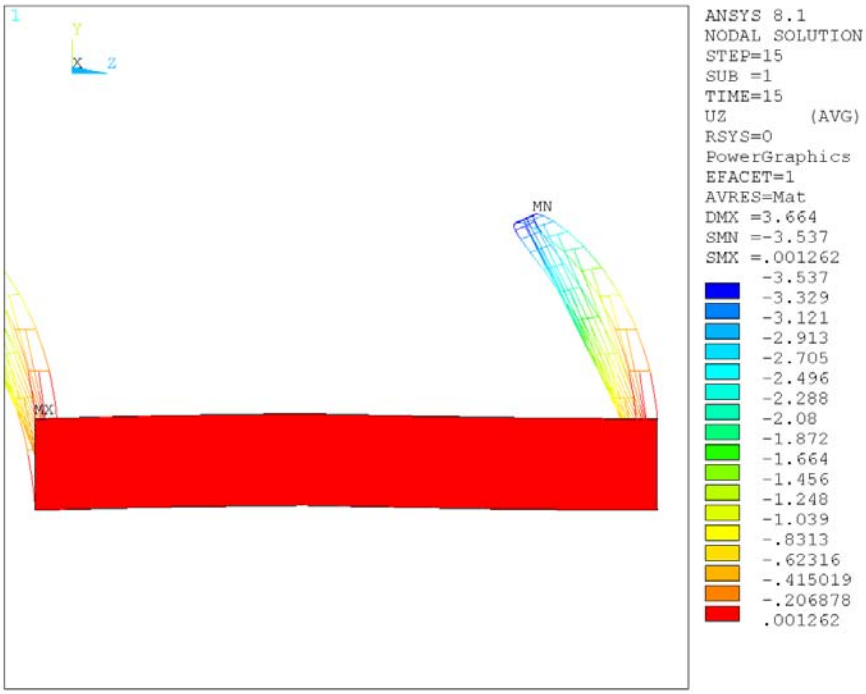

Fig.5.14 step 15 – 14 x design wind load

6. STABILITY OF THE ARCH WITH AN IMPERFECTION FOR TRUCK AND WIND LOAD

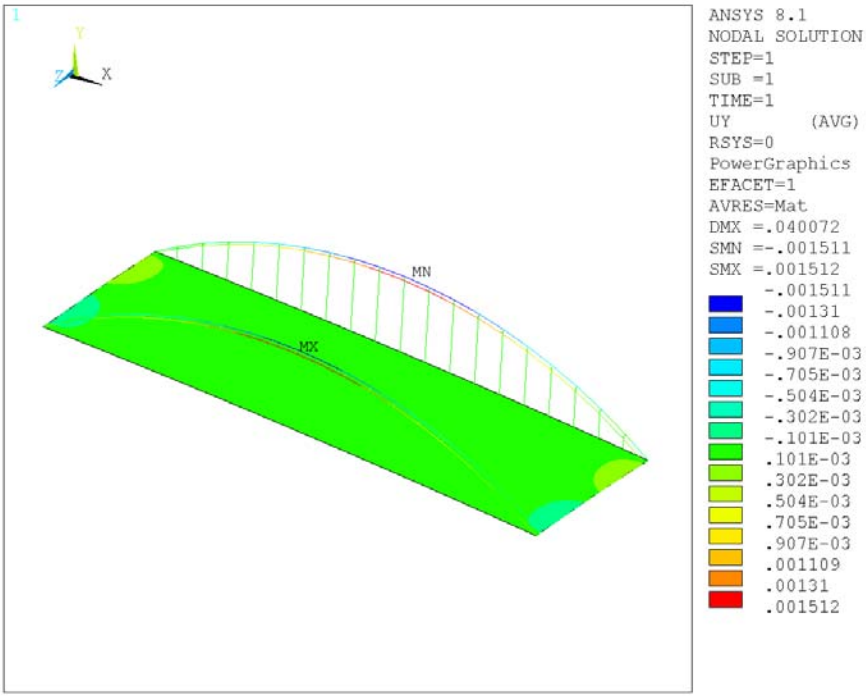

Fig.6.1 Structure with the imperfection

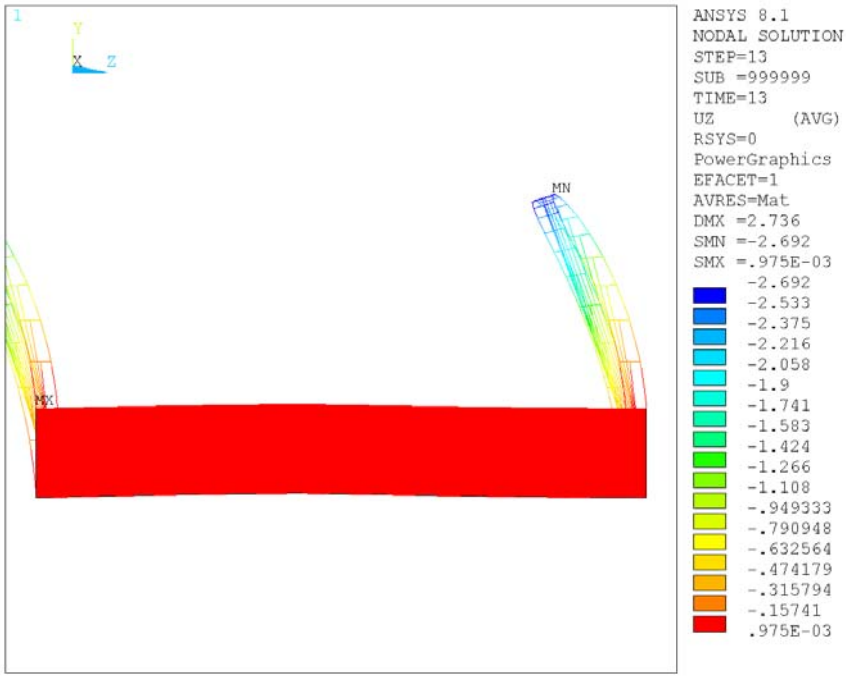

Fig.6.2 step 13 – 12 x design wind load

6. CONCLUSIONS

The divergence of the solution for the structure formed by the arch without an imperfection for wind the load and for the truck and wind load has occurred when the wind load reached value hat correspond to 15 multiple of the design load.

The divergence of the solution for the structure formed by the arch with the imperfection has occurred when the wind load reached value hat correspond to 12 multiple of the design load.

However it is necessary to realize that for these loads the stresses in the arches were higher than ultimate stresses and the horizontal deflection of the arches was as much as 3.67 m (12.04 ft).

Due to the stabilizing effects of the hangers the structure proved to very stable for the design static wind load.

JIRI STRASKY, PH.D.,P.E., 176 CORTE ANITA, GREENBRAE, CA 94904, TEL. (415) 464-0447, FAX.(415) 354 3348
E-mail: j.strasky@usa.net

APPENDIX B

Bottom Chord Test Design Mix

Material	Design/CY	
Cement Type I/II	681	lb.
Class C Fly Ash	402	lb.
47B Sand-Gravel	1059	lb.
C33 Fine Sand	1571	lb.
Glenium 30/30	2.09 (0.25)	lb. (Gal) - Superplasticizer
Rheomac VMA 362	1.17 (0.14)	lb. (Gal) - Vicosity Modifier
Tetragaurd AS20	12.51 (1.50)	lb. (Gal) - Shrinkage-reducer
Total Water	260	lb.
w/c =	0.24	

Note: Make allowance for moisture in aggregates and admixtures. For admixtures, assume 100% moisture

Bottom Chord Test Mix (Actual)

Material	Quantity/CY		% Moisture	Water Wt.	
Cement Type I/II	680.00	lb.	-	-	
Class C Fly Ash	402.86	lb.	-	-	
47B Sand-Gravel	1071.43	lb.	1.90	20.34	lb.
C33 Fine Sand	1597.14	lb.	2.00	31.94	lb.
Glenium 30/30	2.09 (0.25)	lb. (Gal)	100.00	2.09	lb.
Rheomac VMA 362	1.17 (0.14)	lb. (Gal)	100.00	1.17	lb.
Tetragaurd AS20	12.51 (1.50)	lb. (Gal)	100.00	12.51	lb.
Total Water	276.04	lb.	-	-	
Added Water	208.00	lb.	100.00	208.00	lb.
w/c =	0.25				

Cylinder Strengths:

Day	Date	Strength (psi)
0	3/30/2004	
1	3/31/2004	0
6	4/5/2004	5,051
7	4/6/2004	5,490
13	4/12/2004	6,583
13	4/12/2004	6,708
36	5/5/2004	7,209
41	5/10/2004	7,922

Observations: After 24 hours the concrete had yet to gain strength. It could be crushed by hand. It had retained moisture, but hydration had not yet occurred. On day 7, the moisture was still visually apparent within the broken cylinder. By day thirteen, the moisture could no longer be seen.

Recommended Mix – BRS with Admixtures

Material	Design/CY		
Cement Type I/II	705	lb.	
Class C Fly Ash	378	lb.	
47B Sand-Gravel	980	lb.	
C33 Fine Sand	420	lb.	
1/2" BRS Limestone	1340	lb.	
Air Content	2.0	%	
Glenium 30/30	0.25	Gal	- Superplasticizer
Rheomac VMA 362	0.14	Gal	- Vicosity Modifier
Tetragaurd AS20	1.50	Gal	- Shrinkage-reducer
Total Water	260	lb.	
w/c =	0.24		

Note: Make allowance for moisture in aggregates and admixtures. For admixtures, assume 100% moisture

Cylinder Strengths:

Day	Date	Strength (psi)
0	5/5/2004	
1	5/6/2004	2,355
7	5/12/2004	8,093

APPENDIX C

BOTTOM CHORD STRENGTH

The bottom chord strength is presented in interaction diagram as shown in Figure 3.3.1-1 using 100% from the deck slab as an effective flange width.

The points that were used to graph figure 3.3.1-1 are shown in Table 1.

Table 1 the coordinates of the interaction diagram using the full slab width.

ϕPn [kip]	ϕMn [kip-ft]	ϕPn [kip]	ϕMn [kip-ft]
7567.3	4723.2972	7550.98	4829.524
6948.708	5226.7932	6327.91	2396.806
6273.655	5733.136	5910.86	1627.414
5269.663	6425.8502	5425.97	755.5158
4739.681	6776.309	5056.02	99.61566
4239.371	7099.8348	4719.14	-470.99
3766.812	7399.411	4457.40	-872.399
3351.434	7656.6824	4198.72	-1265.27
2926.572	7915.4187	4029.70	-1508.87
2520.165	8157.2952	3820.21	-1818.97
2063.18	8389.8612	3627.56	-2088.21
1578.286	8613.2724	3436.03	-2355.81
1117.684	8823.3455	3230.32	-2621.99
676.9532	9021.3157	3035.07	-2865.44
252.6581	9208.1473	2842.06	-3090
-0.02457	9315.7977	2647.06	-3296.41
-134.3	9372.9878	2398.65	-3342.05
-533.302	9539.6528	2118.74	-3383
-922.481	9697.0059	1867.61	-3414.28
-1676.82	9985.2013	1634.30	-3438.65
-2457.85	10237.149	1388.02	-3459.42
-3248.69	10438.648	179.17	-3468.15
-4056.74	10608.381	-833.73	-3647.77
-4838.78	10749.786	-1639.64	-3778.36
-5816.33	10656.76	-2314.52	-3859.43
-6354.96	7895.7771	-2913.23	-3888.62
-7397.98	5889.1899	-3303.36	-3859.81
-8662.69	4257.65	-3971.25	-3714.75
-9691.99	2710.4775	-6186.88	-2900.92
-10404.6	1463.0197	-8469.37	-1616.07
-11252.3	56.883651	-10366.00	-225.951
		-10479.65	-199.68
		-11252.30	44.92519

The bottom chord strength is also presented in interaction diagram as shown in Figure 8.9-1 using 100% and 70 % from the deck slab as an effective flange width.

The points that were used to graph the 70 % strength values in figure 8.9-1 are shown in Table 2.

Table 2 The coordinates of the interaction diagram using 70% of the slab width.

ϕPn [kip]	ϕMn [kip-ft]	ϕPn [kip]	ϕMn [kip-ft]
7232.5	4037.7739	7216.18	4131.962
6793.3	4445.5274	5993.11	1843.013
6297.64	4869.5536	5576.06	1122.644
5565.093	5455.1223	5091.17	307.7416
5170.247	5758.5504	4721.22	-304.672
4793.713	6042.1834	4384.34	-835.678
4437.356	6306.3122	4122.60	-1206.32
4123.394	6534.6844	3863.92	-1568.78
3805.578	6763.165	3694.90	-1792.52
3503.326	6976.7153	3485.41	-2077.99
3165.598	7182.7206	3292.76	-2324.58
2808.944	7381.2608	3101.23	-2569.67
2471.441	7568.2307	2895.52	-2811.67
2149.636	7744.8687	2700.27	-3032.17
1840.827	7912.1481	2507.26	-3234.04
1566.49	8056.4544	2312.26	-3417.53
1277.696	8207.1607	2074.95	-3440.28
996.6736	8350.3686	1807.53	-3455.41
453.6148	8615.7548	1567.48	-3463.46
-0.09654	8813.6954	1344.09	-3466.03
-121.454	8858.3496	1106.74	-3462.93
-721.832	9067.044	-19.99	-3372.91
-1336.45	9253.4962	-939.01	-3487.29
-1926.95	9416.8782	-1677.87	-3561.59
-2861.95	9419.6158	-2302.46	-3592.17
-3929.28	7030.2267	-2862.06	-3573.42
-5184.06	5248.237	-3222.66	-3515.68
-6445.29	3762.7596	-3758.17	-3343.55
-7471.79	2338.9174	-5329.16	-2585.58
-8180.35	1179.7763	-6932.09	-1500.76
-8997.26	-78.45211	-8271.79	-370.877
		-8365.63	-340.716
		-8997.26	-80.5316

APPENDIX D

SECTION PROPERTIES CALCULATION FOR THE FE MODELING

1. HANGERS

The hangers are grade 150 threaded rods. The threaded rods diameters are 1.75

2. ARCH TOP CHORD

Refer to Figure 8.3.2-1, the cross section properties calculations are as follows:
Modulus of Elastic

$$E_c = 33{,}000 w^{1.5}\sqrt{f'_c} = 33{,}000(0.15)^{1.5}\sqrt{8} = 5421.63\text{ksi}$$

Modular ration

$$n = \frac{E_s}{E_c} = \frac{29000}{5421.63} = 5.35$$

A) Area

$$A_s = \pi(D-t)t = 3.14(12-\frac{1}{2})(\frac{1}{2})(2) = 36.11\text{in}^2$$

$$A_c = \frac{1}{4}\pi D^2 = \frac{1}{4}(3.14)(12-\frac{1}{2}\times 2)^2(2) = 189.97\text{in}^2$$

$$A = A_s + \frac{A_c}{n} = 36.11 + \frac{189.97}{5.35} = 71.62\text{in.}^2$$

B) Moment of Inertia of the section around Z axis

$$I_{SZ} = \pi R^3 t = 3.14(6^3)(\frac{1}{2})(2) = 678.24\text{in.}^4$$

$$I_{CZ} = \frac{1}{4}\pi(6-\frac{1}{2})^4(2) = 1436.65\text{in.}^4$$

$$I_Z = I_{SZ} + \frac{I_{CZ}}{n} = 678.24 + \frac{1436.65}{5.35} = 946.77\text{in.}^4$$

Moment of Inertia of the section around Y axis

$$I_{SY} = I_S + A_s h^2 = 678.24 + 36.11(12^2) = 5878.08\text{in.}^4$$

$$I_{CY} = I_C + A_C h^2 = 1436.65 + 189.97(12^2) = 28792.33\text{in.}^4$$

$$I_Y = I_{SY} + \frac{I_{CY}}{n} = 5878.08 + \frac{28792.33}{5.35} = 11259.82\text{in.}^4$$

C) Density and transferred diameter

$$\rho = \frac{1}{A}(\rho_s A_s + \rho_c A_c) = \frac{1}{71.62}(0.49\times 36.11 + 0.15\times 189.97) = 0.645\,\text{K}/\text{ft.}^3$$

$$D = \sqrt{\frac{4A}{\pi}} = \sqrt{\frac{4(71.62)}{\pi}} = 9.55\text{in.}$$

D) Polar moment of inertia

$$J = I_Y + I_Z = 946.77 + 11259.82 = 12206.59\text{in.}^4$$

3. ARCH BOTTOM CHORD

Refer to Figure 8.3.31, the cross section properties calculations are as follows:

A) Area

$$A_s = 4(24 - \frac{1}{2})\frac{1}{2} = 47\text{in}^2$$

$$A_{c1} = (24 - \frac{1}{2} \times 2)^2 = 529\text{in}^2$$

$$A_{girder} = A_s + \frac{A_{c1}}{n} = 47 + \frac{529}{5.35} = 145.88\text{in.}^2$$

$$A_{c2} = 54.25 \times 7.5 = 406.9\text{in}^2$$

$$A = A_{girder} + \frac{A_{c2}}{n} = 145.88 + \frac{406.9}{5.35} = 221.93\text{in.}^2$$

B) Moment of Inertia of the section around Z axis

$$I_{girder} = I_s + I_{c1} = \frac{1}{12}(24^4 - (24 - 1/2 \times 2)^4)) + \frac{1}{12}(24 - 1/2 \times 2)^4 / 5.35 = 8686.81\text{in.}^4$$

Transformed slab width 54.25/5.35=10.14 in.

$$Y_b = \frac{145.88 \times 12 + (10.14 \times 7.5)(24 + 7.5/2)}{145.88 + 10.14 \times 7.5} = 17.4\text{in.}$$

$$I_Z = (8686.81 + 145.88 \times 5.4^2) + (\frac{1}{12} \times 10.14 \times 7.5^3 + 10.14 \times 7.5 \times (27.25 - 17.4)^2) = 21{,}443.8\text{in.}^4$$

C) Moment of Inertia of the section around Y axis

Transformed slab width 7.5/5.35=1.4 in.

$$Z_b = 17.18\text{in.}$$

$$I_Y = (8686.81 + 145.88 \times (12 - 17.18)^2)$$
$$+ (\frac{1}{12} \times 1.4 \times 54.25^3 + 10.14 \times 7.5 \times (54.25/5.35 - 17.18)^2) = 38749.83in.^4$$

D) Density

$$\rho = \frac{1}{221.93}(0.49 \times 47 + 0.15 \times 529 + 54.25 \times 8) = 0.61\,\text{K/ft}^3$$

e) Polar moment of inertia

$$J = I_Y + I_Z = 60{,}193.63\text{in.}^4$$

4 DECK SLAB

Refer to Figure 8.3.4-1, the cross section properties calculations are as follows:

A) Area = 637.5 in^2

B) Moment of Inertia of the section around Z axis = 2988.3 in^4

5 TURNDOWN BEAM

Refer to Figure 8.3.5-1, the cross section properties calculations are as follows:

A) Area

$$A = \frac{48(24) + 70.5(7.5)}{5.35} = 314.16\text{in.}^2$$

B) Moment of Inertia of the section around Z axis

$$Y_b = \frac{48(24)(12) + 70.5(7.5)(24 + 7.5/2)}{48(24) + 70.5(7.5)} = 16.95\text{in.}$$

$$I_Z = \frac{1}{12}(48)(24^3) + 48(24)(12 - 16.95)^2$$

$$+\frac{1}{12}(70.5)(7.5^3) + 70.5(7.5)(24 + 7.5/2 - 16.95)^2 = 147{,}674.8 in.^4$$

Transfer it to steel material, $I_Z = \frac{147{,}674.8}{5.35} = 27602.8\text{in.}^4$

Moment of Inertia of the section around Y axis

$$Z_b = \frac{48(24)(24) + 70.5(7.5)(70.5/2)}{48(24) + 70.5(7.5)} = 27.54\text{in.}$$

$$I_Y = \frac{1}{12}(24)(48^3) + 48(24)(24 - 27.54)^2$$

$$+\frac{1}{12}(7.5)(70.5^3) + 70.5(7.5)(70.5/2 - 27.54)^2 = 486{,}053.1 in.^4$$

Transfer it to steel material, $I_Y = \frac{486053}{5.35} = 90851.05\text{in.}^4$

D) Density

$$\rho = \frac{1}{314.16}(48(24)(0.15) + 70.5(8)(0.15/2)) = 0.3\ \text{K/ft}^3$$

E) Polar moment of inertia

$$J = I_Y + I_Z = 118453.85\text{in.}^4$$

6 CROSS-BEAMS

Refer to Figure 8.3.6-1, the cross section properties calculations are as follows:

A) Area

$$A = 73.5 + \frac{105(7.5)}{5.35} = 220.7\text{in.}^2$$

B) Moment of Inertia of the section around Z axis

$$Y_b = \frac{73.5(26.34/2) + (105/5.35)(7.5)(26.34 + 7.5/2)}{220.7} = 24.45\text{in.}$$

$$I_Z = 8490 + 73.5\left(24.45 - \frac{26.34}{2}\right)^2$$

$$+\frac{1}{12}\left(\frac{105}{5.35}\right)(7.5^3) + \frac{105}{5.35}(7.5)(26.34 + 7.5/2 - 24.45)^2 = 23214.26in.^4$$

C) Moment of Inertia of the section around Y axis

$$I_Y = 724 + \frac{1}{12}\left(\frac{7.5}{5.35}\right)(105^3) = 135960.6\text{in.}^4$$

D) Density

$$\rho = \frac{1}{220.7}\left(105(8)(0.15/2) + 73.5(0.49)\right) = 0.45\ \text{K/ft}^3$$

E) Polar moment of inertia

$$J = J_{beam} + J_{slab} = 67.3 + \frac{1}{3}\left(\frac{105}{5.35}\right)(7.5^3) = 2827.2\text{in.}^4$$